Low head simple reaction water turbine

A thesis submitted in fulfilment of the requirements for the degree of

Doctor of Philosophy

Abhijit Date
B.Eng.

School of Aerospace, Mechanical and Manufacturing Engineering
Science, Engineering and Technology Portfolio
RMIT University

April 2009

Declaration

I certify that except where due acknowledgement has been made, the work is that of the author alone; the work has not been submitted previously, in whole or in part, to qualify for any other academic award; the content of the thesis is the result of work which has been carried out since the official commencement date of the approved research program; any editorial work, paid or unpaid, carried out by a third party is acknowledged; and, ethics procedures and guidelines have been followed.

Abhijit Date

April 2009

Acknowledgement

This project could not have completed without the support of RMIT University for the endorsement and financing of the project. I am greatly indebted to the following supervisors and guides who graciously lent me their technical expertise and encouragement throughout the project:

- Prof. Aliakbar Akbarzadeh my first supervisor for his guidance in testing, analysis, thesis writing and journal publications
- Mr. Chris Dixon my second supervisor for his guidance in analysis, thesis editing, and resources provision
- Dr John Andrews as a guide for his comments and recommendations during the presentations on this topic at RMIT

Gratitude is expressed the following people for their contribution to the project:

- Patrick Wilkins, David Goodie, Brett Vincent and Adrian from RMIT University for the production of the test rig and turbine prototypes and modification
- All RMIT University Bundoora East Workshop staff
- All members of Energy CARE Group

Special thanks to my parents, my wife and my younger brother.

Abstract

Global warming, climate change, rising fuel prices and sustainable future environment are the main motivations behind this research project. For sustainable future development, entire world has to reduce the green house gas emissions by reducing the use of fossil fuels and relying more on renewable energy sources to support the present and future energy demands. Hydropower is a very good example of renewable energy and it is the most reliable base-load energy source. There is huge untapped technically exploitable hydro energy potential of about 14,000TWh (Taylor, 2004, Sommers, 2004) waiting to be utilised throughout the world. There are few small to medium scale low head hydro turbines commercially available, but they are very expensive for micro power generation at individual level. Therefore, there is an inherent need of a simple low cost and low head hydro turbine that can encourage use of hydropower available in abundant from creeks, small rivers, streams etc. at an individual level.

The aim of the research presented in this thesis is to develop low cost and high performance simple reaction water turbine for electricity production from low head hydro sources. In this thesis, two new innovative designs of simple reaction water turbine are presented and the performance characteristics of their prototypes are investigated experimentally and graphically presented. The theoretical analysis of the simple reaction turbine presented in this thesis highlights the potentials and intrinsic characteristics of simple reaction turbine. The governing equations for ideal situation without losses and practical situation with losses are presented in this thesis. The theoretical analysis predicts the centrifugal pumping effect that allows additional mass of water to flow through the turbine as it starts to rotate faster. Further, the theoretical model for optimum turbine diameter is presented followed by the theoretical analysis of jet-interference phenomenon.

This thesis explains the systematic procedure of manufacturing turbine rotors for both the innovative new designs. Rotary seal arrangements used in the testing of these turbine prototypes are presented with figures and details of suppliers are attached in the appendix. Thesis further illustrates the experimental test rig and its instrumentation used

for testing the prototypes of the new turbine designs. Experimental procedures are explained with illustrative pictures of test rig and its instrumentation.

The experimental investigation presented in the thesis shows the centrifugal pumping effect through the additional flow rate measured as the turbine speed increases. The fluid frictional power loss characteristics of simple reaction turbine are experimentally estimated for stationary and rotary conditions and presented as k-factor in this thesis. Additionally the increase in k-factor with increase in the relative velocity of the water leaving the turbine nozzles is also shown in this thesis. Estimated turbine drag characteristics for both the new turbine designs are also presented. The performance characteristics like turbine power output, electrical power output, turbine efficiency and overall efficiency verses rotational speed for different supply pressures (supply heads) is also presented with examples and illustrative discussion for all new turbine designs.

A case study of the potential low head hydro site in Victoria, Australia is presented with detail turbine sizing and water intake system for small creek using natural stone weir. Simple costing of the entire low head micro hydroelectric installation is presented towards the end of this thesis.

In the conclusion of this research, an optimised low cost and high performance simple reaction turbine design has been developed and presented to be used for electricity production from low head hydro sources.

Table of content

List of Figures

List of Tables

Nomenclature

A	Total exit nozzle area (m^2)
A_s	External surface area of rotor (m^2)
β	Angular distance between two consecutive nozzles (radian)
C_d	Coefficient of discharge
d	Exit nozzle diameter (m)
d_e	Equivalent exit nozzle diameter (m)
D	Turbine diameter (m)
D_A	Average pipe diameter (m)
D_c	Outer diameter of the cover plates (m)
D_m	Mean turbine diameter (m)
D_{opt}	Optimum turbine diameter (m)
δ	Sum of exit nozzle width and turbine wall thickness (m)
η	Theoretical turbine efficiency (%)
η_t	Estimated turbine efficiency, potential to mechanical energy conversion efficiency (%)
$*\eta$	Non-dimensional efficiency
η_o	Overall efficiency (%) – Energy conversion efficiency from turbine mechanical energy output to generator electrical energy output.
f	Coefficient of friction
F_d	Drag force (N)
g	Acceleration due to gravity (m/s^2)

h	height of the rotor (m)
H	Supply head (m)
H_c	Centrifugal Head (m)
H_W	Height of stone weir, (m)
H_G	Gross available head, (m)
H_D	Dynamic head loss in supply pipe, (m)
H_N	Net available head at the inlet to turbine, (m)
I_g	Generator output current (Amp)
k	Factor for fluid frictional power loss
K_e	Voltage constant of the DC motor/generator (Volt/rad/sec)
K_s	Specific speed of turbine
K_t	Torque constant of the DC motor/generator (Nm/amp)
K_L	Head loss coefficient for 90° pipe elbow
L_P	Intake pipe length (m)
L	Distance between external surface of rotor and water splash cover (m)
$\dot{m}$	Mass flow rate of water flowing through the turbine (kg/s)
$\dot{m}_{ideal}$	Ideal mass flow rate of water that should flow through the turbine (kg/s)
$\dot{m}_{real}$	Measured mass flow rate of water flowing through the turbine (kg/s)
$\dot{m}_s$	Mass flow rate of water flowing through a stationary turbine (kg/s)
$*\dot{m}$	Non-dimensional mass flow rate

n	Number of exit nozzles
Q	Volume flow rate of water (m^3/s)
ρ	Density of water (kg/m^3)
R	Turbine radius (m)
R_e	Reynolds number
t	Turbine wall thickness (mm)
$t_{CB'}$	Time required for travel of point C to point B' (sec)
$t_{AB'}$	Time required for travel of point A to point B' (sec)
T	Turbine torque (N-m)
$*T$	Non-dimensional turbine torque
$T_{estimated}$	Estimated torque (N-m)
T_g	Generator shaft input torque (N-m)
T_{loss}	Total torque loss (N-m)
T_s	Turbine stationary torque (N-m)
τ	Time (sec)
θ	Angle between the exiting water jet and tangent to the mean turbine diameter (radian)
w	Exit nozzle width (m)
W_d	Rotor drag power loss (W)
$\dot{W}$	Mechanical power (W)
$*\dot{W}$	Non-dimensional mechanical power
$\dot{W}_E$	Electrical output power from generator (W)

$\dot{W}_{Ff}$	Power loss in fluid friction (W)
$\dot{W}_{Ke}$	Power loss in for kinetic energy with the water jet leaving the turbine at certain absolute velocity (W)
$\dot{W}_{In}$	Estimated hydro input power to the turbine (W)
$\dot{W}_{loss}$	Total power loss (W)
$\dot{W}_{\max}$	Maximum output mechanical power of turbine (W)
$\dot{W}_{T}$	Experimental turbine power output [$\dot{W}_{E}+\dot{W}_{loss}$] (W)
$\dot{W}_{Out}$	Total output power [i.e. $\dot{W}_{T}+\dot{W}_{Ke}+\dot{W}_{Ff}$] (W)
ω	Angular velocity of the rotor (rad/s)
$*\omega$	Non-dimensional angular velocity of rotor
U	Tangential velocity of the nozzles (m/s)
$*U$	Non- dimensional tangential velocity of the nozzles
μ	Viscosity of water (kg/m.s)
μ_{air}	Viscosity of air (kg/m.s)
V_a	Absolute velocity of the water jet leaving the nozzles (m/s)
$*V_a$	Non-dimensional absolute velocity
V_g	Generator output voltage (Volts)
V_{ideal}	Ideal velocity at which water jet should leave the nozzles (m/s)
V_r	Relative velocity of the water jet with respective to nozzle (m/s)
$*V_r$	Non-dimensional relative velocity
x	Center offset between two pipe splits, (m)

$\frac{\Delta y}{\Delta x}$	Terrain slope

List of Acronyms

CPT	Cross pipe turbine (often used in Chapter 3 and Chapter 5)
SRT	Split reaction turbine (often used in Chapter 3 and Chapter 5)
SRT prototype 1	Split reaction turbine with rotor diameter of 243 mm as described in Chapter 3.
SRT prototype 2	Split reaction turbine with rotor diameter of 125 mm as described in Chapter 3.
SRT 125D-120L-8W	Stands for Split reaction turbine with 125mm turbine diameter, 120mm exit nozzle length and 8mm exit nozzle width. (Total exit nozzle area of 0.00192m²)
SRT 125D-120L-5.3W	Stands for Split reaction turbine with 125mm turbine diameter, 120mm exit nozzle length and 5.3mm exit nozzle width. (Total exit nozzle area of 0.00127m²)
SRT 125D-120L-4.2W	Stands for Split reaction turbine with 125mm turbine diameter, 120mm exit nozzle length and 4.2mm exit nozzle width. (Total exit nozzle area of 0.001008m²)
NMS	Nylon Mechanical Seal

Chapter 1 Introduction and Literature Review

1.1 Motivation and Introduction

With the growing understanding of global warming and climate change, it has been acknowledged that traditional dependence on fossil fuel extracts a heavy cost from the environment. Consequently, the benefits from the use of renewable energy have been recognized. At the same time the rapid economic growth of the developing economies such as China, India, Brazil, Vietnam, and Philippines has increased the world energy consumption to record levels (Conti, 2008). The electricity demand is expected to increase at faster rates than the overall energy supply (Taylor, 2004, Conti, 2008). At present majority of electricity is produced from thermal power plants which use coal, gas or oil as the energy source (Sternberg, 2008). There are growing global concerns about the global warming caused by carbon dioxide emissions from the use of fossil fuels, which creates a question about the long-term use of this energy resource. The last decade has shown catastrophic effects of rapid climate change caused by global warming and a consequence increase in awareness about the importance of a sustainable environment. The role of renewable energy in tomorrow's world is of great significance for the global environmental stability. Sun, wind and flowing or stored hydro (water) are considered to be the most common renewable energy sources for power generation. Out of these three renewable energy resources, the advantage of hydro energy is that it can continuously supply energy and can serve as a base power. The annual global hydropower production is very small as compared to the global power consumption. However the technically exploitable hydro power potential available throughout the world is far more than is actually been used as illustrated by the data from Sterngerg, Kaygusz and Taylor (Sternberg, 2008, Taylor, 2004, Kaygusuz, 2004).

<u>World Hydropower scenario (Sommers, 2004, Taylor, 2004)</u>

- Technically exploitable potential 14000 TWh/year
- Economically exploitable potential 8000 TWh/year
- Present hydro power generation 2800 TWh/year

- World electricity production 18580 TWh/year

Table 1.1 Regional hydropower generation and technically exploitable potential (Taylor, 2004, Sommers, 2004)

Regions	Present hydropower generation TWh/yr	Technically exploitable potential TWh/yr
North America	675	2873
South America	596	2880
Europe	727	2741
Asia	754	5174
Australia	17	>30
New Zealand	23	37

Looking at the above estimates it is clear that there is a large potential of hydropower waiting to be exploited. Further there is a large gap between technically exploitable and economically exploitable potential (Khennas, 2000, Khan, 2008) which creates a need for further research in hydropower technology to make it more economic and help to reduce this gap. To date most of the large hydropower sites have been exploited (Bartle, 2002, Jeffs, 1979). However, most of the small and micro hydro sites are yet to be exploited.

Thus keeping in mind that the world currently is still heavily dependent on non-renewable energy sources (fossil fuels) such as coal, oil and natural gases, which are rapidly diminishing and becoming increasingly more expensive, the role of renewable energy has been recognized to be significantly important in sustainable future development. Hydropower is a good example of renewable energy; its present use and potential application to future power generation cannot be underestimated.

The use of moving water to drive machinery traditionally began with undershot and overshot water wheels before evolving to water turbines (Akbarzadeh, 2001). A water turbine gains its energy through the flow of water from a specific head. There are two types of turbine, denoted as impulse and reaction. An impulse turbine consists of a rotor mounted on a shaft free to rotate on a set of bearings. The outer rims of the rotor carries a set of curve blades, a jet of fluid issuing from a nozzle impinges on the blades of the rotor. The change in momentum of the fluid when the fluid hits the blades causing the

wheel to turn is defined as an impulse force (Daugherty, 1954). The process described converts the kinetic energy from the fluid to mechanical work in the shaft producing power in the process. Generally, impulse turbines are restricted to low volume high heads applications with low specific speeds. The specific speed of a turbine is defined as the speed of an ideal, geometrically similar turbine, which yields one unit of power when supplied with one unit of head. In contrast, special designs such as the turgo or cross flow turbines are examples of relatively high specific speed impulse units.

In reaction turbines, the fluid fills all the runner passages completely where the impeller is located, and any head change or pressure drop will occur in the impeller (Daugherty, 1954). The flow shows opposite characteristics to a pump; entering a passage at the larger end and exiting from a smaller gap after releasing all the energy converted through the drop of pressure in the rotating wheel (White, 1986). Barker's Mill was one of the earlier pioneers to outward-flow reaction turbine. Here the fluid enters the center of the rotor via an inlet at the top. A reaction force is created when the fluid exits the nozzle tangentially causing a movement in reverse direction and making the rotor rotate about a defined axis where the rotation mechanism can produce power (Daugherty, 1954).

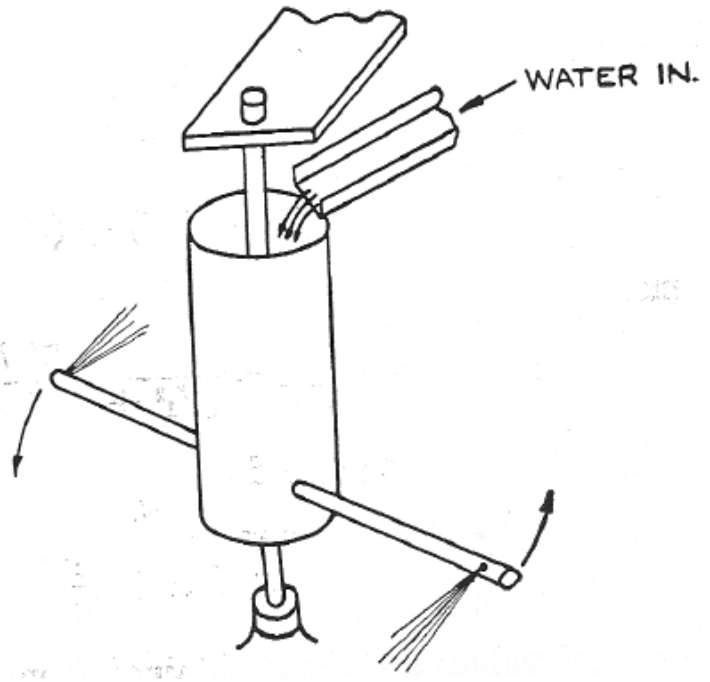

Figure 1.1 Barker's Mill (Shepherd, 1956)

Since early development of simple reaction water turbine (Barker's mill), better and more efficient turbines such as Francis, Fourneyron and Thomson have been invented. However, while subsequent years have seen modifications to increase the efficiency of the Barker's mill turbine design, it is still deemed to be obsolete and not economically viable to be used any more (Duncan, 1970). However, Akbarzadeh et. al. (Akbarzadeh, 2001), have contested that view, believing that a simple reaction turbine design similar to Barker's water turbine is to some extent misunderstood, underutilized and almost forgotten other than for garden sprinklers. In past 8 years Akbarzadeh and some final year undergraduate students have investigated a few simple reaction turbine designs at RMIT (Webb, 1999, Quek, 2001, Quek, 2003). As improvements have been recorded, predicted losses have also been identified. Following the previous research done at RMIT (Webb, 1999, Quek, 2001, Quek, 2003, Akbarzadeh, 2001), here efforts are made to further improve the simple reaction water turbine design for manufacturing simplicity and improved performance. This research thesis investigates two new innovative designs of simple reaction water turbine in detail and finds out the best innovative design of them for manufacturing simplicity and improved performance.

1.2 Aim

The aim of this project is to develop a low cost and high performance simple reaction water turbine for producing electrical power from very low head water resources (head range 0.5m to 5m, equivalent to 5kPa to 50kPa).

The aim can be broken down into following task-oriented objectives:

- Conduct literature review to better understand the current developments.
- Further, enhance the theoretical analysis of simple reaction water turbine following the current body of knowledge.
- Develop theoretical model to predict jet-interference phenomenon and conceptualise ways to utilize it for speed governing.
- Build a new innovative simple reaction water turbine prototype with manufacturing simplicity.

- Selection of suitable rotary seal arrangement to prevent inlet water leak loss
- Investigate the performance characteristics of simple reaction water turbine designs developed in previous step.
- Improve the turbine performance making suitable modifications in the developed turbine designs.
- Identify potential low head hydropower sites in Victoria, Australia through an online survey and conduct a case study for one of these sites for the technical and economic feasibility.

1.3 Methodology

To achieve the above stated objectives literature review of past journal papers and undergraduate theses on the investigation of simple reaction turbine were conducted. Further an enhanced computer model of simple reaction water turbine was developed for optimum turbine sizing for a given head and speed. This computer model can also predict the jet-interference speed. Conceptual design has been proposed to utilize the jet-interference for self-governing the simple reaction turbine to prevent the runaway under no-load condition. Further, the literature review gave better understanding of previous simple reaction turbine designs and their limitations in regards to fulfill the objectives of the present research project. Keeping in mind the objective of developing a turbine design with manufacturing simplicity and knowing the limitations of the previous turbine designs new innovative simple reaction turbine prototypes were developed and manufactured. Several different rotary sealing arrangements were studied and the two most suitable options were tested along with the new innovative turbine prototypes for performance. Following the initial performance investigations, attempts were made to improve the turbine performance by minor or major design modification. Finally, the modified designs were tested for improved performance and characterised. Readers' response survey was conducted with a questionnaire published in an environmental magazine circulated in Melbourne, Australia. Reader's responses to the questionnaire were analysed and some site visits were conducted for potential hydro site data

verification. A case study of a potential low head hydro site in Taggerty, Victoria, Australia was completed and included in this thesis.

1.4 Literature review and background

For thousands of years man has been developing new ways of extracting and converting energy from water. Around 2000 years ago a mathematician from Alexandria, Greece named Hero developed the first reaction turbine called "aeolipile" driven by steam, which worked on a basic reaction principle or Newton's third law of motion as known to us at present. Jet propulsion is another practical application of Newton's third law of motion (for every action, there is an equal and opposite reaction). This is a method of propulsion that uses the reaction produced by the acceleration of a fluid through an orifice or nozzle to move an object forward. This is, in itself, nothing new or revolutionary. Mother Nature has some amazing creatures, which use this principle for their day-to-day activities; one example of this is the squid, which propels itself through the water by a type of jet propulsion. It takes water into its body, and then, using its muscles, adds energy to the water and expels it in the form of a jet to force itself forward through the water.

Man has tried developing mechanical machines working on this reaction principle for centuries, but it is only in the last two centuries that successful applications for power generation and aerospace technology were developed. These developments in the technology came with two working principles for water turbines i.e. impulse and reaction principle (Daugherty, 1954, Duncan, 1970). Most of the conventional and modern day hydro turbines work on impulse or a combination of reaction and impulse principle. The turbine that was based on pure reaction principle was forgotten for a long time and was considered obsolete. In late 17^{th} century Barker an English engineer reinvented and modified the Hero's turbine design to work with potential energy of water stored in dam or reservoir, which is called as Barker's mill (Daugherty, 1954, Duncan, 1970). Since then various inventors have developed new water turbines, which can produce large amount of energy, at different water heads, at high efficiencies. As said the water turbine are classified into two main categories according to their working principles, Impulse and Reaction.

1.4.1 Impulse Turbine

An impulse turbine consists of a rotor mounted on a shaft free to rotate on a set of bearings. The outer rims of the rotor carries a set of curve blades, a jet of fluid issuing from a nozzle impinges on the blades of the rotor. The change in momentum of the fluid when the fluid hits the blades causing the wheel to turn is defined as an impulse force (Daugherty, 1954). The process described converts the kinetic energy from the fluid to mechanical work in the shaft producing power in the process. The Pelton wheel is a good illustration of the above as shown below.

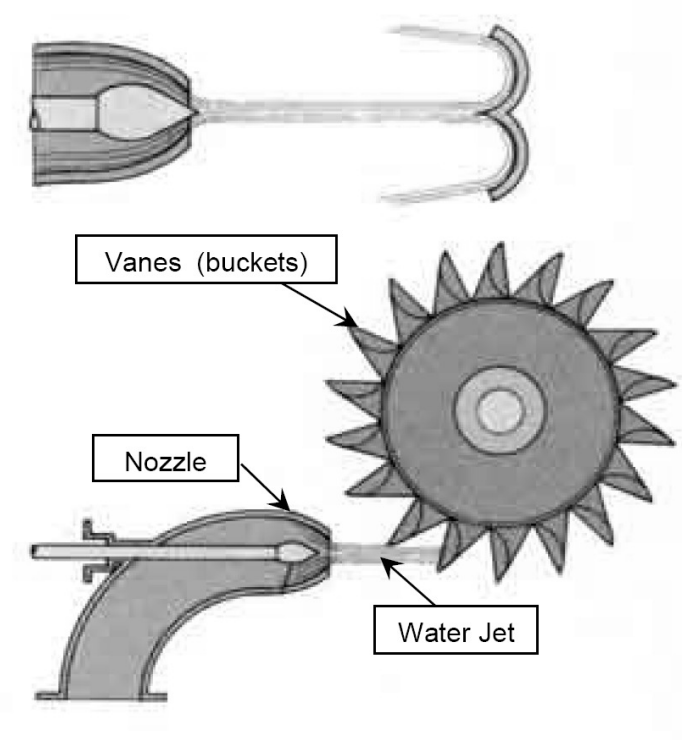

Figure 1.2 Pelton wheel (Ref: Water Wheel Factory, 2009, http://www.waterwheelfactory.com/Pelton.htm)

Generally, impulse turbines are restricted to low volume high heads applications with low specific speeds. As said earlier the specific speed of a turbine is defined as the speed of an ideal, geometrically similar turbine, which yields unit power while supplied with unit head. In contrast, special designs such as the Turgo or crossflow turbines are examples of relatively high specific speed impulse units.

1.4.2 Reaction turbines

In reaction turbines, the fluid fills all the runner passages completely where the impeller is located, and any head change or pressure drop will occur in the impeller (Daugherty, 1954). The flow shows opposite characteristics to a pump; entering into the larger end of a passage and exiting from a smaller gap after releasing all the energy converted through the drop of pressure in the rotating wheel (White, 1986). Barker was one of the earlier pioneers of the outward-flow reaction turbine. In the Barker's mill, the fluid enters the center of the rotor via an inlet at the top. A reaction force is created when the fluid exits the nozzle tangentially causing a movement in reverse direction and making rotor to rotate in a defined axis where the rotation mechanism can produce power (Daugherty, 1954). The characteristics mentioned above are widely used nowadays as a garden sprinkler.

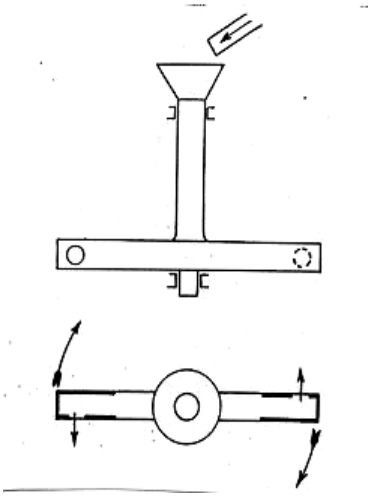

Figure 1.3 Principle of Barker's Mill (Wilson, 1974)

One of the first well-designed in-ward flow pure reaction turbines was built in 1949 by the hydraulic engineer James B. Francis as shown in Figure 1.4. Consequently, all in-ward flow turbines are now known as Francis turbines. A recent innovation has been the improvement on the runner, which resulted in a mixed-flow turbine, still termed a Francis turbine. In this runner, the flow lines have both radial and axial components. A pure axial flow turbine can be called as propeller type or Kaplan turbine as shown in Figure 1.5. The blades of the Kaplan can be adjusted or fixed for appropriate loads (Daugherty, 1954). Francis turbines have adjustable vanes (wicket gates) so as to reduce

exit velocity and create less vibration and bustle. The Kaplan turbine while slightly different in some aspects also has adjustable blades, which can be adjusted even during operation of the machine through gearing (Duncan, 1970). Even though it is more complex than the Francis Turbine, it is known to be more efficient for part loading at low power settings.

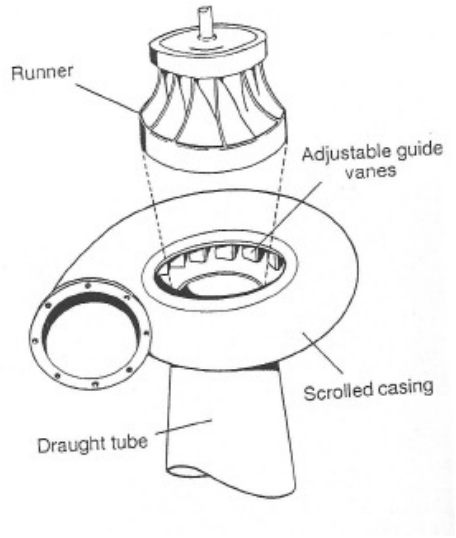

Figure 1.4 Francis Turbine (Harvey, 2005)

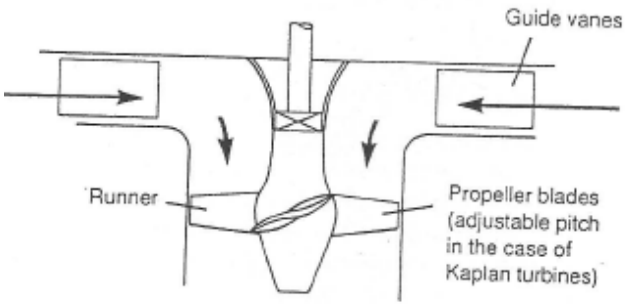

Figure 1.5 Kaplan Turbine (Harvey, 2005)

1.4.3 Comparison of impulse and reaction turbine applicability to high and low head

The reaction turbine utilizes the pressure (head) of the supply water to produce mechanical energy. The water pressure decreases as it moves through the turbine, while producing mechanical energy. This means a reaction turbine utilises hydrostatic head for energy conversation. This characteristic of the reaction turbine makes it suitable for a wide range of heads from very low to medium.

The impulse turbine utilizes the kinetic energy contained in the water jet that hits the turbine blades to produce mechanical energy. The velocity of the water jet is directly proportional change to the water pressure (head). At low head the jet velocity is also low, this means the turbine will not rotate at high speed. The impulse turbine uses the dynamic water head for producing mechanical power. This makes the impulse turbine more suitable for high head applications.

1.4.4 Simple reaction water turbine: Barker's Mill turbine

The earliest ever historically recorded outward-flow turbine is said to be discovered almost 2000 years ago during the first century AD by Hero of Alexandria (Shepherd, 1956). As shown in Figure 1.6 Hero's turbine consists of a hollow metal sphere with nozzles pointing in opposite direction tangentially to the sphere along the same axis. A sealed boiler generates the steam with two tubes connected to both the sphere and the boiler. This will cause the steam to flow into the sphere and coming out of the nozzle therefore resulting in a rotation of the. While the turbine didn't produce power, he demonstrated that steam power could be used to operate machinery. An illustration is shown below.

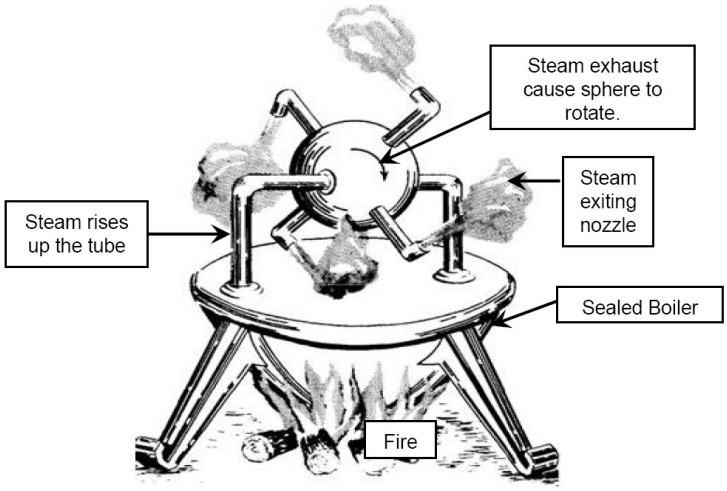

Figure 1.6 Hero's turbine (Shepherd, 1956)

The simple reaction turbine was reinvented by Dr Robert Barker around 1740 and is termed Barker's Mill. The characteristics were similar to Hero's except that the source was water instead of steam. The early design as shown in Figure 1.3 shows the entry of

source of energy came from a tube fed into the top of the turbine causing the rotor to rotate (Wilson, 1974). Further improvements were made by M 1'Abbe' Pupil around 1775, which modified the entry point of the fluid switching from top to bottom entry. Unlike the earlier design when all the loads have to bear by the thrust bearings supporting the moving parts, this innovation resulted in the load of the head being in the opposite direction to the load of moving parts of the turbine as the rising pressure from below counters this load thus acting like a cushion (see Figure 1.7).

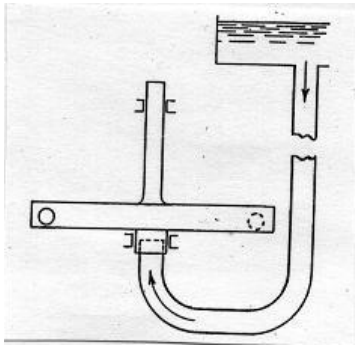

Figure 1.7 Pupil's Turbine (Wilson, 1974)

In 1832 James Whiteland suggested some improvements to Barker's mill (Whiteland, 1832). By 1839, James Whitlaw invented the "Scotch Mill" which also had relatively similar characteristics to the Barker's mill with the exception of the nozzle arm. Whitlaw redesigned the arm making it curve, therefore creating a higher exit velocity, believing that it increases the efficiency of the turbine (Wilson, 1974).

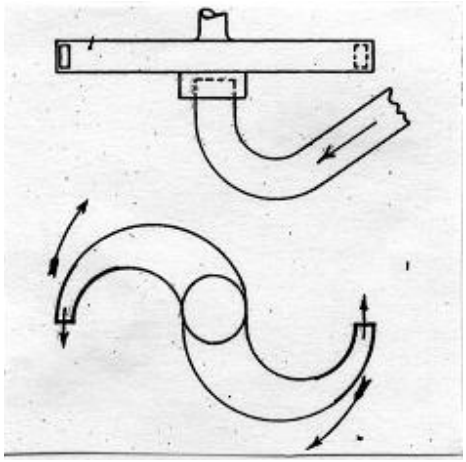

Figure 1.8 Whitlaw's Mill (Wilson, 1974)

Since then, better and more efficient turbines such as Francis, Fourneyron and Thomson have been invented. In present times, Barker's mill is deemed to be obsolete and not economically viable to be used any more (Duncan, 1970).

Most recently Akbarzadeh reviewed this obsolete Hero's turbine design in his paper name parametric analysis of the simple reaction water turbine (Akbarzadeh, 2001), this analysis showed that to large extent the simple reaction water turbine is misunderstood. In his paper Akbarzadeh have identified major geometrical and operational parameters and has developed governing equation for the ideal case of zero friction loss using principles of conservation of mass, momentum and energy. Further, these governing equations are expressed in a non-dimensional form. It is shown that the maximum torque produced by the machine is for the case when the turbine is stationary. At this point, the net output power is zero. As the load torque is decreased, the turbine starts rotating and power is produced. Furthermore, due to a centrifugal pumping effect, the mass flow rate of water through the turbine increases during acceleration. Further decrease in the load torque is accompanied by increase in speed, output power, water mass flow rate and efficiency. It is shown that when the load torque is reduced towards half the value of the torque at the stationary condition, then water mass flow rate, speed and output power approach infinity for an ideal no-frictional loss case. Under this condition the efficiency of the machine approaches unity (Akbarzadeh, 2001). Two simple reaction turbine models were built by Akbarzadeh and some undergraduate students for final year project (Quek, 2001, Quek, 2003, Webb, 1999). These turbine rotors had water passage grove machined in a solid metal disk using a CNC machining process, Figure 1.9 shows a rotor with 400mm diameter and total exit nozzle area of 0.0003125m² tested by Quek (Quek, 2003). The rotor design used in previous research investigations is very expensive and complicated to manufacture, it requires very high skills and specialised machinery. The experimental investigations of these turbine models conducted by Quek and Akbarzadeh (Quek, 2003) revealed a low turbine efficiency of about 45% at head of about 10m to 25m. The expensive machining and the low efficiency showed that these current simple reaction turbine designs need to be made more efficient and cheaper if they are to be economic for use in low head micro-hydro application.

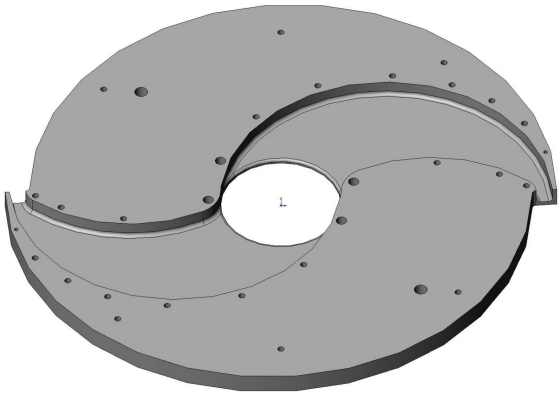

Figure 1.9 Bottom disk of simple reaction turbine with machined water passage grove (Quek, 2003)

1.4.5 Commercially available low head hydro machines

There are several turbine manufacturers who supply hydroelectric units for electricity generation from low head hydro sources. Most of the low head micro hydroelectric units available use impulse type turbines for energy conversion. From the early literature review it is clear that impulse turbine are suitable for high head small flow applications and their energy conversion efficiency drops drastically at low to very low head operation (Harvey, 2005, Waddell, 1999). Due to low cost impulse turbines like Pelton, Cross flow and Turgo are often used even at low to very low head sites. Pelton and Turgo turbine cannot be used when the available head is less then 3m, in this case a Cross flow turbine can convert that low head hydro energy within efficiency of about 60% (Harvey, 2005). As stated in micro-hydro design manual (Harvey, 2005) the unit cost of 2kW cross flow turbine turbines excluding alternator and drive is about US$1000-US$2000, this cost is low as compared to any other commercially available turbines, see Table 1.2.

Table 1.2 Table of cost of different turbines (Harvey, 2005)

Cost of turbines in units of US $1000 excluding alternator and drive						
Shaft power kW	Crossflow	Francis	Single-jet Pelton	Multi-jet Pelton	Turgo	Propeller
2	1 – 2	4 – 6	1 – 4	1 – 3	2 – 4	4 – 6
5	2 – 6	8 – 10	2 – 8	2 – 6	5 – 8	8 – 10
10	2 – 10	15 – 20	2 – 15	2 – 10	8 – 14	15 – 20
20	3 – 14	20 – 30	3 – 20	3 – 15	12 – 20	20 – 30
50	5 – 30	25 – 70	5 – 50	5 – 30	35 – 50	25 – 70
100	30 – 50	40 – 100	40 – 80	15 – 60	55 – 80	40 – 100
150	50 – 80	60 – 120	60 – 100	30 – 80	80 – 100	60 – 120

1.4.6 Savonius wind turbine

Savonius wind turbines are vertical-axis type wind turbine used for converting the power of the wind into mechanical power then to electrical using electric generator. This turbine was invented by the Finnish engineer Sigurd J. Savonius in 1922 (Oakey, 1993, Hau, 2006). Savonius turbines are one of the simplest wind turbines ever designed. Aerodynamically, they are drag type machines in which the differential drag causes the Savonius turbine to spin. Because they are drag-type devices, Savonius turbines extract much less of the wind's power than other similarly sized lift-type turbines. However, they are of extremely simple and cheap construction. As shown in Figure 1.10 when seen from top a two scoop Savonius turbine will look like "S" shape in cross section.

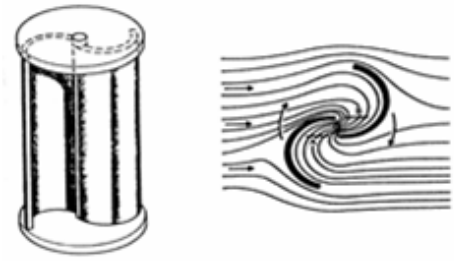

Figure 1.10 Schematic drawing of a two-scoop Savonius wind turbine (Oakey, 1993)

Some times these turbines are made by splitting oil barrels and offsetting them to create the scoops as shown in Figure 1.11. Savonius turbines design has been a motivation and influence for one of the simple reaction water turbine designs in this research.

Figure 1.11 Savonius wind turbine made from oil barrels
(http://www.worldofenergy.com.au/factsheet_wind/07_fact_wind_types.html)

1.5 Organisation of dissertation

The reminder of this dissertation is organised as follows, Chapter 2 introduces a complete study of simple reaction water turbine models; both ideal without fluid friction and practical with fluid friction. Non-dimensional analysis of the simple reaction water turbine governing equations is presented. A jet-interference model is presented with a concept design of a self-governing mechanism. Chapter 3 describes the design, manufacture and costing of the turbine prototypes. Chapter 4 presents the turbine test set-up with its instrumentation and experimental procedure used for prototype testing. Chapter 5 discusses the performance characteristics of turbine prototypes build and tested in this research. Chapter 6 presents case study for one of the surveyed potential site for installation of a micro-hydro power system in Victoria, Australia. Finally, Chapter 7 concludes the complete work highlighting the main contributions and future work required in this research.

1.6 Publications

1. Date A, Akbarzadeh A., 2005, 'Design Analysis and Investigation of a low head simple reaction water turbine', 43rd ANZSES conference, Dunedin, New Zealand.
2. Date A, Akbarzadeh A., 2007, 'Design and cost analysis of low head simple reaction hydro turbine for remote area power supply', International Conference on Renewable Energy for Sustainable Development in the Asia Pacific Region: WREN, Perth, Australia.
3. Date A, Akbarzadeh A., 2009, 'Design and cost analysis of low head simple reaction hydro turbine for remote area power supply', Renewable Energy, 34(2): p. 409-415.

Chapter 2 Theoretical analysis of simple reaction water turbine

2.1 Introduction

In this chapter, the simple reaction water turbine is analysed further following the current body of knowledge. For any hydro machine with even a smallest degree of reaction, the rotor must enclose the water in order to prevent the water from free expansion. A lawn-sprinkler is shown here as a simple reaction turbine in Figure 2.1, where water enters the rotor axially under high pressure or high head and leaves the rotor tangentially with high velocity with respect to the rotor. This type of simple reaction turbine utilises the static head available in the water and converts it to dynamic head within the converging nozzles, which are an integral part of the rotor. The change of momentum of the fluid in the nozzle gives rise to a reaction force which causes the rotor to rotate (Shepherd, 1956).

In an impulse turbine, the reaction force is experienced by the stationary nozzle, which converts the static head to dynamic head. The current body of knowledge on the analysis of a simple reaction turbine is not sufficient for any conclusive account of the performance of a simple reaction turbine; further analysis is required to successfully demonstrate the performance.

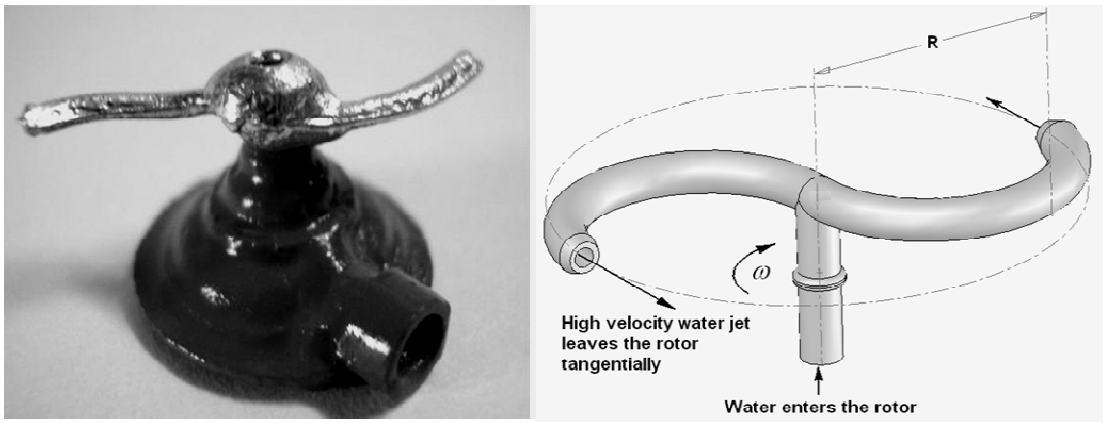

Figure 2.1 Lawn Sprinkler (Simple reaction turbine)

2.2 Analysis of a simple reaction water turbine for ideal situation

Following the work done by A. Akbarzadeh (Akbarzadeh, 2001) on parametric analysis of simple reaction water turbine, here attempts are made to provide governing equations for prediction of the performance of a simple reaction water turbine. These equations are then used for turbine design and performance analysis under specific conditions in the following chapters.

Let us assume that a total head of H (m) is available in a water reservoir and the aim is to convert the potential energy of water to useful work by the means of a simple reaction turbine as shown in Figure 2.2.

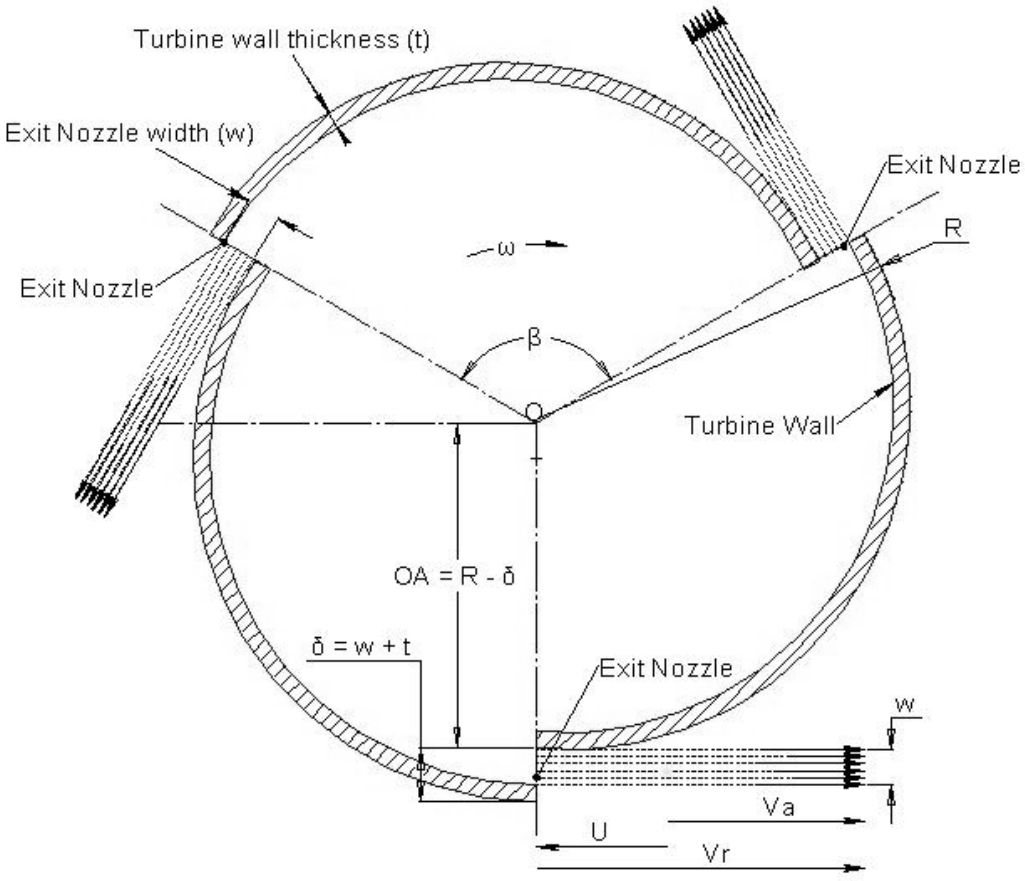

Figure 2.2 Velocity diagram of multiple exits simple reaction turbine rotor

Assume that losses related to flow of water from source, piping, rotor and nozzle are neglected. Mechanical losses such as windage losses due to rotation of the rotor and frictional losses in the bearings are also disregarded (Akbarzadeh, 2001, Date, 2005). The appropriate equations have been derived as follows,

Referring to Figure 2.2 and assuming water to be incompressible, we then have

$$U = R\omega \tag{2.1}$$

$$V_a = V_r - U \tag{2.2}$$

Here, U is the tangential velocity of the turbine in m/s, V_a is the absolute velocity of the water leaving the nozzle with respect to a stationary object in m/s and V_r is the relative velocity of the water leaving the nozzle with respect to the nozzle in m/s. Absolute velocity V_a is the component that determines the torque produced by the turbine.

In case of a simple reaction turbine, there are two components of pressures acting that govern the flow of water through the turbine. The main operating head is created due to physical difference between the water level in the reservoir and the position of the turbine. The secondary head is created due to angular speed of the turbine as discussed by A. Akbarzadeh (Akbarzadeh, 2001).

$$H_c = \frac{\omega^2 R^2}{2g} \tag{2.3}$$

Here, H_c is the centrifugal head in meters and is proportional to the angular speed of the turbine. Assuming ideal condition where there are no fluid frictional losses, the relative kinetic energy would be equal to sum of potential energy and energy due to centrifugal head (Akbarzadeh, 2001).

$$\frac{1}{2}\rho V_r^2 = \rho g(H + H_c) \tag{2.4}$$

So from equation 2.3 & 2.4, we can write the equation for ideal relative velocity as:

$$\therefore V_r = \sqrt{2gH + R^2\omega^2} \tag{2.5}$$

This would be the relative velocity at which water leaves the nozzle in any condition stationary or rotary. If the nozzle is stationary the centrifugal head component $\left(R^2\omega^2\right)$ would be zero as angular speed ω would be zero, and so relative velocity would be proportional to the square root of potential head only.

The mass flow rate $\dot{m}$ of water flowing through the turbine is given as a product of relative velocity of exit jet, the total exit nozzle area $A\ \left(m^2\right)$ of the turbine and density of water ρ in kg/m^3.

$$\therefore \dot{m} = \rho V_r A \qquad 2.6$$

Now substituting equation 2.5 in equation 2.6 we have;

$$\therefore \dot{m} = \rho A\sqrt{2gH + R^2\omega^2} \qquad 2.7$$

From equation 2.7 we can say that when the turbine is stationary, i.e. angular speed $\omega = 0$, the mass flow rate of water flowing through the turbine is at its minimum. The mass flow rate would increase with the increase in rotational speed of the turbine; this is due to the centrifugal pumping effect. This centrifugal pumping effect is mentioned qualitatively by J.R. Ainsworth Davis (Ainsworth, 1910). We would call the minimum flow value as $\dot{m}_s$ as in (Akbarzadeh, 2001).

$$\dot{m}_s = \rho A \times \sqrt{2gH} \qquad 2.8$$

Figure 2.3 shows the effect of centrifugal pumping on the mass flow rate as a function of rotational speeds under different operating heads. (These curves are for a turbine with a total exit area of A = 2 x 10^{-4} m^2 and R = 0.125m)

To estimate the torque *T* produced by the jets of water leaving the turbine we apply conservation of momentum principle which gives,

$$T = \dot{m} V_a R \qquad 2.9$$

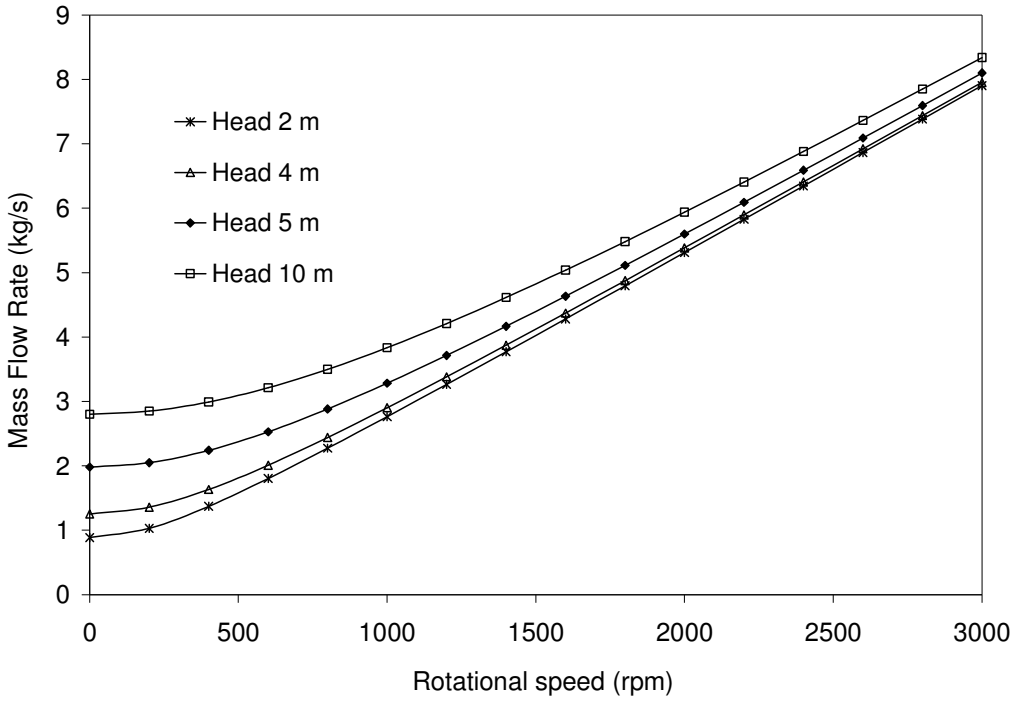

Figure 2.3 Variation of mass flow rate with rotational speed at different water heads

When the turbine is running free under no-load at its maximum possible rotational speed (i.e. when $V_r = U$ and therefore $V_a = 0$ from equations 2.1, 2.2 and 2.5), the torque produced by the turbine would be zero. By similar logic the maximum torque is produced when the turbine is stationary i.e. when $\omega = 0$ and the absolute velocity of the water jet is equal to the relative velocity of that water jet, i.e. $V_a = V_r$. Figure 2.4 shows the variation of turbine torque T with respect to the rotational speed for a turbine with mean effective radius of $R = 0.125m$ and the total exit area $A = 2 \times 10^{-4} m^2$. Here it can be seen the maximum torque $T_{\max} = \dot{m}_s * V_r * R$ corresponds to the stationary condition zero rotational speed. It can also be seen from Figure 2.4 that as the torque is reduced to approximately half the torque value at stationary condition the turbine experiences runaway speed. By reducing the torque the turbine speed is increases which causes the flow rate to increase due to centrifugal pumping. This increase in flow rate further helps to increase the speed of the tubine causing the turbine runaway.

$$T_{\max} = T_s = \dot{m}_s * V_r * R \qquad 2.10$$

Following the discussion on the relation between torque and rotational speed, it's now more convenient to define mechanical power $\dot{W}$ which is measured in Watts. In simple words, power can be defined as a product of torque and angular speed ω in radians per sec.

$$\dot{W} = T\omega \qquad 2.11$$

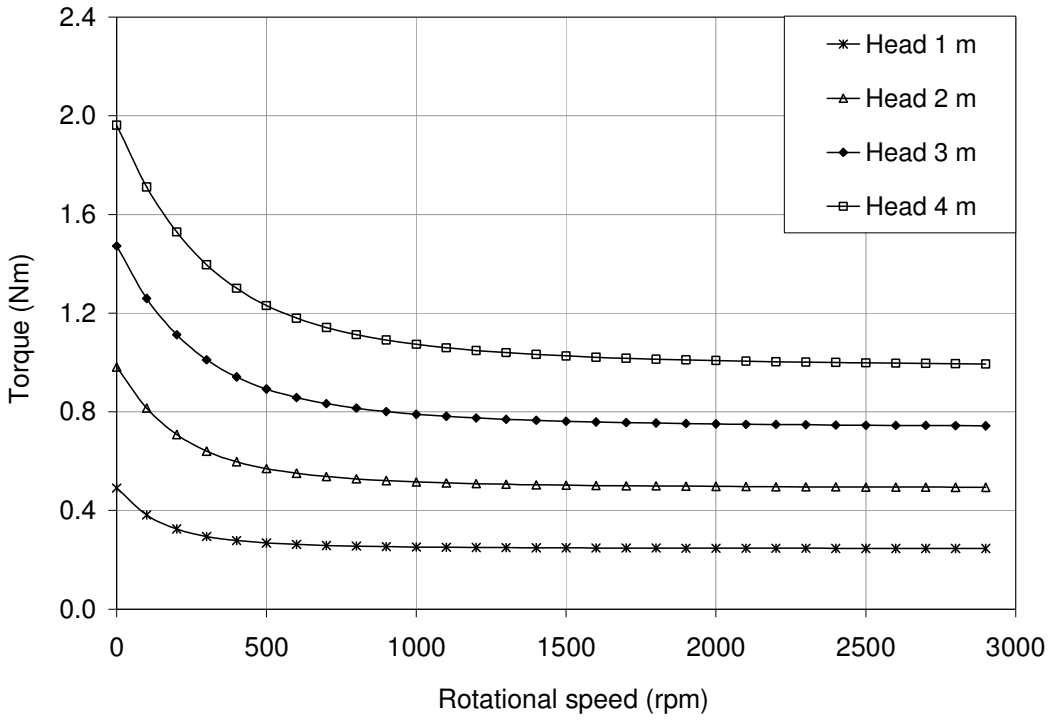

Figure 2.4 Variation of torque with rotational speed at different supply heads

After the power output is defined, an energy balance equation can be written for a simple reaction turbine assuming the ideal situation without any losses. Upon applying the conservation of energy principle to this situation, the total rate of potential energy $\dot{m}gH$ supplied to the turbine at any given rotational speed would be equal to the mechanical power output plus the kinetic energy lost as a result of absolute velocity of the water jet leaving the turbine $\frac{1}{2}\dot{m}V_a^2$. Therefore, we can write the energy balance equation as follows,

$$\dot{m}gH = \dot{W} + \frac{1}{2}\dot{m}V_a^2 \qquad 2.12$$

Therefore, mechanical power output $\dot{W}$ can be written as follows,

$$\dot{W} = \dot{m}gH - \frac{1}{2}\dot{m}V_a^2 \qquad 2.13$$

$$\therefore T\omega = \dot{m}gH - \frac{1}{2}\dot{m}V_a^2 \qquad 2.14$$

Now the efficiency η of the simple reaction turbine to convert the potential energy available in the water from the reservoir to mechanical power can be written as follows,

$$\eta = \frac{\dot{W}}{\dot{m}gH} \qquad 2.15$$

Following the basic analysis of an ideal simple reaction turbine, here efforts are made to do some further analysis on the simple reaction turbine for ideal operating conditions. It can be seen from equation 2.5 that as the angular speed ω of the turbine is increased, the relative velocity V_r approaches the nozzle velocity U, hence it can be seen from equations 2.1 and 2.2 that the absolute velocity V_a approaches zero. By consideration of equations 2.9 and 2.11 it can be seen that if V_a approaches zero the torque and power approach zero, for a fixed mass flow rate and such fixed flow rate situations are considered for a simple reaction steam turbine in Hsu and Leo (Leo, 1960). However, as has been shown in equation 2.7 and Figure 2.3 the centrifugal action is such as to make the mass flow rate increase with speed. The combined effect on the torque and the power of these two opposing trends of decreasing V_a and increasing mass flow rate is not apparent, and is explored subsequently in this chapter. Duncan *el al* (Duncan, 1970) states that when relative velocity V_r is equal to the velocity of the turbine $U = R\omega$ i.e. $V_r = R\omega$, then the power is zero, but do not explore the aforementioned combined effect on power of mass flow rate approaching infinity as V_r and $U = R\omega$ approaches each other at high speed. Similarly Daugherty (Daugherty, 1954) associates the runaway speed condition with zero torque due to the absolute velocity approaching zero without considering the opposing trend of mass flow rate approaching infinity. Duncan *el al* (Duncan, 1970) however discusses the tendency towards instability of the outward flow turbines. Instability in this context is the characteristic of having a self-enhancing runaway tendency if the torque is reduced. By contrast, inward flow turbines such as

Thomson and Francis are self governing to some extent in that a speeding up causes a build up of centrifugal pressure that tends to reduce the inward mass flow and hence the torque.

In the all the previous equations R, A and H are known geometrical parameters, ρ is the density of water and *g* is the acceleration due to gravity. Here the solutions of the above algebraic equations are offered based on the load torque *T*. By solving the equations from 2.1 to 2.15, the equations relating the seven unknowns (i.e., U, V_a, V_r, ω, $\dot{m}$, $\dot{W}$ and η) to known parameters of the system are developed. The solutions are offered in a non-dimensional form for ease of presentation and generalization of the results. From equation 2.5, 2.8 and 2.10 at $\omega = 0$ we can write the equation for stationary torque as follow: (when $\omega = 0$, $V_r = \sqrt{2gH}$)

$$T_s = 2\rho AgHR \qquad 2.16$$

Now non-dimensional parameters are defined as in (Akbarzadeh, 2001):

$$*T = \frac{T}{T_s} \qquad 2.17$$

$$*\dot{m} = \frac{\dot{m}}{\dot{m}_s} \qquad 2.18$$

$$*V_a = \frac{V_a}{\sqrt{2gH}} \qquad 2.19$$

$$*V_r = \frac{V_r}{\sqrt{2gH}} \qquad 2.20$$

$$*U = \frac{U}{\sqrt{2gH}} \qquad 2.21$$

$$*\omega = \frac{\omega}{\left(\frac{\sqrt{2gH}}{R}\right)} \qquad 2.22$$

$$*\dot{W} = \frac{\dot{W}}{\dot{m}_s (gH)} \qquad 2.23$$

The solutions to the equations 2.1, 2.2, 2.6, 2.9, 2.11, 2.13 and 2.15 can be obtained based on equations 2.9 and 2.16 and using the definitions introduced in equation 2.17 to 2.23.

Using $*T$ as the independent variable enables explicit expressions to be obtained for the other non-dimensional variables in equation 2.17 to 2.23.

$$*V_a = \sqrt{2*T - 1} \qquad 2.24$$

$$*V_r = \frac{*T}{\sqrt{2*T - 1}} \qquad 2.25$$

$$*U = \frac{1 - *T}{\sqrt{2*T - 1}} \qquad 2.26$$

$$*\dot{m} = \frac{*T}{\sqrt{2*T - 1}} \qquad 2.27$$

$$*\omega = \frac{1 - *T}{\sqrt{2*T - 1}} \qquad 2.28$$

$$*\dot{W} = \frac{2*T(1 - *T)}{\sqrt{2*T - 1}} \qquad 2.29$$

$$*\eta = 2(1 - *T) \qquad 2.30$$

The above equations can provide the complete characteristics of an idealized simple frictionless reaction water turbine working at any head.

The universal characteristics of this turbine are presented graphically in Figure 2.5 using the dimensionless torque $*T$ as the independent variable. Reducing the load torque applied to turbine from the stationary to runaway condition corresponds to moving from right to left on the horizontal axis. Figure 2.5 shows the graphical representation of

parameters $*V_a, *\omega, *\dot{m}, *\dot{W}$ and $*\eta$ as a function of non-dimensional torque $*T$. At the right hand end of the graph in Figure 2.5 the turbine is stationary and, as already discussed the mass flow rate through the turbine is at its least value when the turbine is not rotating. At this point to balance the torque from the reaction to the flow of water $\dot{m}_s$ through the turbine exit nozzles given by equation 2.8, a load torque equal to the value of stationary torque T_s given by equation 2.16 needs to be applied. At this point the value of non-dimensional torque $*T$ defined in equation 2.17 and is equal to one (i.e. $*T = 1$). Since the machine is stationary i.e. $*\omega = 0$, no power is produced i.e. $*\dot{W} = 0$ and efficiency $\eta = 0$. Further $*V_a$ is at its maximum i.e. $*V_a = 1$.

If the turbine is allowed to rotate by reducing the load torque, the mass flow rate would increase due to the centrifugal effect. As the turbine starts to rotate it starts to produce power, the efficiency increases and the absolute velocity of the exiting fluid decreases.

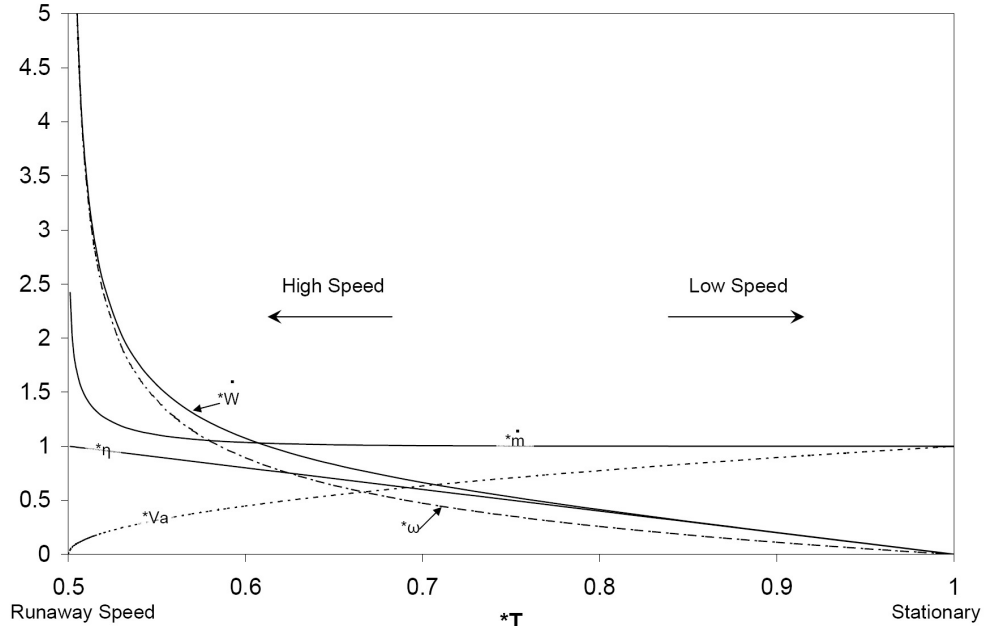

Figure 2.5 Graphical presentation of parameters $*V_a, *\omega, *\dot{m}, *\dot{W}$ and η as a function of $*T$

Apart from efficiency which is linear function of $*T$, the rate of change of the other functions $*\omega, *\dot{m}, *\dot{W}$ increase with decrease of $*T$. The rate of change (as evident

from equations 2.24 to 2.29 and shown in Figure 2.5) subsequently increases and approaches infinity as the $*T$ approaches the value of ½ the stationary torque. It can be seen that the most efficient case will be when no absolute kinetic energy is left in the exiting stream, i.e. $*V_a = 0$. In addition, this occurs when $*T = 1/2$, i.e. when the load torque is reduced to half the torque that was applied to hold the turbine stationary. At this point the mass flow rate through the turbine is infinite and the turbine is producing infinite power. In reality off course the windage, mechanical frictional losses and the fluid frictional losses would prevent the turbine from spinning at infinite angular speed and so the turbine would not produce infinite power at unit efficiency.

As seen from the analysis, the runaway speed of the turbine under consideration happens at $*T = 1/2$ and not at $T = 0$. This is contrary to the statements and the conclusions made by Daugherty (Daugherty, 1954) who associated the zero torque with the infinite speed condition. We can say that ½ $< *T \leq$ 1 and as a result $\rho AgHR < T \leq 2\rho AgHR$.

The nature of an ideal simple reaction turbine as shown in Figure 2.5 is illuminating, which shows how the efficiency increases with increase in angular speed. Figure 2.5 further shows how a simple reactions turbine pumps more water through the turbine as the angular speeds increases due to centrifugal pumping effect. This centrifugal pumping effect significantly increases the power production capacity of this turbine and presents an opportunity to develop a compact water turbine for low head hydro-power applications with low specific energy.

2.2.1 Simple reaction turbine and specific speed

Specific speeds are commonly used as a tool for comparison of the characteristics of similar hydraulic machines. Here this tool is applied to simple reaction water turbine, by using the formulation provided by Turton (Turton, 1995) for the specific speed of turbines, the following relation between specific speed and efficiency of a simple reaction turbine has been derived as discussed by Akbarzadeh (Akbarzadeh, 2001).

$$K_s = \frac{\omega\sqrt{Q}}{(gH)^{3/4}} \qquad 2.31$$

Where Q (m^3/s) is the volume flow rate of water given by,

$$Q = \frac{\dot{m}}{\rho} \tag{2.32}$$

Using equations 2.8, 2.18, 2.22, 2.27, 2.28 and 2.32 we get,

$$K_s = 2^{-3/4} \times \frac{\sqrt{A}}{R} \times \frac{\eta\sqrt{2-\eta}}{(1-\eta)^{3/4}} \tag{2.33}$$

The effect of geometry on the relation between specific speed and efficiency is expressed in terms of $\frac{\sqrt{A}}{R}$. However this can be changed to ratio of diameters i.e. $\frac{D}{d}$ where $D = 2R$ and d is the diameter of the nozzle. Defining an equivalent exit nozzle diameter d_e as,

$$d_e = \frac{2}{\sqrt{\Pi}} \times \sqrt{A} \tag{2.34}$$

Using the relation for the equivalent exit nozzle diameter from equation 2.34, we can re-write equation 2.33 as follows,

$$K_s = 2^{-3/4} \times \sqrt{\Pi} \times \frac{d_e}{D} \times \frac{\eta\sqrt{2-\eta}}{(1-\eta)^{3/4}} \tag{2.35}$$

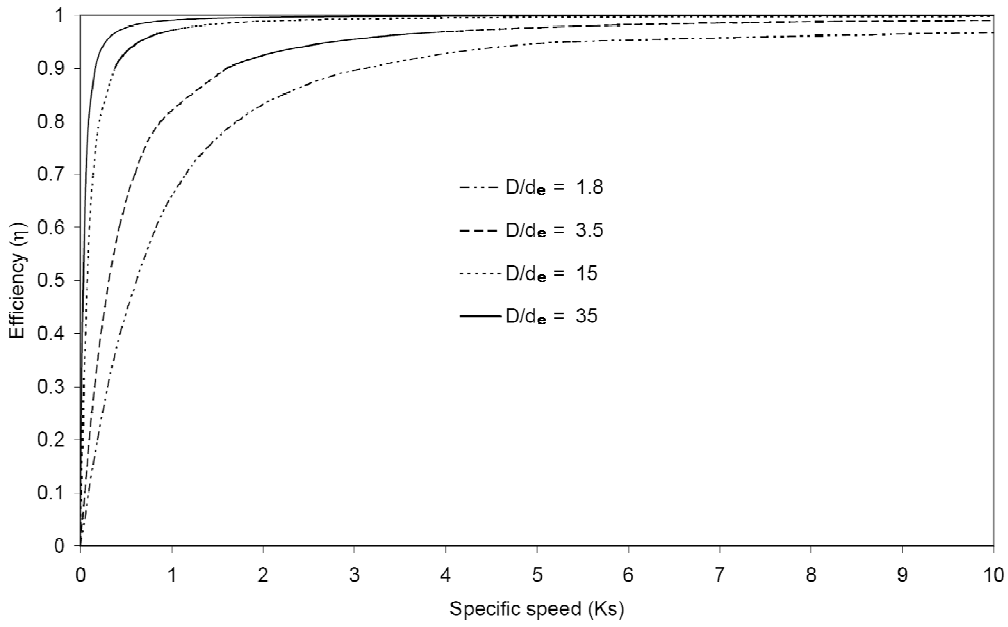

Figure 2.6 Variation of efficiency with specific speed for various diameter ratios

It is not possible to present η as a function of K_s in an explicit form (Akbarzadeh, 2001). However, the variation of η as a function of K_s is presented for several values of diameter ratio. It is seen in Figure 2.6 that a simple reaction turbine achieves higher efficiency for machines of higher diameter ratio $\left(\frac{D}{d_e}\right)$, i.e. for a given diameter D, a smaller nozzle exit area will improve efficiency. Since we relate capacity of the turbine to the nozzle exit area, we can then say that for the same specific speed and rotor diameter, machines of smaller capacities would be more efficient (Inclusion of the frictional effects may of course cause such a conclusion to be revised). It can be also seen from Figure 2.6 that efficiency of a simple reaction turbine improves as the specific speed K_s increases. Considering the definition of K_s in equation 2.44 this is equivalent to saying higher efficiencies are achieved at high rotational speeds, higher flow rates and lower heads. This can be considered as an important conclusion in relation to the characteristics of simple reaction water turbine.

2.3 Analysis of simple reaction water turbine considering losses and for practical operating condition

Now if we consider real operating condition there would be considerable amount of energy loss associated with the flow of water through the simple reaction water turbine (Date, 2009). Factor that would represent the fluid frictional energy loss associated with the fluid flow through the turbine has been introduced and defined in this section. This factor will be called the k-factor throughout this thesis.

For practical situation, the energy balance equation would be different from that in an ideal situation, as there would be some energy lost due to fluid friction mainly at the exit nozzles due to the high velocity of exiting water jets. So in this situation the energy balance equation 2.12 would be re-written as follows,

$$\dot{m}gH = \dot{W} + \frac{1}{2}\dot{m}V_a^2 + \frac{1}{2}\dot{m}kV_r^2 \qquad 2.36$$

Here the term $\frac{1}{2}\dot{m}kV_r^2$ represents the fluid frictional power loss associated with the flow of water through the turbine exit nozzles, and $\frac{1}{2}\dot{m}V_a^2$ represents the kinetic power loss associated with the absolute velocity of the exiting water jet, $\dot{W}$ represent the shaft power (mechanical power) produced by the turbine and the $\dot{m}gh$ represents the input hydro power supplied to the turbine.

Obviously, there would be a decrease in mechanical power produced if there is an increase in fluid frictional power loss i.e. if the *k*-factor increases, which is clear from the following equation,

$$\dot{W} = \dot{m}gH - \frac{1}{2}\dot{m}V_a^2 - \frac{1}{2}\dot{m}kV_r^2 \qquad 2.37$$

On using 2.1, 2.2, 2.5, 2.6, 2.9, 2.11 to solve the equations 2.37, one gets the equation for relative velocity in a real situation which is as follows,

$$\therefore V_r = \sqrt{\frac{1}{(1+k)}} \times \sqrt{2gH + R^2\omega^2} \qquad 2.38$$

In a situation where *k*-factor of the exit nozzle is known we can use this equation 2.38 to estimate the relative velocity independent of exit area.

Further, if we have experimental data from a performance test on a simple reaction water turbine, one would be able to use the following equation to estimate the *k*-factor of the simple reaction water turbine under test. Equation 2.38 has been re-arranged to obtain the following equation.

$$\therefore k = \frac{2gH + R^2\omega^2}{\left(\frac{\dot{m}}{\rho A}\right)^2} - 1 \qquad 2.39$$

Here $V_r = \frac{\dot{m}}{\rho A}$ is estimated from the experimentally measured value of mass flow rate or volume flow rate, measured total exit nozzle area and density of water. From the

above equations, we can say that if we keep the supply head constant then the *k*-factor will be a function of angular speed and the relative velocity.

2.3.1 Torque, mass flow and rotational speed characteristics

Figure 2.7 shows the variation of torque T and mass flow rate $\dot{m}$ with respect to the rotational speed for a turbine with rotor radius $R = 0.125m$, the total exit area $A = 2\times10^{-4} m^2$ and an assumed k-factor of 0.05. After considering, the fluid frictional losses associated with the flow of water through the turbine exit nozzles it can be seen from Figure 2.7 that the turbine will not experience runaway condition in real operation due to the power loss in the turbine.

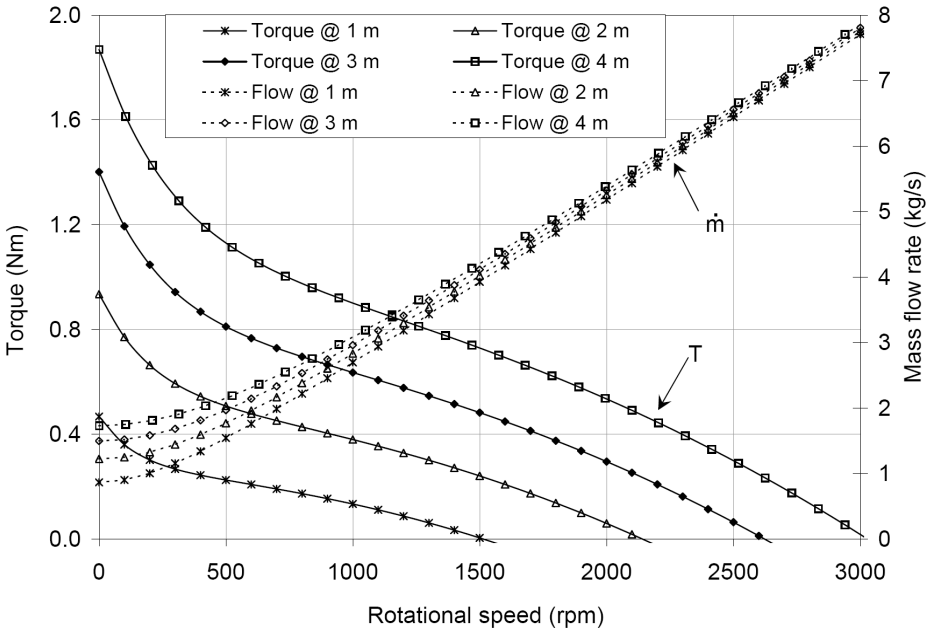

Figure 2.7 Variation of torque with rotational speed at different supply heads

Further, it can also be seen that as the load torque is decreased the angular speed of the turbine will increase causing the mass flow rate of water flowing through the turbine to increases but will not reach a value close to infinity. The variation of $\dot{m}$ with rotational speed is almost linear and the effect of supply head on mass flow rate vanishes at high rotational speeds. It is also seen that for a practical situation with fluid frictional loss the simple reaction turbine will never experience the runaway condition of infinite speed.

2.3.2 Power characteristics

The power curves shown in Figure 2.8 are theoretical predictions for a simple reaction water turbine with rotor radius of $R = 0.125m$, total nozzle exit area of $A = 2\times10^{-4}\,m^2$ and an assumed k-factor of 0.05. Figure 2.8 show that for a practical situation with losses the power produced by the turbine never reaches infinity. The power curves for a simple reaction turbine model can be experimentally estimated by initially allowing the simple reaction turbine to rotate at its maximum possible speed under no external load and at constant supply head while all the variables are recorded. Then gradually increase the load on the turbine in steps and record the variables for each step, while the supply head is kept constant. The point of maximum power shifts to higher speeds at higher heads.

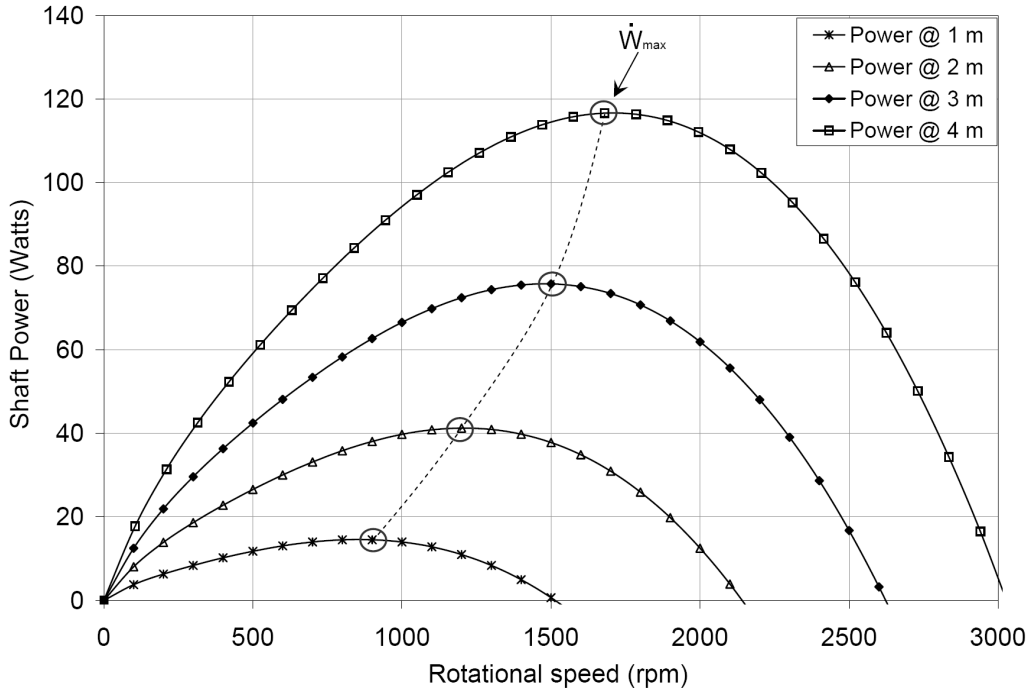

Figure 2.8 Variation of power with rotational speed at different supply heads

2.3.3 Effect of fluid friction on turbine efficiency characteristics

From the analysis of an ideal simple reaction turbine it was previously concluded that the faster the turbine runs the more efficient it will be. However, after the efficiency analysis of simple reaction turbine with fluid frictional losses is carried out and presented as in Figure 2.9 it is seen that the maximum efficiency depends on the value of k-factor.

Figure 2.9 shows the predicted efficiency curves for a turbine with a rotor diameter of 0.12m operating under a constant head of 5m for different values of k-factors. For example, it can be seen that with a k-factor of 0.1 the maximum turbine efficiency is 70%, where as if the k-factor was higher at a value of 0.15 then the efficiency will decrease to 65%.

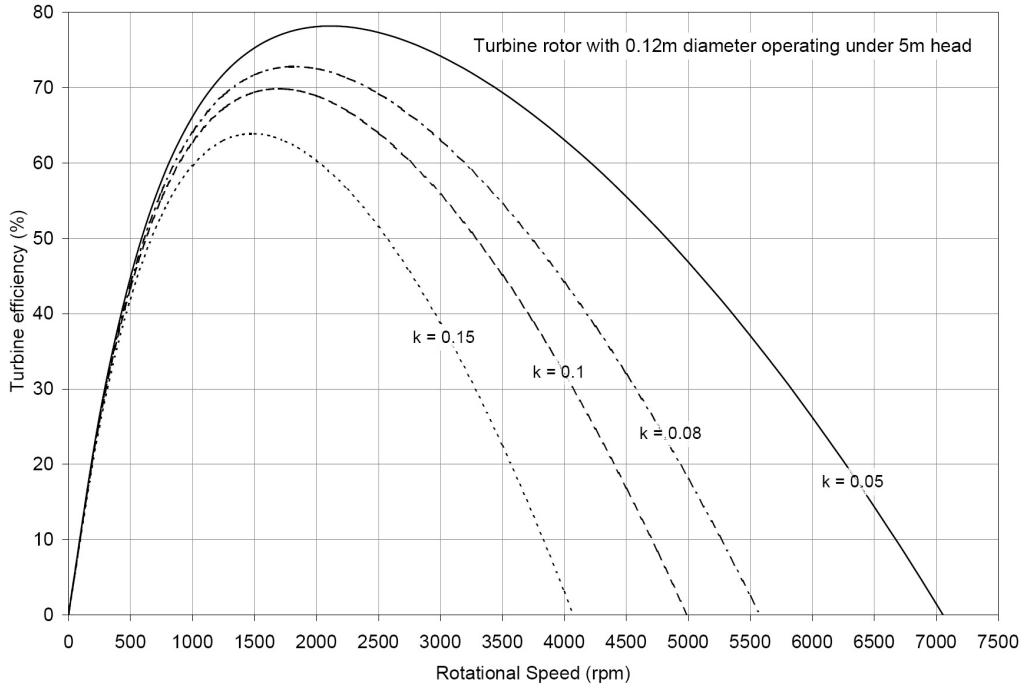

Figure 2.9 Effect of k-factor on turbine efficiency

2.4 Simple reaction turbine optimum rotor diameters

Here a new term "Optimum diameter" has been introduced; an optimum diameter is defined as the diameter corresponding to the maximum efficiency point for a given angular speed at a constant operating head. For a given rotational speed and constant operating head there is only one rotor diameter for which the turbine would have highest efficiency. Optimum diameter is independent of power; it only depends on head, rotational speed and k-factor as can be seen from equation 2.41.

Following is the derivation for optimum diameter equation. From equations 2.1, 2.2, 2.9, 2.11, 2.15 and 2.38 we get,

$$\eta = \frac{R\omega}{gH}\left[-R\omega + \sqrt{\frac{1}{1+k}} \times \sqrt{2gH + R^2\omega^2}\right] \qquad 2.40$$

Now differentiating equation 2.40 with respect to turbine radius R and equating it to zero for maximum efficiency condition $\frac{d\eta}{dR} = 0$, we get,

$$D_{opt} = 2R_{opt} = 2 \times \frac{\sqrt{gH}}{\omega} \times \sqrt{\left(\sqrt{\frac{1+k}{k}}\right) - 1} \qquad 2.41$$

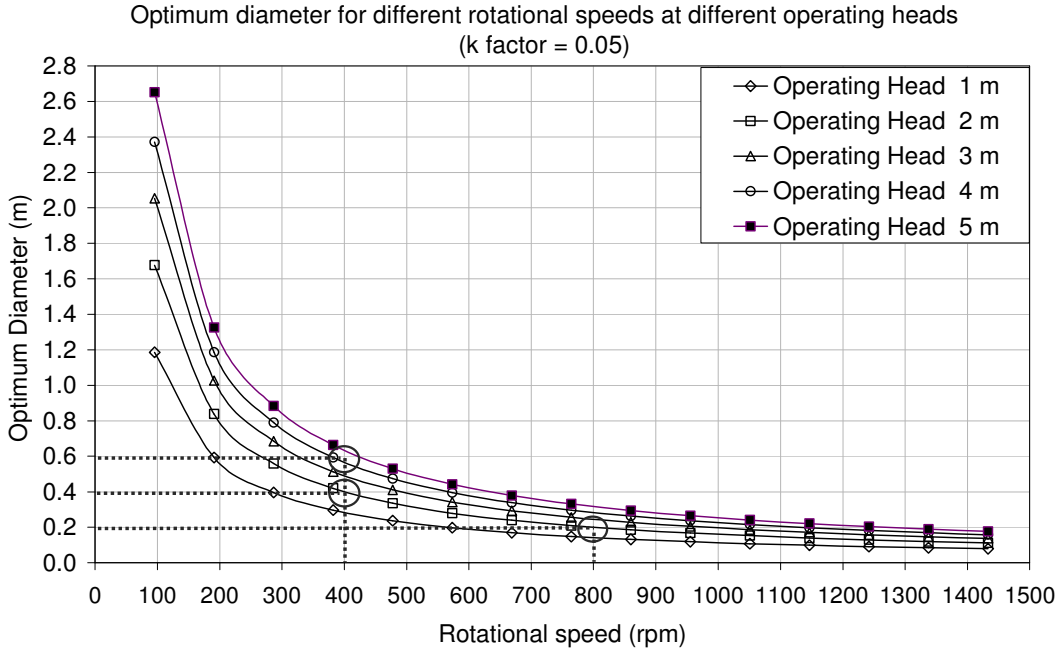

Figure 2.10 Optimum turbine diameter v/s rotational speed for various operating heads

Using equation 2.41 and an assumed k-factor of 0.05 the curves shown in Figure 2.10 have been estimated for a simple reaction turbine. It is observed that for the constant head, optimum turbine diameter decreases with increase in the rotational speed. Initially the rate of decrease in optimum turbine diameter is substantially high, but reduces with increase in rotational speed and eventually assumes an almost linear variation. It is interesting to note that the effect of the head on the optimum turbine diameter diminishes at higher speeds. For example, it is observed from Figure 2.10 that a simple reaction turbine operating at a constant head of 2m and rotating at 400 rpm has an optimum diameter of 0.4m, while at the same rotational speed at higher head of 4m the optimum diameter is 0.6m. While at a higher rotational speed such as 800 rpm the optimum

diameters for 2m and 4m heads are very close to each other. Similar to this Figure 2.10 also shows that beyond 800 rpm the variation of optimum diameter with rotational speed and head is diminishing for this situation of k-factor as 0.05. It is also very clear from Figure 2.10 that for operating head of 5m or less, to achieve rotational speed of 1500 rpm to produce electrical power at 50Hz AC using 4 pole AC motor the turbine diameter would have to be less than 0.2m. Smaller turbine diameter will limit the nozzle exit area and there by limit the power output capacity of such a turbine. Further, the jet interference phenomenon also limits the width of the exit nozzle, which has been discussed in detail in the following sections.

2.5 Phenomenon of jet-interference in a simple reaction turbine

For a simple reaction turbine, there is a certain rotational speed before which there is no interference between the turbine and the water jet, which can be called the non-interference speed. Beyond the non-interference rotational speed, the jet of water exiting will hit point C on the turbine as shown in Figure 2.11 and will try to push the turbine in the opposite direction to the current rotation, which causes a reduction in net torque produced and hence reducing the rotational speed of the turbine (Date, 2009). Therefore, the maximum rotational speed that a turbine can reach under a constant head and no load condition will decrease if there is any jet interference. This limits the width of the exit nozzle thereby limiting the power output capacity of the turbine.

With reference to Figure 2.11, we have $\delta = w + t$ and $\beta = \frac{2\Pi}{n}$, where δ represents the sum of nozzle exit width (w) and the turbine wall thickness (t), β is the angle between the two consecutive nozzles and n is the number of nozzles.

As shown in Figure 2.11 the jet interference will occur when the time required for the jet of water exiting from point A to reach point B equals the time required for point C on the turbine to reach point B. To delay this phenomenon the jet of water could be directed at an angle θ to the tangent. However, doing this will reduce the reaction torque experienced by the turbine. The equation for the non-interference speed can be derived for this condition when time CB' equals time AB' as follows,

$$t_{CB'} = t_{AB'} \tag{2.42}$$

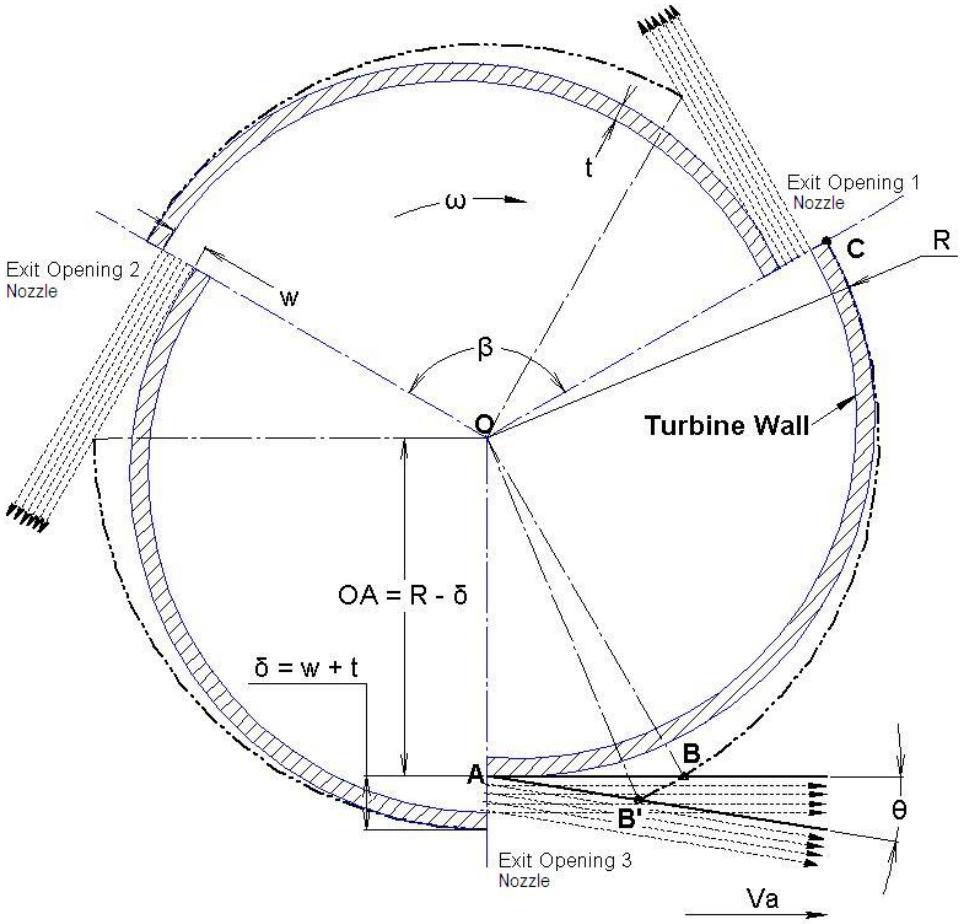

Figure 2.11 Interference of rotor and jet

$$\frac{\angle COB'}{\omega} = \frac{AB'}{V_a} \tag{2.43}$$

From geometry of the turbine we can write, (detail steps shown in Appendix F)

$$\angle COB' = \beta - \frac{\pi}{2} + \theta + ArcSin\left[(R-\delta)\times\frac{\sin\left(\frac{\pi}{2}+\theta\right)}{R}\right] \tag{2.44}$$

And

$$AB' = \frac{R}{\sin\left(\frac{\pi}{2}+\theta\right)}\times\sin\left(\frac{\pi}{2}-\theta-ArcSin\left[(R-\delta)\times\frac{\sin\left(\frac{\pi}{2}+\theta\right)}{R}\right]\right) \tag{2.45}$$

Now from equation 2.1, 2.2, 2.38, 2.43, 2.44 and 2.45 we get,

$$\therefore \omega_{\text{int}} = \sqrt{\frac{2 \cdot C_1 gH}{(1 - C_1 R^2)}} \qquad 2.46$$

$$Where \Rightarrow C_1 = \left(\frac{C}{(1 + CR\ )} \right)^2 \cdot \frac{1}{(1 + k)} \qquad 2.47$$

And,

$$Where \Rightarrow C = \frac{\beta - \frac{\pi}{2} + \theta + ArcSin\left[(R - \delta) \times \frac{\sin\left(\frac{\pi}{2} + \theta \right)}{R} \right]}{\frac{R}{\sin\left(\frac{\pi}{2} + \theta \right)} \times \sin\left(\frac{\pi}{2} - \theta - ArcSin\left[(R - \delta) \times \frac{\sin\left(\frac{\pi}{2} + \theta \right)}{R} \right] \right)} \qquad 2.48$$

It can be seen from the equation 2.46, 2.47 and 2.48 that there are number of physical parameters that determine the interference speed, for example if the value of β is increased the value of non- interference speed would increase and vice-versa. Similar to that the smaller the diameter of the turbine and the smaller the width of the exit nozzles the higher would be the non-interference speed.

Figure 2.12 presents the variation of jet-interference with changing exit nozzle width for a constant operating head of 2m. It can be seen from Figure 2.12 that the optimum rotor diameter at 1000 rpm is about 0.16m and how the exit nozzle width affects the jet-interference speed for a simple reaction turbine with a rotor diameter of 0.16m. A 0.16m diameter rotor with exit nozzle width of 6 mm will experience jet-interference at around 1040 rpm that is just above the rotational speed corresponding to the optimum diameter curve of 1000 rpm. Similarly, for exit nozzle widths of 8 mm, 10 mm and 12 mm the simple reaction turbine with a rotor diameter of 0.16m will experience jet-interference at three different speeds below 1000 rpm. Any point under the optimum diameter curve represents occurrence of jet-interference before the turbine can reach the maximum efficiency point for 2 m operating head and k-factor as 0.05.

To increase the power output capacity of a simple reaction turbine for a given rotor diameter and operating at a constant head, the nozzle exit area has to be increased. Increasing the exit nozzle width *w* for a constant nozzle length will increase the exit

nozzle area; thereby increasing the power output capacity for same diameter simple reaction turbine operating under constant hydrostatic head.

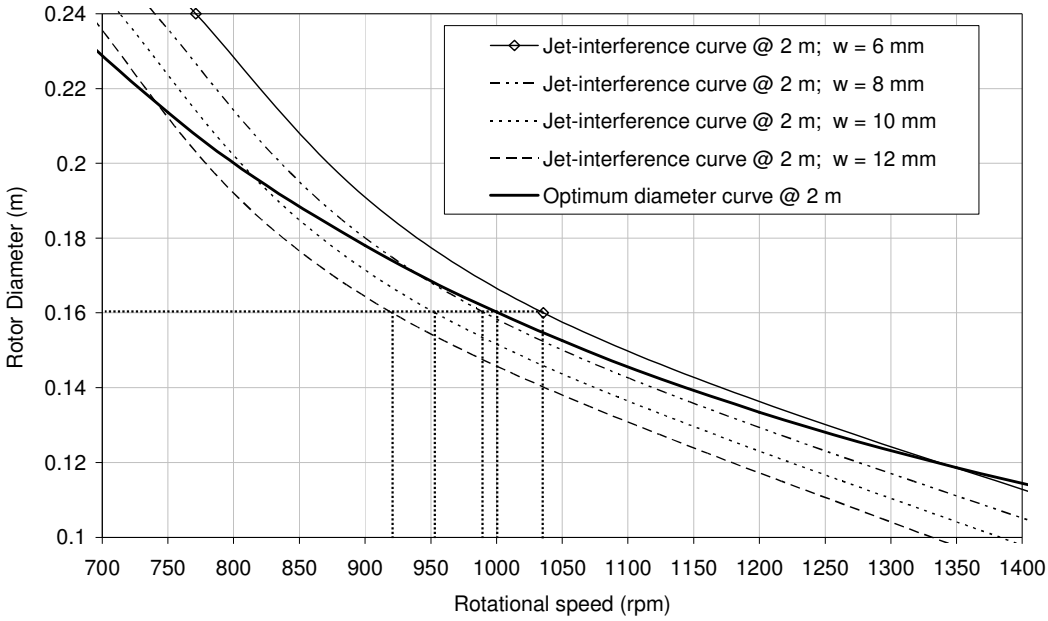

Figure 2.12 Variation of jet-interference with changing exit nozzle width

2.5.1 Concept of self governing simple reaction turbine

The hindrance of jet interference can be utilized to our benefit for preventing the run-away of the simple reaction turbine rotor at no-load condition which can some times be setback of this type of turbines (Date, 2009). By adding a simple speed damper at the ends of the nozzle as shown in Figure 2.13 and by controlling the size of the damper we can control the maximum run-away speed at no-load conditions. So as soon as the turbine runs at slightly higher speed then desired the jet will hit the dampers and slow down the turbine. With a speed damper in place the jet-interference will occur at a lower speed then that without a speed damper, this is explained by solving equation 2.43 for both the situations of with and without speed dampers. It can be seen from Figure 2.13 that $\angle C_1OB_2$ is smaller then $\angle COB'$ and distance AB_2 is larger then distance AB. Therefore, the time required for point C_1 to reach point B_2 will be less then the time required for point C to reach point B'. So when equation 2.43 is solved to calculate ω for both the situations the interference speed for situation with damper give lower speed value.

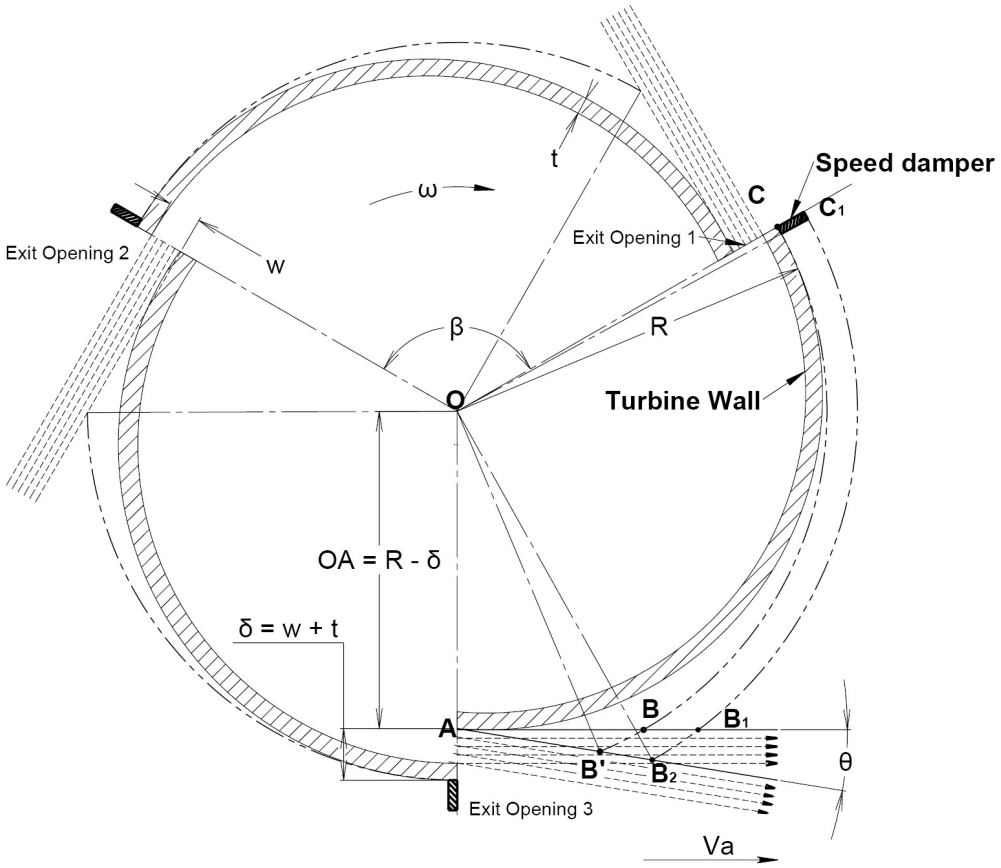

Figure 2.13 Concept drawing for self governing simple reaction turbine with speed dampers

2.6 Theoretical analysis of drag friction losses on the rotor

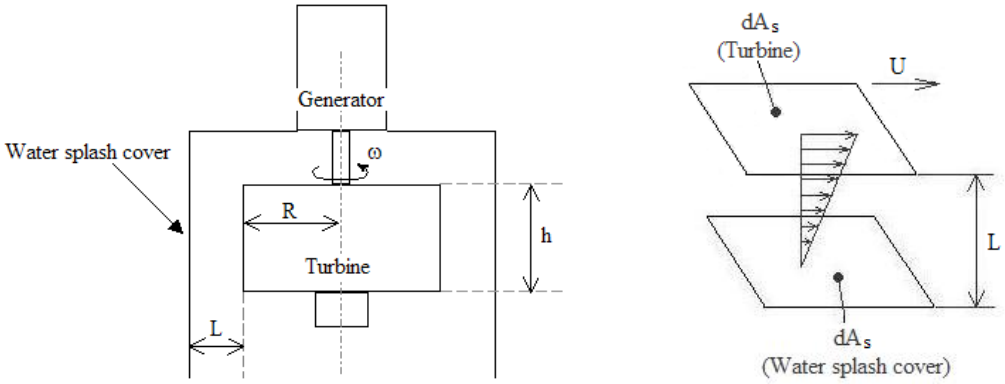

Figure 2.14 Velocity diagram to analyse rotor drag

Shear stress is defined as force per unit area $\frac{dF_d}{dA_s}$, surface area of the turbine $A_s = 2\pi Rh$. Shear strain is defined as ratio of displacement due to shear stress to the transverse L. In solid stress is proportional to strain, but in a fluid having laminar flow shear stress is proportional to the rate of change of strain (Sears, 1955). The strain is equal to $\frac{U\tau}{L}$ and its rate of change is $\frac{d}{d\tau}\frac{U\tau}{L} = \frac{U}{L}$.

$$\frac{dF_d}{dA_s} \alpha \frac{U}{L} \tag{2.49}$$

Viscosity of air μ_{air} (kg/m.s) is used as proportionality constant.

$$\frac{dF_d}{dA_s} = \mu_{air} \frac{U}{L} \tag{2.50}$$

Integration of above equation results in following

$$\int dF_d = \int \mu_{air} \frac{U}{L} dA_s \tag{2.51}$$

$$F_d = \mu_{air} \frac{U}{L} A_s \tag{2.52}$$

$$F_d = \frac{2\pi\mu_{air} R^2 \omega h}{L} \tag{2.53}$$

$$W_d = F_d R\omega \tag{2.54}$$

$$R_e = \frac{\rho UL}{\mu} = \frac{\rho R\omega L}{\mu} \tag{2.55}$$

$$R = \frac{R_e \mu}{\rho\omega L} \tag{2.56}$$

$$W_d = \frac{2\pi\rho R^4 \omega^3 h}{R_e} \tag{2.57}$$

Assuming coefficient of friction $f = \frac{2}{R_e}$ for laminar flow, and substituting in the above equation we get,

$$W_d = f\pi\rho R^4 \omega^3 h \tag{2.58}$$

The detail derivation of the above equation is discussed in the boundary layer theory by (Schlichting, 1955). For turbulent flow $f = 0.184(R_e)^{-0.2}$ (Incropera, 2002).

2.7 Summary

The analysis of simple reaction turbine for ideal situation revelled that the mass flow rate increases as the rotational speed of the turbine is increased. Further it is seen that the simple reaction turbine experiences runaway speeds when the load torque is reduced to half the maximum torque (i.e. torque at zero rotational speed). It is also seen that for ideal situation the simple reaction turbine will have maximum efficiency at half the maximum load torque.

The analysis of simple reaction turbine when considering losses and for practical operating condition showed similar mass flow rate and rotational speed characteristics. So the flow rate increases with increase in rotational speed. Here a k-factor is introduced that represents the fluid frictional energy loss associated with the fluid flow through the turbine. Equation to estimate the value of k-factor from experimental data has been derived and presented in this chapter. It is seen that if the supply head is kept constant, the *k*-factor depends on angular speed and the relative velocity. Further, it is seen that as the load torque is decreased the angular speed of the turbine will increase causing the mass flow rate of water flowing through the turbine to increases but will not reach a value close to infinity. The variation of $\dot{m}$ with rotational speed is almost linear and the effect of supply head on mass flow rate vanishes at high rotational speeds. It is also seen that for a practical situation with fluid frictional loss the simple reaction turbine will never experience the runaway condition of infinite speed. The point of maximum power shifts to higher speeds at higher heads. Further in this chapter the equation for optimum turbine diameter was derived and presented. Finally the phenomenon of jet-interference is discussed and a concept self-governing system is presented that uses the jet-interference for useful purpose.

Chapter 3 Design, manufacture and costing of simple reaction water turbine

3.1 Introduction

Following the theoretical analysis of simple reaction turbine conducted in previous chapter, here efforts are made to use that analysis to design and configure prototypes of simple reaction turbines. This chapter describes two new designs of simple reaction water turbines and their manufacturing methods. In case of the simple reaction water turbine the water enters into the turbine axially from an intake pipe attached to the bottom of the turbine through a rotary seal and exits tangentially through nozzles located on the outer periphery of the turbine. This chapter also describes the design for three different rotary seal arrangements, which can be used to prevent water leakage at the inlet without major frictional losses.

3.2 Simple reaction turbine

Here two different simple reaction turbine designs and their manufacture methods are proposed, which are later used to manufacture the turbine prototypes in this research. Emphasise is given on simple and low cost manufacturing while designing the turbine prototypes. The potential application of this turbine is more likely in remote and economically poor areas. Consequently the material is that is widely and easily available in most remote areas is selected for making a turbine prototype. Standard plumbing pipes and fittings of steel or plastic are easily available these days. Further advantages and limitations of these designs for potential use in low heads power generation systems are also discussed.

3.2.1 Design 1 - Cross pipe reaction water turbine

Cross pipe reaction water turbine is built from standard pipe fittings assembled as shown in as shown in Figure 3.1. The main component of this turbine is the cross pipe fitting which holds the other turbine parts in position, for this reason the turbine is named as “Cross Pipe Turbine” (CPT). Here the 90° pipe bends or pipe elbows helps direct the

water to leave at tangent to the turbine diameter. At the outer end of the elbow a solid stream nozzle is connected directly or through a reduction bush. This solid stream nozzle helps to produce a solid jet of water leaving the turbine. A solid stream water jet would produce a higher tangential reaction force (torque) then a normal jet.

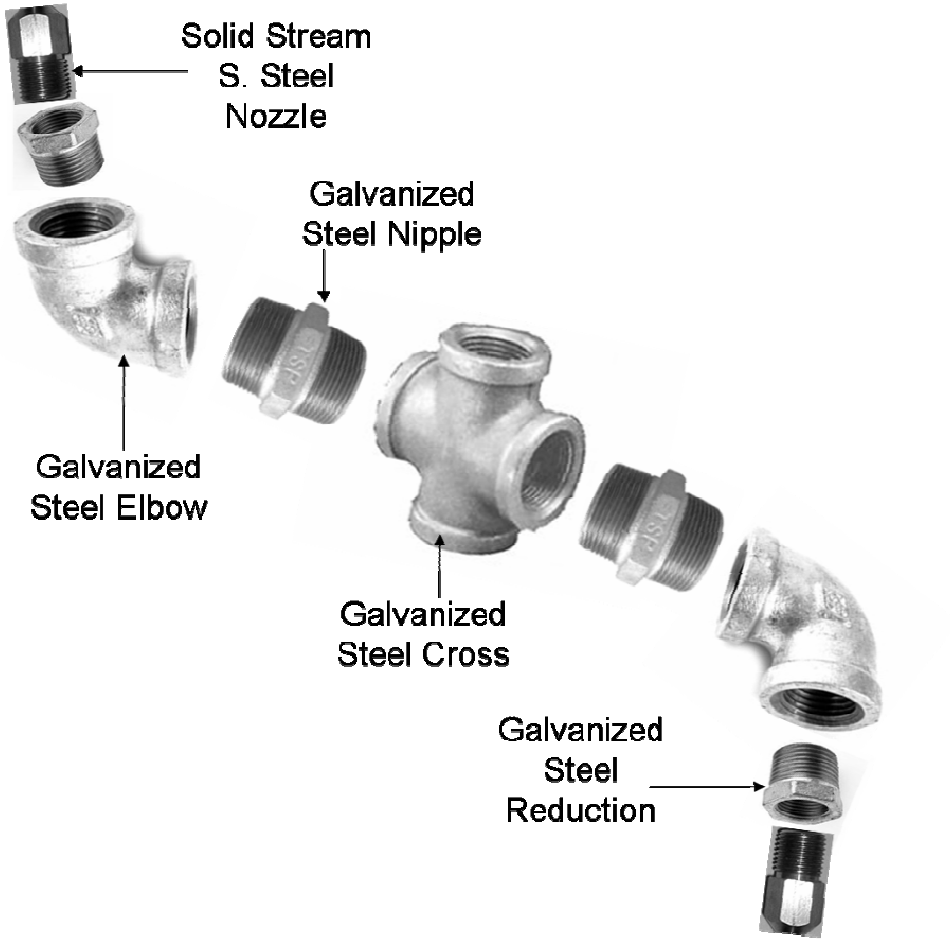

Figure 3.1 Cross pipe turbine parts

As shown in Figure 3.2 the CPT prototype is build from a 3" cross pipe at the center and the two arms made from 3" male adapter fittings. Each is fitted with 3" to 2" reduction elbow to guide the exit water jet in the tangential direction to the rotor diameter. Due to the fixed dimensions of the standard 3" pipe cross, the diameter of the turbine cannot be reduced below 400 mm even while using shortest possible standard pipe fittings. At the end of both the elbows, two solid stream nozzles with exit diameter of 15.9 mm (5/8") are attached through the reduction bush.

With this design it is very hard to build the turbine that has small turbine diameter and large nozzle exit areas. This is the desired attribute for low head water turbines as they have to handle large volume flow rates because of low specific energy available in the low head water sources. Further, it was clear from the experiments that a significant amount of energy is lost to overcome the air drag created due to the two separate arms of this turbine. The cross pipe reaction turbine prototype was tested and was found to be inefficient and slow rotating due to large diameter and low head combination. Detail turbine characteristics and experimental data analysis has been presented in Chapter 5. Due to constraints on turbine diameter presented by the dimensions of the standard pipe fittings and the turbine inefficiency, CPT design is not pursued further.

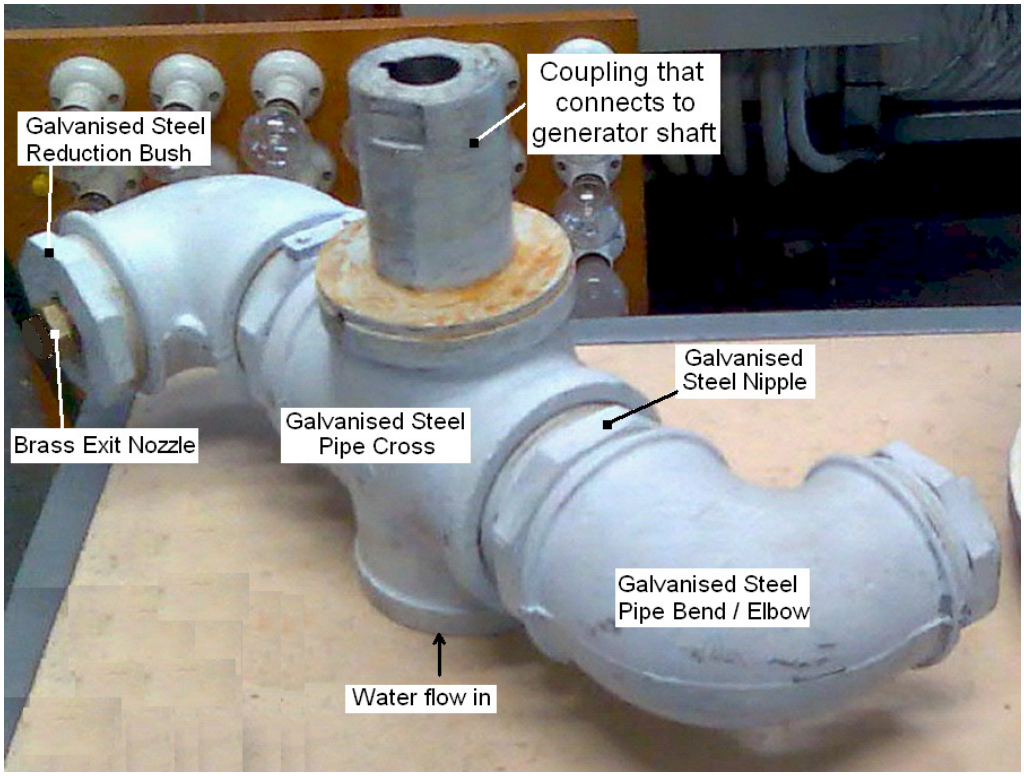

Figure 3.2 Cross pipe reaction turbine made from standard pipe fittings

3.2.2 Design 2 - Split reaction turbine design

Keeping in mind the main objectives of this research (i.e. low cost and manufacturing simplicity) another innovative simple reaction turbine design is developed and presented in this section. This new design has very simple geometry, it can be

manufactured using a very basic skill set and can be made from locally available materials (so low cost). The split reaction turbine can produce power from very low head hydro-sites (head range ≥0.3m and flow rate of ≥10 litres per second). This simple reaction turbine is named as "Split Reaction Turbine" after its method of manufacturing. Figure 3.3 shows the concept drawing of this type of turbine rotor. Water enters the split reaction water turbine axially under static pressure from the opening on bottom cover and leaves the split reaction turbine tangentially with high velocity from the exit nozzle openings located on the outer periphery of the turbine (see Figure 3.3).

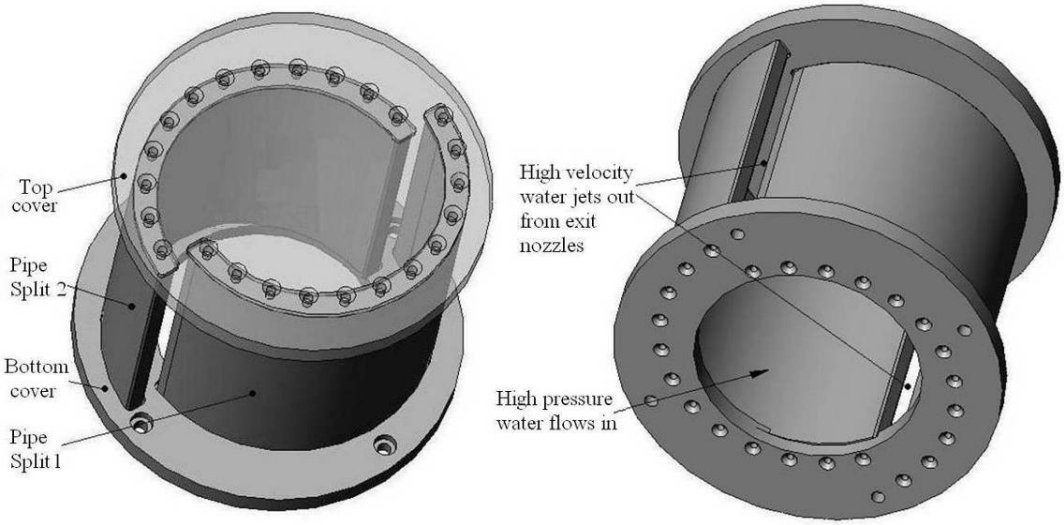

Figure 3.3 Split reaction turbine concept drawing

After the limitations presented by the CPT design, a more flexible turbine design was developed which would allow variation of the turbine diameter and exit nozzle area independent of each other. The idea of split pipe reaction turbine is influenced by "*Savonius wind rotor"* (Saha and Rajkumar, 2006, Menet, 2004, Oakey, 1993), the suggestions by James Whiteland (Whiteland, 1832), and also the need to develop an inexpensive low head simple water turbine. As shown in Figure 3.4, the split reaction turbine is manufactured using a simple fabrication method of splitting a pipe in two halves and attach these two halves to a top and bottom cover, with centers of the halves off-set to each other. The turbine exit nozzle width is determined by the center off-set distance and the pipe wall thickness. This method of fabricating is thought to be the simplest method for manufacturing a simple reaction turbine and hence the name "Split

Reaction Turbine". At several occasions in this thesis SRT is used as an acronym for "Split Reaction Turbine".

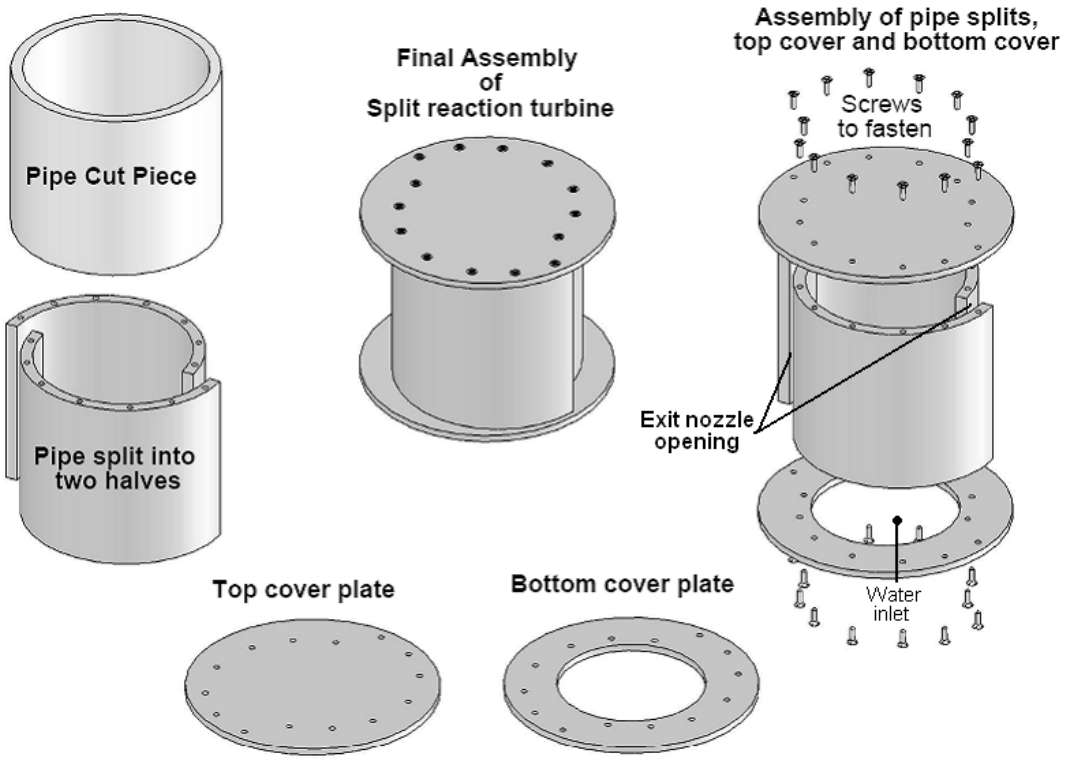

Figure 3.4 Steps in Building a Split Reaction Water Turbine

Figure 3.4 show the steps to build the split reaction turbine, here the piece of pipe is split into two halves, then these splits are drilled and tapped on the flat faces to hold the screws which would fasten the top and bottom cover to the splits. The top and bottom cover plates are made from same material as that of the pipe. The locating holes to attach the pipe splits are drilled on both the plates. In addition to this, the top plate will need some arrangement to connect the turbine to the electric generator (for example, provision to connect a flange coupling), the bottom plate has a hole at the center for the water to flow into the turbine and arrangement to connect the inlet port to guide the rotary seal which is connected to the stationary intake pipe.

It is advised to use plastic pipe and plastic cover and use screws to fasten the pipe splits and covers because of the following main advantages,

- Corrosion resistant: Plastic has good anti-corrosive properties

- Minimum or no balancing is required due to light weight material, simple facrication and ease to maintain symmetry.

Using steel pipe and steel covers for the turbine and weld them together to build the turbine would have following main disadvantages,

- Steel turbine is likely to rust, and would require some kind of rust proof coating to protect it.
- There might be some distortion in the turbine symmetry due to thermal stresses induced during welding and this would require the turbine to be balanced before it can be used.

In remote farming communities' animal feed trough are readily available, which these days are made from split plastic pipes, which could be used to build a split reaction turbine.

3.2.2.1 Building a Split Reaction Turbine

Split reaction turbine configuration depends upon following factors

- Available head
- Available flow rate or desired power output
- Desired rotational speed (i.e. operating speed of a electric generator)

As discussed in Chapter 2, for constant head operations the power output from the turbine will depend upon the amount of water flow through the turbine, and the amount of water that can flow through the turbine depend upon the total exit nozzle area. Further, the total exit nozzle area depends upon the number of exit nozzles, the width of each exit nozzle and the height of each exit nozzle.

Example Question: Design a split reaction turbine for operating head of 2.5m and for two different flow rates of 35 l/s (≈ 860W potential) and 45 l/s (≈ 1100W potential). Assume: k-factor of 0.1, angular speed of 100 rad/s (≈ 955 rpm), number of exit nozzles as two and turbine height of 0.15m (which is equal to nozzle height).

Solution: From equation 2.41 and the given and assumed data, the optimum turbine diameter is calculated to be 0.151m (151mm) for both the flow rates, as the optimum turbine diameter only dependents on head and angular speed.

Relative velocity of the water jet leaving the turbine exit nozzle is calculated as 9.81 m/s from equation 2.38, this value is same for both the flow rates as it only dependents on head, angular speed and k-factor (which are constant).

The total exit nozzle area for 35 l/s is calculated as 0.00357m² by dividing the flow rate (m³/s) by relative jet velocity (m/s). So the exit nozzle width of each nozzle is calculated as 0.0119m by dividing the total exit nozzle area by number of nozzles and by height of each nozzle. Similarly, the total exit nozzle area for 45 l/s is calculated to be 0.00459 m² and exit nozzle width of each nozzle as 0.0153m.

The turbine pipe size and material selection is done from the available standard pipe sizes. Here PVC pressure pipe class PN9 with a nominal diameter of 150 mm is selected from the Australian Standards AS/NZS 1477:2006 (Australian Standards, 2006). The mean outside diameter of this pipe is 160.5 mm and the mean wall thickness is 5.9 mm, so the inside diameter of the pipe is about 148.7 mm. The turbine built with this pipe would have a mean turbine diameter of $D_m = 160.5 - 5.9 = 154.6mm$ (here the $5.9mm$ is the wall thickness), which is very close to the calculated optimum diameter (151mm) for 2.5m head. The mean turbine diameter is the distance between the centers of both the exit nozzles as shown in Figure 3.5. This pipe is then cut to 0.15m length and split into two halves. Figure 3.5 shows the projections of pipe splits on the cover plate for the purpose of assembly. Here it is advised to drill clearance hole at the marked locations for the screws on the both the cover plates, where as the screw holes on the pipe splits should be tapped. This would help to achieve water tight joints between pipe splits and covers.

For the turbine with two exit nozzles the relation between the center off-set (x), the exit nozzle width (w) and the split pipe wall thickness (t) is given by,

$$x = w + t \qquad 3.1$$

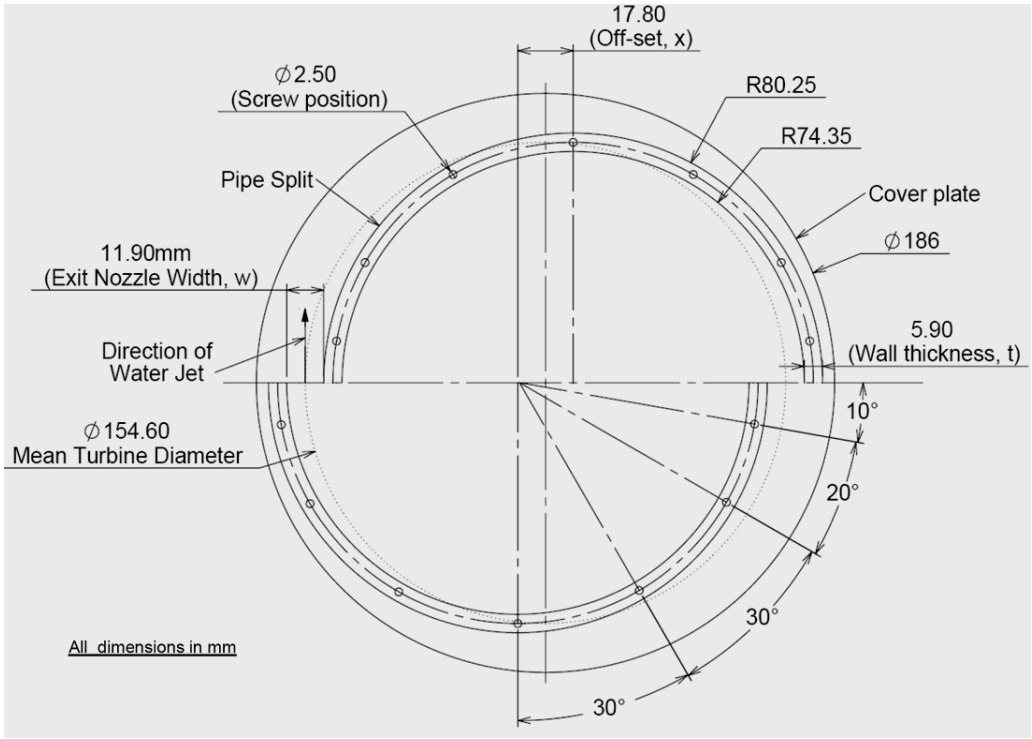

Figure 3.5 Projections of pipe splits over the cover plate

3.2.2.2 Manufacture of split reaction turbine – Prototype 1

First split reaction turbine prototype is built from cut piece of the plastic pipe with 250 mm nominal diameter, which was available at the RMIT University Workshops (scrap yard). As the supply head and flow rate could be controlled in laboratory operation of this turbine, it was not required to design this prototype for a specific operating head. The objective of building this prototype turbine was to do experimental performance analysis under different operating heads and estimate parameters like k-factor, power output and efficiency. Building of this turbine also confirmed the manufacturing simplicity of the SRT design.

Figure 3.6 shows the measured dimensions of the plastic pipe and the pipe splits with the mean wall thickness of 6.5mm. The pipe must be machined and squared to the desired turbine height (i.e. equal to the exit nozzle height) before it is split into two halves. In this research, the maximum possible turbine height that could accommodate in the turbine test rig was estimated to be 120 mm, so the exit nozzle height of the first prototype split reaction turbine limited to 120 mm. The pipe is split into two halves (semi

circular splits) (Note: use the saw blade with minimum thickness to prevent major loss of material on the splits while cutting). While splitting the pipe 1mm material is lost on each split.

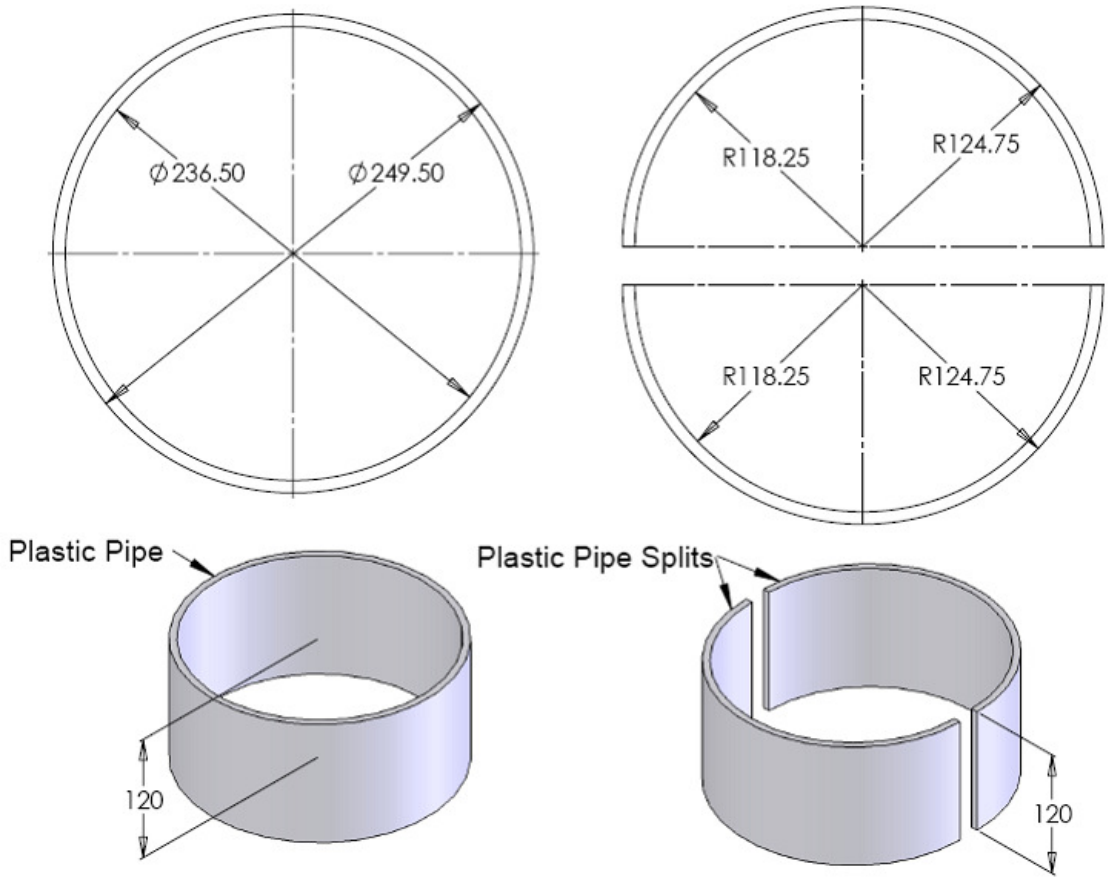

Figure 3.6 Plastic pipe and pipe splits *(All dimensions in mm)*

Once the pipe is split into two halves, in the next step the flat faces of the pipe splits are drilled and tapped symmetrically. The objectives of the fastening screws are to hold the pipe splits in position and to prevent water leakage from the interface of pipe split and the cover plates. The screw holes should be positioned symmetrically on both the faces of either pipe split. Figure 3.7 shows the number of holes and their positions used to build the split reaction turbine prototype 1. It is recommended to have the first screw position as close to the outer edge of the split, which in this case is shown at an angle of 10° (see Figure 3.7). The remaining holes there after could be located at a larger angular distance and should be positioned symmetrically. The number of screws that should be used to assemble the turbine depends upon how square the splits are machined

and how flat are the cover plates to which the splits would be fastened (Note: for not very flat cover plates use extra screws to achieve leak proof interface).

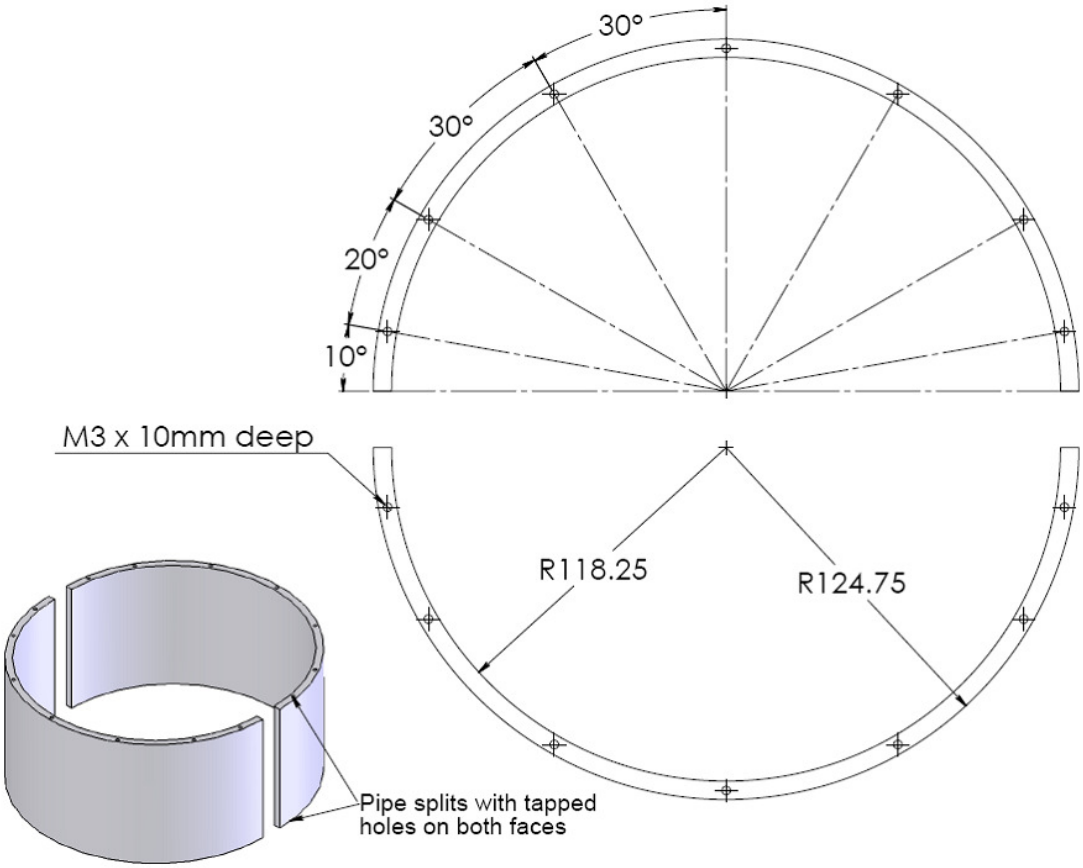

Figure 3.7 Machining of screw holes on pipe splits (All dimensions in mm)

Once the pipe splits are ready, the next step is to machine the top and bottom cover plates. Figure 3.8 shows the position of the pipe splits on the cover plates with a center off-set of 12.5 mm to get a 6 mm exit nozzle width ($x = w + t$). The outer diameter of the cover plate is machined to be at least equal to the sum of mean turbine diameter plus the pipe wall thickness plus the width of one exit nozzle ($D_c = D_m + t + w$). (Note: the mean turbine diameter is the distance between the middle of one exit nozzle to the middle of opposite exit nozzle). The cover plates should have clearance holes for the screws to fasten the pipe splits, this will help to achieve a leak proof connection interface between the pipe split and cover plates. The mechanical power is transmitted to the generator using a flange coupling, which is connected to the top cover plate of the

turbine. The water enter into the turbine through the inlet port connected to the bottom cover plate, inlet port also guides the rotary seal.

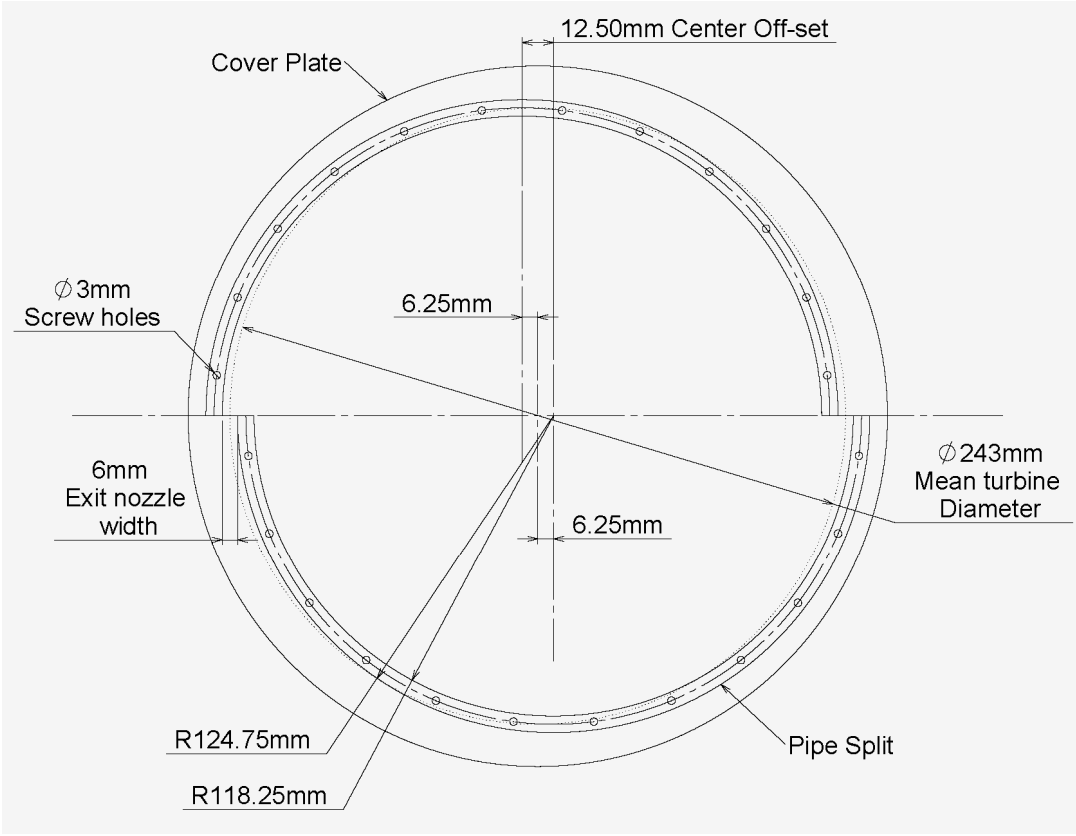

Figure 3.8 Split pipe position on the cover plates *(All dimensions in mm)*

Figure 3.9 shows a complete assembly of the split reaction turbine prototype 1 with two exit nozzles and mean turbine diameter of 243 mm. This prototype has a total exit nozzle area of 0.00144m² with two exit nozzles (each 120mm in height and 6mm wide). Figure 3.9 also shows the flange coupling attached to the top cover plate and the inlet port attached to the bottom cover plate. During the initial trials water leak was located at the interface of the pipe splits and the cover plates. Silicon gel was applied at the interface from inside and outside to prevent the water leak. This water leak is attributed to the poor fastening between the cover plates and pipe splits. The inlet port guides the rotary seal, which directs the water into the turbine while prevents leakage at the rotary joint. Different rotary seal arrangements that can be used with simple reaction water turbine have been discussed in the later part of this chapter.

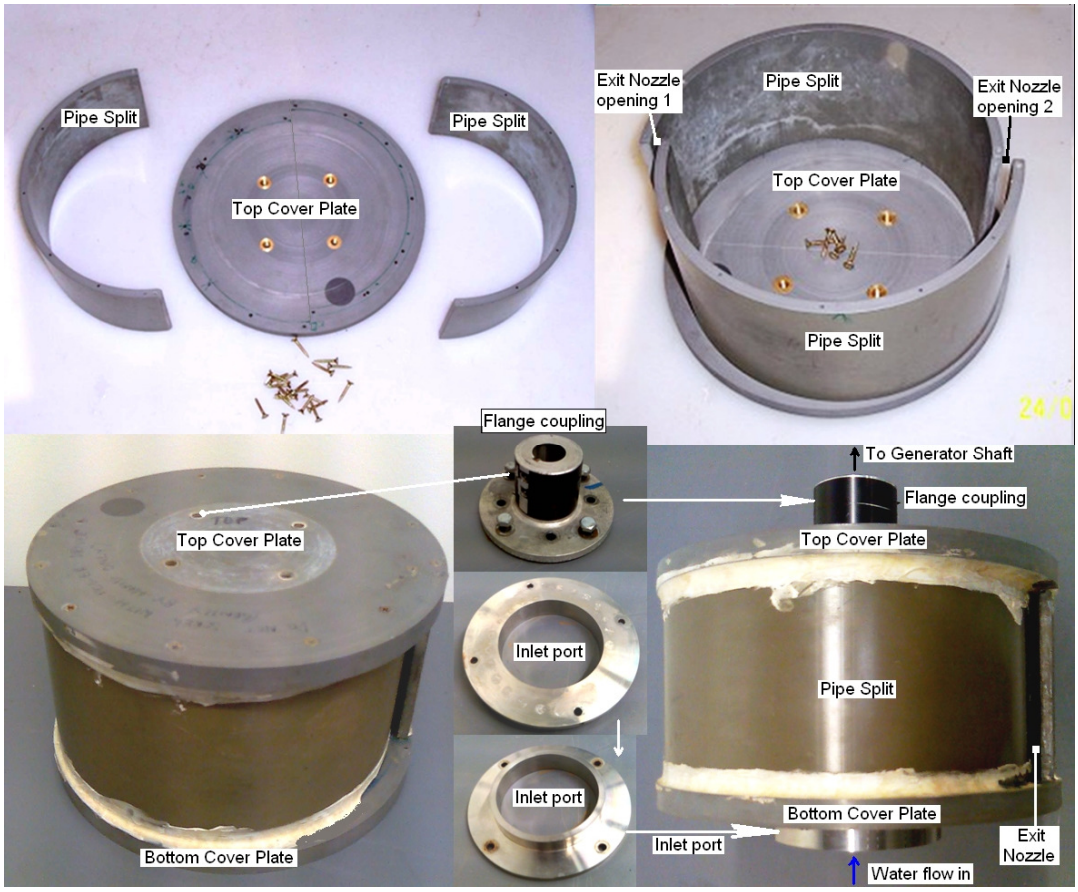

Figure 3.9 Split reaction turbine - Prototype 1

Table 3.1 shows the cost analysis for SRT prototype 1. The cost of plastic pipe is not considered as it was available from the RMIT workshop scrap yard. The retails pipe of such pipe is about AU$20.

Table 3.1 Split pipe turbine – Prototype 1 (can produce upto 1kW)

All amounts in AU$				
Item	Material cost	Labor hours $20 per hour	Labor Cost	Total
Plastic pipe OD 250mm x 120mm long	Free ($20)	N/A	N/A	N/A ($20)
Splitting the plastic pipe	-	2hrs	$40	$40
Plastic discs Ø300mm x 5mm thick (Qty 02)	$20	4 hr	$80	$100
Bolts / Screws (Qty 48)	$6	N.A.	N.A.	$6
Assembly and balancing	N.A.	2 hr	$40	$40
Total				$186 ($206)

3.2.2.3 Manufacture of split reaction turbine – Prototype 2

Figure 3.10 shows the pressures pipe coupling and its splits used to build the SRT prototype 2. This prototype was build to run at higher rotational speeds under low head, this was achieved by reducing the mean turbine diameter.

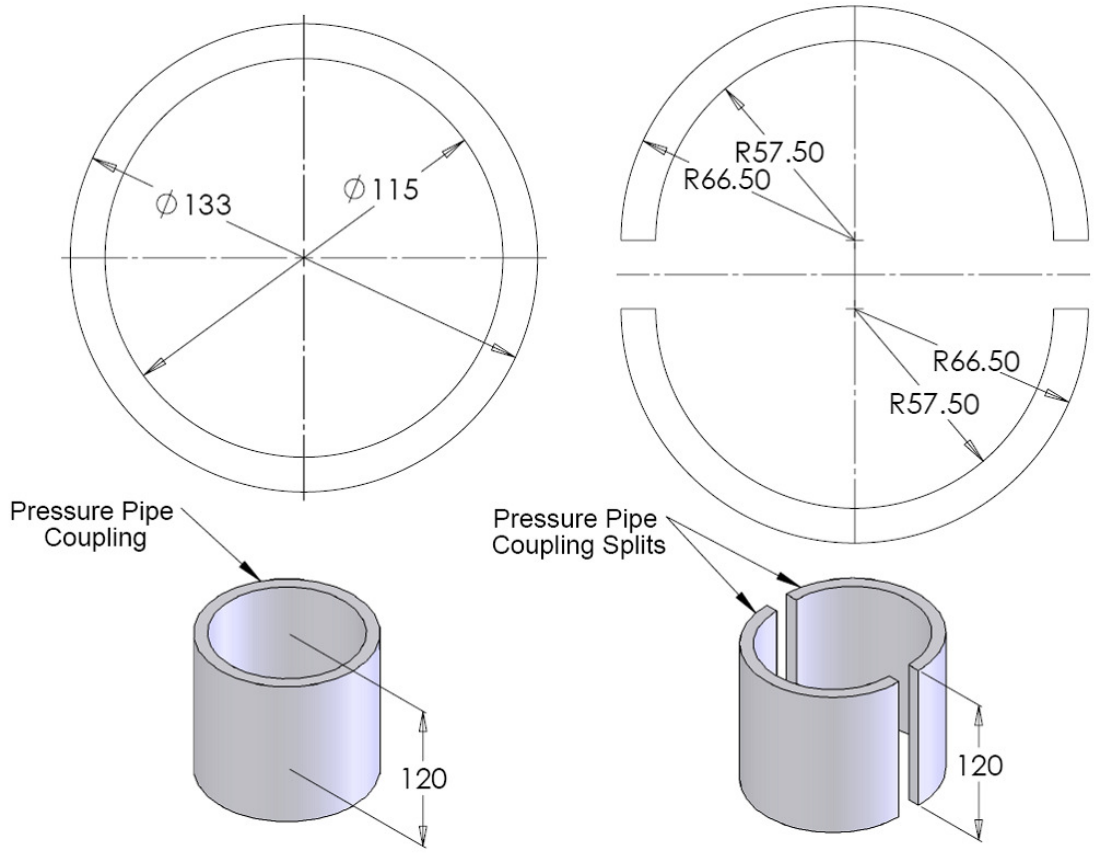

Figure 3.10 PVC pressure pipe coupling and splits *(All dimensions in mm)*

The SRT prototype 2 was build from a PVC pressure pipe coupling class PN18 (Australian Standards, 2006), which was donated to us by a local plumbing supplier. This pressure pipe coupling has an outer diameter of Ø133 mm and wall thickness of 9 mm. The turbine height was kept at 120 mm, the same as prototype 1. The mean turbine diameter is equal to the product of average pipe diameter and cosine of the jet exit angle $D_m = D_A \times \cos ine(\theta)$ (see Figure 3.11 and Figure 3.13). If the water jet emit tangent to the turbine diameter (i.e. jet exit angle is 0°) then $\cos ine(0) = 1$ and so the mean turbine diameter will be equal to the average diameter of the pipe from which the turbine is build (where average pipe diameter $D_A = (D_{OD} + D_{ID})/2$). In this case, the measured outer

diameter and the inner diameter of the pressure pipe coupling are measured as Ø133 mm and Ø115 mm respectively, so the average pipe diameter is Ø124 mm. To reduce the mean turbine diameter below the average pipe diameter, the splits were machined at the edges to allow water to leave at and angle of 10° to the tangent, so the mean turbine diameter is Ø122.12 mm. Figure 3.11 shows the splits machined to achieve a jet exit angle of 10°.

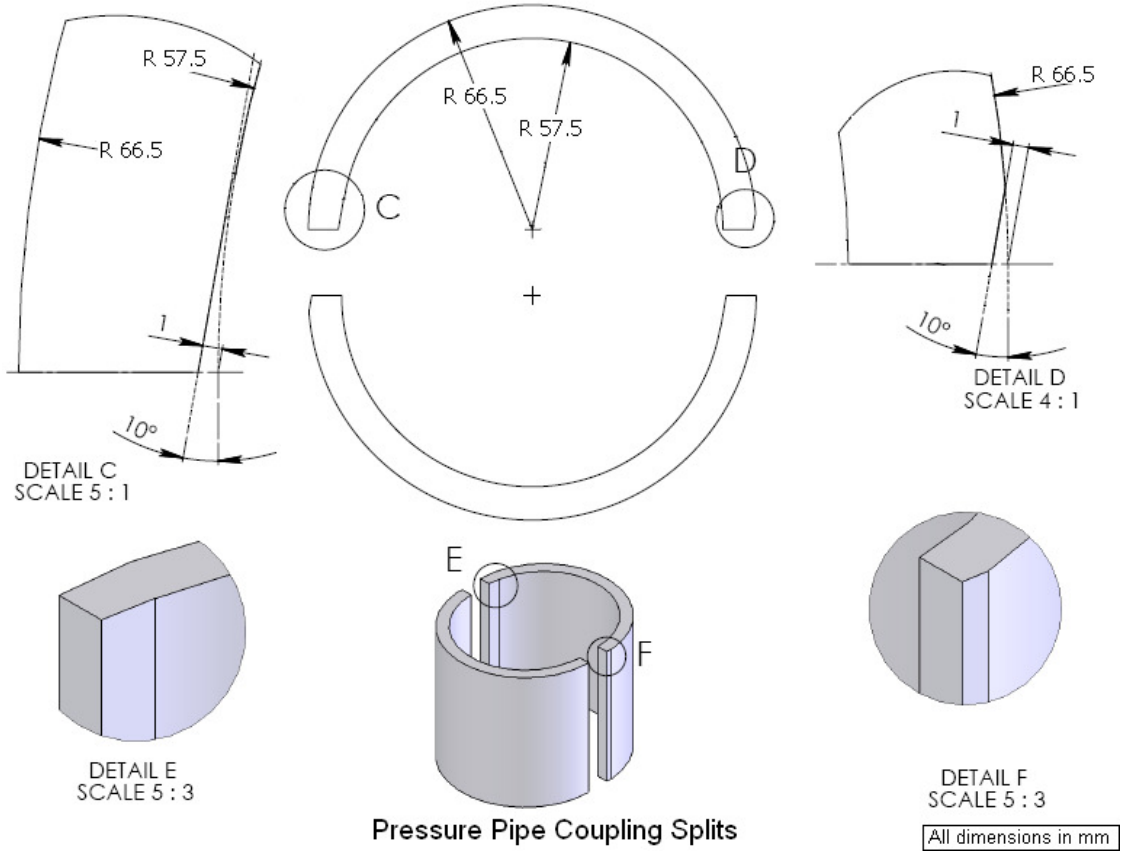

Figure 3.11 Tapper on splits for jet to exit at an angle

Figure 3.12 shows the position of screw holes machined on the pipe splits to build the split reaction turbine prototype 2. It is recommended to have the first hole as close as possible to the outer edge of the split, which in this case is shown at an angle of 7.5°. As mentioned earlier, while testing prototype 1 water leakage was observed at the interface of the cover plates and pipe splits, so to prevent this happening in the prototype 2 extra screws are used to join the pipe splits to the cover plates.

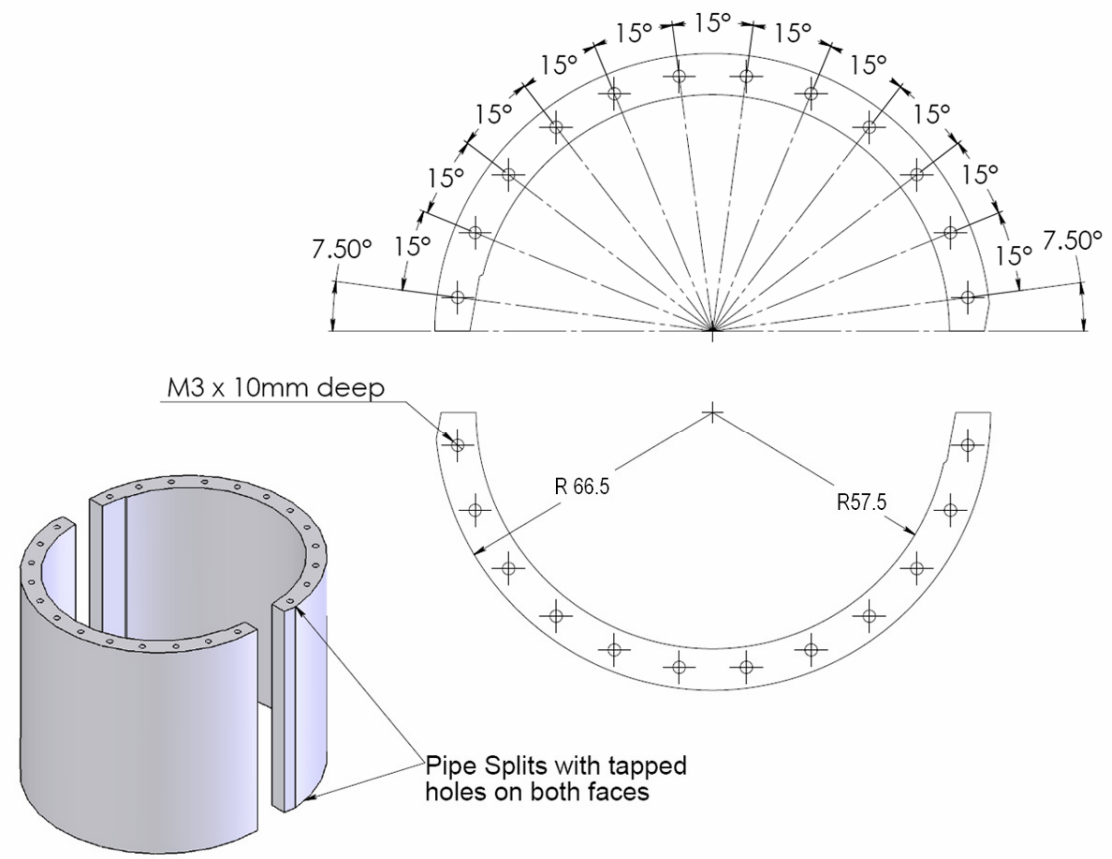

Figure 3.12 Machining of screw holes on splits (All dimensions in mm)

In the next step the top and bottom cover plates are machined to get the desired exit nozzle width. Figure 3.13, Figure 3.14, and Figure 3.15 shows three cover plates with projection of the pipe splits with three different center offsets to achieve three different exit nozzle widths. The exit nozzle widths of 8 mm, 5.3 mm and 4.2 mm were achieved with the center offsets of 17.2 mm, 14.5 mm and 13.4 mm respectively.

Figure 3.13, Figure 3.14, and Figure 3.15 also shows the jet exit angle of 10° and the mean turbine diameter. To guide the water jet leaving the turbine in the desired direction (i.e. 10° exit angle) an additional center off-set of 6 mm on Z-axis is provided. This helped to achieve a 6 mm jet guide on the exit nozzle.

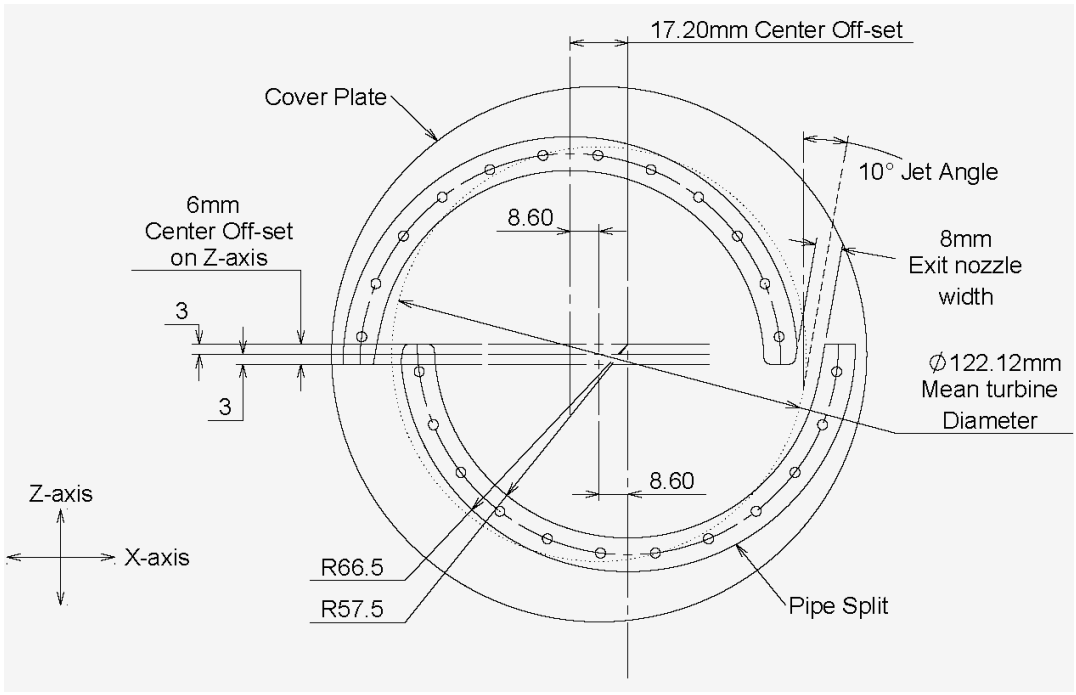

Figure 3.13 SRT Prototype 2 – Cover plate 1 with exit nozzle width of 8mm

(All dimensions in mm)

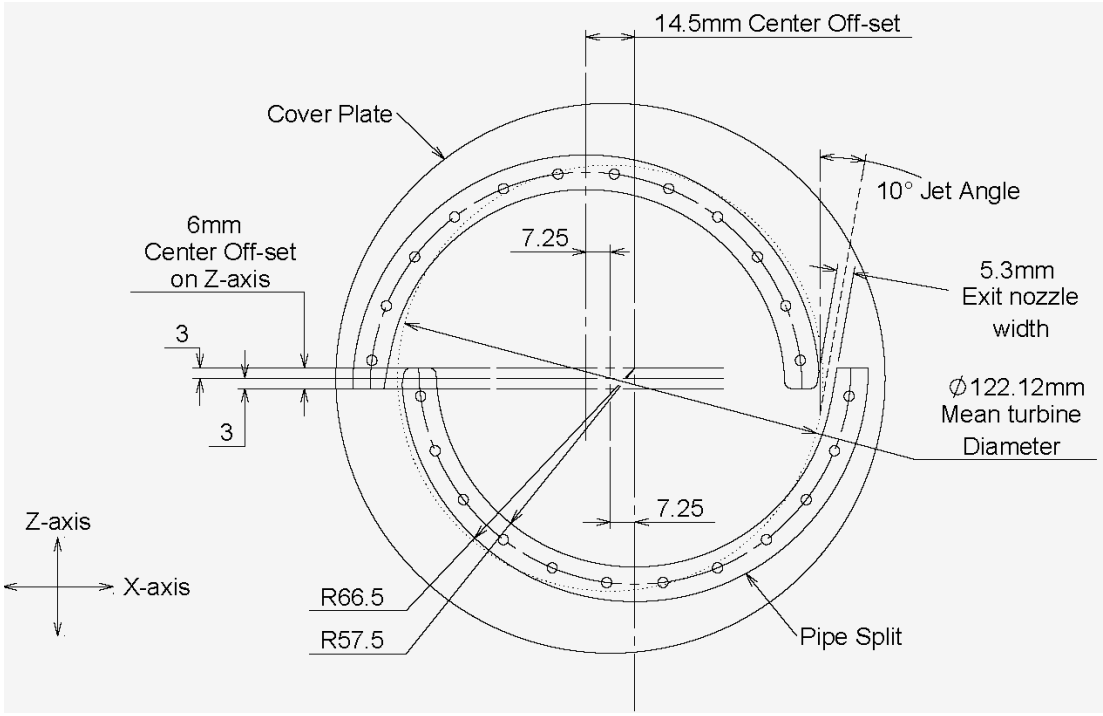

Figure 3.14 SRT Prototype 2 – Cover plate 2 with exit nozzle width of 5.3mm

(All dimensions in mm)

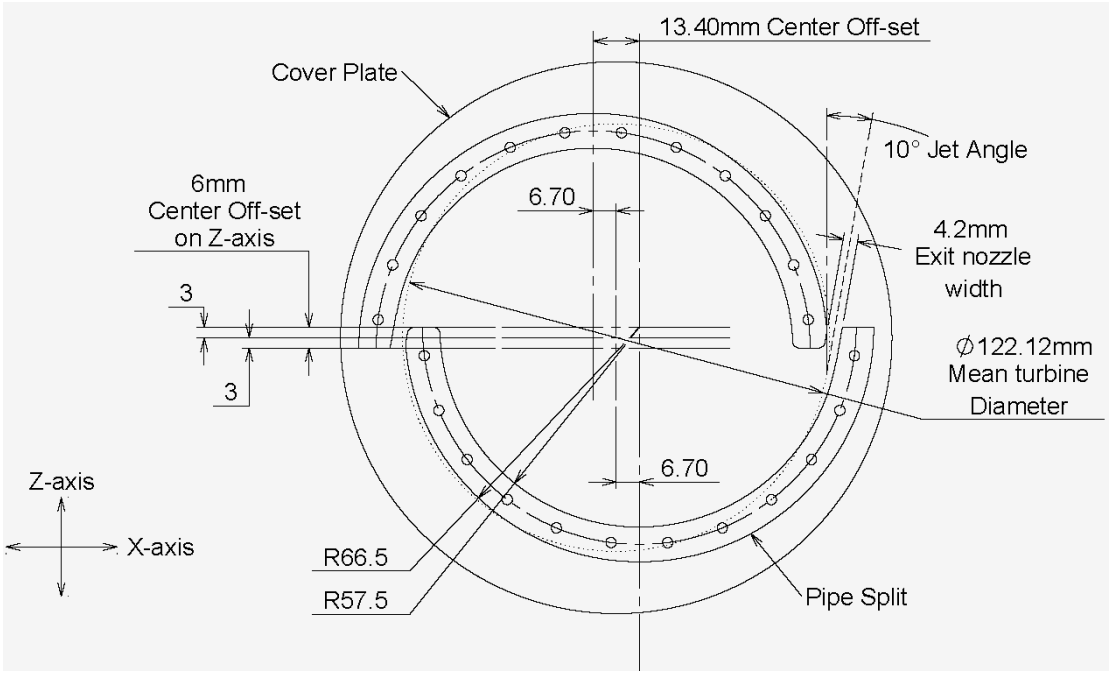

Figure 3.15 SRT Prototype 2 – Cover plate 3 with exit nozzle width of 4.2mm

(All dimensions in mm)

Figure 3.16 shows the complete assembly of SRT prototype 2 with the flange coupling attached to the top cover plate and the inlet port connected to the bottom cover plate. Figure 3.16 also show the pictures of the pipe splits and the Ø3 mm tapped holes along the flat faces of the split for connecting to the top and bottom plate. Figure 3.16 also shows the actual pictures of top and bottom cover plates. The flange coupling and inlet port from SRT prototype 1 are reused in SRT prototype 2. The flange coupling transmits the power produced by the turbine to the electric generator. The inlet port guides the rotary seal and the water into the turbine.

By changing the centre off-sets the exit nozzle widths are changed as shown in Figure 3.13, Figure 3.14 and Figure 3.15 . There was no water leakage at the interface of the splits and the cover plates in SRT prototype 2. Figure 3.16 shows four tapped holes, 90° apart on the top cover plate to connect the flange coupling. Similarly the inlet port is connected to the bottom cover plate with four bolts (see Figure 3.16).

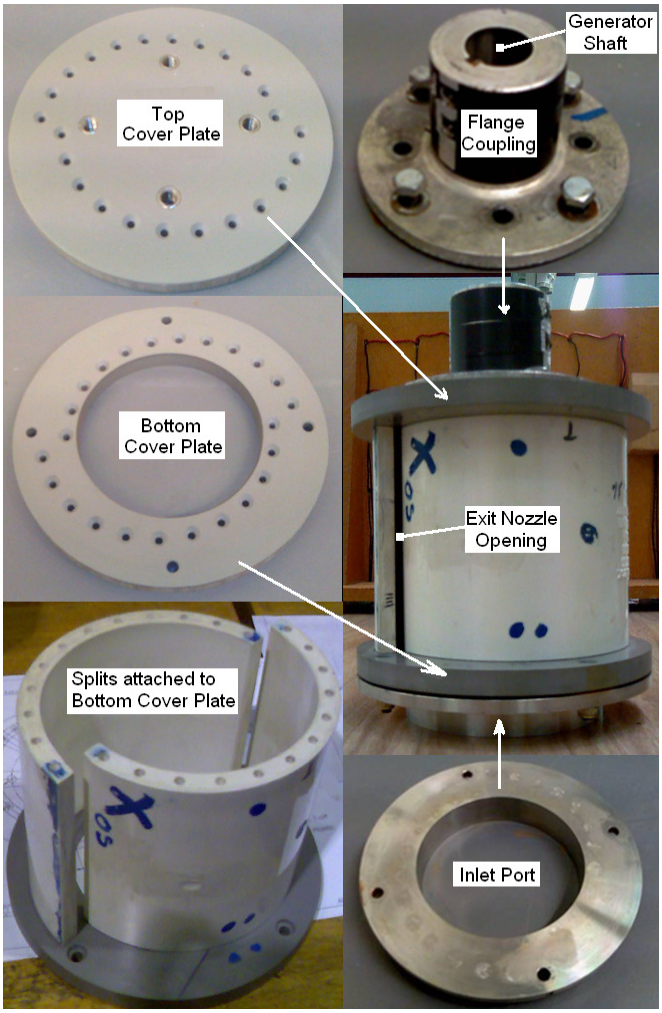

Figure 3.16 Split reaction turbine - Prototype 2

3.3 Inlet Rotary Seal arrangement

To prevent water leakage from the inlet of the simple reaction turbine a rotary seal is connected at the inlet. Proper selection of the rotary seal is very critical for this application. Following are the main factors that are considered in the seal selection,

- Cost and availability: The seal should be inexpensive and easily available.
- Frictional power loss due to the seal: The seal should have minimum frictional power losses.
- Simplicity: The seal should be simple to install.
- Durability: The seal should have long life.

After considering these factors two rotary seal arrangements are selected for use with low head simple reaction turbine, these rotary seal arrangements are V-ring lip seal arrangement and mechanical seal arrangement. The V-ring lip seal arrangement is inexpensive, has medium frictional power loss, is simple to install and has good life. While the mechanical seal arrangement has very low friction, is easy to install and has reasonable life, they are expensive to buy. The cost of commercially available mechanical rotary seal arrangement with seal diameters above 50mm get too high. So a simple and low cost method to manufacture a customised mechanical seal with large diameter has been discussed in this section.

3.3.1 V-ring lip seal

The V-ring rotary seal arrangement has been shown in the Figure 3.17; here the V-ring seal is mounted on the stationary supply pipe with seal support ring holding the seal in correct position. The lip of the stationary V-ring seal is pressed against the rotating stainless steel seal ring by the pressure of the incoming water. The rotating stainless steel seal ring is connected to the inlet port, which rotates with the turbine. This type of rotary seal arrangement is very effective against preventing water leakage.

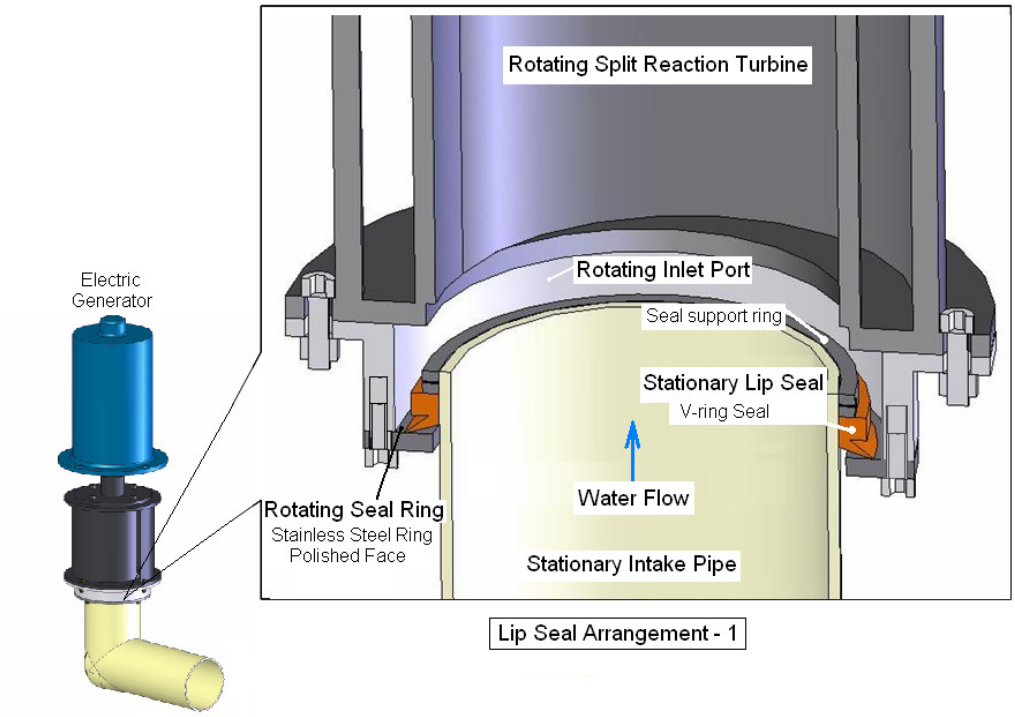

Figure 3.17 V-ring lip seal arrangement 1

This method of rotary sealing is tested with both the split reaction turbine prototypes. Standard Forsheda V-ring seal (manufactured by Busak&Shamban; Part number TWVA00900) with inner seal diameter range of Ø88-93 mm is used with both the prototypes. The contact face of stainless steel rotating seal ring is polished to achieve minimum friction and wear on the V-ring seal. As per the recommendations by Busak&Shamban V-ring seal installation guide (see Figure - E.8 to Figure - E.14, Appendix E), for nitrile rubber V-ring seal the opposite contact surface should be Stainless steel. Figure 3.18 shows the V-ring seal arrangement; here the special V-ring seal with extra long lip is used. Here the V-ring seal is mounted on the stationary intake pipe with a seal support ring to hold the V-ring in position. The lip of the stationary V-ring seal touches the inner surface of the inlet port. The incoming water pressure pushes the extra long lip against the inner face of the rotating inlet port inner. This prevents the water leakage. Here the need of additional steel ring connected to the inlet port as that in previous V-ring seal arrangement is eliminated. However, this type of sealing arrangement is not recommended for heads above 3m, because under higher pressures the extra long lip bends and slips into the gap between the inlet port and the V-ring seal, which causes high water leakage and high frictional power loss.

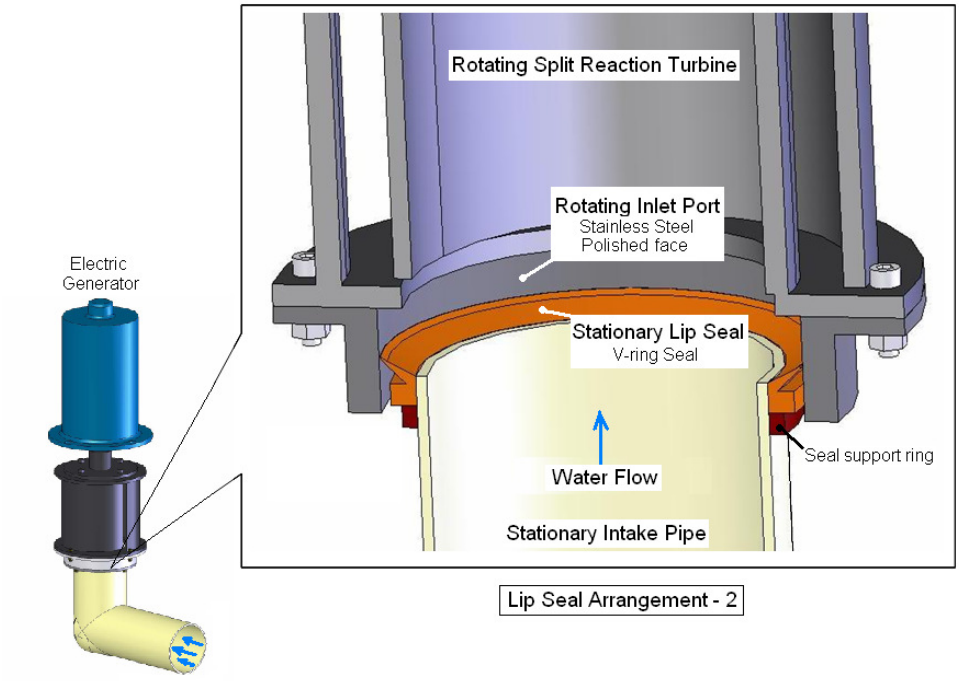

Figure 3.18 V-ring lip seal arrangement 2

The experimentally estimated frictional power loss for the V-ring lip seal is seen to vary with the supply head. As the supply head increases the frictional power loss increases. The testing technique used for the estimation of the frictional power loss is discussed in Chapter 4 and the power loss test results are presented in Chapter 5.

3.3.2 Mechanical seal

The mechanical seal is the surface-to-surface contact rotary seal where the sealing is achieved by pressing to polished faces against each other. This type of rotary seal arrangement performs excellently at any supply pressure. Usually the stationary surface is made from material, which is soft and has very good self-lubricating properties like carbon, graphite or nylon. While the rotating surface is made from, wear resistant materials like ceramic or stainless steel.

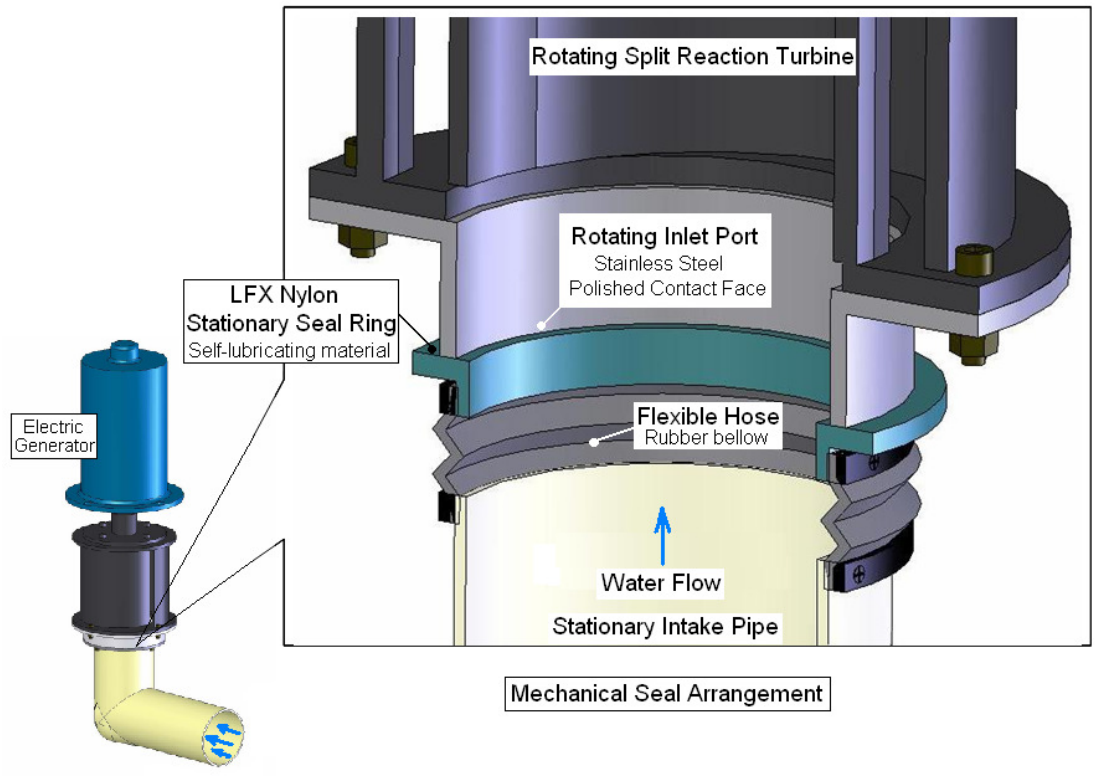

Figure 3.19 Mechanical seal – Contact surface LFX nylon and Stainless Steel

Figure 3.19 and Figure 3.20 shows the rotary mechanical seal with the SRT prototype. The stationary surface of this seal is made from LFX type nylon material, which has very good self lubricating properties. The rotating inlet port surface is made

from stainless steel. The contact face of the inlet port is polished to reduce the friction. The nylon ring is connected to the stationary intake pipe with steel wire reinforced flexible hose. The steel wire reinforced flexible hose is connected to the nylon ring and intake pipe using cable ties. The testing technique used for the estimation of frictional power loss when using the mechanical seal arrangement is discussed in Chapter 4 and the power loss test results are presented in Chapter 5.

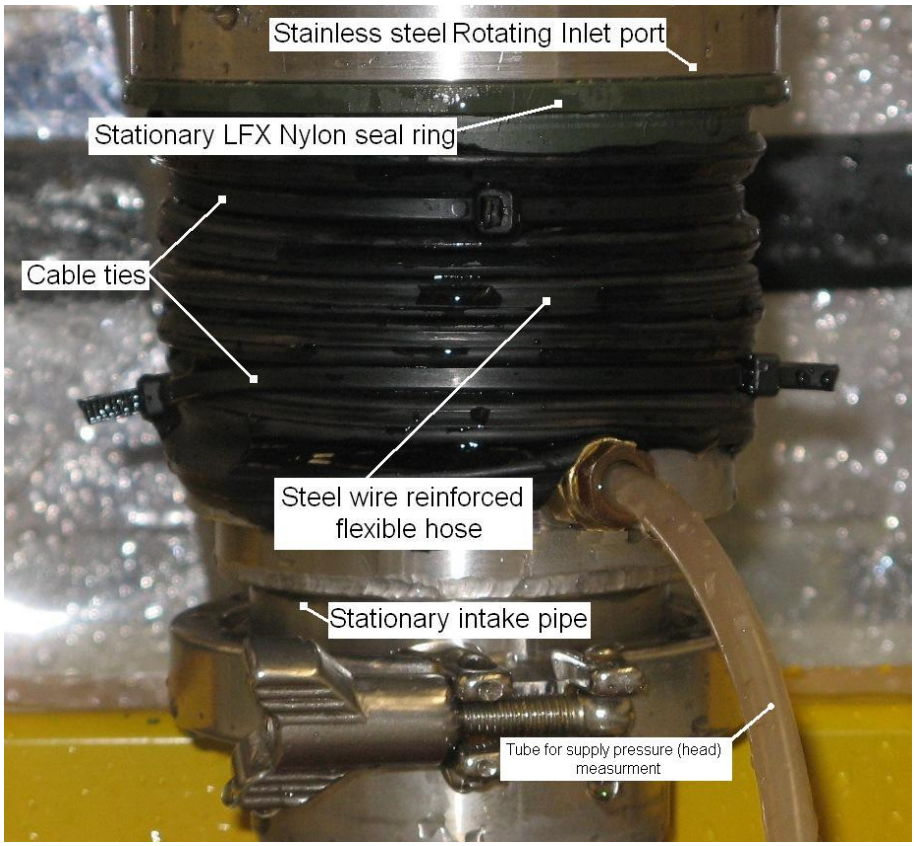

Figure 3.20 Picture of actual LFX Nylon-Stainless steel seal

Chapter 4 Turbine test rig and test procedure

4.1 Introduction

This chapter describes the instrumentation of the turbine test rig and the experimental procedures used for performance study of all the simple reaction turbine prototypes. In the first section of this chapter, the main parts of the turbine test rig are described in detail covering the details of instrumentation used in the experimental performance analysis of the simple reaction water. The following section of this chapter describes the test procedures/techniques used for the experimental analysis of all the simple reaction turbine prototypes.

4.2 Turbine test rig

Figure 4.1 shows the schematic diagram of the turbine test rig used for the performance analysis of the simple reaction turbine prototypes. This test rig is divided into two main sections

- Hydraulic power input unit, which is comprised of water pump, flow meter, pressure gauge, delivery pipe, and flow control system.
- Power output unit comprised the simple reaction water turbine with the inlet rotary seal arrangement, the electric generator, the electric load, the tachometer and the electric power-measuring device (i.e. voltmeter and ammeter).

Here the water stored in the water tank (tank capacity 0.5m³) is pressurised with the water pump and then this pressurised water is supplied to the turbine. After the water turbine extracts the mechanical power from the water, it is discharged back into the water tank for re-circulation through the systems. The mechanical power produced by the turbine is transmitted to the electric generator through the solid flange coupling. Then the electric power produced by the generator is dumped into the rheostat or globe bank (electric load). The voltage and current are measured with multi-metres, this helps estimate the electrical power output.

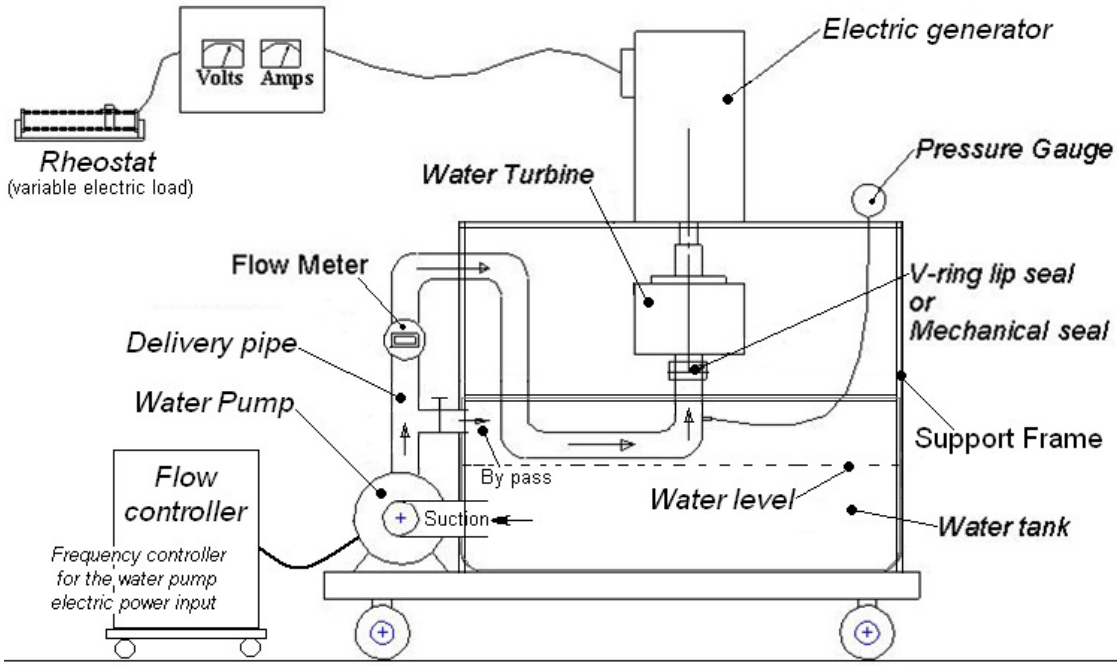

Figure 4.1 Schematic diagram of test rig

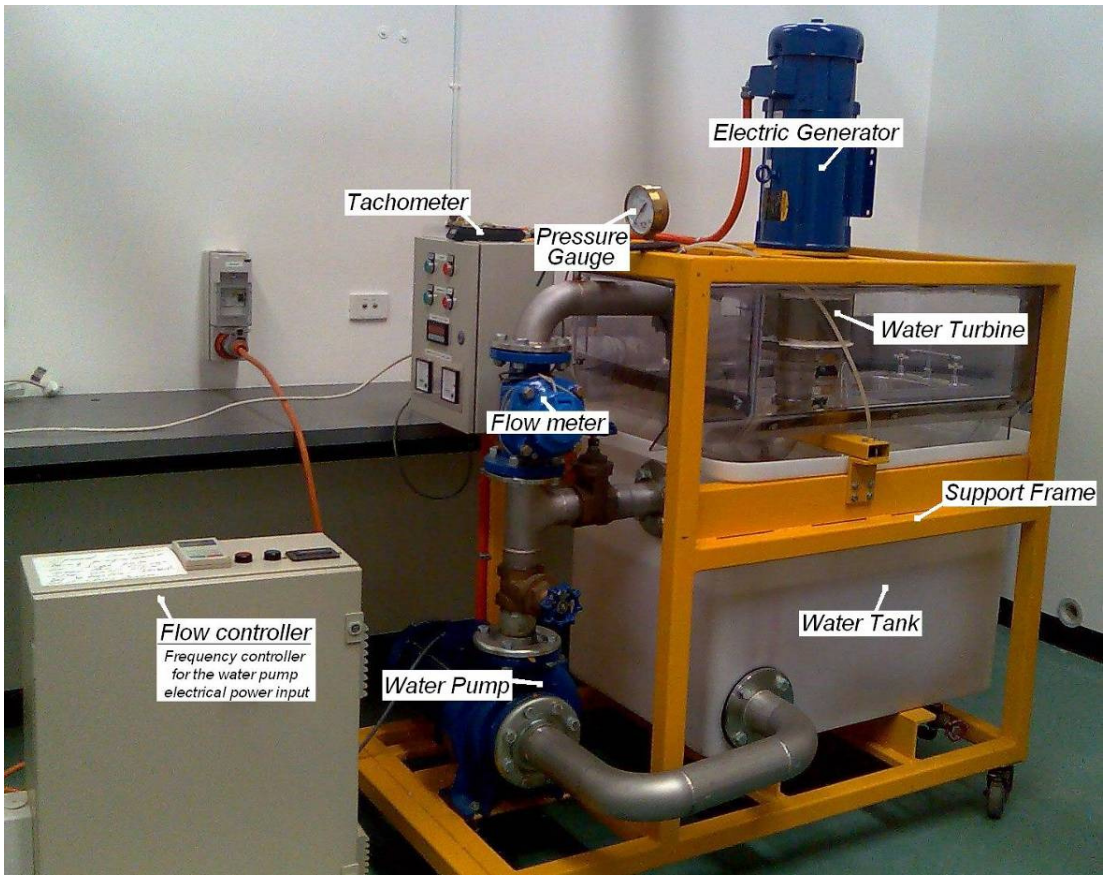

Figure 4.2 Picture of the turbine test rig

Figure 4.2 shows the picture of the turbine test rig, which is constructed for the testing of the simple reaction turbine prototypes. The support frame is constructed from rectangular hollow steel bars and is fabricated by Drummond Steel Services, Melbourne, Australia. The plastic water tank (Model R340/610) is purchased from Team Systems, Melbourne, Australia. Universal Plumbing Company, in Melbourne, Australia, did the installation of water pump and flow meter with the supply and delivery pipe plumbing on the steel support frame. The electric generator, pressure gauge, tachometer, flow controller and the water turbine were added to this turbine test unit at RMIT University workshop.

4.2.1 Hydraulic power input unit

Figure 4.3 shows the hydraulic power input unit consisting of water pump, water flow meter, pressure gauge, suction and delivery pipe and flow control system (frequency controller for water pump electric input power). The selection of all the hydraulic input unit components is based on the maximum operating head and maximum flow rate estimated for turbine performance testing. Here the estimated maximum supply head and maximum flow rate is 5m and 90m³/hr respectively.

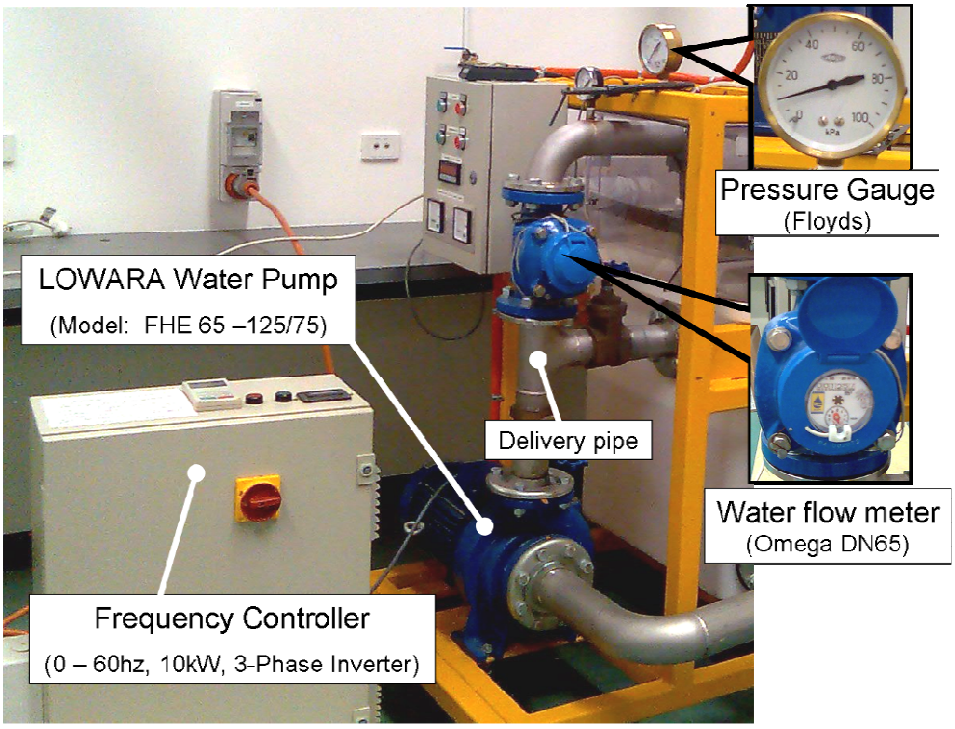

Figure 4.3 Hydraulic power input unit components

The 7.5kW centrifugal pump (model number is FHE 65-125/75, see details in Appendix E) manufactured by LOWARA is selected for the test rig. This pump operates on 415volts 3-phase 50Hz power supply and has delivery pipe internal diameter of Ø72mm. As shown in Figure 4.1 and Figure 4.2 the delivery pipe is connected to four bends, these are 90° smooth bends with assumed head loss coefficient $K_L = 0.9$ (Cengel Y., 2006) and flow meter before the inlet to the turbine. For the delivery pipe diameter of Ø72mm (cross-sectional area of $4.1\text{x}10^{-3}$ m^2) and a flow rate of 90m³/hr (0.025 m³/sec) the velocity of the water flowing through the turbine is equal to $V = 0.025 \big/ 4.1\times10^{-3} = 6.14$ m/sec. The Renolds number for this water flow is estimated as $R_e = \frac{\rho VD}{\mu} = \frac{998\times6.14\times0.072}{1.002\times10^{-3}} = 440315.21$. It is seen that the flow is turbulent with Renolds number greater than 20000, so the coefficient of friction is estimated using the following equation $f = 0.184\times(R_e)^{-0.2} = 0.0137$. The major head loss in the 3m long delivery pipe is equal to $h_{major} = f\times\frac{L\times V^2}{D\times2g} = 1.09m$. The minor head loss in each of the 90° smooth bends is estimated as $h_{\min or} = K_L\times\frac{V^2}{2g} = 1.72m$, so the sum of head loss in the bends is equal to 1.72 x 4 = 6.92m. Therefore the total head loss (major plus minor head loss) in the delivery pipe from the pump to the turbine inlet is estimated to be about 8m (Cengel Y., 2006). Figure 4.4 shows the hydraulic characteristics of the FHE65-125/75 water pump, it can be seen from curve 65-125/75 that this pump can deliver a flow rate of 90m³/hr at a delivery head of 23m. The net available head at the inlet to the turbine after deducting the dynamic head loss of 8m in the delivery pipe is estimated to be about 15m (not including the head loss in flow meter).

In addition to the head loss in the delivery pipe, the head loss in the water flow meter is also considered. Removable element WOLTMAN water meter DN65 (nominal diameter Ø65mm) with the flange connection is selected. This flow meter can measure the flow rate of 50m³/hr and above with an accuracy of ±98% (i.e. ±2% error). From Figure 4.5 the head loss in the water flow meter size DN65 for a flow rate of 90m³/hr was estimated as 1.5m. So the net head available at the inlet to the turbine was estimated as

13.5m (i.e. pump delivery head 23m minus total head loss in delivery pipe 8m minus the head loss in water flow meter 1.5m).

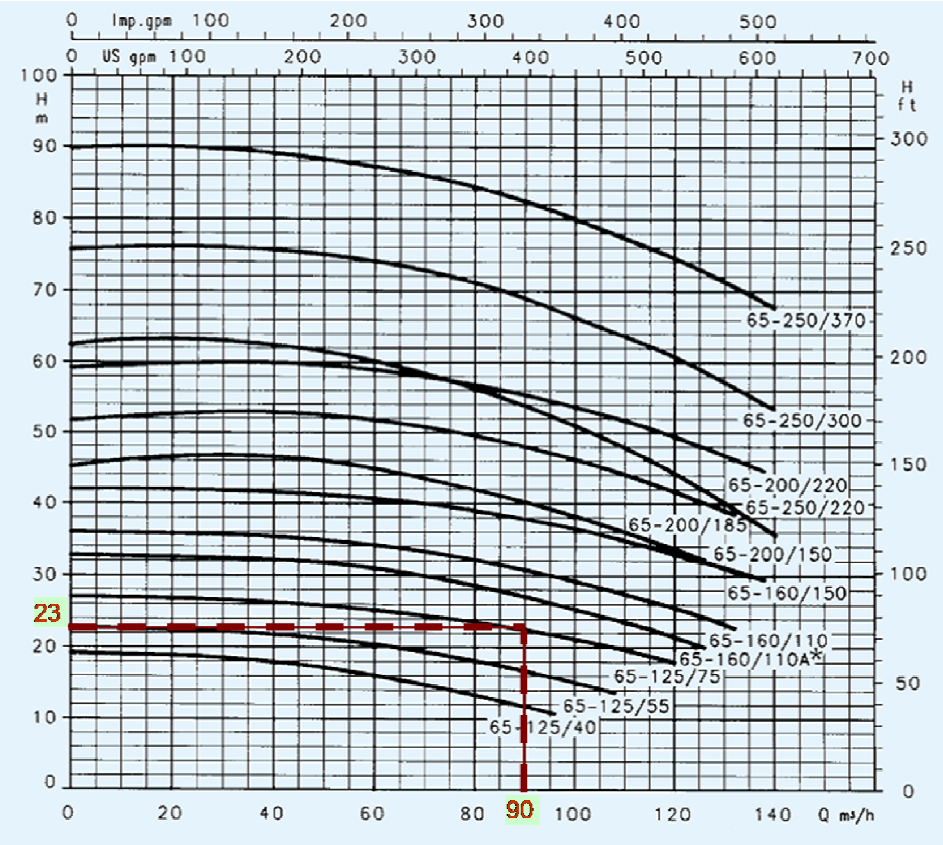

Figure 4.4 Manufacturers specifications for water pump FHE65-125/75 (source: Lowara centrifugal pump FH series techincal catlogue, see Appendix E)

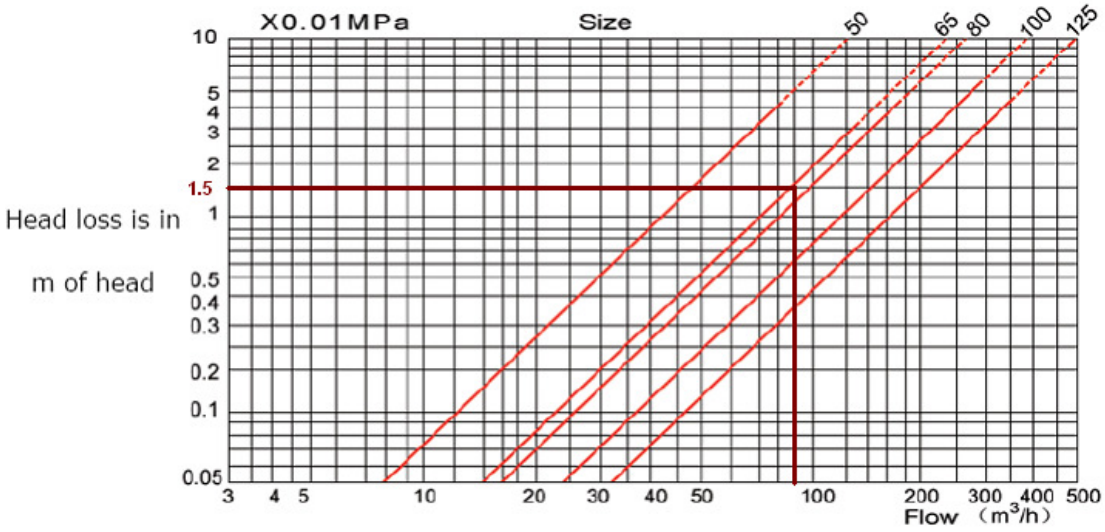

Figure 4.5 Head loss characteristics for the Omega flow meter (source: Technical catalogue Omega Flow meter)

As shown in Figure 4.3 mechanical pressure gauge is used to measure the supply pressure to the turbine with the pressure measuring range of 0 to 100 kPa (Floyds, Ø100mm brass dial). As per manufacturer's specifications, the measurement error on a full-scale display for this pressure gauge was ±1%. Low range pressure gauge was later used for the testing of SRT prototype 2 to measure the supply pressures below 30kPa with greater accuracy. This low range pressure gauge has the measuring span of 0 to 10PSI (approximately 0 to 69kPa) with the measuring error of ±1% full-scale display (FSD).

Here the 15kW variable frequency sign wave inverter is used for flow control during the performance testing of the turbine prototypes. To control the delivery water flow rate and head from the pump, the frequency controller is connected inline with the electric power supply to the water pump. By controlling the frequency of the electrical power supplied to the water pump, the impeller speed is controlled and in turn the delivery flow rate and head is controlled.

4.2.2 Power output unit

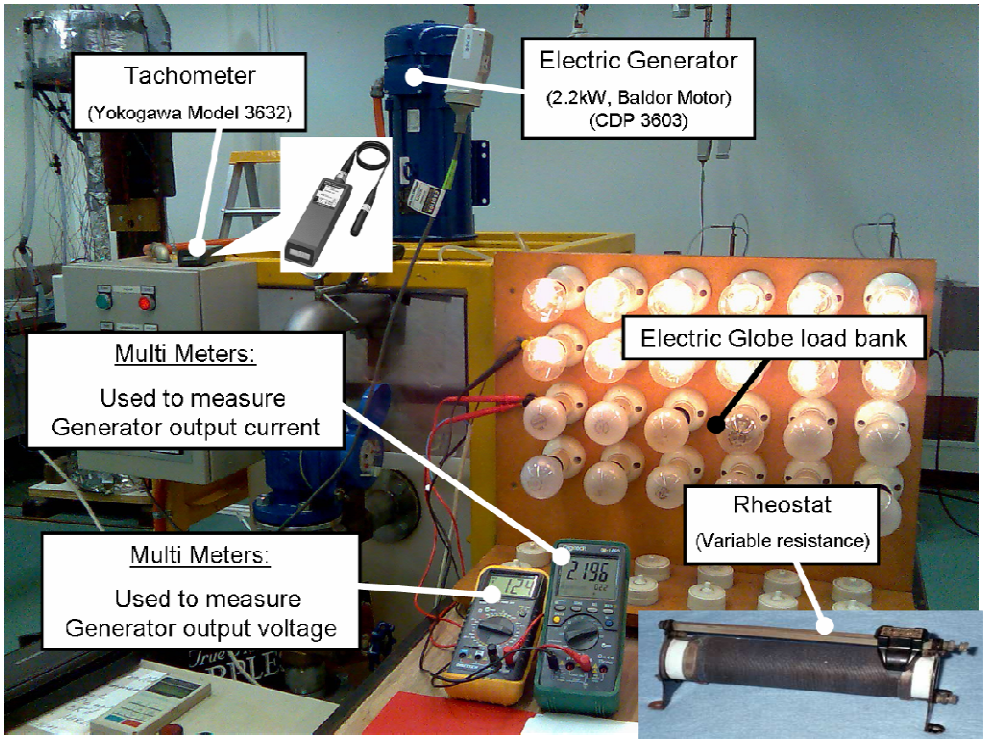

Figure 4.6 Power output unit

Figure 4.6 shows the power output unit that consists of the simple reaction water turbine, the inlet rotary seal arrangement, electric generator, electric load, tachometer and electric power-measuring device (i.e. voltmeter and ammeter). As shown in Figure 4.1, Figure 4.2 and Figure 4.6 the simple reaction turbine is connected to the electric generator. Here the permanent magnet DC motor (Capacity: 2.2kW, Manufacturer: Baldor, Catalogue No.: CDP3603) is used in reverse as an electric generator (motor data sheet in Appendix E). The non-contact photo probe tachometer is used to measure the rotational speed of the turbine. This tachometer has the measuring accuracy of ±1rpm for range of 60 to 4000rpm. Output electric power from this DC generator is dumped in the variable electric load. Rheostat and Globe bank are the two types of variable loads used in the testing. An electric globe load bank is good means to visually demonstrate the power production, as well as to measure the performance, but fine-tuning of load is not possible. However, with a rheostat, fine-tuning of load is possible but it does not have the ability to visually demonstrate the power production in the form of visible light. The generator output voltage and current are measured on two separate multi-metres. The measurement error specified by the multi-metre manufacturers is ±1.5% for DC voltage (range 1V – 1000V) and ±2.5% for DC current (range 10mA – 20A).

The electrical power output from the electric generator is less then the mechanical power supplied to the generator shaft. This is due to the sum of all electrical power losses (i.e. iron losses, eddy current losses, copper loss) plus the sum of frictional power loss in the generator bearing and the generator armature windage power loss (air drag). All these losses are added to the electrical power output from the generator to estimate the mechanical power produced by the turbine.

4.3 Test and performance estimation procedure summary

In this section all the test techniques used for the experimental analysis of all the simple reaction turbine prototypes are discussed. The objective of this analysis is to determine the performance of these turbines under different hydrostatic heads. Following are the test techniques used in this analysis:

- Stationary test: This test technique measures the amount of water flowing through the stationary rotor at different hydrostatic heads and it helps to estimate the stationary torque produced by the turbine.
- Power test: This test technique measures the input water flow rate and hydrostatic head; this is then used to estimate the input power ($\dot{m}gh$). At the same time this test technique also helps to estimates the power produced by the rotating turbine at different hydrostatic heads and different rotational speeds. This data is later used to estimate the dynamic k-factor and the turbine performance.
- Power loss estimation: This test estimates the DC motor/generator power loss, turbine drag loss and rotary seal mechanical friction loss.
- DC motor/generator shaft power estimation procedure.

4.3.1 Stationary test

The stationary test is carried under different hydrostatic supply heads. This technique helps to estimate the stationary torque produced by the turbine. The stationary torque is equivalent to the maximum torque that turbine can produce at a certain hydrostatic supply head. It also helps to estimate the stationary water flow rate through the turbine. This is equivalent to the minimum water flow rate that a constant hydrostatic supply head can produce. Finally, this test technique helps to estimate the stationary k-factor of the turbine.

All the turbine prototypes discussed in Chapter 3 have been tested with this technique. Figure 4.7 shows the experimental set-up used in the stationary test. During the stationary test, torque arm is connected to the turbine shaft and the force sensor (Dana Load cell capacity 20kgf), the force sensor measures the tangential force at the torque arm F_{LC}, this is used to estimate the stationary torque. The force sensor is secured rigidly to the test rig frame as shown in Figure 4.7. From this measurement, the torque is deduced and hence the total reaction force of the exiting water jets. Here water is supplied at constant hydrostatic head, the supply pressure/head is monitored on the

pressure gauge, the flow rate is monitored on the flow meter and the is force (proportional to torque) is monitored on the force sensor indicator, at the same time all these parameters are also recorded. In the stationary test, the flow rate is only dependent on the supplied hydrostatic head as there is no centrifugal pumping effect present that could alter the flow rate. All the data is recorded manually on data sheet, this data is later transferred to the excel spreadsheet.

Table 4.1 shows the arrangement of the stationary test data sheet used to record the stationary test results. The volume flow rate of the water flowing through the turbine is equal to the measured volume of water in m³ using flow meter divided by the time measured on stopwatch.

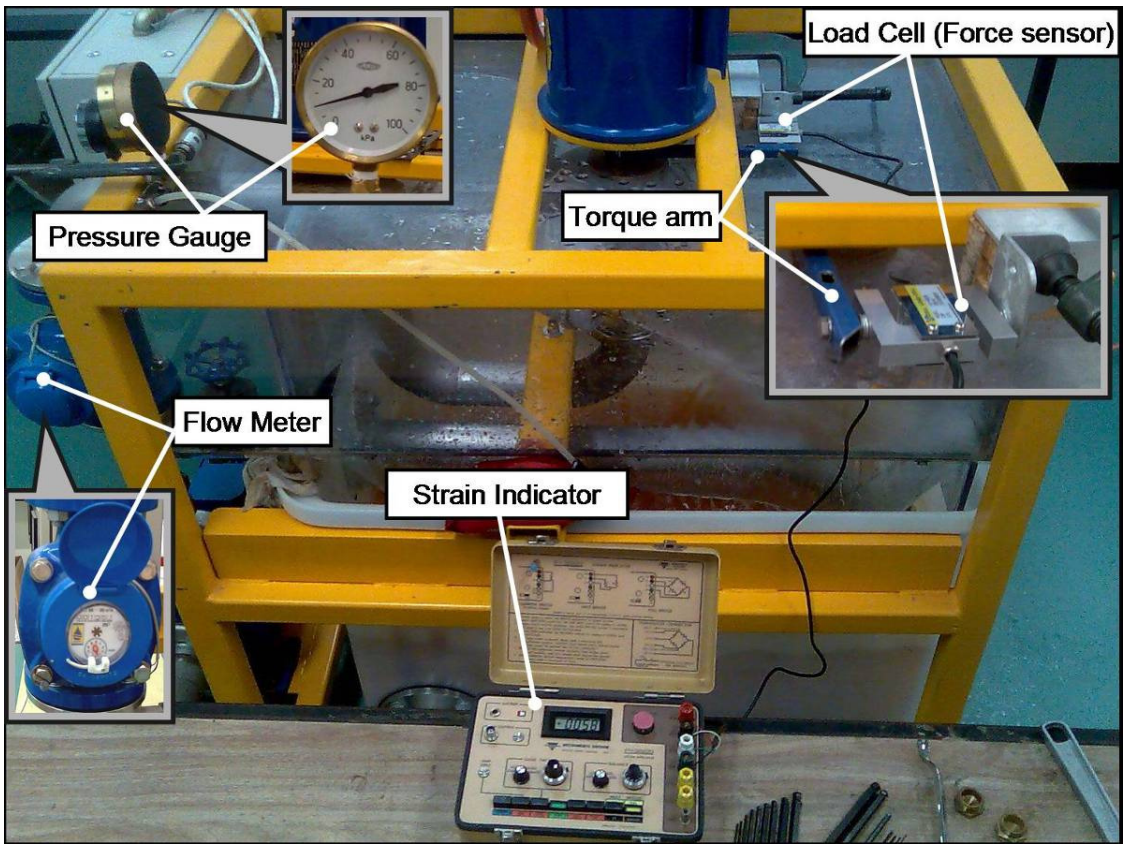

Figure 4.7 Stationary torque and flow rate measurement set-up

The relative velocity V_r of the water jet at both the exit nozzles is equal to the total volume flow rate of water supplied to the turbine divided by the total exit nozzle area. Using this value of relative velocity and equation 2.39 from Chapter 2 the value of

k-factor is calculated. Ideally the torque produced at the turbine shaft T_{shaft} should be equal to the estimated torque, here estimated torque is equal to product of absolute velocity V_a, total mass flow rate $\dot{m}$ and mean turbine radius R as shown is equation 2.10 (when the turbine is stationary (i.e. $\omega = 0 \,\&\, \therefore U = 0$) the absolute velocity V_a is equal to the relative velocity V_r). The turbine shaft torque is equal to the product of the measured force F_{LC} (N) at the turbine shaft times the torque arm length L_{arm} (m). The stationary test results for all the turbine prototypes are analysed and discussed in the Chapter 5.

$$T_{shaft} = F_{LC} \times L_{arm} \qquad 4.1$$

Table 4.1 Arrangement of stationary test data sheet

Simple reaction turbine type: _____ Torque arm length L_{arm} = _____			
Obs. No.	Pressure gauge reading (kPa)	Time required for $V =$ ___ m^3 water flow through turbine t (Sec)	Force transducer reading F_{arm} (N)
1			
2			
3			
4			
5			
6			
7			
8			
9			

4.4 Power Test

Power test is used to measure the overall performance of a turbine prototype. During this test the hydrostatic supply head is kept constant while the load on the turbine is varied. This technique helps to estimate the maximum power produced by a turbine for a constant hydrostatic head and the maximum energy conversion efficiency (overall efficiency) of the hydroelectric unit. It also helps to estimate the water flow rate while turbine is rotating. Here the flow rate increases with the increase in rotational speed due to centrifugal pumping effect as discussed in Chapter 2. Further, this test technique helps to estimate the variation of k-factor with rotational speed. The measured data assists in

the overall energy balance analysis of the hydroelectric unit. All the turbine prototypes discussed in Chapter 3 are tested with this technique.

Figure 4.8 shows the turbine test rig and its instrumentation used for the power test. Here the flow meter measures the volume flow rate of water flowing through the turbine, the pressure gauge measures the hydrostatic supply pressure at the inlet to the turbine, the tachometer measures the rotational speed of the turbine, and the two multi-metres are used to measure the output voltage and current from the D.C. generator. The frequency controller seen in Figure 4.8 is used to regulate the supply water pressure. The supply pressure to the turbine is controlled by the adjusting the frequency of the electrical power supplied to the water pump through this frequency controller.

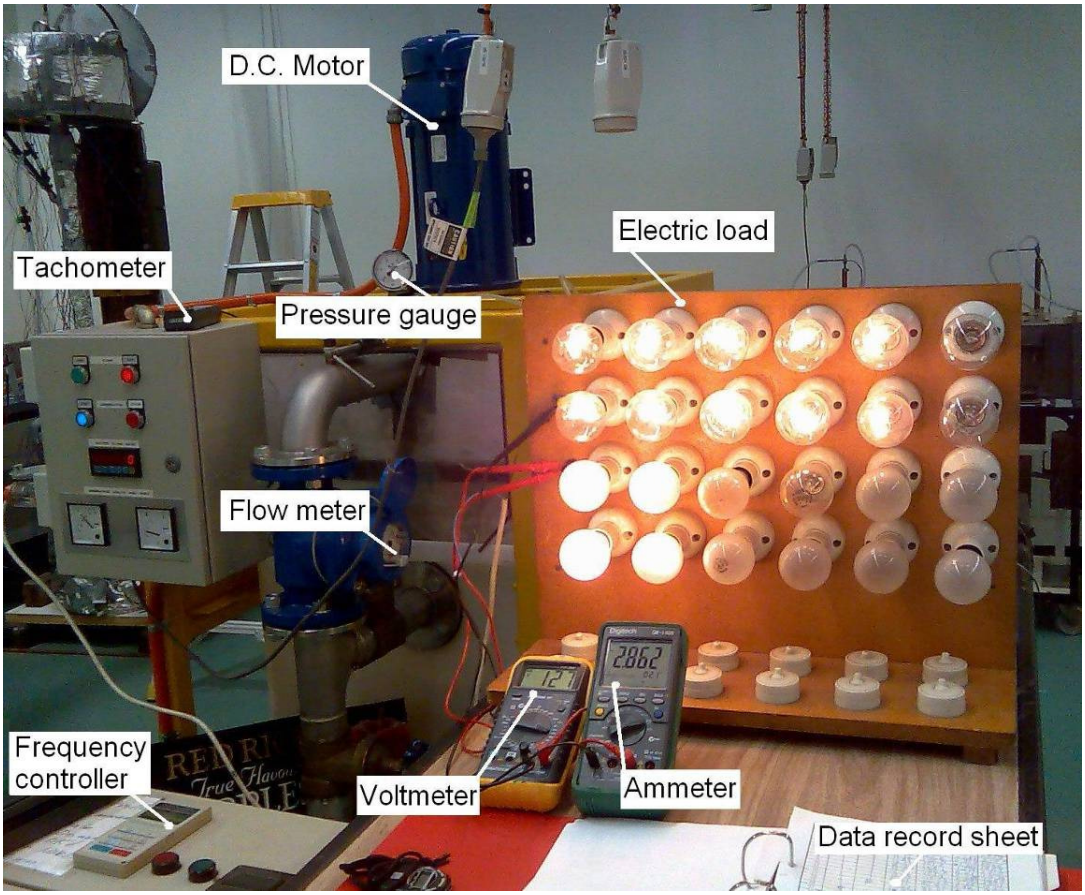

Figure 4.8 Power measurement test

All the prototypes are tested with power test technique at different hydrostatic supply pressures/heads (range 10-80kPa; i.e. 1m to 8m) to estimate their performance characteristics. At the beginning of a power test, the turbine is allowed to rotate free

without any electric load or some times with very small electrical load, while the supply pressure is held constant. At the same time parameters like flow rate, rotational speed, output voltage, and output current are recorded. Then the electric load is gradually increased in steps, this tends to decrease the rotational speed of the turbine. This decrease in rotational speed reduces the centrifugal pumping effect causing the supply pressure to increase slightly. The supply pressure is then adjusted to its original value with the frequency controller connected to the water pump. The parameters like supply pressure, flow rate, rotational speed, output voltage and output current are recorded for each step when load is increased. The increase in load is continued till the turbine slows down to about quarter of no-load rotational speed (initial maximum rotational speed). This procedure is repeated for different supply pressures to analysis the performance characteristics of all turbine prototypes for low hydrostatic heads range 1-8m (i.e. ≈10-80kPa). All the data is recorded manually on data record sheet, which is later transferred to the excel spreadsheet. Table 4.2 shows the arrangement of the power test data sheet used to record the power test data.

Table 4.2 Arrangement of power test data sheet

Measured test data for SRT Prototype 1 (Ø243mm and total nozzle exit area 0.00144 m²)				
Supply Pressure (kPa)	Time required for 0.4m³ of water to flow through the turbine (sec)	Gen Output Voltage V_g (Volts)	Gen Output Current I_g (Amps)	Rotational Speed (rpm)

4.5 Turbine and DC generator power estimation procedure

The mechanical power produced by the turbine is equal to sum of electrical power output, plus the power lost in DC generator, plus the power lost in overcoming turbine air drag plus the power lost in friction at the rotary seal. For a permanent magnet D.C. motor/generator only a few constants and equations linking them are needed to describe

the relationship between speed, torque and current (Enfield, 2005). The D.C. motor torque constant K_t is defined as the ratio between the torque and the current; in the metric system its unit is Nm/amp. In the metric system K_t has the same numerical value as the voltage constant K_e (unit Volt/rad/sec) for a D.C. motor (Enfield, 2005). Following are the equations linking the speed, torque and current, (later used to estimate the mechanical shaft power)

$$T_g = K_t \times I_g + T_{loss} \qquad 4.2$$

Here T_g is the torque applied to the generator shaft by the water flow through the turbine (Nm), I_g is the generator output current (Amp) and T_{loss} is the sum of lost torque (Nm).

Further T_{loss} is expressed as the sum of torque lost in DC motor/generator (bearing friction and ohmic loss) plus torque lost to overcome the friction at rotary seal plus the torque lost to overcome the turbine air drag,

$$T_{loss} = \frac{\dot{W}_{loss}}{\omega} \qquad 4.3$$

Here $\dot{W}_{loss}$ total power loss i.e. sum of power loss in DC motor, rotary seal and turbine air drag.

The electrical power output from the D.C. motor/generator $\dot{W}_E$ (Watts) can be estimated using following equation,

$$\dot{W}_E = K_t \times I_g \times \omega = V_g \times I_g \qquad 4.4$$

Here I_g is the generator output current (Amp), V_g is the generator output voltage (Volts), K_t is the torque constant of the DC generator/motor.

Finally the turbine output power (i.e. the actual mechanical power output from turbine before turbine drag removes some) $\dot{W}_T$ (Watts) is estimated using following equation,

$$\dot{W}_T = \dot{W}_E + \dot{W}_{loss} \quad 4.5$$

The DC motor/generator constants K_e and K_t is estimated by using the equations discussed by Max Enfield (Enfield, 2005) and the performance data provided in the Baldor publication "Direct Current Motors" catalogue E-104. The numerical value of K_e and K_t is estimated as 0.902 using equation suggested by Max Enfield (Enfield, 2005). The total power loss $\dot{W}_{loss}$ is estimated as discusses in section 4.6.

4.6 Power loss estimation

The estimation of total power loss between the turbine and electric generator is required for accurate performance analysis and turbine efficiency estimation. The aim of the power loss test is to estimate the total power lost while converting mechanical output power from the turbine to the electrical output power from the generator. The individual power loss components for DC motor, rotary seal and turbine air drag are estimated for verification and design optimisation purpose. External DC power is supplied to the DC motor/generator and the power consumption by DC motor/generator at different rotational speeds is recorded, this helps to estimate the individual power loss components associated with the DC motor, the inlet rotary seal (V-ring lip seal or mechanical surface contact seal) and the turbine air drag. This test involves three steps, in the first step, DC power is supplied to the DC motor/generator alone (turbine is not attached) and power consumption by the DC motor/generator at different rotational speeds without any external load is measured using the test set-up as shown in Figure 4.9. Data from this test estimates the power losses associated with the DC motor as tabulated in Table 4.3.

Table 4.3 Measured power loss associated with the DC motor/generator alone

Supply Voltage V (Volt)	Supply Current I (Amp)	Speed (rpm)	Power Loss V*I (Watt)
9.9	0.104	105	1.0
19.1	0.189	203	3.6
28.4	0.263	301	7.4
37.9	0.327	402	12.4
47.2	0.379	501	17.9
54.6	0.428	580	23.4
65.9	0.432	700	28.5
75.3	0.448	799	33.7
85.2	0.464	904	39.5

94.4	0.477	1002	45.0
103.9	0.487	1103	50.6
113.2	0.503	1202	57.0
122.6	0.514	1301	63.0
132.0	0.521	1401	68.8
141.5	0.524	1502	74.1
151.2	0.523	1605	79.0
160.4	0.516	1703	82.7
169.7	0.514	1801	87.2
179.2	0.511	1902	91.5
188.8	0.509	2004	96.0

In the second step, the turbine is connected to the DC motor/generator without a rotary seal as shown in Figure 4.10. Then DC power is supplied to the DC motor/generator, while the corresponding power consumption is measured for different rotational speeds. Here the power consumed by the DC motor/generator is equal to the sum of power loss associated with the DC motor/generator and turbine air drag. The difference between the power loss measured in this test and the power loss measured in the previous test (DC motor alone) helps estimate the power loss component representing the turbine air drag.

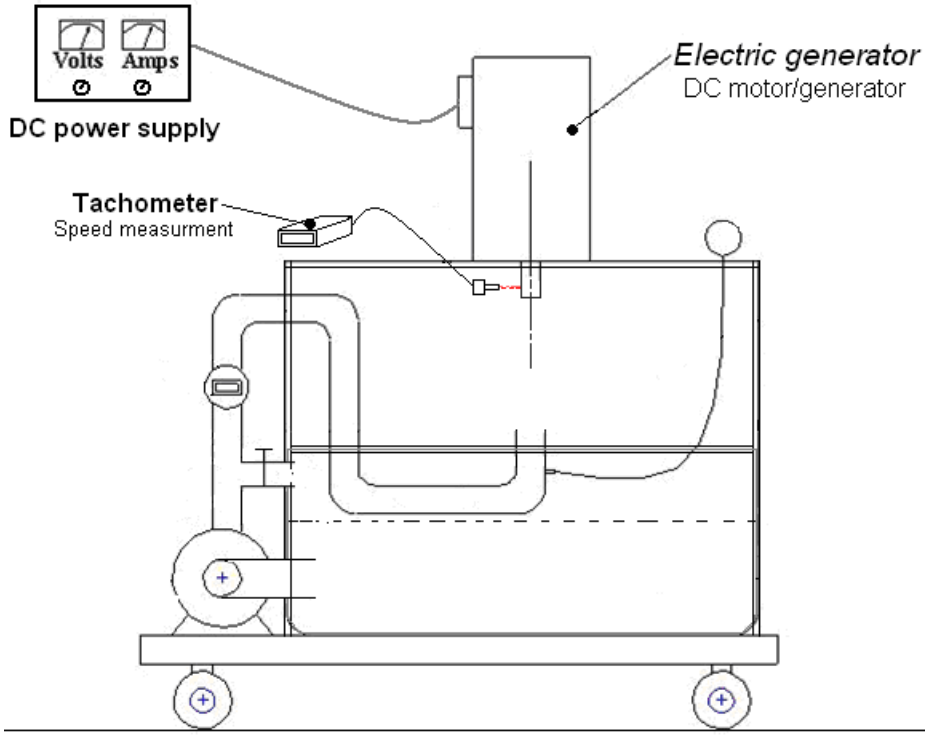

Figure 4.9 Schematic of the experimental set-up for measurement of power loss associated with the DC motor/generator

In the third step to estimate, the power loss associated with the rotary seal two slightly different procedures are used for two different rotary seal arrangements namely V-ring rotary seal arrangement and NMS arrangement. Both these sealing arrangements are discussed in Chapter 3 section 3.3. To estimate the power loss associated with the mechanical seal (NMS), the turbine with the inlet rotary seal (Mechanical seal) is connected to the DC motor/generator as shown in Figure 4.11. Now DC power is supplied to the DC motor/generator, while the corresponding power consumption is measured for different rotational speeds. Here the power consumed by the DC motor/generator is equal to the total power loss associated with the DC motor/generator, turbine air drag and inlet rotary seal friction. The difference between the total power loss and sum of power loss associated with the DC motor and turbine air drag estimated in earlier steps gives the power loss component representing the rotary seal frictional power loss.

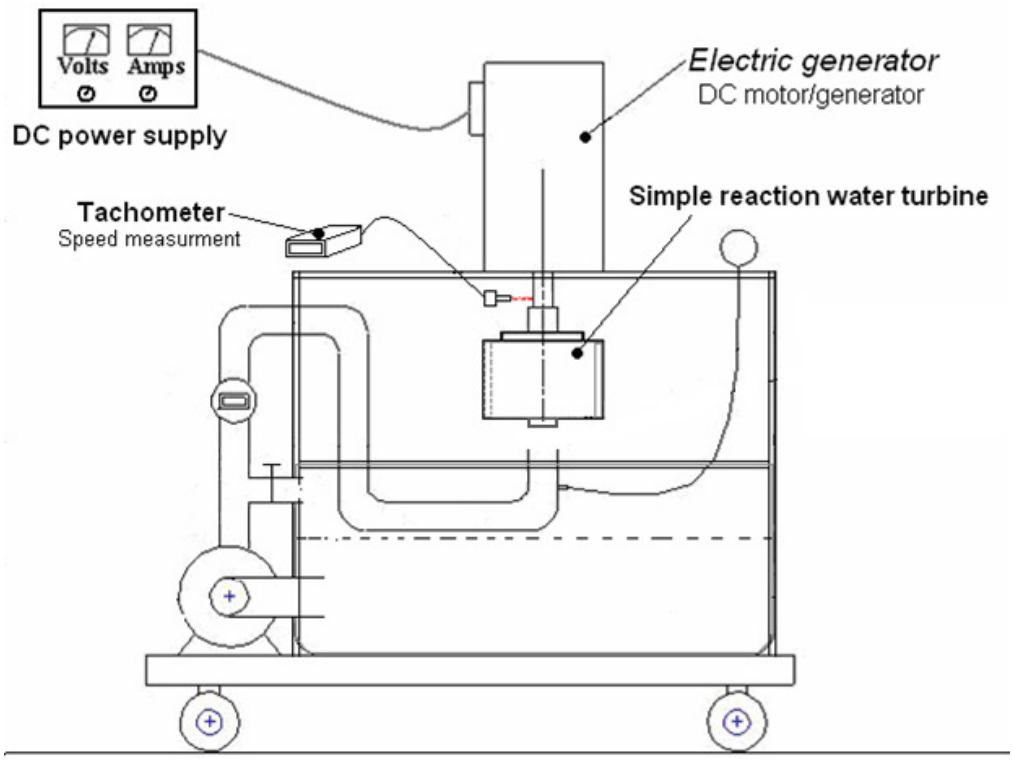

Figure 4.10 Schematic of the experimental set-up to estimate power loss associated with the turbine drag

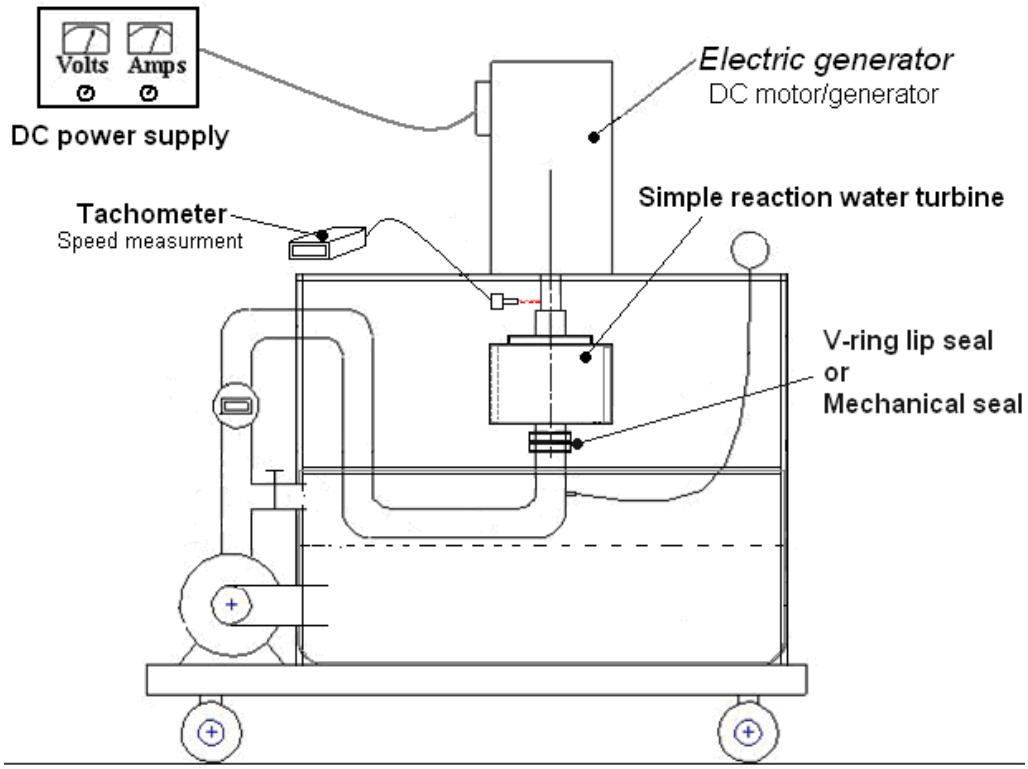

Figure 4.11 Schematic of the experimental set-up for measurement of total power loss

For the power loss estimation when using a V-ring lip seal arrangement same procedure is repeated with some additional constraints. As discussed in Chapter 3 section 3.3 the V-ring lip seal arrangement requires some water pressure to effectively seal the rotary joint and V-ring lip seal arrangement shows different frictional characteristics at different pressures. The friction between stationary surface and rotary surface increases with increase in supply water pressure, this is due to increased surface contact that is achieved at higher pressure (i.e. better sealing). So when testing for the frictional power loss in the V-ring lip seal water pressure has to be applied without allowing the water to pass through the turbine preventing any turbine reaction torque. V-ring lip seal power loss at different pressures is estimated by blocking the turbine nozzles and then applying the water pressure while the DC power is supplied to the DC motor/generator (turbine nozzles are blocked with rubber plugs). The power consumed by the DC motor/generator is measured for different rotational speeds. This procedure is repeated for a range of water pressures from 10kPa to 80kPa to estimate the increasing frictional power loss with increase in pressure. This test procedure is repeated for all turbine prototypes. Now the

power loss associated with friction in V-ring rotary seal is equal to the difference between the power consumption measured in this step minus the sum of power consumption measured in first two steps for corresponding rotational speed.

Chapter 5 Discussion and validation of experimental results

5.1 Introduction

The objective of the experimental analysis is to investigate and compare the performance of the two simple reaction turbine designs proposed in this research. This chapter will discuss the performance analysis based on the experimental data collected from different performance tests carried on all the simple reaction turbine prototypes designed during this research. The following sections will discuss the performance characteristics of stationary turbine i.e. zero power produced and performance characteristics of turbine producing power.

5.2 Stationary performance characteristics of cross pipe turbine

Figure 5.1 shows the comparison between the estimated torque based on flow rate measurement and the shaft torque based on the force measurement taken from the stationary test unit shown in Figure 4.7, the stationary test procedure used to conduct this test is explained in section 4.3.1 of Chapter 4. Ideally, both the estimated and measured torque values should be equal. Figure 5.1 also shows the minimum amounts of water flowing through the cross pipe turbine at different hydrostatic supply pressures at different conditions; this CPT has a diameter of 400mm and total turbine nozzle exit area of 0.000397m². When the turbine is stationary, the flow rate only depends on the supply pressure and total nozzle exit area, as there is no centrifugal pumping effect present. The stationary flow rate data is used to estimate the theoretical stationary torque (estimated torque) based on the flow rate and estimated exit velocity of the water jet. As discussed in Chapter 2, the estimated turbine torque is the product of total mass flow rate, turbine radius and absolute velocity of the water leaving the nozzles (see equation 2.9, Chapter 2, absolute velocity equals relative velocity at stationary condition).

For example, from Table 5.1 and Figure 5.1 at a pressure of 30kPa the volume of water flowing through the turbine is 2.94L/s; taking the density of water @ 20°C as 1000kg/m³, the estimated mass flow rate is equal to $\dot{m}$ = 2.94kg/s. So the absolute

velocity (exit jet velocity) of water leaving the nozzles is equal to,

$$V_a = \frac{2.94\times10^{-3}}{0.000397} = 7.412\ m/s$$

Radius of the turbine is equal to 200mm.

Therefore, the estimated torque is equal to

$$T_{estimated} = \dot{m}V_a R = 2.94\times7.412\times0.2 = 4.361 Nm$$

Table 5.1 Measured flow rate and force transducer readings at different pressures for CPT

CPT Prototype (Ø400mm) Torque arm = 0.211m			
Obs. No.	Pressure gauge reading (kPa)	Time required for $V = 0.1m^3$ water flow through turbine t (Sec)	Force transducer reading F_{arm} (N)
1	10	58.43	6.66
2	20	41.44	12.90
3	30	33.95	20.63
4	40	29.48	26.81
5	50	26.43	33.10
6	60	24.19	40.73
7	70	22.44	46.70
8	80	21.03	52.83

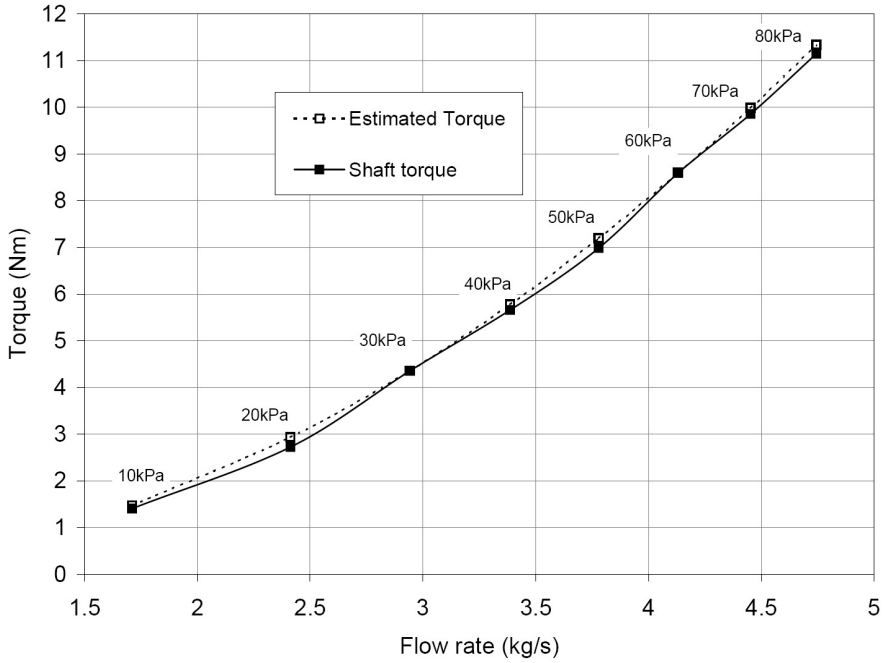

Figure 5.1 Torque comparison and minimum flow rates at different pressures for CPT

As discussed in section 4.3.1 of chapter 4 the shaft torque T_g is measured using a force sensor (load cell) connected to the turbine shaft through the torque arm of 0.211m length. Table 5.1 shows the force measurements for different pressures and the corresponding flow rates. The shaft torque is calculated from this measured data. For example, from Table 5.1 at 30kPa pressure the measured force acting on the torque arm of 0.211m length is 20.633N.

Therefore, $T_g = 20.63 \times 0.211 = 4.354 Nm$

Figure 5.1 shows comparison between the estimated torque and the measured shaft torque for stationary condition. Theoretically, the measured shaft torque should be equal to the estimated torque. However, it can be seen that on few occasions the measured shaft torque is less then the estimated torque and this deviation is very consistent. This deviation in two torque values is attributed to instrumental error, the inaccuracy in the estimation of the actual total exit nozzle area and the turbine diameter. The uncertainty analysis of the measured data from this experiment shows a relative uncertainty of ±3.66% in the estimation of the estimated torque based on the flow rate and a relative uncertainty of ±1.11% in the estimation of shaft torque (see Table - C-9 in Appendix C).

Figure 5.2 shows the estimated k-factor for stationary condition at different pressures. When the turbine is stationary the value of k-factor increases with increase in supply pressure, this is due to increase in flow rate and as a result increase in the velocity of the water leaving the exit nozzles at higher pressures. As discussed in Chapter 2 the k-factor represents the fluid frictional power loss associated with the turbine and the exit nozzles. When the turbine is stationary (i.e. ω=0) there is no centrifugal pumping effect so for the given turbine geometry the value of k-factor will remain constant at constant supply pressure. The k-factor is estimated from the data measured from the stationary test and using equation 2.39 (see Chapter 2).

For example, at 30kPa pressure (i.e. $H \approx 3m$), the measured flow rate is 2.94L/s and the angular speed if zero as the turbine is stationary (i.e. ω=0). The turbine radius is 200mm and the total exit nozzle area of CPT is 0.000397m². The real exit velocity is

equal to the total flow rate divided by the total exit nozzle area, making the exit velocity at 30kPa equal to 7.40m/s as seen in Figure 5.2.

Therefore, $k = \frac{2gH + R^2\omega^2}{\left(\frac{\dot{m}}{\rho A}\right)^2} - 1 = \frac{2\times 30 + 0}{\left(\frac{2.94}{1000 * 0.000397}\right)^2} - 1 = 0.09$

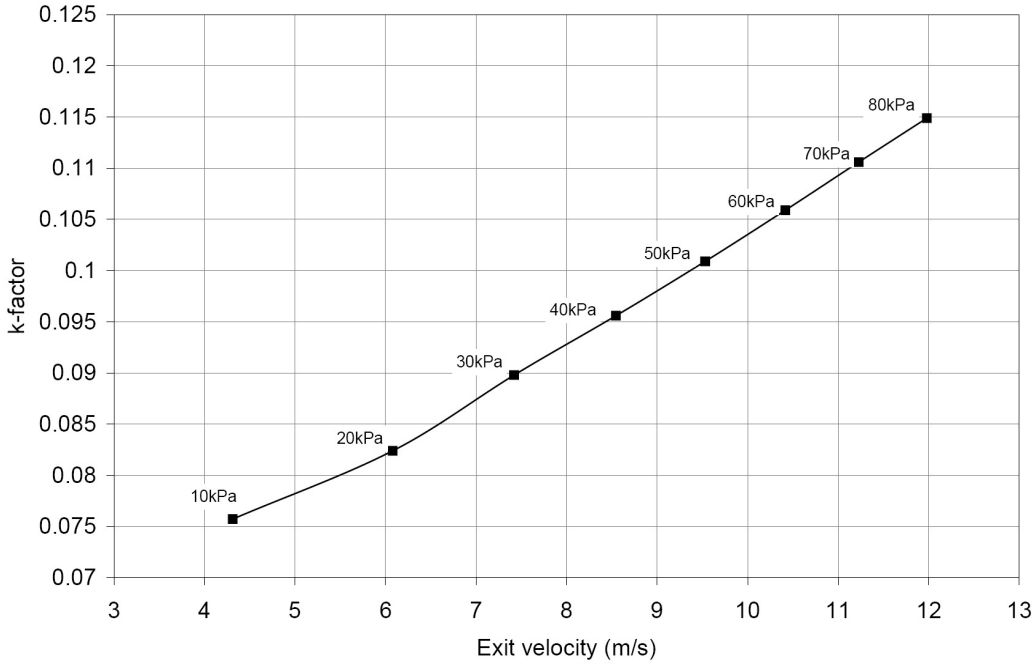

Figure 5.2 Experimentally estimated k-factor for CPT at stationary condition

In classic fluid dynamic analysis of a nozzle or an orifice a term called coefficient of discharge (C_d) is used to represent fluid frictional loss. The coefficient of discharge is equal to ratio of measured mass flow rate to the ideal mass flow rate i.e. $C_d = \frac{\dot{m}_{real}}{\dot{m}_{ideal}}$ (White, 1986). Here $\dot{m}_{real}$ is equal to the measured flow rate, while the $\dot{m}_{ideal} = \rho \times A \times V_{ideal}$ (i.e. equal to the product of density of water times the total exit nozzle area times the ideal velocity $V_{ideal} = \sqrt{2gH}$). Example of calculated coefficient of discharge for a supply pressure of 30kPa (i.e. gH) and total exit nozzle area is equal to 0.000397m² is shown below,

$$V_{ideal} = \sqrt{2gH} = \sqrt{2*30} = 7.75 m/s$$

Assuming density of water equal to 1000kg/m³,

$$\dot{m}_{ideal} = \rho \times A \times V_{ideal} = 1000 \times 0.000397 \times 7.75 = 3.08 kg/s$$

From Figure 5.1 and Table 5.1 the measured mass flow rate is equal to 2.95kg/s.

Therefore, $C_d = \frac{\dot{m}_{real}}{\dot{m}_{ideal}} = \frac{2.95}{3.08} = 0.958$

5.3 Performance characteristics of rotating cross pipe turbine

Figure 5.3 shows the electrical power and flow rate characteristics of CPT at constant supply pressure with V-ring lip rotary seal arrangement (as shown in Figure 3.17 in Chapter 3) attached at the inlet to prevent any water leakage. The test procedure used to conduct this power test is explained in section 4.4 of Chapter 4. The CPT has a mean turbine diameter of 400mm and total exit turbine nozzle area of 0.000397m² (two 15.9mm diameter solid stream nozzles). It can be seen that the water flow rate increases at constant supply pressure with increase in rotational speed. This shows the centrifugal pumping effect causing the flow rate to increase at higher rotational speed. Further, it can be seen from Figure 5.3 that the effect of static head on the flow rate starts to diminishes at higher rotational speeds, as predicted by the theoretical analysis of simple reaction turbine discussed in Chapter 2.

Table 5.2 Measured electrical power output and supply flow rate at two sample supply pressures from the CPT

Supply Pressure (kPa)	Speed (rpm)	Time required for 0.1m³ of water to flow through the turbine (s)	Gen. Output Voltage (Volt)	Gen. Output Current (Amp)	Flow Rate (L/s)	Flow rate (m³/s)	Electrical Power (W)
30	290	26.84	27.32	0.00	3.73	0.00373	0.00
30	252	28.15	23.76	0.47	3.55	0.00355	11.22
30	227	29.02	21.38	0.73	3.45	0.00345	15.57
30	218	29.32	20.56	0.79	3.41	0.00341	16.27
30	210	29.60	19.78	0.88	3.38	0.00338	17.39
30	200	29.93	18.84	1.00	3.34	0.00334	18.86

30	188	30.32	17.71	1.15	3.30	0.00330	20.28
30	174	30.77	16.39	1.30	3.25	0.00325	21.32
30	156	31.33	14.70	1.50	3.19	0.00319	22.00
30	140	31.79	13.19	1.70	3.15	0.00315	22.45
30	124	32.22	11.68	1.89	3.10	0.00310	22.09
30	93	32.94	8.76	2.21	3.04	0.00304	19.36
30	74	33.30	6.97	2.48	3.00	0.00300	17.29
Supply Pressure (kPa)	Speed (rpm)	Time required for 0.2m³ of water to flow through the turbine (s)	Gen. Output Voltage (Volt)	Gen. Output Current (Amp)	Flow Rate (L/s)	Flow rate (m³/s)	Electrical Power (W)
80	525	32.06	49.46	0.00	6.24	0.0062	0.0
80	489	32.97	46.06	0.65	6.07	0.0061	30.1
80	470	33.46	44.27	1.03	5.98	0.0060	45.6
80	447	34.05	42.11	1.43	5.87	0.0059	60.2
80	423	34.68	39.85	1.88	5.77	0.0058	75.1
80	403	35.20	37.96	2.24	5.68	0.0057	85.0
80	378	35.85	35.61	2.65	5.58	0.0056	94.4
80	350	36.57	32.97	3.12	5.47	0.0055	102.9
80	316	37.41	29.77	3.69	5.35	0.0053	109.8
80	286	38.14	26.94	4.09	5.24	0.0052	110.1
80	264	38.63	24.87	4.38	5.18	0.0052	108.9
80	227	39.44	21.38	4.90	5.07	0.0051	104.8
80	197	40.04	18.56	5.49	5.00	0.0050	101.9
80	164	40.61	15.45	6.03	4.92	0.0049	93.2

The flow rate data collected from the power test of the CPT is used to estimate the dynamic k-factor. Figure 5.3 and Table 5.2 also shows the electrical power produced by CPT for 30kPa and 80kPa supply pressures. For 30kPa supply pressure the maximum electrical power of 22.45W is produced at about 140rpm. It can be seen that the maximum power point (MPP) for this type of turbine depends on the supply pressure and as the supply pressure is increased the MPP shifts to the higher rotational speed. At 80kPa the maximum electrical power of 110.1W is produced at about 286rpm. It can be seen that the maximum no load rotational speed of the CPT at 30kPa (i.e. ≈ 3m head) supply pressure is only 290rpm, this is due to the large diameter of the turbine. As discussed in section 2.4 in Chapter 2, for turbine to rotate at high speed at low heads a small diameter rotor is required. Most of the electric generators perform poorly at low speeds. As a result the direct coupling of low speed hydro turbines to electric generators is not efficient. Low speed turbines require additional speed step-up power transmission, such as gearbox, belt pulley or chain and sprocket. This adds an extra cost of speed

change transmission components, and add to the installation cost of micro-hydro or low head hydro systems, making the low head micro hydro a weak competitor. Even at higher supply pressure of 80kPa (i.e. ≈ 8m head) the no load rotational speed of CPT is only 525rpm and the maximum power is produced at almost half this speed (i.e. 286rpm). So a large diameter turbine for low head micro-hydro installation is not suitable for producing electrical power very efficiently.

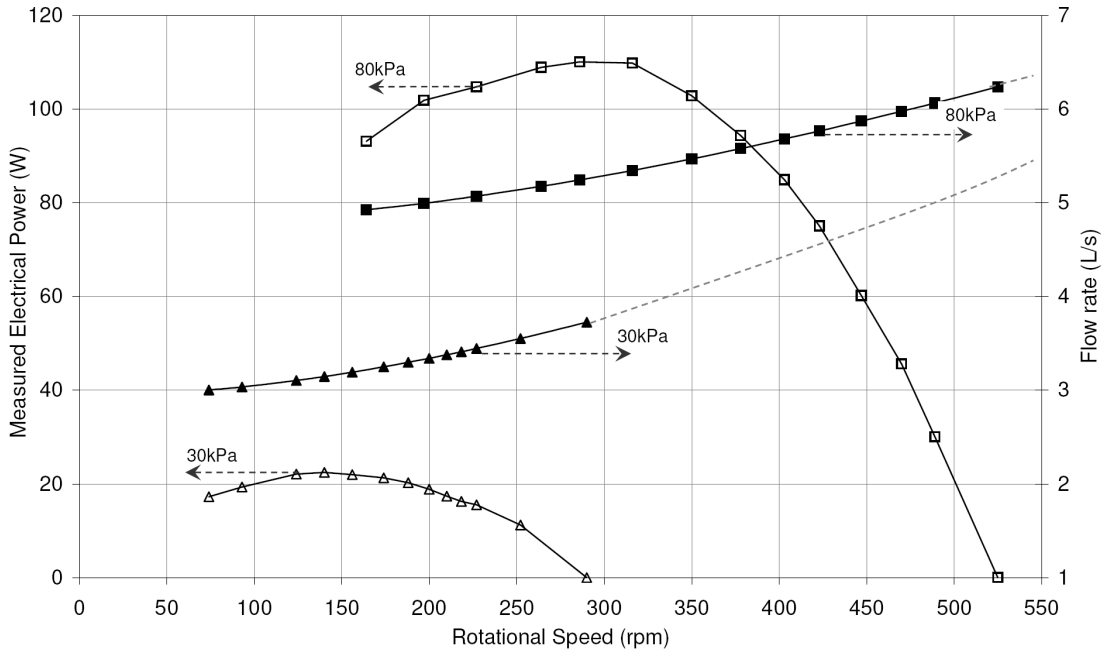

Figure 5.3 Measured electrical power and flow rate characteristics of CPT

5.3.1 Fluid frictional loss characteristics (k-factor)

Figure 5.4 and Table 5.3 shows the characteristic of the estimated *k*-factor for CPT. As discussed in Chapter 2 the k-factor represents the fluid frictional power losses and is a function of rotational speed and flow rate. The relative velocity of the exiting water jets is directly proportional to the flow rate. With the increase in rotational speed, the flow rate increases due to centrifugal pumping effect and so does the relative velocity. A linear increase in the value of k-factor with relative velocity is observed from Figure 5.4. It can be said from Figure 5.4 and Table 5.3 that the dependency of k-factor on the relative velocity is more prominent at higher rotational speeds because more water tends to flow through the same exit nozzle area of the turbine at constant supply pressure due to

the centrifugal pumping effect. It is seen from Figure 5.4 that the increasing trend of k-factor as seen in the stationary tests is also seen during the rotary power test and the values of k-factor estimated from stationary and power test are very close for corresponding relative velocity values.

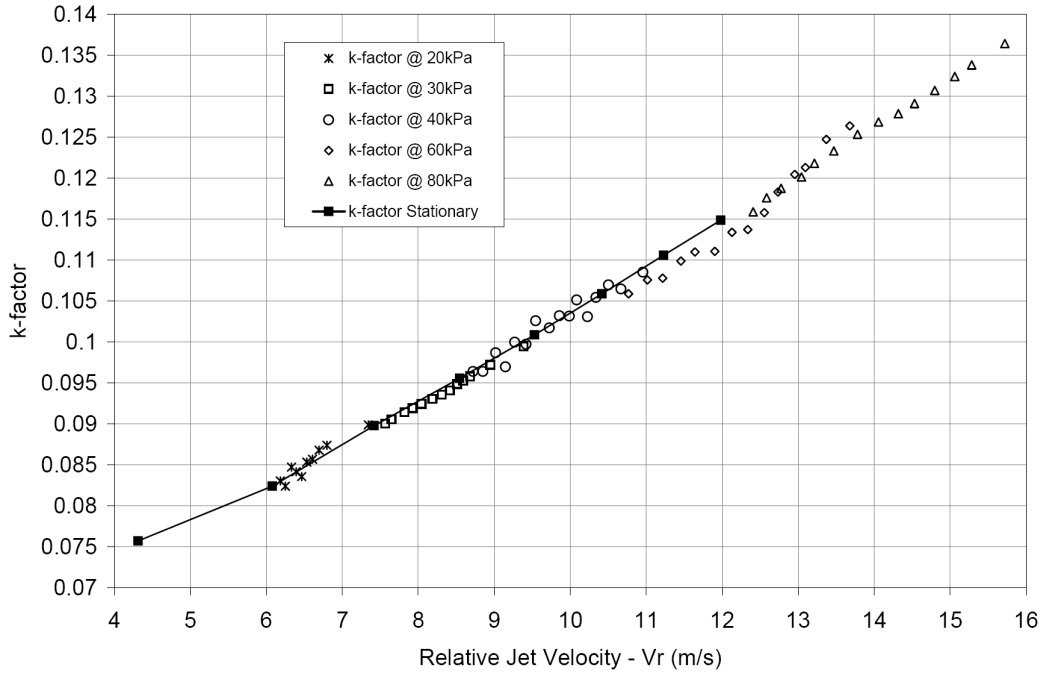

Figure 5.4 Estimated k-factor characteristics at relative jet velocities for CPT

The k-factor values are estimated using equation 2.39 (see Chapter 2) and the experimental data collected from power test carried on CPT as shown in Table 5.2. The estimated values of relative and absolute velocities of water jet and the linear velocity of the nozzle in opposite direction to the flow of water for two sample supply pressures are shown in Table 5.3 with estimated values for the corresponding k-factor. Following is a solved example of k-factor estimation at 30kPa supply pressure and 200rpm, the effective turbine radius is 0.2m,

$$k = \frac{2gH + R^2\omega^2}{(V_r)^2} - 1 = \frac{2\times 30 + (0.2)^2 \times (20.9)^2}{(8.42)^2} - 1 = 0.094$$

Further, at 200rpm the fluid frictional power loss is estimated as discussed in Chapter 2 using the fluid frictional power loss component $\frac{1}{2}\dot{m}kV_r^2$ of equation 2.36.

Table 5.3 Estimated values of k-factor at different rotational speeds and corresponding relative velocity of the exit jet for CPT at two sample pressures

Supply pressure (kPa)	Flow rate (m^3/s)	Speed (rpm)	V_r (m/s)	U (m/s)	V_a (m/s)	*k*-factor
30	0.00373	290	9.39	6.07	3.32	0.099
30	0.00355	252	8.95	5.28	3.67	0.097
30	0.00345	227	8.68	4.75	3.93	0.096
30	0.00341	218	8.59	4.57	4.02	0.095
30	0.00338	210	8.51	4.40	4.12	0.095
30	0.00334	200	8.42	4.19	4.23	0.094
30	0.00330	188	8.31	3.94	4.37	0.094
30	0.00325	174	8.19	3.64	4.54	0.093
30	0.00319	156	8.04	3.27	4.78	0.092
30	0.00315	140	7.93	2.93	4.99	0.092
30	0.00310	124	7.82	2.60	5.22	0.091
30	0.00304	93	7.65	1.95	5.70	0.091
30	0.00300	74	7.57	1.55	6.02	0.090
Supply pressure (kPa)	Flow rate (m^3/s)	Speed (rpm)	V_r (m/s)	U (m/s)	V_a (m/s)	*k*-factor
80	0.0062	525	15.72	10.99	4.73	0.136
80	0.0061	489	15.28	10.24	5.05	0.134
80	0.0060	470	15.06	9.84	5.22	0.132
80	0.0059	447	14.80	9.36	5.44	0.131
80	0.0058	423	14.53	8.85	5.68	0.129
80	0.0057	403	14.32	8.44	5.88	0.128
80	0.0056	378	14.06	7.91	6.14	0.127
80	0.0055	350	13.78	7.33	6.45	0.125
80	0.0053	316	13.47	6.61	6.85	0.123
80	0.0052	286	13.21	5.99	7.23	0.122
80	0.0052	264	13.04	5.53	7.52	0.120
80	0.0051	227	12.77	4.75	8.02	0.119
80	0.0050	197	12.58	4.12	8.46	0.118
80	0.0049	164	12.41	3.43	8.97	0.116

5.3.2 Power loss characteristics

Figure 5.5 shows the power loss characteristics curves for the DC motor, V-ring rotary seal and the cross pipe turbine drag operating at two sample pressures of 30kPa and 80kPa. It can be seen from Figure 5.5 that the V-ring frictional power loss increases with increase in the supply pressure; this is due to increase in the surface contact force between the V-ring lip and the rotating stainless steel ring attached to the inlet port of the turbine as illustrated in Figure 3.17 of Chapter 3. These power loss values are added to the electrical power generated at respective supply pressure and rotational speeds to get the power produced by the turbine as discussed in section 4.5 of Chapter 4. As shown in Figure 5.5 second order polynomials are drawn to fit the power loss curves and then the

equations for each of these polynomial curves is used to estimate the exact value of power loss at different rotational speeds. For example as shown in Figure 5.5, power loss associated with V-ring lip seal operating at 80kPa is represented by $y = 0.0006 * x^2 - 0.0324 * x + 25.721$ (here y is the power loss in V-ring lip seal and x is the corresponding rotational speed).

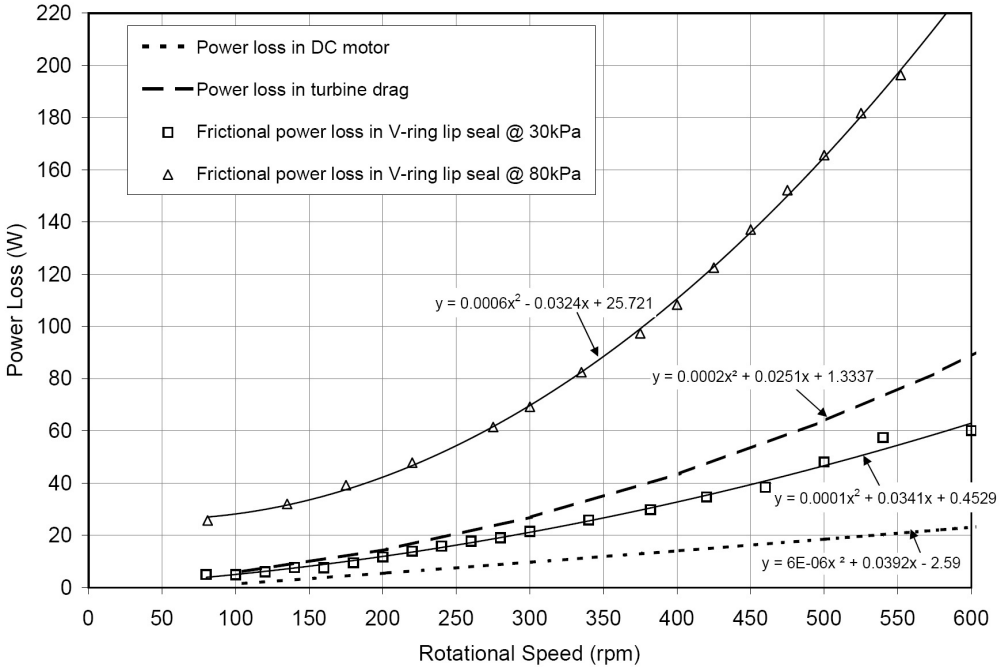

Figure 5.5 Measured power loss characteristic curves associated with DC motor, V-ring rotary seal and the turbine drag for CPT at 30kPa and 80kPa supply pressure

Figure 5.5 also shows power loss in the DC motor/generator, which is very small as compared to other power loss components. The power loss due to turbine air drag is higher then the frictional power loss in the V-ring rotary seal when the turbine is operating at 30kPa. While at 80kPa pressure the frictional power loss in the V-ring rotary seal exceeds the power loss in turbine air drag. This shows the major power loss is associated with V-ring lip seal and turbine drag. As the CPT design has two protruding arms, there is significant amount of power required to over come the air drag on the turbine. This makes the CPT to slow down causing further power loss; the power is lost in form of kinetic energy of the water leaving the turbine. The absolute velocity of the water jet leaving the turbine is high at low rotational speed. It can be seen from Table 5.2 and Table 5.3 that even at zero electrical load the absolute velocity is not zero or even

any were close to zero (For example, at 80kPa and 525rpm absolute velocity is 4.73m/s while the electrical load is zero, see Table 5.3) .

5.3.3 Turbine power and turbine efficiency

Table 5.4 and Figure 5.6 shows the estimated power output and efficiency characteristics of the CPT with V-ring seal. In Table 5.4 $\dot{W}_T$ represents the mechanical power produced by the turbine and $\dot{W}_E$ represents the electrical power generated by the DC motor/generator. As discussed in Chapter 4 the turbine power is estimated by adding the sum of power loss in DC motor/generator, rotary seal and turbine drag to the electrical power output from the generator. For example from Figure 5.5 at 80kPa supply pressure and 286rpm the individual power loss components are calculated as follows,

Power loss in V-ring rotary lip seal (90mm diameter V-ring seal) @ 80kPa and 286rpm is, , $y = 0.0006*(286)^2 - 0.0324*286 + 25.721 = 65.53W$

Power lost to overcome turbine air drag at 286rpm is,

$$y = 0.0002*(286)^2 + 0.0251*286 + 1.3337 = 24.87W$$

Power loss in DC motor/generator at 286rpm is,

$$y = 0.000006*286^2 + 0.0392*286 - 2.59 = 9.11W$$

Therefore the sum of total power loss is equal to 65.53+24.87+9.11 = 99.49W this is then added to the measured electrical power of 110.1W to get the turbine power of 209.59W, as shown in Table 5.4.

Table 5.4 Estimated power outputs and energy conversion efficiencies for CPT at 80 kPa supply pressure (sample)

Supply pressure (kPa)	Flow Rate (L/sec)	Turbine Speed (rpm)	Electrical Power $\dot{W}_E$ (W)	Total Power Loss $\dot{W}_{Loss}$ (W)	Turbine Power $\dot{W}_T$ (W)	Turbine efficiency $\eta_t = \frac{\dot{W}_T}{\dot{m}\,gh}$ %	Overall efficiency $\eta_o = \frac{\dot{W}_E}{\dot{m}\,gh}$ %
80	6.24	525	0.00	263.31	263.31	52.76	0.00
80	6.07	489	30.08	232.75	262.83	54.16	6.20
80	5.98	470	45.60	217.46	263.06	55.01	9.54
80	5.87	447	60.21	199.73	259.94	55.33	12.82

80	5.77	423	75.07	182.13	257.20	55.75	16.27
80	5.68	403	84.96	168.18	253.14	55.69	18.69
80	5.58	378	94.36	151.65	246.01	55.12	21.14
80	5.47	350	102.87	134.33	237.20	54.21	23.51
80	5.35	316	109.84	115.00	224.84	52.58	25.68
80	5.24	286	110.10	99.49	209.59	49.96	26.24
80	5.18	264	108.93	89.03	197.96	47.80	26.30
80	5.07	227	104.78	73.22	177.99	43.88	25.83
80	5.00	197	101.88	62.01	163.89	41.01	25.50
80	4.92	164	93.16	51.36	144.51	36.68	23.65

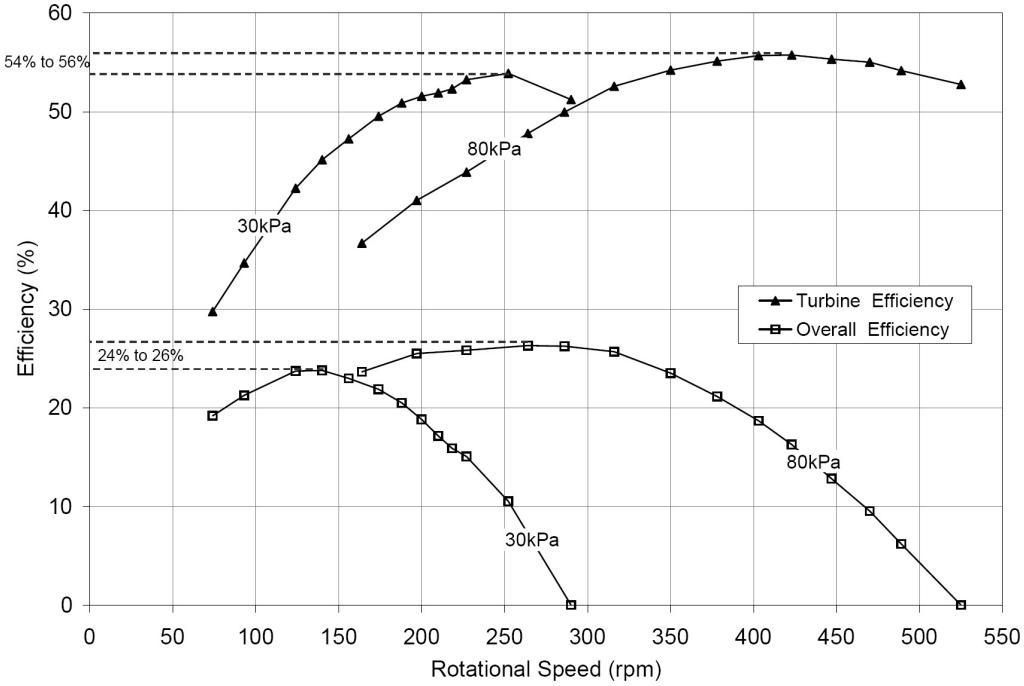

Figure 5.6 Estimated turbine and electrical efficiency curves for CPT

Figure 5.6 shows the turbine efficiency and the overall efficiency of CPT, it can be seen that the overall efficiency is about 24% to 26%. This low efficiency is attributed to the small amount of power supplied to the generator, as the DC generator used for testing has high power capacity and its performance is poor at low power (torque). Further it can be observed from Figure 5.6 that CPT can convert low head hydro energy to mechanical energy with an efficiency of around 54% to 56%. CPT also shows very constant turbine efficiency characteristics over a wide range of rotational speeds, i.e. from Figure 5.6 at 30 kPa and 240 rpm turbine efficiency is about 54%, similarly at 80 kPa and 470 rpm the turbine efficiency is about 54%. However, the power loss to overcome the turbine drag is large and so this design of two arms is not efficient. Because

of this a simple reaction turbine with disk shape rotor is proposed and investigated further in this research.

5.3.4 Energy balance analysis

Energy balance analysis is done to verify the accuracy and dependability of the experimental data and procedures. Figure 5.7 and Table 5.5 shows the energy balance of sample data from the performance tests conducted on the CPT, this is based on the governing equation 2.36 discussed in Chapter 2. The rate of energy input is estimated from the measured flow rate and the measured supply pressure as $\dot{m}\,gH$. The mechanical turbine power is estimated as discussed earlier in section 5.3.3 and section 4.5 in Chapter 4. The fluid frictional power loss is estimated from the measured flow rate, estimated k-factor and estimated relative velocity as $\frac{1}{2}\dot{m}\,kV_r^{\,2}$. In addition, the kinetic power lost with the water leaving the turbine is estimated from the measured flow rate and estimated absolute velocity as $\frac{1}{2}\dot{m}V_a^{\,2}$. For example, it can be seen from Figure 5.7 and Table 5.5 at 350rpm the input power is 437.54W, where as the sum of output is equal to the 416.16W, this shows that there is an error of 21.39W in the estimation (i.e. ≈ 5%). This error may be due to instrumental uncertainty and the fact that the turbine rotates in wet environment (water drops splashing) while producing power where as the turbine drag power loss is estimated only in normal atmospheric air and there will be small amount of unaccounted power loss. Overall the energy balance around the maximum power point and the maximum efficiency point is within ±8%.

Finally the instrumentation uncertainty analysis shows the maximum relative uncertainty of ±4.19% in the estimation of the total output power $\dot{W}_{Out} = \dot{W}_T + \dot{W}_{Ff} + \dot{W}_{Ke}$ and the relative uncertainty of ±2.69% in the estimation of the hydro input power $\dot{W}_{In}$ (see Table - C-19, Appendix C), making the overall relative uncertainty of ±6.9%. After considering this fact of relative instrumental uncertainty of ±6.9% and some small amount of unaccounted power loss in turbine drag when operating under wet environment (splashing water droplets), it can be said that the overall energy

balance analysis gives good confidence in the experimental data measurements and procedures used in the performance testing of the CPT.

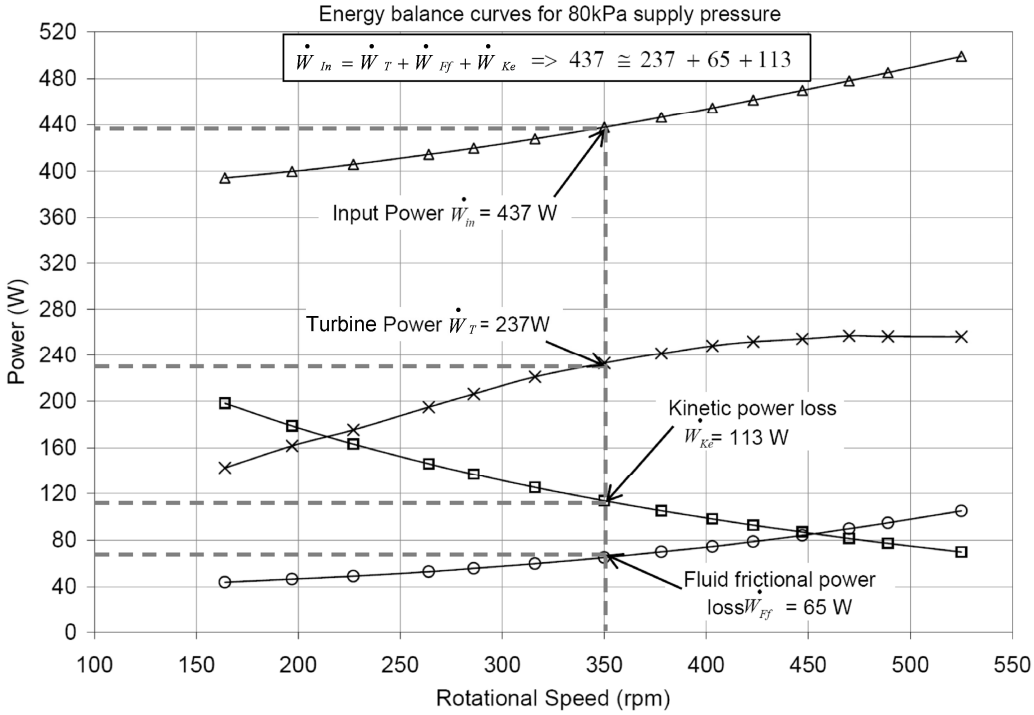

Figure 5.7 Energy balance curves of CPT performance test results

Table 5.5 Energy balance analysis for CPT tested under a supply pressure of 80kPa

Supply pressure (kPa)	Turbine Speed (rpm)	Turbine power $\dot{W}_{T}$ (W)	+	Fluid Frictional loss $\dot{W}_{Ff}$ (W)	+	Kinetic power loss $\dot{W}_{Ke}$ (W)	=	Sum of output power $\dot{W}_{Out}$ (W)	≈	Input hydro power $\dot{W}_{In}$ (W)
80	525	263.31	+	105.15	+	69.75	=	438.21	≈	499.11
80	489	262.83	+	94.79	+	77.20	=	434.81	≈	485.24
80	470	263.06	+	89.74	+	81.44	=	434.24	≈	478.17
80	447	259.94	+	84.04	+	86.88	=	430.86	≈	469.83
80	423	257.20	+	78.63	+	92.90	=	428.73	≈	461.39
80	403	253.14	+	74.46	+	98.24	=	425.85	≈	454.59
80	378	246.01	+	69.91	+	105.24	=	421.16	≈	446.30
80	350	237.20	+	65.09	+	113.87	=	416.16	≈	437.54
80	316	224.84	+	59.79	+	125.53	=	410.16	≈	427.65
80	286	209.59	+	55.76	+	136.91	=	402.26	≈	419.54
80	264	197.96	+	52.90	+	146.21	=	397.07	≈	414.13
80	227	177.99	+	49.14	+	163.19	=	390.32	≈	405.64
80	197	163.89	+	46.53	+	178.79	=	389.21	≈	399.60
80	164	144.51	+	43.93	+	198.31	=	386.76	≈	393.97

5.4 Stationary performance characteristics of SRT prototype 1

Figure 5.8 shows the comparison between the estimated torque based on flow rate measurement and the shaft torque based on the force measurement taken from the stationary test unit shown in Figure 4.7, the stationary test procedure used to conduct this test is explained in section 4.3.1 of Chapter 4, ideally both these torques should be equal. Figure 5.8 further shows the minimum amount of water flowing through the SRT prototype 1 at different supply pressures at stationary conditions. The SRT prototype1 has a mean turbine diameter of 243 mm and the total exit nozzle area of 0.00144m². When the turbine is stationary, the flow rate depends on the supply pressure and total exit nozzle area. When the turbine is stationary, there is no centrifugal pumping effect in action. The stationary flow rate data is used to estimate the theoretical stationary torque (estimated torque) based on the flow rate and estimated exit velocity of the water jet. As discussed in Chapter 2, the estimated torque of turbine is a product of total mass flow rate, turbine radius and absolute velocity of the water leaving the nozzles (see equation 2.9, Chapter 2).

For example, from Table 5.6 and Figure 5.8 at 25kPa pressure the volume flow rate of water flowing through the turbine is 9.926L/s. Assuming the density of water @ 20°C equal to 1000kg/m³ the mass flow rate is equal to $\dot{m}$ = 9.926kg/s. Further, as the turbine is stationary the relative velocity and the absolute velocity of the water jet are equal. Here it is assumed that all water particles leave the turbine tangentially like a solid water jet. Therefore, the absolute velocity of water leaving the nozzles is equal to,

$$V_a = \frac{9.926\times10^{-3}}{0.00144} = 6.893 \ m/s$$

Radius of the SRT prototype 1 is equal to 121.5mm.

Therefore, the estimated torque is equal to

$$T_{estimated} = \dot{m}V_a R = 9.9\times6.893\times0.1215 = 8.312Nm$$

As discussed in section 4.3.1 of chapter 4 the shaft torque T_g is measured using a force sensor (load cell) connected to the turbine shaft through the torque arm of 0.19m

length. Table 5.6 shows the force measurements for different pressures and the corresponding flow rates. The shaft torque is calculated from the measured data, for example from Table 5.6 at 25kPa pressure 41.27N of force is acting on the torque arm of 0.19m length.

Therefore, $T_{shaft} = 41.27 \times 0.19 = 7.84 Nm$

Table 5.6 Measured flow rate and force transducer readings at different pressures for SRT prototype 1

SRT Prototype 1 (Ø243mm) Torque arm = 0.19m			
Obs. No.	Pressure gauge reading (kPa)	Time required for $V = 0.2m^3$ water flow through turbine t (Sec)	Force transducer reading F_{arm} (N)
1	10	31.61	16.74
2	15	25.87	24.90
3	20	22.47	33.00
4	25	20.15	41.27
5	30	18.45	48.41
6	35	17.13	57.05
7	40	16.07	64.24
8	45	15.20	72.67
9	50	14.46	81.52
10	55	13.83	89.20

Theoretically the measured shaft torque should be equal to the estimated torque. However, it can be seen from Figure 5.8 that the measured shaft torque is less then the estimated torque and this deviation is very consistent. This deviation in two torque values is attributed to number of factors namely instrumental uncertainty, uncertainty in the estimation of the total exit nozzle area and the assumption that all water particles leave the turbine tangentially. In reality, it was seen during the stationary test that the exit water jet scatters while it leaves the turbine nozzles and does not leave as a solid stream jet. This scattering of the water jet produces less torque as compared to the solid stream water jet.

The percentage difference in the estimated and the measured shaft torque over the range of pressure is estimated to be approximately –6% (see Table - C-1, Appendix C). While the uncertainty analysis of the measured data shows a relative uncertainty of ±4.41% in the estimation of the estimated torque based on the flow rate (see Table - C-6,

Appendix C) and a relative uncertainty of ±1.13% in the estimation of shaft torque (see Table – C-7, Appendix C).

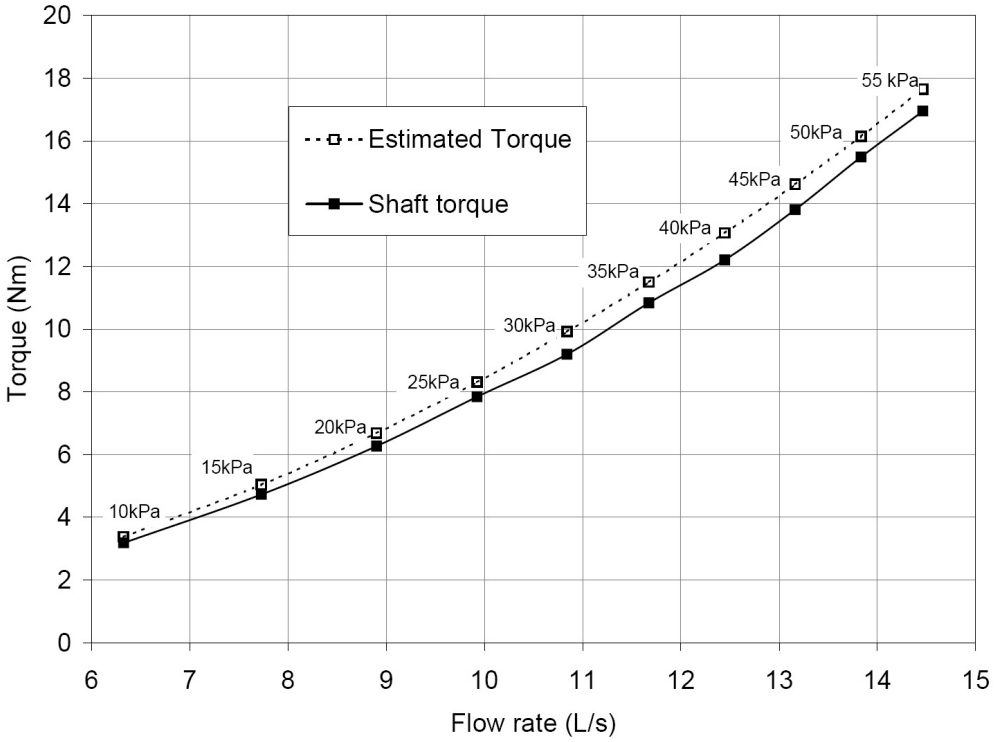

Figure 5.8 Comparison between shaft torque and estimated torque for SRT prototype 1

Figure 5.9 shows the estimated k-factor for stationary condition for different exit velocities at different supply pressures. When the turbine is stationary the value of k-factor increases with increase in supply pressure, this is due to increase in flow rate and in turn the velocity of the water leaving the exit nozzles at higher pressures. As discussed in Chapter 2 the k-factor represents the fluid frictional power loss associated with the turbine and exit nozzles. When the turbine is stationary (i.e. $\omega=0$) there is no centrifugal pumping effect so for the given turbine geometry the value of k-factor will remain constant for a constant supply pressure. The k-factor is estimated from the data measured during the stationary test of SRT prototype 1 and using equation 2.39 from Chapter 2. This information is important for SRT computer modelling and performance prediction.

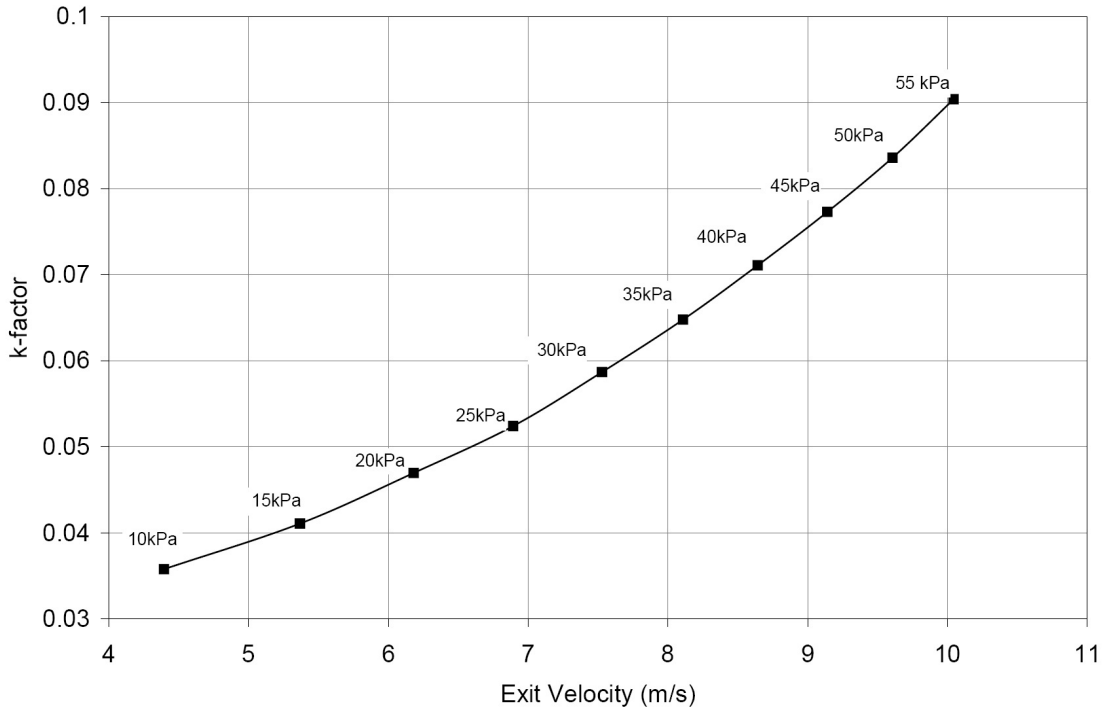

Figure 5.9 Experimentally estimated k-factor at different pressures for SRT prototype 1

For example, at 25kPa pressure (approximately 2.5m water head), the estimated mass flow rate is 9.926kg/s and the angular speed is zero as the turbine is stationary (i.e. ω=0). The mean turbine radius is 121.5mm and the total exit nozzle area for SRT prototype 1 is 0.00144m². The exit velocity is equal to the total volume flow rate (m³/s) divided by the total exit nozzle area, thus the exit velocity at 25kPa is equal to 6.893m/s as seen in Figure 5.9.

Therefore @ 25kPa, $k = \frac{2gH + R^2\omega^2}{\left(\frac{\dot{m}}{\rho A}\right)^2} - 1 = \frac{2\times 25 + 0}{\left(\frac{9.926}{1000 * 0.00144}\right)^2} - 1 = 0.052$

5.5 Performance characteristics of SRT prototype 1

Figure 5.10 shows the electrical power and flow rate characteristics of SRT prototype1 at constant supply pressure with V-ring rotary seal arrangement as shown in Figure 3.17 in Chapter 3 which is attached at the inlet to prevent any water leakage. SRT prototype 1 has the mean turbine diameter of 243mm and total exit turbine nozzle area of 0.00144m² as discussed in design and manufacture of SRT prototype 1 in section 3.2.2.2

of Chapter 3. It can be seen from Figure 5.10 that at constant supply pressure the water flow rate increases with increase in rotational speed. This is due to the effect of centrifugal pumping as discussed in the theoretical analysis of simple reaction turbine in Chapter 2. The governing equation for the mass flow rate when the turbine is rotating is written as $\dot{m} = \frac{\rho A\sqrt{2gH + R^2\omega^2}}{\sqrt{1+k}}$. It can be seen from Figure 5.10 that the effect of static head on the flow rate diminishes at high rotational speed.

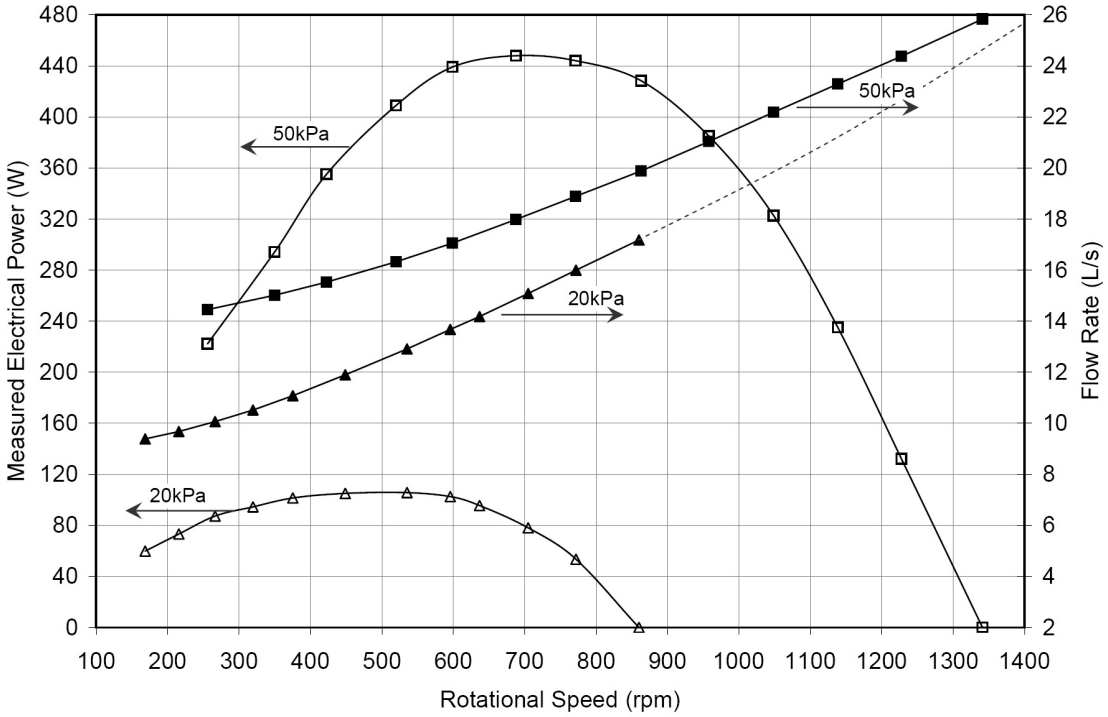

Figure 5.10 Measured electrical power and flow rate characteristics of SRT prototype 1 with V-ring lip seal at the inlet

It is clear from the experimental results shown in Table 5.2 and Table 5.7 that SRT prototype 1 spins at higher speeds than CPT at same supply pressures (head), this is mainly due to smaller turbine diameter. The SRT design has the advantage of flexibility to vary the turbine diameter without having to vary the total exit nozzle area and vice versa.

The flow rate data collected from the power test of the SRT is used to estimate the dynamic k-factor. Figure 5.10 also shows the maximum power point for SRT prototype 1 at 20kPa and 50kPa supply pressures. For 20kPa supply pressure the maximum electrical

power of 105.7W is produced at about 535rpm and at 50kPa supply pressure the maximum electric power is 447.8W @ 688rpm. So it can be said that the maximum power point (MPP) for SRT prototype 1 depends on the supply pressure and as the supply pressure is increased the MPP shifts to a higher rotational speed. Further it can be seen from Figure 5.10 that at 50kPa supply pressure the electrical power output at 520rpm is 409W and at 869rpm is 428W (almost constant and very close to MPP). From these observations, it can be said that SRT prototype 1 has an optimum operating speed between 500rpm to 900rpm at 50kPa. So SRT prototype 1 design is suitable for installation at micro-hydro site with net head of 5m (≈50kPa). At 5m head SRT prototype 1 can generate 50 Hz AC when coupled with 8 pole electrical generator operating at 750rpm.

Table 5.7 Estimated electrical power and flow rate data for SRT prototype 1 with V-ring seal arrangement

Supply Pressure (kPa)	Speed (rpm)	Time required for 0.4m³ of water to flow through the turbine (s)	Gen. Output Voltage (Volt)	Gen. Output Current (Amp)	Flow Rate (L/s)	Flow rate (m³/s)	Electrical Power (W)
20	860	23.24	75.5	0	17.22	0.0172	0.0
20	772	24.96	71.2	0.75	16.01	0.0160	53.4
20	705	26.47	63.0	1.24	15.11	0.0151	78.1
20	637	28.15	57.2	1.67	14.21	0.0142	95.5
20	596	29.20	52.5	1.95	13.67	0.0137	102.6
20	535	30.93	46.4	2.28	12.91	0.0129	105.7
20	449	33.55	39.5	2.66	11.88	0.0119	105.1
20	375	36.03	33.6	3.02	11.08	0.0111	101.4
20	320	37.95	27.6	3.42	10.53	0.0105	94.5
20	267	39.65	22.6	3.87	10.07	0.0101	87.3
20	216	41.27	16.8	4.35	9.68	0.0097	73.2
20	169	42.51	12.2	4.91	9.39	0.0094	59.9
Supply Pressure (kPa)	Speed (rpm)	Time required for 0.4m³ of water to flow through the turbine (s)	Gen. Output Voltage (Volt)	Gen. Output Current (Amp)	Flow Rate (L/s)	Flow rate (m³/s)	Electrical Power (W)
50	1341	15.46	131.2	0.00	25.47	0.0255	0.0
50	1228	16.38	114.9	1.15	24.13	0.0241	132.1
50	1139	17.14	105.9	2.22	23.10	0.0231	235.0
50	1049	18.00	96.8	3.33	22.05	0.0220	322.6
50	958	18.98	87.7	4.39	21.02	0.0210	385.0
50	863	20.08	78.7	5.44	19.93	0.0199	428.3
50	771	21.13	69.4	6.40	18.91	0.0189	444.0
50	688	22.20	60.8	7.37	18.01	0.0180	447.8

50	599	23.41	51.3	8.56	17.12	0.0171	439.0
50	520	24.46	43.1	9.49	16.39	0.0164	409.0
50	423	25.71	33.0	10.77	15.58	0.0156	355.1
50	350	26.58	25.0	11.77	15.06	0.0151	294.2
50	256	27.62	17.3	12.83	14.51	0.0145	222.2

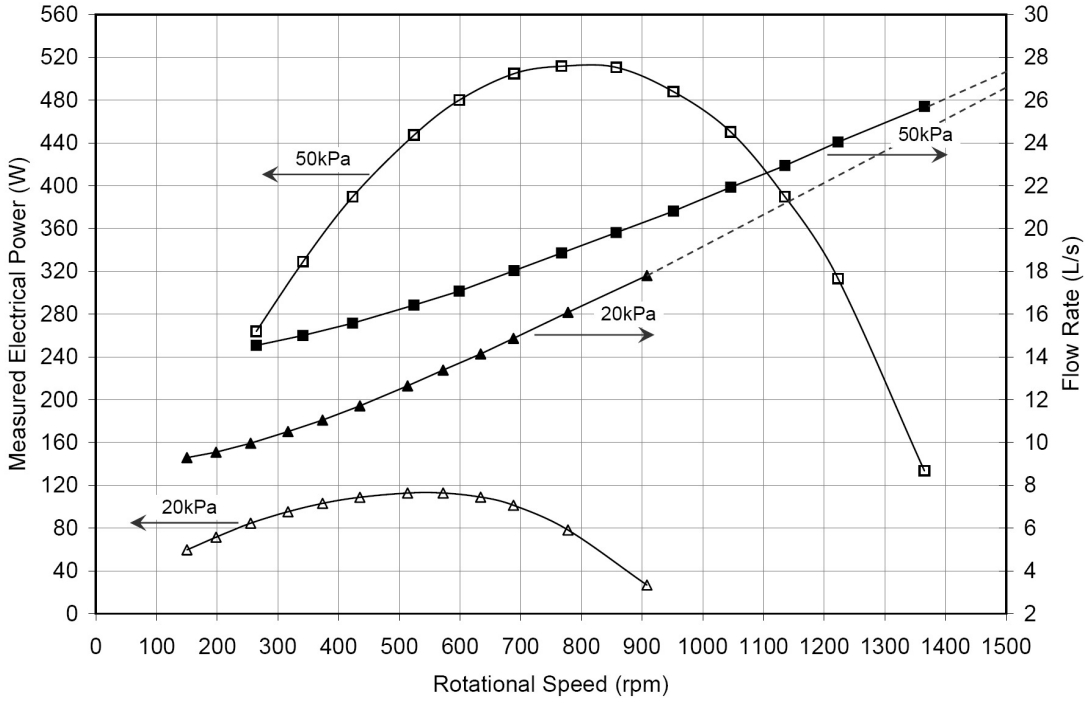

Figure 5.11 Measured electrical power and flow rate characteristics of SRT prototype 1 with mechanical seal NMS at the inlet

SRT prototype 1 is also tested with the nylon mechanical seal arrangement connected at the inlet to prevent water leakage. Figure 5.11 and Table 5.8 shows the electrical power and flow rate characteristics of the SRT prototype1 at constant supply pressure with the mechanical seal attached at the inlet. Preliminary observations of Figure 5.10 and Figure 5.11 shows that SRT prototype1 produces more electrical power and spins faster with the NMS arrangement as compared to the V-ring lip seal arrangement. This shows that the NMS has less frictional power loss as compared to V-ring seal. The rotary seal power loss test results are discussed in the following section. Most importantly, it is observed that both V-ring lip seal and NMS arrangement perform excellently in the prevention of water leaks.

Table 5.8 Measured electrical power and flow rate data for SRT prototype 1 with NMS arrangement

Supply Pressure (kPa)	Speed (rpm)	Time required for 0.4m³ of water to flow through the turbine (s)	Gen. Output Voltage (Volt)	Gen. Output Current (Amp)	Flow Rate (L/s)	Flow rate (m³/s)	Electrical Power (W)
20	908	22.37	85.53	0.31	17.84	0.0178	26.70
20	778	24.85	73.29	1.07	16.07	0.0161	78.22
20	688	26.86	64.81	1.56	14.86	0.0149	101.21
20	634	28.21	59.71	1.82	14.15	0.0142	108.82
20	572	29.87	53.90	2.09	13.36	0.0134	112.79
20	513	31.59	48.36	2.33	12.64	0.0126	112.64
20	435	34.05	40.97	2.65	11.72	0.0117	108.69
20	374	36.08	35.19	2.93	11.06	0.0111	103.16
20	317	38.00	29.82	3.19	10.51	0.0105	95.19
20	255	40.02	24.02	3.52	9.98	0.0100	84.48
20	198	41.74	18.65	3.84	9.57	0.0096	71.53
20	150	42.98	14.13	4.22	9.29	0.0093	59.58
Supply Pressure (kPa)	Speed (rpm)	Time required for 0.4m³ of water to flow through the turbine (s)	Gen. Output Voltage (Volt)	Gen. Output Current (Amp)	Flow Rate (L/s)	Flow rate (m³/s)	Electrical Power (W)
50	1365	15.55	128.58	1.04	25.66	133.49	0.0257
50	1223	16.63	115.19	2.72	24.01	313.12	0.0240
50	1135	17.36	106.94	3.64	23.00	389.70	0.0230
50	1046	18.17	98.55	4.57	21.97	450.14	0.0220
50	952	19.12	89.65	5.44	20.88	487.87	0.0209
50	857	20.15	80.76	6.32	19.81	510.53	0.0198
50	767	21.20	72.27	7.08	18.83	511.63	0.0188
50	689	22.17	64.89	7.78	18.00	504.67	0.0180
50	599	23.34	56.41	8.51	17.11	480.04	0.0171
50	524	24.32	49.36	9.06	16.41	447.25	0.0164
50	423	25.63	39.85	9.78	15.58	389.64	0.0156
50	341	26.61	32.14	10.24	15.00	328.98	0.0150
50	264	27.44	24.90	10.60	14.55	263.83	0.0145

5.5.1 Fluid frictional loss characteristics (k-factor)

Figure 5.12 and Figure 5.13 shows the characteristic curves of the estimated *k*-factor for SRT prototype 1. As discussed in Chapter 2 the k-factor represents the fluid frictional power losses and is a function of rotational speed and flow rate. While the relative velocity of the exiting water jets is directly proportional to the flow rate, with the increase in rotational speed, the flow rate increases due to centrifugal pumping effect and so does the relative velocity. A linear increase in the value of k-factor with relative velocity is observed from Figure 5.12 and Figure 5.13. It can be said from Figure 5.12 and Figure 5.13 that the dependency of k-factor on the relative velocity is more

prominent at higher rotational speeds because more water tends to flow through the same exit nozzle area of the turbine at constant supply pressure due to the centrifugal pumping effect. It can be seen from Figure 5.12 and Figure 5.13 that the increasing trend of k-factor in the stationary test and the rotary power test is very similar.

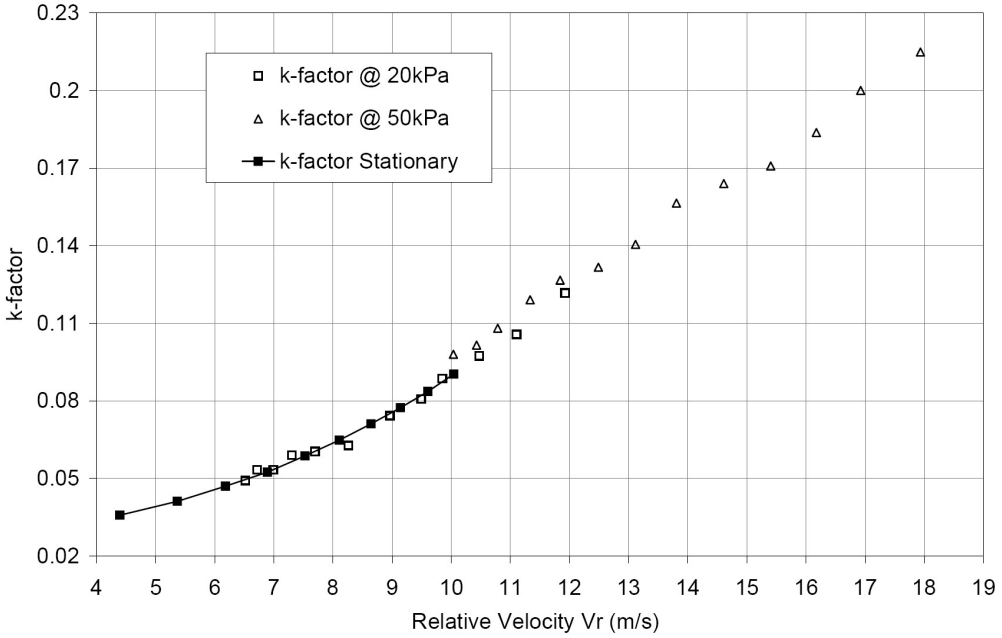

Figure 5.12 Estimated k-factor characteristics of SRT prototype 1 with V-ring lip seal at the inlet

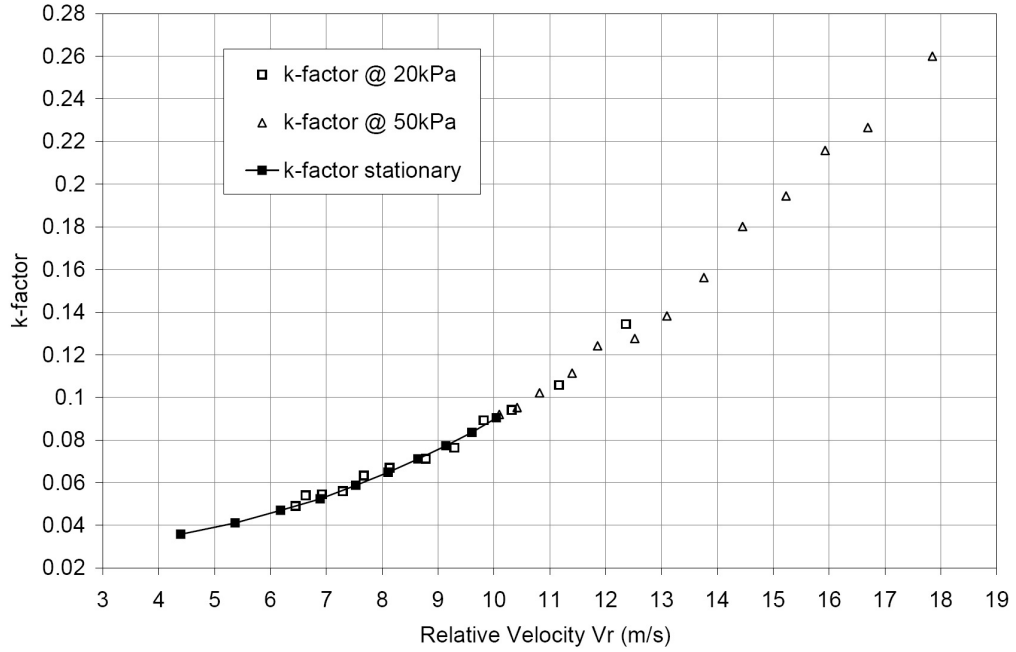

Figure 5.13 Estimated k-factor characteristics of SRT prototype 1 with mechanical seal NMS at the inlet

Table 5.9 shows the estimated values of V_r, V_a, U and the estimated values for the corresponding *k*-factor. The *k*-factor is estimated using equation 2.39 (see Chapter 2) and the experimental data collected from power test carried on SRT prototype-1. Following is a solved example of k-factor estimation at 50kPa supply pressure and 1049 rpm as shown in Table 5.9. The effective turbine radius is 0.1215m.

$$k = \frac{2gH + R^2\omega^2}{(V_r)^2} - 1 = \frac{2\times 50 + (0.1215)^2 \times (109.8)^2}{(15.4)^2} - 1 = 0.1708$$

The tendency of increase in the value of *k*-factor with increase in relative velocity is confirmed from repeated experiments and data analysis. The variation of k-factor is more dependent on relative velocity (V_r) and is a weak function of supply pressure (Head). The frictional power loss is proportional to the square of relative velocity even if k-factor is constant. The fact that k-factor is increasing with V_r, means fluid frictional power loss increases even more than usual with increase in V_r. Values of k-factor at very high relative velocities can be predicted through a stationary turbine test by simulating flow rates that are achieved at high rotational speeds using high pressure pumps. These predictions of k-factor can be then used as a basis for computer modeling of a SRT for real life installations at different low head hydro sites.

Table 5.9 Estimated values of k-factor at different rotational speeds and corresponding relative velocity of the exit jet for SRT prototype 1 with V-ring seal

Supply pressure (kPa)	Flow rate (m³/s)	Speed (rpm)	Vr (m/s)	U (m/s)	Va (m/s)	k-factor
20	0.0172	860	11.93	10.94	0.99	0.1217
20	0.0160	772	11.11	9.82	1.29	0.1057
20	0.0151	705	10.47	8.97	1.51	0.0974
20	0.0142	637	9.85	8.10	1.75	0.0886
20	0.0137	596	9.49	7.58	1.92	0.0807
20	0.0129	535	8.96	6.81	2.16	0.0742
20	0.0119	449	8.26	5.71	2.56	0.0627
20	0.0111	375	7.70	4.77	2.92	0.0604
20	0.0105	320	7.31	4.06	3.24	0.0590
20	0.0101	267	6.99	3.39	3.60	0.0533
20	0.0097	216	6.72	2.74	3.97	0.0533
20	0.0094	169	6.52	2.15	4.37	0.0491
Supply pressure (kPa)	Flow rate (m³/s)	Speed (rpm)	Vr (m/s)	U (m/s)	Va (m/s)	k-factor
50	0.0258	1341	17.94	17.05	0.88	0.2149
50	0.0244	1228	16.92	15.61	1.31	0.2000

50	0.0233	1139	16.17	14.48	1.69	0.1838
50	0.0222	1049	15.40	13.34	2.07	0.1708
50	0.0210	958	14.61	12.18	2.43	0.1640
50	0.0199	863	13.81	10.98	2.83	0.1565
50	0.0189	771	13.12	9.81	3.31	0.1405
50	0.0180	688	12.49	8.75	3.74	0.1317
50	0.0171	599	11.84	7.61	4.23	0.1267
50	0.0163	520	11.33	6.61	4.72	0.1191
50	0.0155	423	10.78	5.37	5.41	0.1081
50	0.0150	350	10.43	4.45	5.98	0.1016
50	0.0145	256	10.04	3.26	6.78	0.0980

5.5.2 Power loss characteristics

Figure 5.14 shows the individual power loss characteristics of the DC motor, V-ring rotary seal and the SRT prototype 1 air drag operating at two sample pressures of 20kPa and 50kPa. It can be seen from Figure 5.14 that the frictional power loss increases with increase in the supply pressure, this is due to increase in the surface contact force between the V-ring lip and the rotating stainless steel ring attached to the inlet port of the turbine as illustrated in Figure 3.17 of Chapter 3. These power loss values are added to the electrical power generated at given supply pressure and respective speeds to get the actual shaft power produced by the turbine as discussed in section 4.6 of Chapter 4.

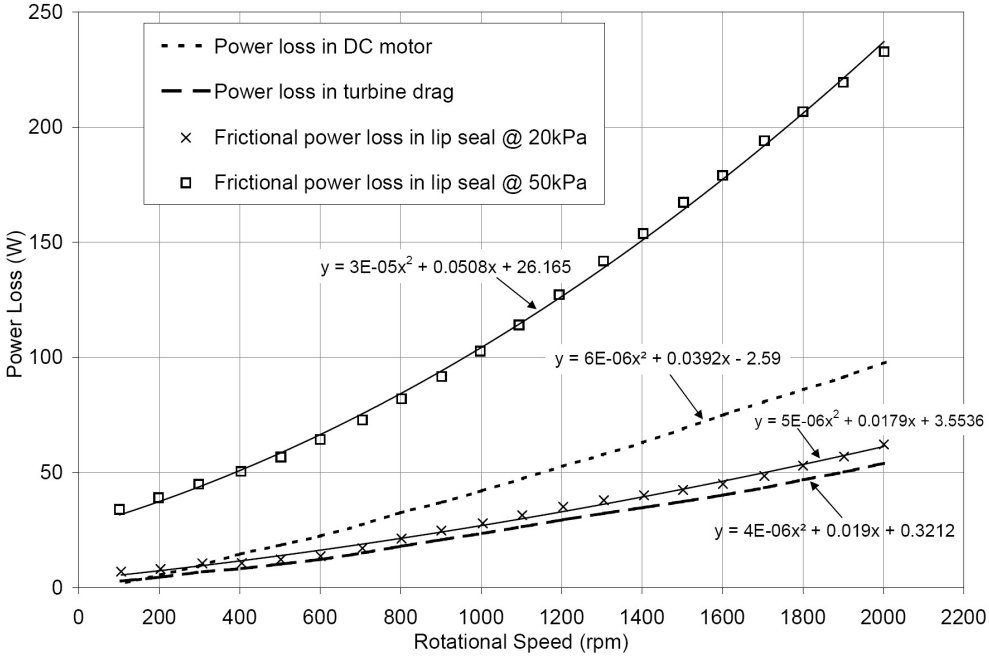

Figure 5.14 Power loss curves for SRT prototype 1 with V-ring lip seal (V-ring friction plus turbine air drag)

As shown in Figure 5.14 the second order polynomials are drawn to fit the individual power loss curves and then the equations for each of these polynomial curves are used to estimate the exact value of power loss at different rotational speeds. For example as shown in Figure 5.14, power loss associated with V-ring lip seal operating at 50kPa is represented by $y = 0.00003x^2 + 0.0508x + 26.165$ (here y is the power loss in V-ring lip seal and x is the corresponding rotational speed). After the comparison of Figure 5.5 and Figure 5.14 it can be said that SRT prototype1 has less air drag as compared to the CPT design, this is due to the disk like shape of SRT prototype 1. The V-ring rotary seal arrangement are suitable for micro-hydro applications as they are readily available and are very inexpensive. A 100mm V-ring lip seal made by SKF costs approximately Australian $6 (retail price).

Figure 5.15 shows the individual frictional power loss curves for DC motor, mechanical seal (NMS) and turbine drag. The mechanical seal (NMS) does not require water pressure for its operation as did the V-ring rotary lip seal arrangement and so the frictional power loss associated with it is independent of the supply pressure and only varies with rotational speed. Further from Figure 5.14 and Figure 5.15, it can be said that the NMS arrangement has much less frictional power loss as compared to the V-ring rotary seal arrangement. However, the V-ring lip seal is cheaper to purchase and easier to install.

As shown in Figure 5.15 second order polynomials are drawn to fit individual power loss curves and then the equations for each of these polynomial curves are used to estimate the values of power loss at different rotational speeds. Then these power loss values are added to the electrical power generated for respective speeds to get the actual turbine power produced by the turbine as discussed in section 4.6 of Chapter 4. The experiments have showed that both V-ring lip seal arrangement and NMS arrangement have excellent performance in preventing water leak at the rotary inlet joint. The only advantage of NMS arrangement over V-ring rotary seal arrangement is less frictional power loss. The disadvantage of NMS arrangement is that they are expensive and not readily available.

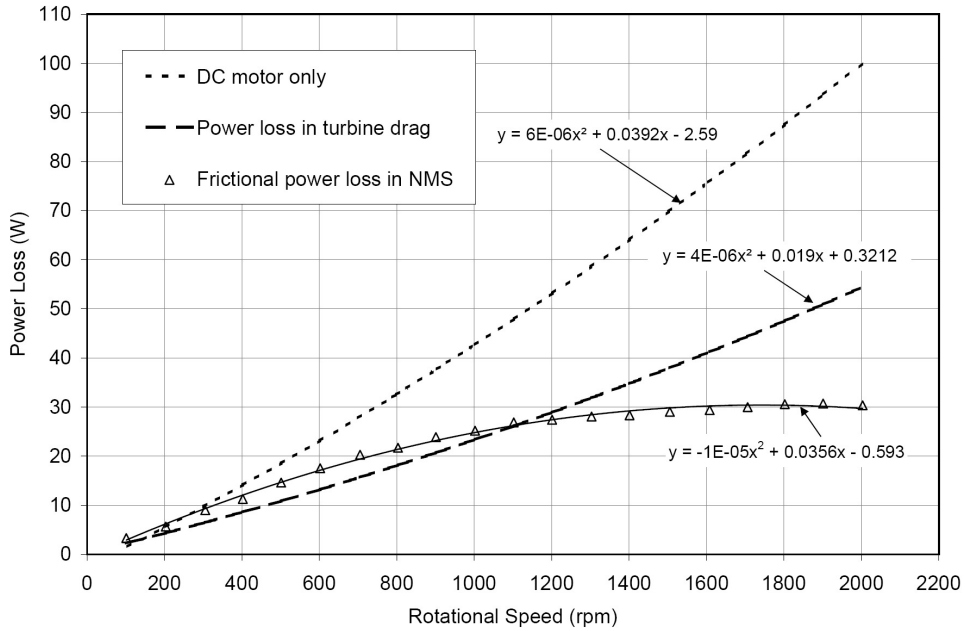

Figure 5.15 Power loss curves for SRT prototype 1 with mechanical seal (mechanical seal friction plus turbine air drag)

5.5.3 Turbine power and turbine efficiency

Table 5.10 and Table 5.11 show sample performance data of SRT prototype 1 operating at 50kPa pressure with V-ring rotary seal arrangement and NMS arrangement respectively. In Table 5.10 and Table 5.11 $\dot{W}_T$ represents the actual turbine power (mechanical power) produced by the turbine, $\dot{W}_E$ represents the electrical power generated by the DC generator and $\dot{W}_{loss}$ represents the power loss in the DC generator, rotary seal and turbine air drag. As discussed in Chapter 4 the turbine power is estimated by adding the sum of power loss in DC generator, rotary seal and turbine air drag to the electrical power output from the generator. For example from Figure 5.14 at 50 kPa supply pressure and 599 rpm the individual power loss components are calculated as follows,

Power loss in V-ring lip seal @ 50 kPa and 599 rpm is, (100 mm diameter V-ring seal) $y = 0.00003 * 599^2 + 0.0508 * 599 + 26.165 = 67.35W$

Power loss in turbine air drag at 599 rpm is,

$$y = 0.000004 * 599^2 + 0.019 * 599 + 0.3212 = 13.14W$$

Power loss in DC motor/generator at 599 rpm is,

$$y = 0.000006 * 599^2 + 0.0392 * 599 - 2.59 = 23.04W$$

Therefore the sum of total power loss is equal to 67.35+13.14+23.04 = 103.53W this is added to the measured electrical power of 439W@599rpm to get the turbine power of 542.53W@599rpm, as shown in Table 5.10.

Table 5.10 Estimated power outputs and energy conversion efficiencies for SRT prototype 1 at 50 kPa supply pressure with V-ring lip seal (sample)

Supply pressure (kPa)	Flow Rate (L/sec)	Turbine Speed (rpm)	Electrical Power $\dot{W}_E$ (W)	Total power Loss $\dot{W}_{Loss}$ (W)	Turbine Power $\dot{W}_T$ (W)	Turbine efficiency % $\eta_t = \frac{\dot{W}_T}{\dot{m}\,gh}$	Overall efficiency % $\eta_o = \frac{\dot{W}_E}{\dot{m}\,gh}$
50	25.83	1341	0.0	242.0	242.00	18.74	0.00
50	24.37	1228	132.1	218.0	350.11	28.73	10.84
50	23.29	1139	235.0	199.9	434.86	37.34	20.18
50	22.18	1049	322.6	182.2	504.79	45.51	29.09
50	21.04	958	385.0	165.0	550.03	52.29	36.60
50	19.88	863	428.3	147.8	576.04	57.94	43.08
50	18.89	771	444.0	131.8	575.78	60.97	47.01
50	17.98	688	447.8	117.8	565.64	62.90	49.80
50	17.05	599	439.0	103.5	542.53	63.63	51.49
50	16.32	520	409.0	91.4	500.39	61.32	50.12
50	15.53	423	355.1	77.1	432.18	55.66	45.73
50	15.02	350	294.2	66.9	361.16	48.10	39.19
50	14.45	256	222.2	54.4	276.61	38.28	30.75

Table 5.11 Estimated power outputs and energy conversion efficiencies for SRT prototype 1 at 50 kPa supply pressure with NMS arrangement (sample)

Supply pressure (kPa)	Flow Rate (L/sec)	Turbine Speed (rpm)	Electrical Power $\dot{W}_E$ (W)	Total power Loss $\dot{W}_{Loss}$ (W)	Turbine Power $\dot{W}_S$ (W)	Turbine efficiency % $\eta_t = \frac{\dot{W}_T}{\dot{m}\,gh}$	Overall efficiency % $\eta_o = \frac{\dot{W}_E}{\dot{m}\,gh}$
50	25.70	1365	133.49	125.18	258.67	20.13	10.39
50	24.04	1223	313.12	111.84	424.96	35.36	26.05
50	22.94	1135	389.70	103.63	493.32	43.02	33.98
50	21.93	1046	450.14	95.27	545.41	49.74	41.06
50	20.81	952	487.87	86.41	574.28	55.19	46.89
50	19.81	857	510.53	77.55	588.08	59.37	51.54

50	18.86	767	511.63	69.10	580.73	61.59	54.26
50	18.03	689	504.67	61.75	566.42	62.84	55.99
50	17.07	599	480.04	53.31	533.35	62.49	56.24
50	16.41	524	447.25	46.29	493.54	60.14	54.50
50	15.58	423	389.64	36.82	426.46	54.76	50.03
50	15.00	341	328.98	29.14	358.12	47.75	43.87
50	14.54	264	263.83	21.93	285.76	39.31	36.30

Figure 5.16 and Figure 5.17 shows the turbine efficiency and the overall efficiency of SRT prototype 1. It can be seen that at 50 kPa supply pressure the peak overall efficiency with V-ring rotary seal arrangement is about 51%, where as that with NMS arrangement the peak overall efficiency increases to around 57%. This increase in overall efficiency can be attributed to the less frictional power loss in NMS arrangement. Further, it can be seen from Figure 5.16 and Figure 5.17 that at 20kPa supply pressure the overall efficiency of SRT prototype 1 with V-ring rotary seal arrangement is better than NMS arrangement. This observation shows that the NMS arrangement has better performance when used at higher supply pressures than the V-ring rotary seal arrangement.

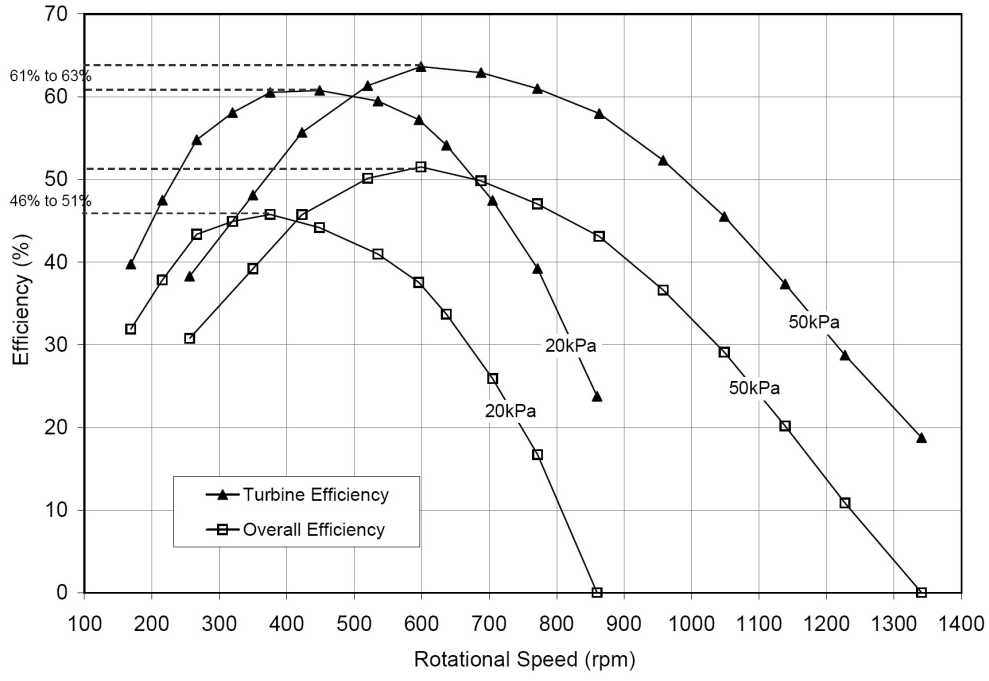

Figure 5.16 Estimated turbine efficiency and electrical efficiency characteristics of SRT prototype 1 with V-ring lip seal at the inlet

Further the SRT prototype1 demonstrates high energy conversion efficiency as compared to the CPT design, Barkers mill simple reaction water turbine and the simple reaction water turbines developed at RMIT in earlier development projects (Webb, 1999, Quek, 2003). SRT prototype-1 can convert low head hydro energy to mechanical energy with an efficiency of around 61% to 63%. SRT prototype 1 shows constant turbine efficiency characteristics over a wide range of rotational speeds, i.e. from Figure 5.16 at 20kPa and 370rpm turbine efficiency is about 60%, similarly at 50kPa and 800rpm the turbine efficiency is still 60%. This makes the SRT design a very flexible option to be used for power production from a wide range of low head resources as an alternative to the present commercially available micro-hydro turbines.

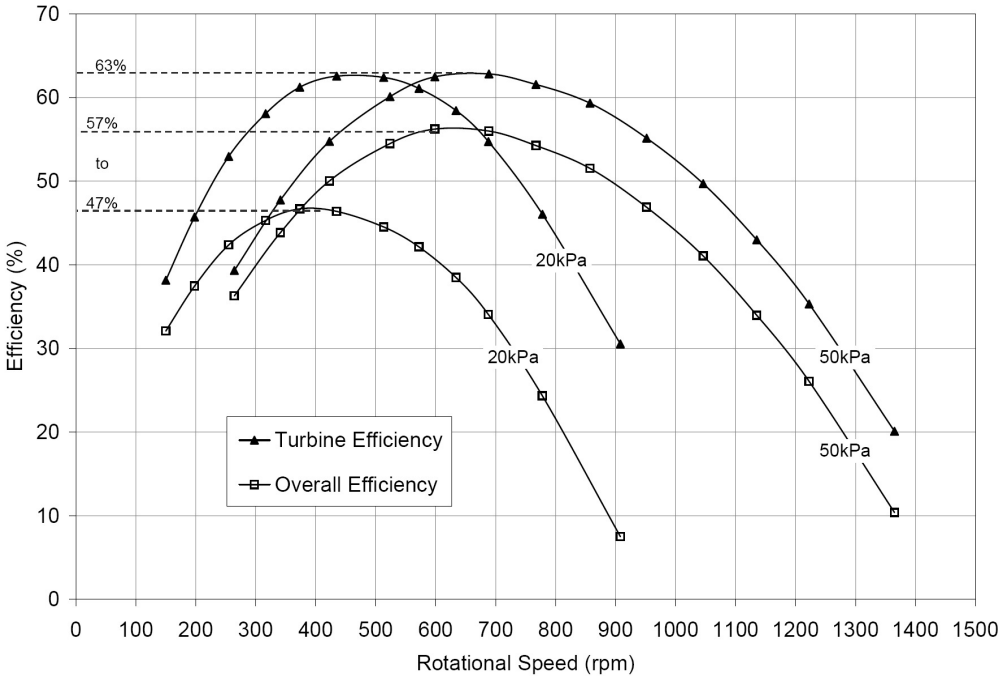

Figure 5.17 Estimated turbine efficiency and electrical efficiency characteristics of SRT prototype 1 with mechanical seal NMS at the inlet

5.5.4 Energy balance analysis

Energy balance analysis is done to verify the accuracy and dependable of the experimental data and procedures. Figure 5.18 and Figure 5.19 shows the energy balance of sample data from the performance tests conducted on the SRT prototype 1, this is based on the governing equation 2.36 as discussed in Chapter 2. The energy input is

estimated from the measured flow rate and the measured supply pressure as $\dot{m}gH$. The mechanical turbine power is estimated as discussed earlier in section 5.3.3 and in section 4.5 of Chapter 4. The fluid frictional power loss is estimated from the measured flow rate, estimated k-factor and estimated relative velocity as $\frac{1}{2}\dot{m}kV_r^2$. And the kinetic power lost with the water leaving the turbine is estimated from the measured flow rate and estimated absolute velocity as $\frac{1}{2}\dot{m}V_a^2$. For example it can be seen from Figure 5.18 and Table 5.10 at 688rpm the input power is 899.2W, where as the sum of output is equal to the 876.23W, this shows that there is an error of 22.9W in the estimation (i.e. ≈ 3%). This error may be due to instrumentation uncertainty and the fact that the turbine rotates in wet environment (water drops splashing) while producing power where as the turbine air drag power loss is estimated only in normal atmospheric air and there will be small amount of unaccounted power loss present there. Overall, the energy balance around the maximum power point and the maximum efficiency point is within ±7%.

Table 5.12 Estimated power outputs and energy conversion efficiencies for SRT prototype-1 at 50 kPa supply pressure with V-ring lip seal (sample)

Supply pressure (kPa)	Turbine Speed (rpm)	Turbine power $\dot{W}_T$ (W)	+	Fluid Frictional loss $\dot{W}_{Ff}$ (W)	+	Kinetic power loss $\dot{W}_{Ke}$ (W)	=	Sum of output power $\dot{W}_{Out}$ (W)	≈	Input hydro power $\dot{W}_{In}$ (W)
50	1341	242.00	+	892.65	+	10.06	=	1144.70	≈	1291.4
50	1228	350.11	+	697.97	+	21.01	=	1069.09	≈	1218.5
50	1139	434.86	+	559.93	+	33.41	=	1028.19	≈	1164.5
50	1049	504.79	+	449.56	+	47.49	=	1001.84	≈	1109.1
50	958	550.03	+	368.15	+	61.91	=	980.09	≈	1051.9
50	863	576.04	+	296.57	+	79.69	=	952.30	≈	994.1
50	771	575.78	+	228.29	+	103.31	=	907.38	≈	944.4
50	688	565.64	+	184.69	+	125.90	=	876.23	≈	899.2
50	599	542.51	+	151.45	+	152.32	=	846.27	≈	852.6
50	520	500.39	+	124.79	+	181.79	=	806.98	≈	816.0
50	423	432.18	+	97.60	+	227.36	=	757.13	≈	776.5
50	350	361.16	+	82.94	+	268.41	=	712.52	≈	750.8
50	256	276.61	+	71.31	+	332.26	=	680.19	≈	722.6

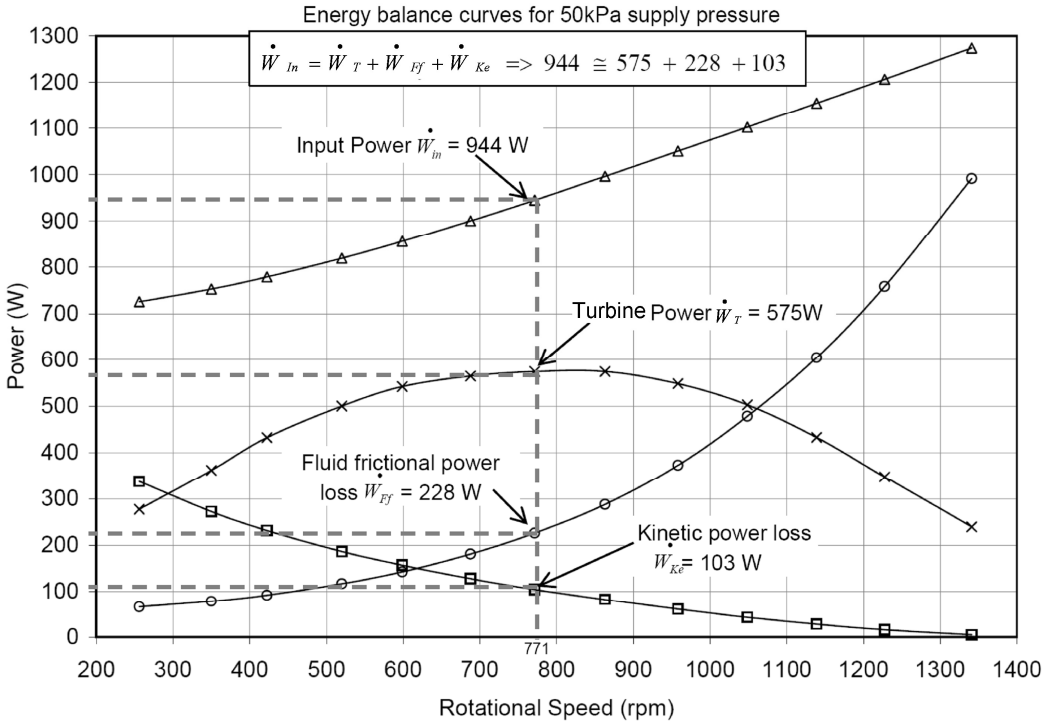

Figure 5.18 Energy balance analysis of SRT prototype 1 with V-ring lip seal at the inlet

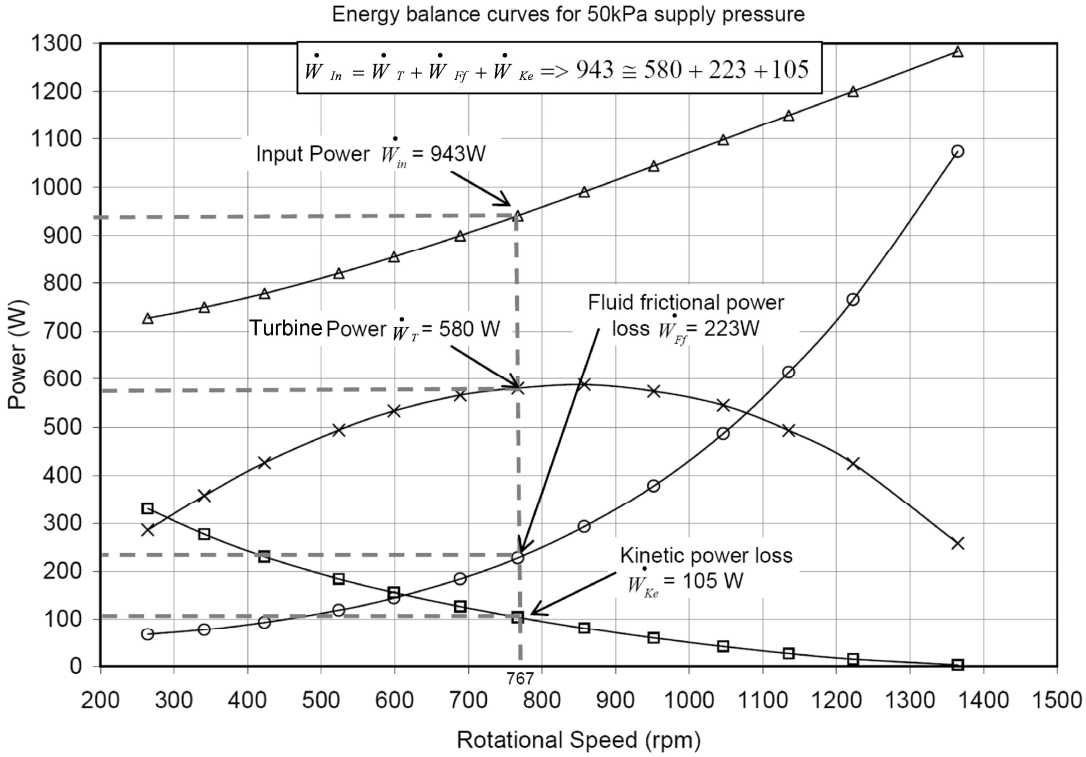

Figure 5.19 Energy balance analysis of SRT prototype 1 with mechanical seal NMS at inlet

The instrumental uncertainty analysis shows the relative uncertainty of ±4.98% in the estimation of the total output power $\dot{W}_{Out} = \dot{W}_T + \dot{W}_{Ff} + \dot{W}_{Ke}$ and a relative uncertainty of ±2.70% in the estimation of the hydro input power $\dot{W}_{In}$ (see Table - C-17, Appendix C), making the net instrumental uncertainty of ±7.7 %. After considering this fact of relative instrumental uncertainty of ±7.7% and some amount of unaccounted power loss in turbine drag estimation in wet environment, it can be said that the overall energy balance analysis shows good confidence in the experimental data measurements and procedures used in the performance testing of the SRT prototype1.

5.6 Stationary performance characteristics of SRT prototype 2

Figure 5.20 shows the comparison between the estimated torque based on flow rate measurement and the shaft torque based on the force measurement taken from the stationary test unit shown in Figure 4.7, the stationary test procedure used to conduct this test is explained in section 4.3.1 of Chapter 4. Ideally, both the estimated and measured torque values should be equal. Figure 5.20 also shows the minimum amount of water flow through the SRT prototype 2 at different pressures. SRT prototype2 has a mean rotor diameter of 125mm (effective turbine diameter of 123.1mm, due to the exit nozzles oriented at 10° angle to tangent, see section 3.2.2.3 of Chapter 3) and total turbine nozzle exit area of 0.00192m² at stationary conditions. When the SRT is stationary the flow rate depends on the supply pressure and total nozzle exit area, as there is no centrifugal pumping effect present. The stationary flow rate data is used to estimate the theoretical stationary torque (estimated torque) based on the flow rate and estimated exit velocity of the water jet. As discussed in Chapter 2, the estimated turbine torque (see equation 2.9, Chapter 2) is a product of total mass flow rate, turbine radius and absolute velocity of the water leaving the nozzles (absolute velocity equals relative velocity at stationary condition).

For example, from Table 5.13 and Figure 5.20 at 25kPa pressure the volume of water flowing through the turbine is 13.17L/s; taking the density of water @ 20°C as 1000kg/m³ the mass flow rate will be equal to $\dot{m}$ = 13.17kg/s.

Table 5.13 Measured flow rate and force transducer readings at different pressures for SRT prototype 2 with exit nozzle width of 8mm

SRT Prototype 2 (Ø125mm, nozzle width 8mm) Torque arm = 0.211m			
Obs. No.	Pressure gauge reading (kPa)	Time required for $V = 0.1m^3$ water flow through turbine t (Sec)	Force transducer reading F_{arm} (N)
1	5	16.85	5.06
2	10	11.93	10.08
3	15	9.77	15.03
4	20	8.47	20.09
5	25	7.59	24.79
6	30	6.94	29.95
7	35	6.44	35.12
8	40	6.04	40.33
9	45	5.70	44.69

Therefore, the absolute velocity (exit velocity) of water leaving the nozzles will be equal to, $V_a = \frac{13.17 \times 10^{-3}}{0.00192} = 6.86 \ m/s$

Mean effective radius of this turbine is equal to 61.5mm.

Therefore the estimated torque is equal to,

$$T_{estimated} = \dot{m} V_a R = 13.2 \times 6.86 \times 0.0615 = 5.511 Nm$$

As discussed in chapter 4 the shaft torque is measured using a force transducer (load cell with strain indicator) connected to the turbine shaft with a torque arm of 0.211m length. Table 5.13 shows the force measurements for different pressures and the corresponding flow rates. The shaft torque is calculated from this measured data, for example from Table 5.13 at a pressure of 25kPa the measured force acting on the torque arm of 0.211m length is 24.79N.

Therefore, $T_{shaft} = 24.79 \times 0.211 = 5.23 Nm$

Figure 5.20 shows comparison between the estimated torque and the measured shaft torque for the stationary condition. Theoretically, the measured shaft torque should be equal to the estimated torque. It can be seen from Figure 5.20 that the measured shaft torque is very close to the estimated torque and any deviation is very small and consistent. For the SRT prototype2 the exit nozzle is designed with 6mm jet guidance

(split pipe overlap, see Figure 3.13 in Chapter 3), this nozzle guide helps the water to leave the turbine as a solid stream jet. To some extent, this goal seems to be fulfilled, as there is very small deviation in the measured and estimated torque values. As compared to the SRT prototype1 the SRT prototype2 shows better match of measured and estimated torque values. Any small deviation in two torque values is attributed to instrumental error and the inaccuracy in the estimation of the actual total exit nozzle area. The uncertainty analysis of the measured data from this experiment shows a relative uncertainty of ±5.68% in the estimation of the estimated torque based on the measured flow rate and a relative uncertainty of ±1.11% in the estimation of shaft torque (see Table - C-11, Appendix C).

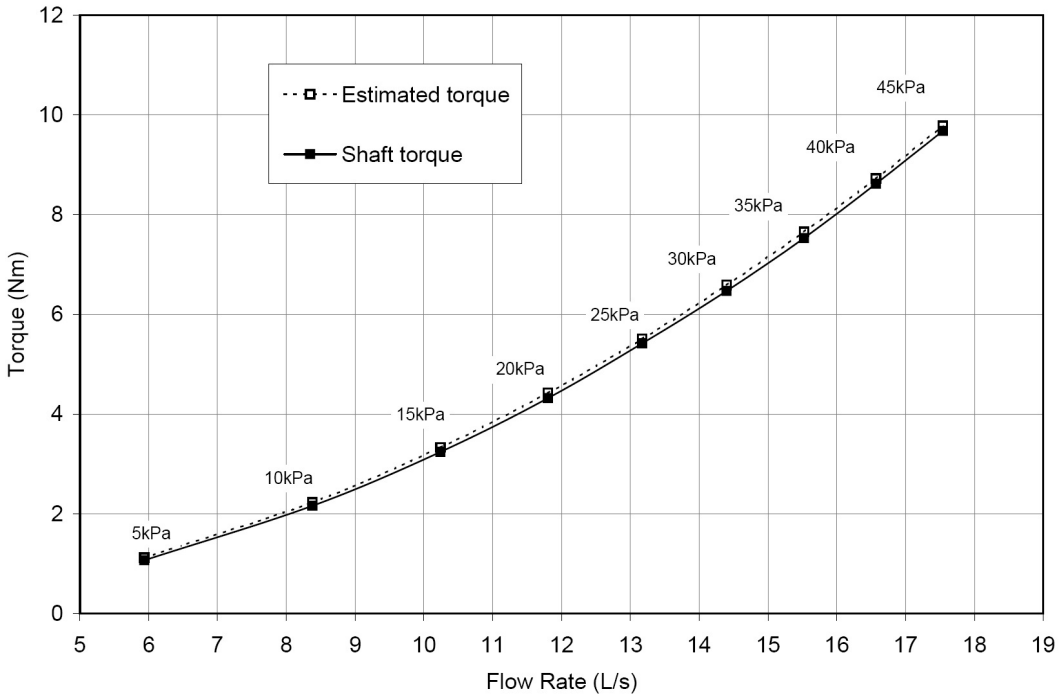

Figure 5.20 Torque comparison and minimum flow rates at different pressures for SRT prototype 2 with exit nozzle width of 8mm

Figure 5.21 shows the estimated k-factor for the stationary condition at different pressures. When the turbine is stationary the value of k-factor increases with increase in supply pressure, this is due to increased flow rate, this results in increase in the velocity of the water leaving the exit nozzles. As discussed in Chapter 2 the k-factor represents the fluid frictional power loss associated with the turbine body and exit nozzles. When the

turbine is stationary (i.e. ω=0) there is no centrifugal pumping effect so for the given turbine geometry the value of k-factor will remain constant for the given supply pressure. The k-factor is estimated from the stationary test results and using equation 2.39 from Chapter 2. It can be seen that even for stationary condition value of k-factor increases with higher exit velocity. This information is valuable for SRT computer modelling and performance prediction.

For example, at a pressure of 25kPa (i.e. $H \approx 2.5m$), the flow rate is 13.17L/s and angular speed if zero as the turbine is stationary (i.e. ω=0). The effective mean turbine radius is 61.5mm and the total exit nozzle area is 0.00192m². Here the exit velocity is equal to the total flow rate divided by the total exit nozzle area, making the exit velocity at 25kPa equal to 6.86m/s as shown in Figure 5.21.

Therefore, $$k = \frac{2gH + R^2\omega^2}{\left(\frac{\dot{m}}{\rho A}\right)^2} - 1 = \frac{2 \times 25 + 0}{\left(\frac{13.17}{1000 * 0.00192}\right)^2} - 1 = 0.062$$

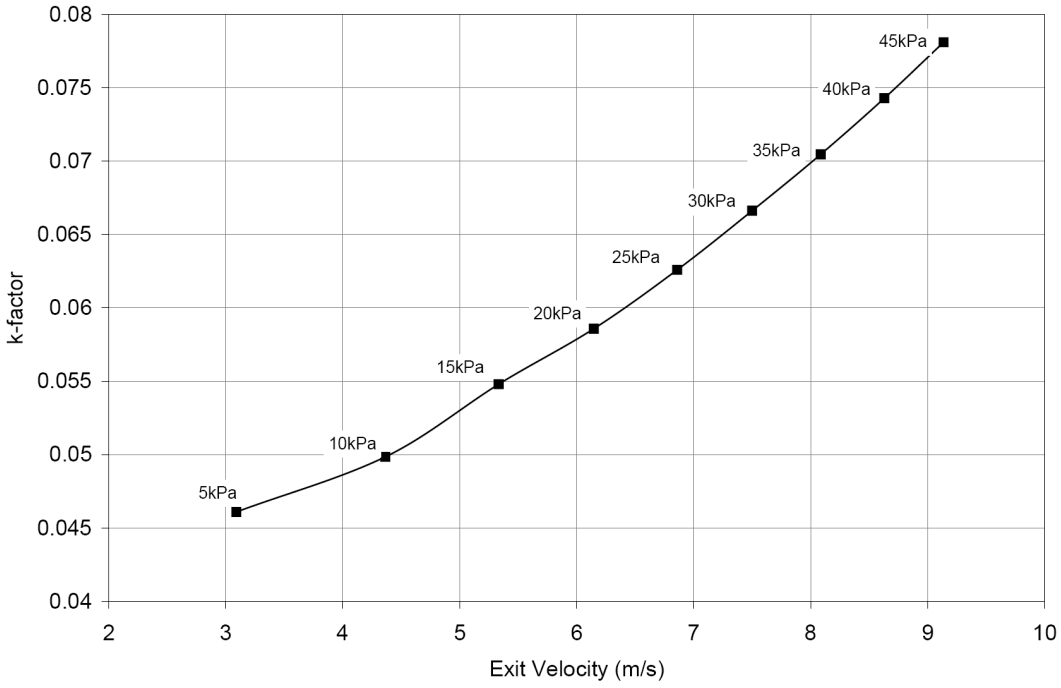

Figure 5.21 Experimentally estimated k-factor for SRT prototype 2 with exit nozzle width of 8mm

5.7 Performance characteristics of rotating SRT prototype 2

Figure 5.22 and Figure 5.23 shows the electrical power and flow rate characteristics of SRT prototype 2 (SRT-125D-120L-8W) at two sample supply pressures with V-ring rotary seal arrangement and NMS arrangements as discussed in Chapter 3 (Figure 3.17 and Figure 3.19). The test procedure used to conduct this power test is explained in section 4.4 of Chapter 4. SRT prototype 2 has a mean effective turbine diameter of 123mm and total exit nozzle area of 0.00192m² (120mm x 8mm x 2 nozzles). The centrifugal pumping action is evident from the rising water flow rate at constant supply pressure at increased rotational speed as seen from Figure 5.22 and Figure 5.23. As predicted in the theoretical analysis (see Figure 2.7 of Chapter 2) at high speeds the flow rate tends to become almost a linear function of rotational speed. Further, it is also observed that the effect of hydro static pressure (head) on the flow rate diminishes at higher rotational speeds, the projected flow rate curves are seen to come closer as if eventually at some very high speed they would merge. This trend of flow rates merging is predicted in the theoretical analysis shown in Figure 2.7 of Chapter 2. As discussed in the theoretical analysis of simple reaction turbine in Chapter 2 the governing equation for the mass flow rate is written as $\dot{m} = \frac{\rho A\sqrt{2gH + R^2\omega^2}}{\sqrt{1+k}}$.

The flow rate data collected from this power test of the SRT prototype2 is used to estimate the dynamic k-factor. Figure 5.22 also shows the maximum power point for SRT-125D-120L-8W at 13.79kPa and 41.37kPa supply pressures. For 13.79kPa supply pressure the maximum electrical power of 80W is produced at about 600rpm, where as at 41.37kPa the maximum electrical power of 458W is produced at about 1300rpm. This shows that the maximum power point (MPP) of SRT prototype 2 depends on the supply pressure and is seen to shift to higher speed as the supply pressure is increased. Further it is observed from Figure 5.22 that power output remains very constant over a wide range of rotational speeds, for example at 41.37kPa supply pressure the electrical power output at 900rpm is 395W and at 1500rpm is 410W (almost constant and very close to MPP). These observations show that SRT-125D-120L-8W has an optimum operating speed range of 900rpm to 1500rpm at 41.37kPa (4.2m head). So SRT prototype 2 can be

coupled with a 4 pole electrical generator operating at 1500rpm to produce 50Hz electrical power from 4.2m to 5m head hydro source.

SRT prototype2 tests with NMS arrangement shows more electrical power generation at 41.37kPa pressure as compared to the V-ring rotary seal arrangement and the turbine spins at faster speed, this is due to less frictional power loss when using NMS arrangement as compared to V-ring rotary seal arrangement at high pressure. The frictional power loss associated with the NMS arrangement remains constant with respect to pressure and so at low pressure of 13.79kPa the electrical power produced when using NMS is less then when using V-ring rotary seal arrangement. Most importantly, it is observed that both V-ring rotary seal arrangement and NMS arrangement perform excellently in the prevention water leakage.

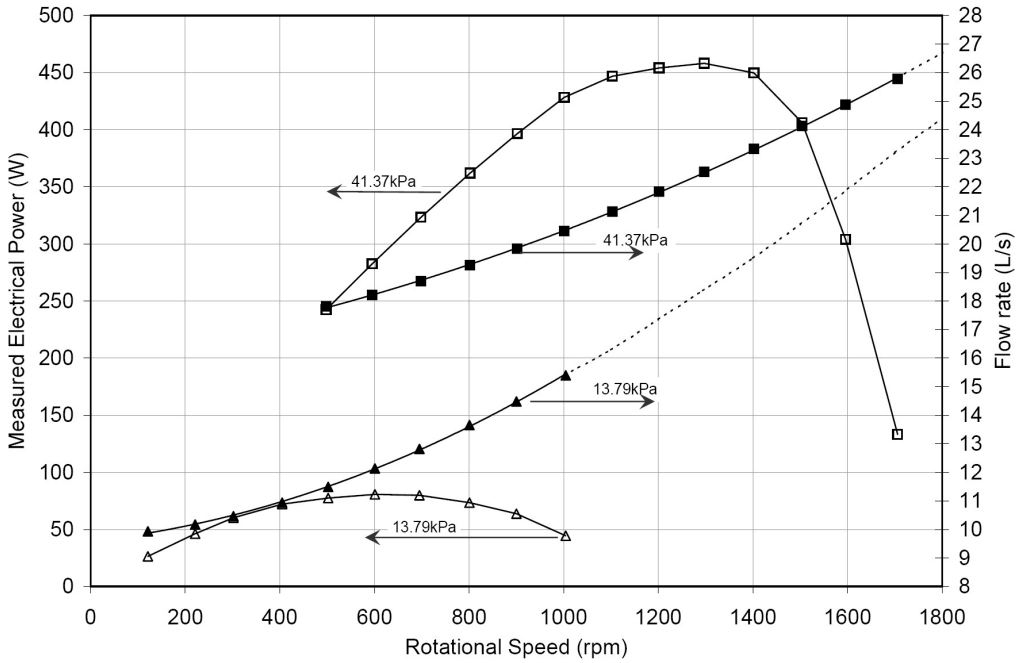

Figure 5.22 Estimated performance characteristics of SRT 125D-120L-8W with V-ring seal

It is clear from the experimental results that SRT prototype2 spins at much higher speeds than SRT prototype1 and CPT even at lower supply pressures, this is because SRT prototype 2 has smaller turbine diameter. The advantage of SRT design is the flexibility of varying the turbine diameter without having to vary the total nozzle area and vice versa.

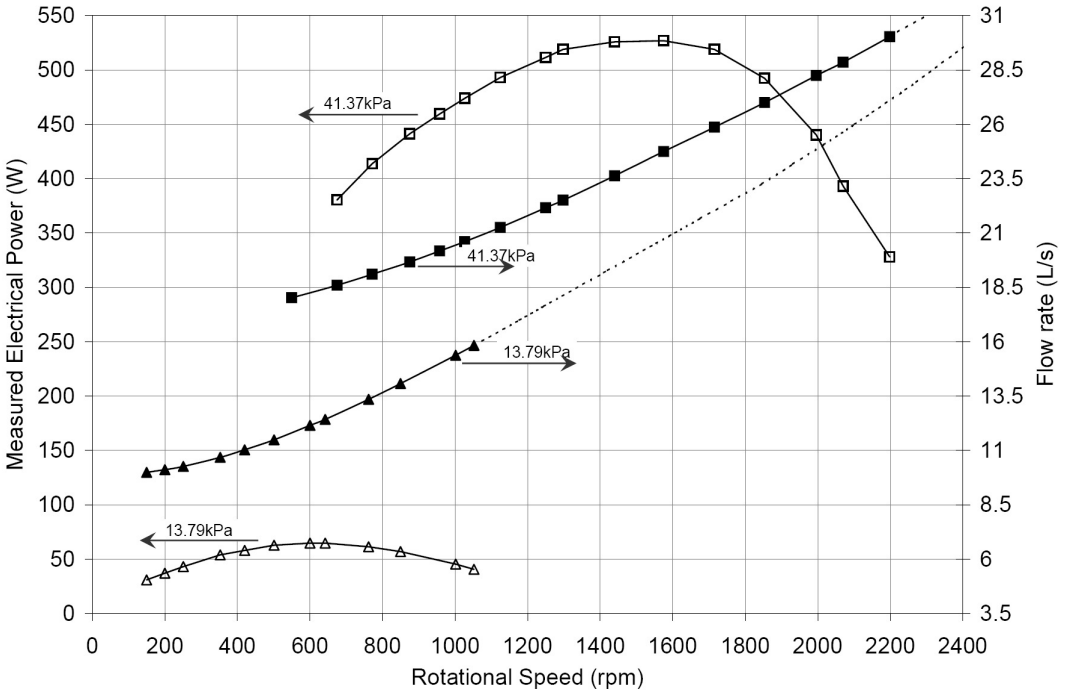

Figure 5.23 Estimated performance characteristics of SRT 125D-120L-8W with NMS rotary seal

5.7.1 Fluid Frictional loss characteristics

Figure 5.24 and Figure 5.25 shows the characteristic curves of the estimated *k*-factor for SRT-125D-120L-8W with V-ring rotary seal arrangement and NMS arrangements for stationary and rotary conditions. The k-factor represents the fluid frictional losses and is a function of relative velocity as discussed in Chapter 2. While the relative velocity of the exiting water jets is directly proportional to the flow rate, with the increase in rotational speed, the flow rate increases due to centrifugal pumping action and so does the relative velocity. The k-factor is seen as a linear function of relative velocity from Figure 5.24 and Figure 5.25. The k-factor values are estimated using equation 2.39 from Chapter 2 and the experimental data collected from the power test conducted out on SRT prototype 2 (data tables in Appendix B). Following is a solved example of k-factor estimation at 41.37kPa supply pressure and rotational speed of 1001rpm, from Figure 5.22 the total flow rate corresponding to 1000rpm (41.37kPa) is 20.5L/s. The total exit nozzle area of turbine SRT prototype2 under investigation is 0.00192m², so the relative velocity of exit jet is 10.7m/s.

$$\therefore k = \frac{2gH + R^2\omega^2}{(V_r)^2} - 1 = \frac{2\times 41.37 + (0.0615)^2 \times (104.7)^2}{(10.7)^2} - 1 = 0.09$$

The increasing trend of k-factor as seen in the stationary tests is also seen from the power test results shown in Figure 5.24 and Figure 5.25. Further the values of k-factor estimated from stationary test and power test are very close for corresponding relative velocity values. The tendency of increase in the value of k-factor and in turn further increase in fluid frictional losses with increase in relative velocity is confirmed from repeated experiments and data analysis. The variation of k-factor is more dependent of relative velocity for V_r and is a weak function of supply pressure (Head). Values of k-factor at very high relative velocities can be predicted through a stationary turbine test by simulating flow rates that are achieved at high rotational speeds using high-pressure pumps. These predictions of k-factor can be used as a basis for computer modeling of a SRT for real life installations at different low head hydro sites.

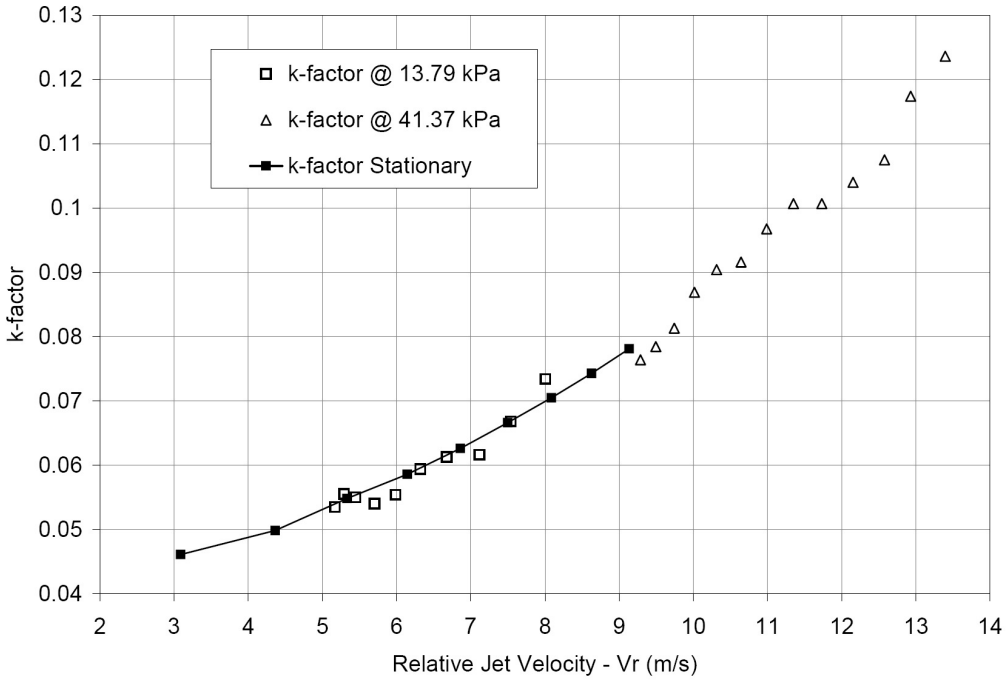

Figure 5.24 Estimated k-factor characteristics for SRT 125D-120L-8W with V-ring rotary seal arrangement

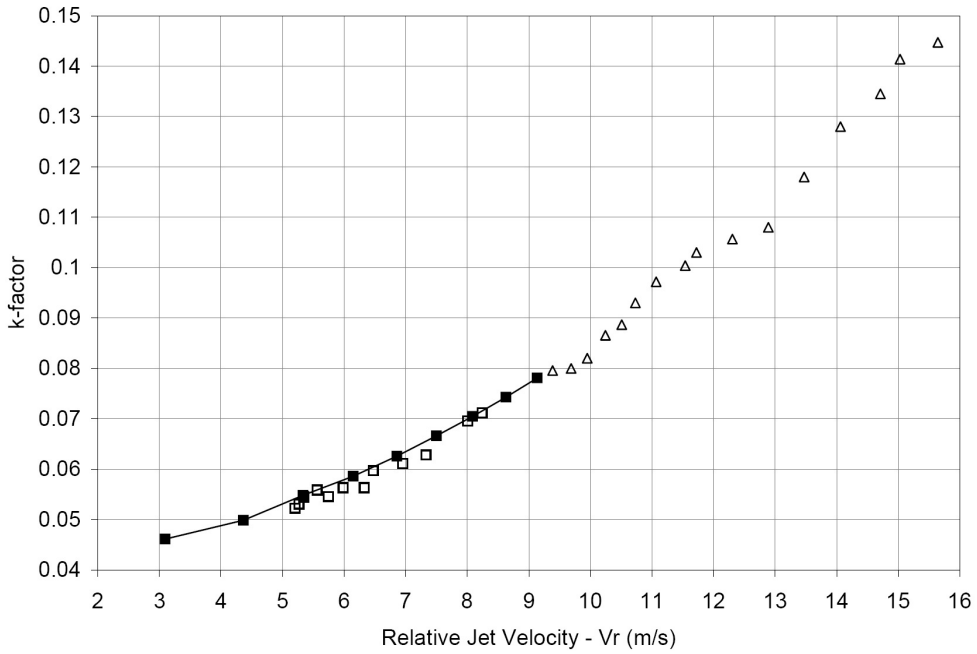

Figure 5.25 Estimated k-factor characteristics for SRT 125D-120L-8W with NMS rotary arrangement

5.7.2 Power loss characteristics

Figure 5.26 shows the individual power loss characteristics of DC motor, V-ring rotary seal and the SRT prototype2 drag operating at two sample pressures of 13.79kPa and 41.37kPa. It can be seen from Figure 5.26 that the frictional power loss in V-ring rotary arrangement increases with increase in the supply pressure. This is due to increase in the surface contact force between the V-ring lip and the rotating stainless steel ring attached to the inlet port of the turbine as illustrated in Figure 3.17 of Chapter 3. The total power loss value is added to the electrical power generated at the given supply pressure and given speed to get the turbine power produced as discussed in section 4.6 of Chapter 4. As shown in Figure 5.26 second order polynomials are drawn to fit individual power loss curves and then the equations for each of these polynomial curves is used to estimate exact value of power loss at different rotational speeds. It can be seen from the comparison of Figure 5.5, Figure 5.14 and Figure 5.26 that the SRT prototype2 has the least power loss. This is due to reduced turbine drag as compared to the SRT prototype1 and CPT design as the SRT prototype2 has a smaller diameter with a disk shape.

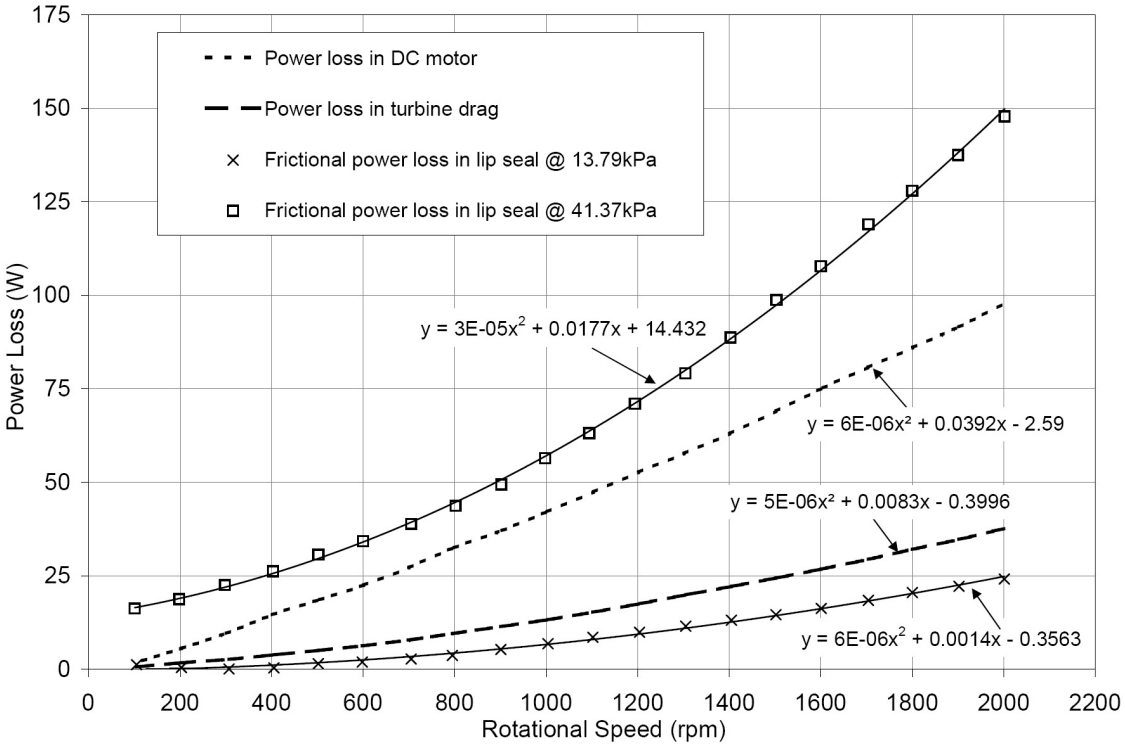

Figure 5.26 Estimated power loss characteristics of DC motor, V-ring rotary seal and turbine drag for SRT prototype-2

Figure 5.27 shows the individual components of frictional power loss curve for DC motor, NMS arrangement and turbine drag. The NMS arrangement does not require water pressure for its operation and so the frictional power loss associated with NMS arrangement is independent of the supply pressure and only varies with rotational speed. Further from Figure 5.26 and Figure 5.27 it can be said that the NMS arrangement has less frictional power loss as compared to V-ring seal arrangement at higher pressures. As shown in Figure 5.27 second order polynomials are drawn to fit individual power loss curves and then the equations for each of these polynomial curves are used to estimate exact value of power loss at different rotational speeds. Then these power loss values are added to the electrical power generated to get the turbine power as discussed in section 4.6 of Chapter 4. The experiments have showed that both V-ring rotary arrangement and NMS arrangement perform excellently in preventing water leakage at the rotary joint. The advantage of the NMS arrangement is the characteristics of less frictional power loss, but these seals are expensive.

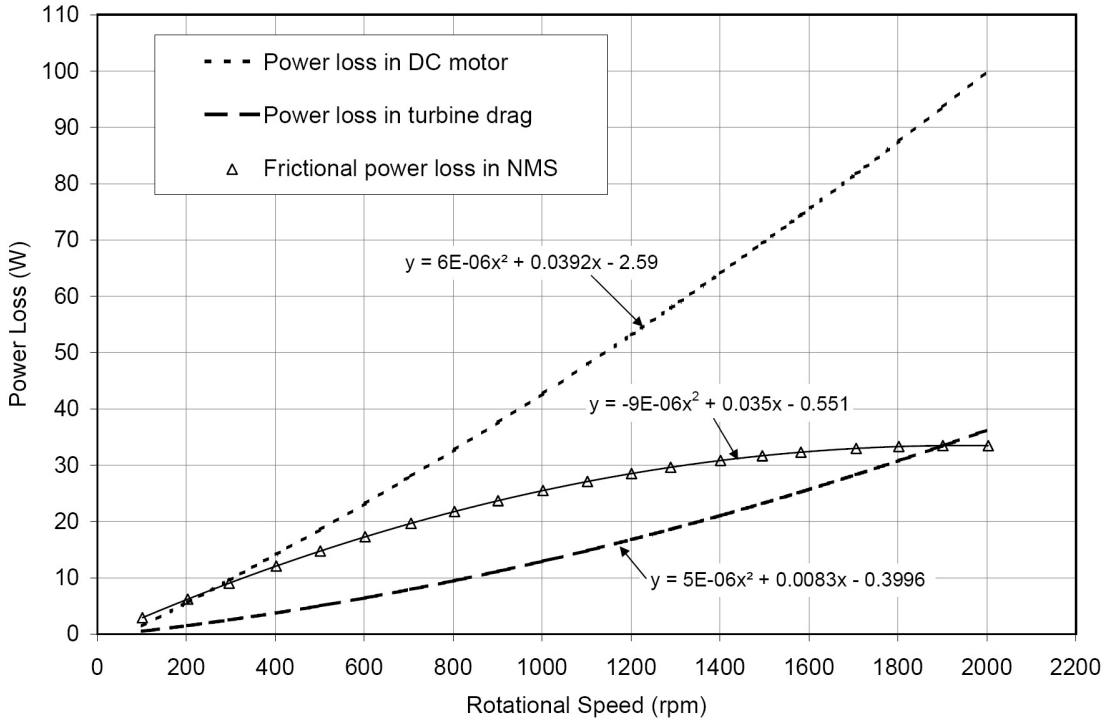

Figure 5.27 Estimated power loss characteristics of DC motor, V-ring rotary seal and turbine drag for SRT prototype-2

Example of the theoretical estimation of drag friction power loss on rotor for SRT prototype 2 is shown below,

SRT prototype has a diameter of 0.124m and a height of 0.12m. The distance between turbine outer surface and anti-water splash cover is considered to be 0.1m. At ω = 100 rad/s the turbine outer surface velocity is U = 6.28m/s.

Consider the turbine is surrounded with air at 25C temperature. At this temperature the air has a density of 1.19kg/m^3 and viscosity of 1.98 x 10^{-5}N.s/m (Incropera, 2002). For this condition the Renolds number is estimated to be R_e = 37743.4 based on equation 2.55. Therefore the flow is turbulent and so the friction coefficient is estimated using $f = 0.184(R_e)^{-0.2} = 0.022$ (Incropera, 2002). Therefore, from equation 2.58 the power loss due to windage in dry air is estimated as 0.148 Watts.

Similarly consider the turbine is surrounded with water at 20C temperature. At this temperature the water has a density of 998kg/m^3 and viscosity of 9.65 x 10^{-4}N.s/m (Incropera, 2002). For this condition the Renolds number is estimated to be R_e = 649475.6 based on equation 2.55. Therefore the flow is turbulent and so the friction coefficient is estimated using $f = 0.184(R_e)^{-0.2} = 0.0127$ (Incropera, 2002). Therefore from equation 2.58 the power loss due to drag in water is estimated as 70.3 Watts.

Where as in a real condition the turbine runs in a wet environment and it is hard to estimate the exact amount of suspended water particles in the air. From Figure 5.27 the experimental results show that the turbine drag loss at 980rpm is about 12.53 Watts, which is within the range of theoretical prediction. This shows that the experimental procedure used is reliable and reasonably accurate.

5.7.3 Turbine power and turbine efficiency

Table 5.14 and Table 5.15 show sample data at 41.37kPa of estimated power output and efficiency characteristics of SRT prototype-2 with V-ring seal arrangement and NMS arrangement respectively. Here $\dot{W}_E$ represents the electrical power generated by the DC generator, $\dot{W}_{loss}$ represents the power loss in the DC generator, rotary seal and turbine drag and $\dot{W}_T$ represents the actual turbine power (mechanical power) produced by the turbine. As discussed in Chapter 4 the turbine power is estimated by adding the sum of power loss in DC generator, rotary seal and turbine drag to the electrical power output from the generator ($\dot{W}_T = \dot{W}_E + \dot{W}_{loss}$). For example from Figure 5.26 at 41.37kPa supply pressure and 1103rpm the individual power loss components are calculated as follows, Power loss in V-ring rotary seal arrangement @ 41.37 kPa and 1103rpm is, (90 mm diameter V-ring seal) $y = 0.00003 * 1103^2 + 0.0177 * 1103 + 14.432 = 70.45W$

Power loss in turbine drag at 1103 rpm is,

$y = 0.000005 * 1103^2 + 0.0083 * 1103 - 0.3996 = 14.84W$

Power loss in DC motor/generator at 1103 rpm is,

$$y = 0.000006 * 1103^2 + 0.0392 * 1103 - 2.59 = 47.95W$$

Therefore the sum of total power loss is equal to 70.45+14.84+47.95 = 133.24W this is then added to the measured electrical power of 447W @ 1103rpm to get the turbine power of 580W, as shown in Table 5.14. Figure 5.28 and Figure 5.29 shows the turbine efficiency and the overall efficiency of SRT prototype-2. It can be seen that at 41.37kPa supply pressure the peak overall efficiency of SRT prototype 2 with V-ring rotary seal arrangement is about 51%, where as that with NMS arrangement the peak overall efficiency increases to about 56%. This increase in electrical efficiency is due to fact that there is less frictional power loss with NMS arrangement at high pressures as compared to V-ring rotary arrangement.

Table 5.14 Estimated turbine and overall efficiencies of SRT 125D-120L-8W with V-ring rotary seal

Supply pressure kPa [PSI] (m of H_2O)	Flow Rate (L/sec)	Turbine Speed (rpm)	Electrical Power $\dot{W}_E$ (W)	Total power loss $\dot{W}_{loss}$ (W)	Turbine Power $\dot{W}_T$ (W)	Turbine efficiency $\eta_t = \frac{\dot{W}_T}{\dot{m} gH}$ %	Overall efficiency $\eta_o = \frac{\dot{W}_{loss}}{\dot{m} gH}$ %
41.37 [6] (4.2)	25.72	1706	133.25	242.00	375.26	35.26	12.52
41.37	24.83	1596	304.02	219.94	523.95	51.02	29.60
41.37	24.15	1504	406.07	202.25	608.32	60.90	40.65
41.37	23.33	1402	449.76	183.44	633.20	65.60	46.59
41.37	22.52	1297	458.17	164.98	623.14	66.88	49.17
41.37	21.79	1202	454.05	149.05	603.10	66.90	50.37
41.37	21.10	1103	446.78	133.24	580.02	66.45	51.18
41.37	20.44	1001	428.26	117.79	546.05	64.58	50.65
41.37	19.80	902	396.54	103.61	500.15	61.05	48.41
41.37	19.23	802	362.03	90.10	452.14	56.84	45.51
41.37	18.71	698	323.31	76.93	400.24	51.72	41.78
41.37	18.23	595	282.62	64.75	347.37	46.06	37.48
41.37	17.83	498	242.42	54.08	296.50	40.19	32.86

Further the SRT prototype-2 demonstrates high energy conversion efficiency as compared to SRT prototype 1, CPT and other simple reaction water turbine designs developed at RMIT during earlier projects (Webb, 1999, Quek, 2003). SRT prototype2 can convert low head hydro energy to mechanical energy with an efficiency of around 65% to 67%. From Figure 5.28 it can be seen that at 13.79kPa pressure and 600rpm the turbine efficiency is about 65% while at 41.37kPa pressure and 1400rpm the turbine

efficiency is still about 65%, this observation shows that SRT prototype 2 has high efficiency characteristics over a wide range of rotational speeds. It can be seen from Figure 5.28 and Figure 5.29 that at 13.70kPa pressure the overall efficiency with V-ring rotary seal arrangement is better then that with NMS arrangement. This is because of the fact that at low pressures the frictional power loss in V-ring rotary seal arrangement is very small, where as the frictional power loss with NMS arrangement remains constant with respect to supply pressure and only varies with rotational speed.

Table 5.15 Estimated turbine and overall efficiencies of SRT 125D-120L-8W with NMS rotary seal

Supply pressure kPa [PSI] (m of H_2O)	Flow Rate (L/sec)	Turbine Speed (rpm)	Electrical Power $\dot{W}_E$ (W)	Total power loss $\dot{W}_{loss}$ (W)	Turbine Power $\dot{W}_T$ (W)	Turbine efficiency $\eta_t = \frac{\dot{W}_T}{\dot{m}gH}$ %	Overall efficiency $\eta_o = \frac{\dot{W}_{loss}}{\dot{m}gH}$ %
41.37 [6] (4.2)	30.04	2198	328.00	176.47	504.47	40.60	26.40
41.37	28.86	2070	393.02	165.45	558.47	46.78	32.92
41.37	28.25	1996	440.17	159.12	599.29	51.29	37.67
41.37	27.00	1853	492.45	146.93	639.39	57.25	44.09
41.37	25.87	1715	518.94	135.25	654.19	61.13	48.49
41.37	24.75	1575	526.98	123.48	650.46	63.53	51.47
41.37	23.63	1440	525.85	112.21	638.05	65.27	53.79
41.37	22.51	1298	518.88	100.42	619.31	66.51	55.73
41.37	22.16	1250	511.58	96.46	608.04	66.33	55.80
41.37	21.25	1125	493.04	86.18	579.22	65.87	56.07
41.37	20.60	1027	473.93	78.16	552.09	64.78	55.61
41.37	20.18	958	459.51	72.54	532.05	63.74	55.05
41.37	19.67	875	441.36	65.80	507.17	62.33	54.24
41.37	19.10	772	413.77	57.48	471.26	59.64	52.36
41.37	18.60	675	380.55	49.68	430.23	55.91	49.45
41.37	18.02	550	332.61	39.69	372.30	49.94	44.62

The modified exit nozzle design with 6mm of split pipe overlap for guiding the water in form of solid jet has proven to be effective to some extend. This is evident from the improved turbine performance. Also as discussed in the stationary test analysis in section 5.6 the measured torque and the estimated torque are seen to be approximately equal. This shows that there is little to almost no scattering of the water jets leaving the exit nozzles.

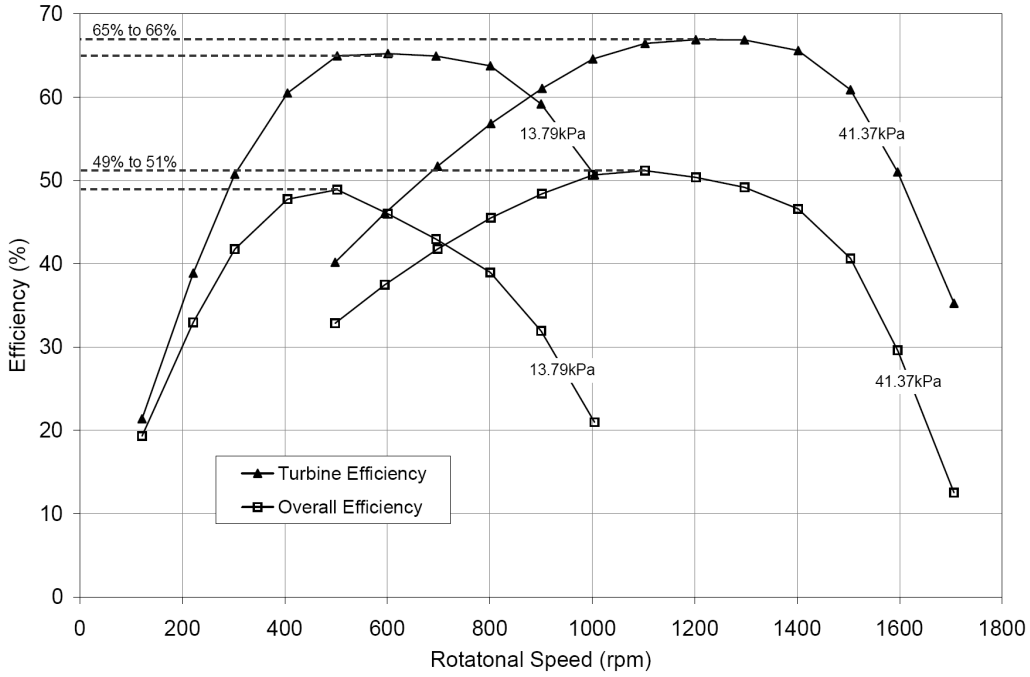

Figure 5.28 Estimated turbine and electrical efficiencies characteristics of SRT 125D-120L-8W with V-ring rotary seal

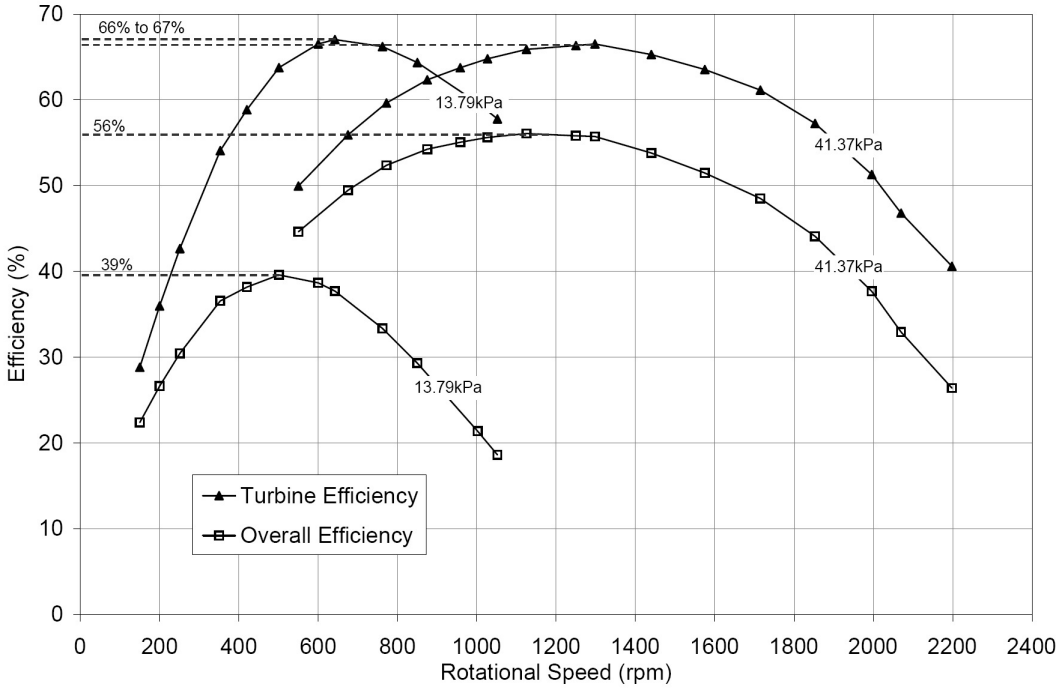

Figure 5.29 Estimated turbine and electrical efficiencies characteristics of SRT 125D-120L-8W with NMS rotary seal

5.7.4 Energy balance analysis

Energy balance analysis is carried out to verify the accuracy and dependability of the experimental data and procedures. Figure 5.30 and Figure 5.31 shows the energy balance of sample data from the performance tests conducted on the SRT prototype2, this is based on the governing equation 2.36 discussed in Chapter 2. The energy input is estimated from the measured flow rate and the measured supply pressure as $\dot{m}gH$. The turbine power is estimated as discussed earlier in section 4.5 (see Chapter 4). The fluid frictional power loss is estimated from the measured flow rate, estimated k-factor and estimated relative velocity as $\frac{1}{2}\dot{m}kV_r^2$. And the kinetic power lost with the water leaving the turbine is estimated from the measured flow rate and estimated absolute velocity as $\frac{1}{2}\dot{m}V_a^2$. For example, it can be seen from Figure 5.30 at 1400rpm the input power is 965W, where as the sum of output is equal to the 931W, this shows that there is an error of 34W in the estimation (i.e. ≈ 4%). This error may be due to instrumental uncertainty and the fact that the turbine rotates in wet environment (additional drag from splashing of water drops) while producing power where as the turbine drag power loss is estimated only in normal atmospheric air and there will be small amount of unaccounted power loss present there. Overall, the energy balance around maximum power point is within ±8%.

Finally the instrumental uncertainty analysis shows a maximum relative uncertainty of ±5.89% in the estimation of the total output power $\dot{W}_{Out} = \dot{W}_T + \dot{W}_{Ff} + \dot{W}_{Ke}$ and a relative uncertainty of ±3.75% in the estimation of the hydro input power $\dot{W}_{In}$ (see Table - C-18, Appendix C), making a possible instrumental uncertainty of ±9.64%.

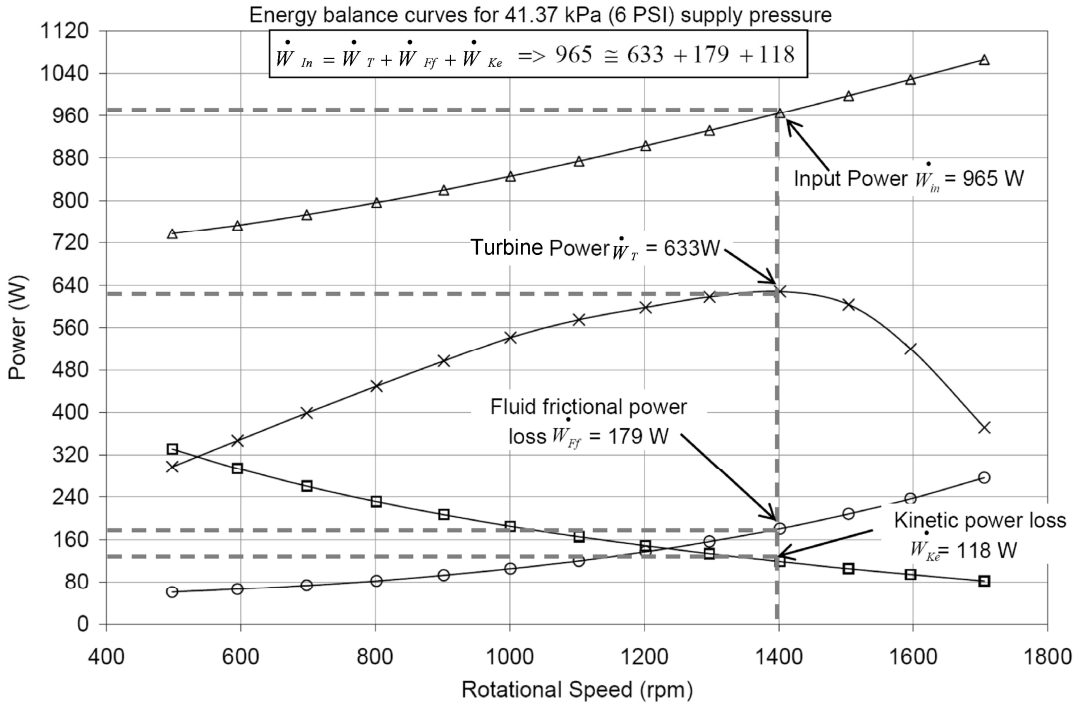

Figure 5.30 Energy balance curves for SRT 125D-120L-8W with V-ring rotary seal

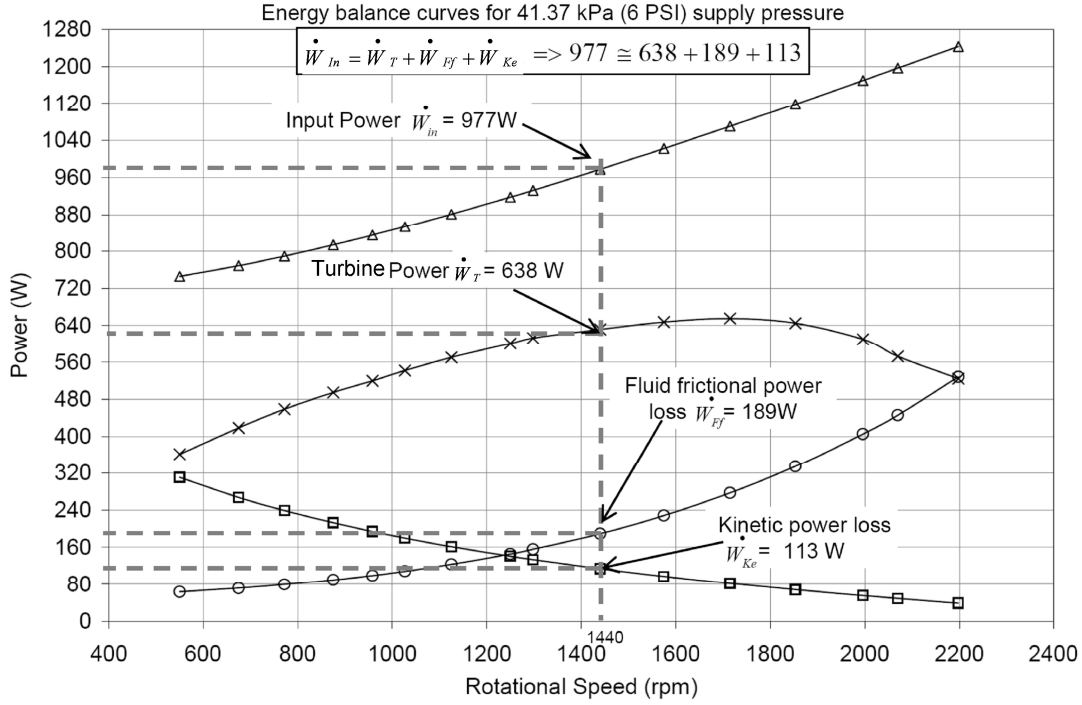

Figure 5.31 Energy balance curves for SRT 125D-120L-8W with NMS rotary seal

After considering this fact of relative instrumental uncertainty of ±9.64% and some amount of unaccounted power loss in turbine drag under water drops, it can be said

that the overall energy balance analysis shows good confidence in the experimental data measurements and procedures used in the performance testing of the SRT prototype 2.

5.8 Summary

The objectives of this experimental analysis have been fulfilled, in that performance characteristics of all three prototypes have been satisfactorily measured, analysed and presented in this chapter.

Stationary tests on the CPT and all SRT prototypes showed a very close match between measured and estimated stationary torque values. This confirmed the reliability of the stationary test set-up. Further, it is observed that the fluid frictional losses are mainly dependent on the exit velocity (relative velocity) of the water leaving the turbine. The dependency of k-factor on relative velocity presents a possibility of testing simple reaction turbine models only under stationary conditions and still being able to predict the dynamic performance of these turbines using the value of k-factor from stationary tests carried out over a range of relative velocities.

Power output and power loss tests conducted on all the simple reaction turbine prototypes showed that CPT design has a significant amount of turbine drag loss compared to the SRT design. The reduced drag losses in the SRT are due to the disk shape design. All the turbine prototypes showed similar k-factor characteristics for stationary and rotary conditions. This helped to further confirm that the k-factor is a strong function of the relative velocity of the water leaving the turbine.

The maximum no-load speed of CPT (400mm diameter) is observed to be about 530rpm at 80kPa. Where as it is observed that SRT prototype1 (243mm diameter) runs at maximum no-load speed of 1365rpm at 50kPa supply pressure, further reducing the turbine diameter makes the simple reaction turbine spin at faster speeds as was the case of SRT ptototype2 (123mm effective turbine diameter), which could reach a maximum no-load speed of about 2200rpm. It was concluded that the CPT design is very difficult to build to desired diameter and desired exit nozzle areas. It is not possible to make a small diameter CPT turbine with large nozzle exit area using standard pipefittings. The SRT

design has that flexibility of changing the turbine diameter and exit nozzle area independent of each other.

It was seen from the comparison of the power loss test results with the V-ring rotary seal arrangement and the NMS arrangement that, the NMS has less frictional power losses which are almost a linear function of rotational speed; where as in case of V-ring seal the frictional power loss also depend on supply pressure in addition to rotational speed. It was observed that a V-ring lip seal perform poorly at higher pressure. Main advantages of using a V-ring seal are its simplicity to use/install, easy availability and low cost, where as NMS is not readily available for diameters above 100mm and are very expensive.

The turbine efficiency of CPT is about 55% (turbine efficiency), where as the turbine efficiency of SRT prototype1 is about 62% and SRT prototype2 is about 66%. This shows that SRT design is a better option and moreover a SRT design with some amount of split pipe overlap as exit nozzle guide for solid stream exit jets has better energy conversion performance. Overall energy balance analysis and uncertainty analysis has showed good confidence in the experimental procedures and the instrumentation used.

SRT prototype 2 was built to easily change the exit nozzle area as discussed in Chapter 3 section 3.2.2.3. SRT prototype 2 with 5.3mm (SRT-125D-120L-5.3W) exit nozzle width and 4.2mm (SRT-125D-120L-4.2W) exit width has been tested and their experimental results are supplied in Appendix B section B.1 and section B.2. These results show strong characteristic resemblance with SRT-125D-120L-8W. It is seen that as the nozzle exit area is reduced by reducing the exit nozzle width the power output drops and the overall efficiency of the hydroelectric system decreases due to inefficient operation of DC generator at part load. The turbine efficiency for all the SRT prototype 2 models is constant over a range of supply head and rotational speed.

In the conclusion, statement for this chapter it can be confidently said that a “Split reaction turbine (SRT)” design is very flexible, with good energy conversion efficiency and is an economic alternative to the presently available commercial turbines for use at low head hydro sites for electricity generation.

Chapter 6 Potential site survey and Case study

6.1 Introduction

This chapter describes the site surveys done as a part of the research and the hydrology involved in doing a micro hydro site survey. This chapter is divided into the following sections:

- The first section discusses the hydrology study techniques used in the survey of potential ultra low head sites (Head measurement, Flow measurement and Geology study)
- In the second section a case study of one site has been discussed

Here the smallest flow method has been used to determine the potential of all the hydro sites surveyed. The smallest flow method is the simplest and the most accurate method used to determine the power output capacity of a hydro project. In this method the smallest flow in the stream is determined (in the driest period of the year) and the hydroelectric system is designed for that flow rate. For this method to work all that is required is some certainty that next year or in some future year after the hydro system is installed this smallest flow would still be available in the driest period of the year (Harvey, 2005). This kind of certainty can be predicted with the availability of the past minimum flow rate data for that stream. This data could be measured or could be just a guessed value by the property owners for at least the past 10 years.

6.2 Hydrology study literature review

The hydrology study of a potential hydropower site involves estimation of the available flow rate and head. The suitability of any hydro site depends upon the available head and minimum water flow rate to produce the desired amount of power. So it is very important to accurately determine the available head and minimum flow rate. There are various methods that can be implemented for measuring the available head and the flow rate, in this section some of these methods have been discussed in detail, which were used in the potential site survey as a part of this research project.

6.2.1 Head measurements

The first approach to determine the available head could be by using local maps. This represents a quick first look at the various possibilities in the region, but does not represent a careful measurement of head. As head is the most important factor in design and costing of a hydro scheme it must be measured accurately with an accuracy of $\pm 3\%$ (Harvey, 2005). For an accurate measurement of the available head, it is recommended to take more than one measurement of the head, as it is possible to make mistakes while measuring. It is also recommended to use two different methods to measure the head for a single site and then try to obtain agreement of the measured readings. If the measured readings do not agree closely with each other, then it is recommended to table further measurements until agreement is achieved. There are number of methods to measure head; some are more suitable for low head sites and inaccurate on high head sites, while some are only suitable for high head sites. It's always recommended to use a head measurement method suitable for the type of site (high head or low head) and the availability of the instruments (Wilson, 1983, Whyte, 1985, Harvey, 2005). Some of the head measurement methods are listed below,

Table 6.1 Comparison of head measurement techniques (Harvey, 2005)

Method	***Comments***	***Advantages and limitations***	***Accuracy***	***Precautions***
Water-filled tube and rods	Weight: Light Expense: Low	Long-winded for high heads	Approx 95%	Repeat measurements
Sprit level and plank (or string)	Weight: Light Expense: Low	Unsuitable for long gentle slops, slow to use. Best done with two people	Approx 95% on steep slopes, 80-90% on gentle slopes	Repeat measurements
Builders' levels (Dumpy level)	Weight: Heavy Expense: Can be hired, since in common use	Not good on wooded sites Fast	Very good	Liable error Calculations can introduce errors
Map	Map-reading skills Weight: Light Expense: Low	High heads only Wrong site may be identified	Depends on quality and scale of map	Map may be incorrect Check correct site identified

6.2.1.1 Water-filled tube

This method is suitable for low head sites and so is used for head measurement at one of the sites. The equipments required for this method are nylon hose (transparent), height marker (measuring tape) and a record sheet. This method can be reasonably accurate if used properly. A single measurement is not sufficient to get accurate readings; at least two of three separate measurements must be taken. Figure 6.1 shows the use of this method (Harvey, 2005). This method can even be used on long distances without using long tube; this is done in steps and later all the heights are added to get the total head.

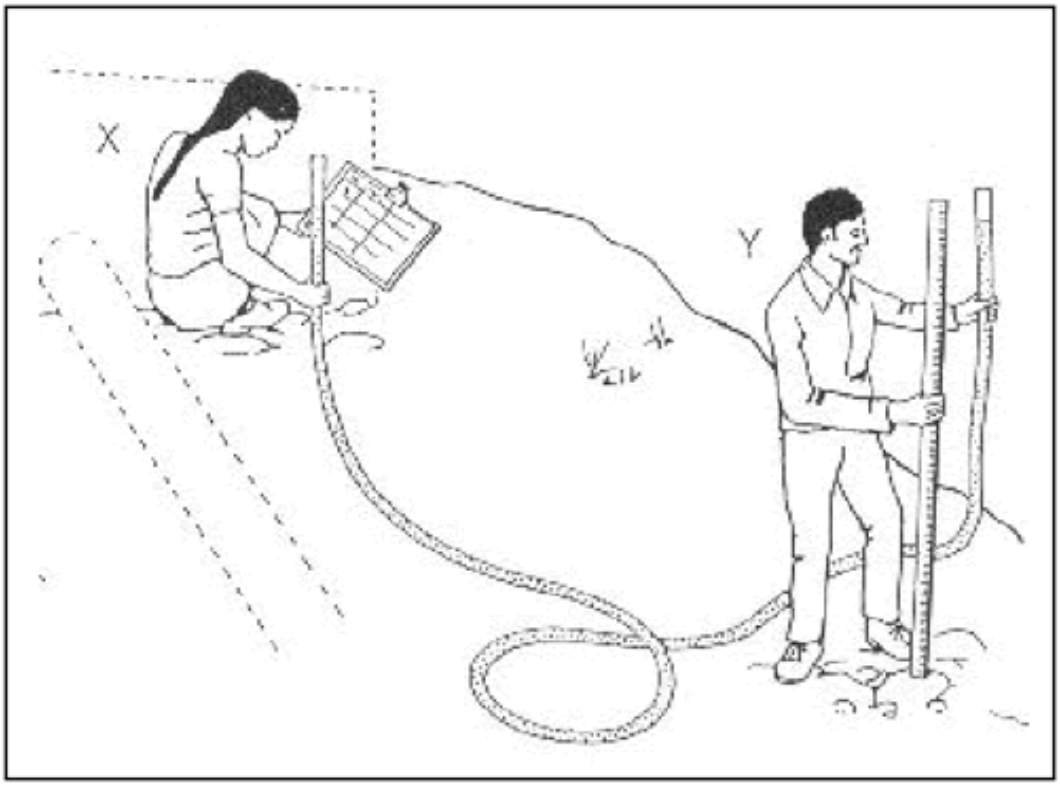

Figure 6.1 Water filled tube method (Harvey, 2005)

6.2.1.2 Builders' levels (Dumpy level)

This method is suitable for low head sites. However, the equipment is expensive and heavy. As the owners of one of the sites under survey are architects, they preferred to use this method for head measurement. Builders for survey very commonly use this method so the equipment is easily available on rent.

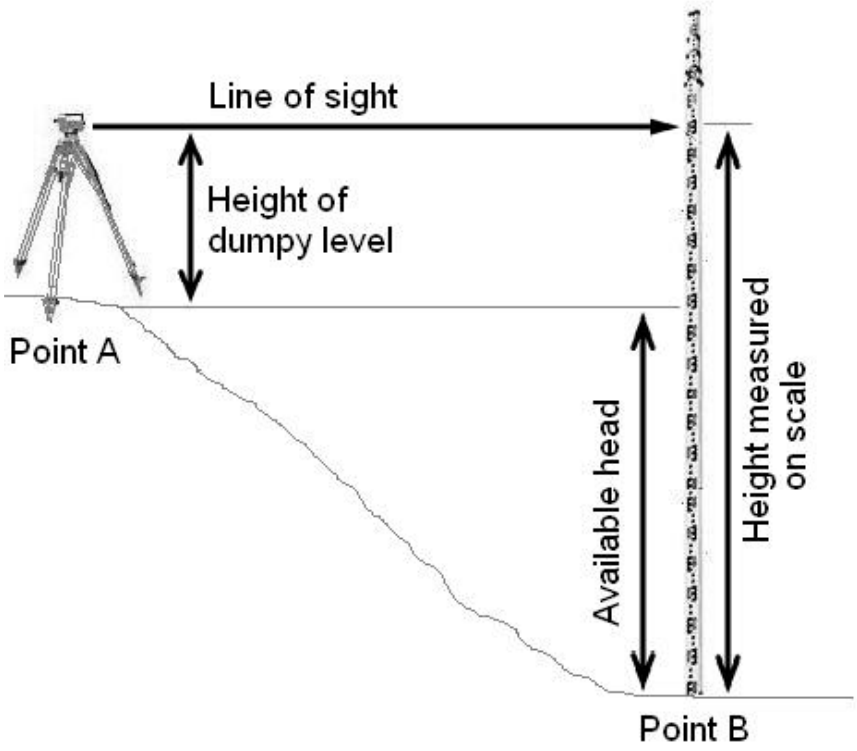

Figure 6.2 Builders level (Dumpy level) measurement technique (Harvey, 2005)

6.2.2 Flow measurement

Accurate flow measurement is very critical in the design of micro-hydro systems. For low head sites the power producing capacity mainly depends on the available water flow. To protect the aquatic life in and around the water stream it is desirable not to use more than 50% of the total annual average flow for hydropower systems. Flow predictions should not be based on single flow measurement, as it will lead to wrong flow predictions in most of the cases. It is desired to take daily flow measurements over a year to accurately predict the average flow. When daily measurement is not possible, a weekly flow measurement can also be used for annual average of the flow. Some times a conservative approach is used for flow measurements, where a daily flow measurement is recorded only during the driest period of the year, which predicts a minimum average flow. The main reason to use this kind of approach is to design a hydro system that can operate even during the dry periods without affecting the aquatic life. The following flow

measurement techniques are used in the hydrology study of the potential sites in this research.

6.2.2.1 The bucket method

This is the simplest way of measuring the flow; it is only suitable for small flow measurements. The whole flow to be measured is diverted into a bucket as shown in Figure 6.3 and the time required to fill the bucket is recorded. The volume of the bucket is then divided by the measured time to get the volume flow rate. The disadvantage of this method is that the whole flow must be channelled into the bucket, which often requires temporary dam so the method is only practical for small water streams.

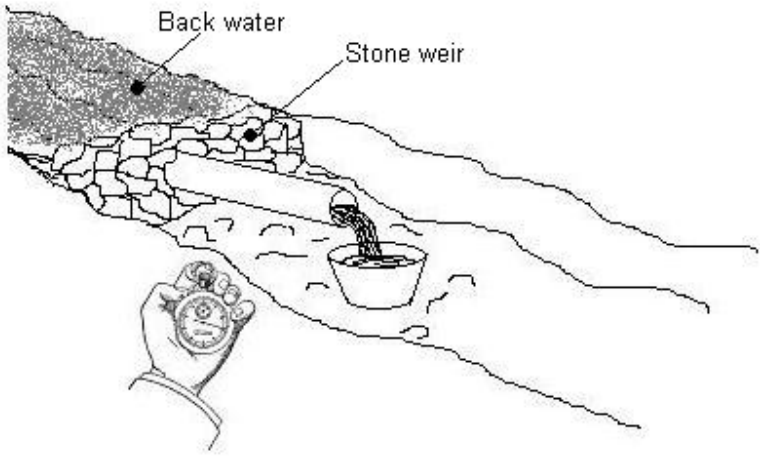

Figure 6.3 Bucket flow measurment method

6.2.2.2 The float method

An approximate cross-sectional profile of the streambed is charted over a known length of the stream. A float which can submerge in the water but which will not sink to the bottom is allowed to flow with the stream and is timed over the known length of a section of the stream as shown in Figure 6.4. This process is repeated for different sections across the stream width and the results are averaged to obtain the flow velocity. Then the volume flow rate is obtained as a product of the mean cross-sectional area of the stream and the average flow velocity as shown in Figure 6.4. Some more flow measuring techniques used for hydrology study are salt gulp method, propeller device method, stage control method and weir method (Harvey, 2005).

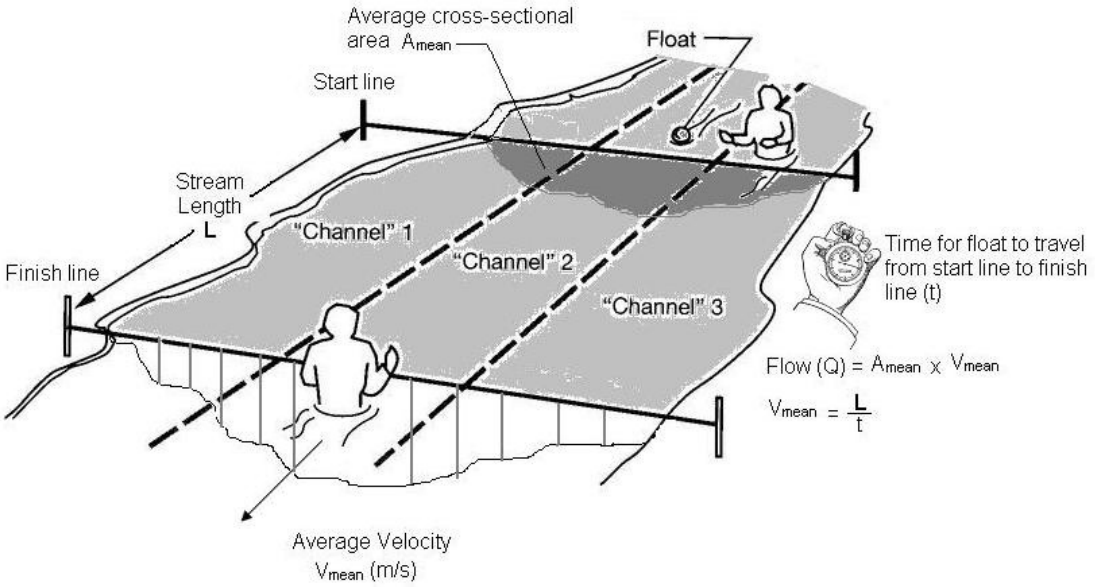

Figure 6.4 Float flow measurement method (Harvey, 2005)

6.3 Case study of potential hydro sites

The case study of a potential hydro site involves hydrology study, design of system layout, design of turbine, generator selection, design of energy storage system and economic analysis. The head and flow measurement techniques discussed earlier are used for the hydrology study of the potential sites. In the system layout the water extraction method is selected based on the available head and 50% of the average flow. Provision is made in the layout to allow the remaining 50% of water to flow through the normal stream to sustain the surrounding environment. Selection of proper diameter and length of intake pipe is very critical in case of low-head micro hydro schemes, so as to keep the fluid frictional losses to minimum. The split reaction turbine is then designed for the net head available at the end of the intake pipe and for the corresponding flow. The generator selection is based on power requirement (A.C. or D.C.) and distance of the load from the generator. The energy storage system is designed as standalone or grid interactive system depending on the distance to the nearest grid and the amount of power produced. A standalone system is used if the grid is far and power produced is small. Economic analysis considers capital and maintenance cost of the system and is then compared with the expenses involved to obtain grid connection.

6.3.1 Site 1 – Taggerty, Victoria

Taggerty is located approximately 110km North East of Melbourne as shown in Figure 6.5. There is not grid connection available at the property; the nearest grid location is about 1.5km away. The property owner has obtained a cost estimate to get their property grid connected for AU$60,000. The present daily energy requirement of the farm (≈ 11 Acres) and house (2 occupants) is about 16kWh, out of which about 4-5kWh is required for pumping water from the creek to the storage pond on the farm.

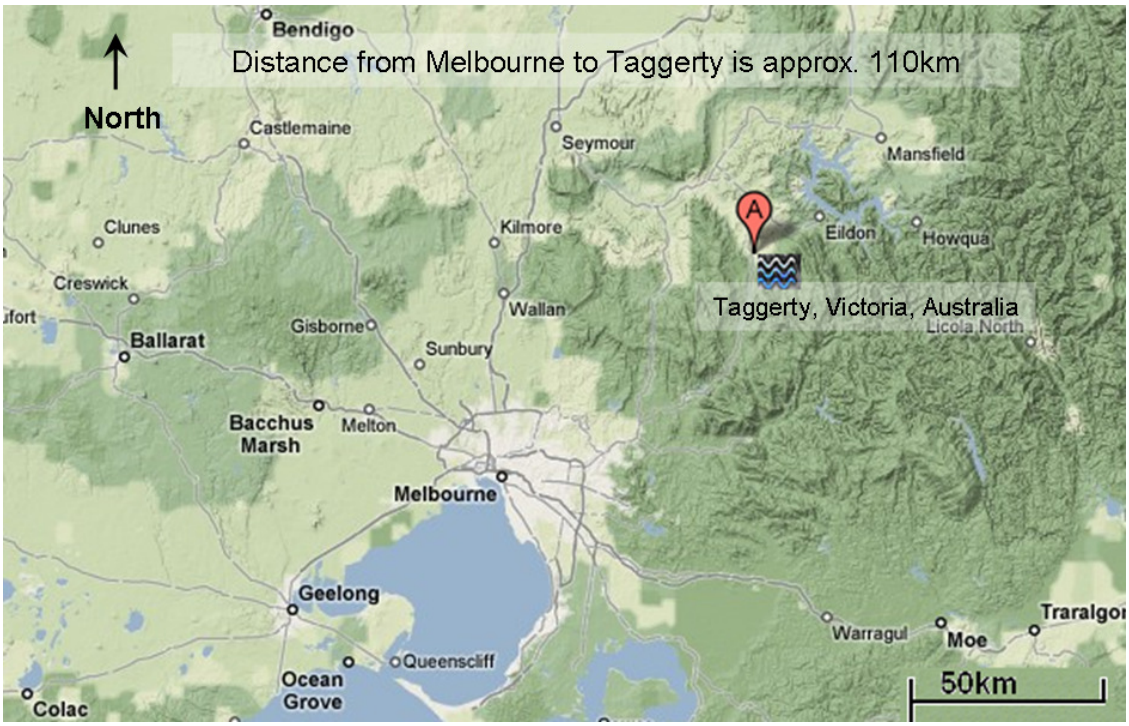

Figure 6.5 Location of- Site1 with reference to Melbourne, Australia (Ref: Google Earth)

The property is spread over 160 acres with a small farm and a medium size creek that flows along the east boundary as shown in Figure 6.6. The water required for the farm and household use is pumped from the creek and stored in a shallow storage pond on the farm. At present petrol engine (power 5HP; 3.7kW) driven water pump is used to pump the water from the creek and deliver it to the pond (5m static head + 11m dynamic head loss @ 10L/s). The current delivery pipe from the creek to the storage pond is a 3-inch diameter PVC pipe. The storage pond has around 300m² of surface area and is 0.5-1m deep. During cultivation period of the year the daily water requirement of farm about 75m³.

Figure 6.6 Supply catchment's from which water will be captured; Site1: Taggerty, Victoria, Australia (Ref: Google Earth)

6.3.1.1 Hydrology study

Hydrology study of this site was carried out over the driest period of the year (i.e. December to January 2007). As one of the property owners is an architect she preferred to use builder's level (dumpy level) for head measurement. The measured head was 3m over a 300m distance (i.e. slope $\Delta y/\Delta x = 0.01$). Flow rate was measured with float method as the water stream under consideration was very wide and that was not suitable for bucket method. The first flow measurement was recorded on 10th November 07. This was followed by alternate week measurement of the flow taken by the property owners till the last measurement taken on 26th January 08. The average flow was measured to be 63 litres per second as shown in Table 6.2.

Table 6.2 Flow measurement data with float method (Site1, Taggerty)

Flow measurement Date (dd/mm/yy)	Stream length (m)	Average time for float to travel stream length (sec)	Average stream velocity (m/s)	Average cross-section area over stream length (m^2)	Volume flow rate (m^3/sec)	Volume flow rate (l/sec)
10-Nov-07	10	31.62	0.316	0.213	0.0674	67

24-Nov-07	10	32.58	0.307	0.213	0.0654	65
8-Dec-07	10	34.13	0.293	0.213	0.0625	62
22-Dec-07	10	35.25	0.284	0.213	0.0605	60
12-Jan-08	10	36.44	0.274	0.213	0.0585	59
26-Jan-08	10	34.68	0.288	0.213	0.0615	61
Average flow rate over driest period of the year (l/s)						**63**

6.3.1.2 Hydro system layout

Water from the creek will be captured via small stone weir. Figure 6.7 shows the proposed location for the weir. The captured water would then be carried to the low head hydroelectric unit located on the dry land 150m down the stream via 0.15m diameter PVC pipe (see Figure 6.8 and Figure 6.9). The used water from the turbine will then be discharged back into the creek. The stonewall will be constructed from natural materials (i.e. stones, boulders and mud) thereby ensuring that the water which is not used for the hydro scheme will continue to flow through the weir. Only 50% of total flow will be used for the hydro scheme, which is about 30L/s. The net head available at the hydro unit is estimated taking into account the dynamic head loss in the intake water pipe and the gross head available as shown in Table 6.3 and Table 6.4.

Table 6.3 Gross head estimations

Intake pipe diameter (mm)	Intake pipe length L_P (m)	Terrain down slope ($\Delta y/\Delta x$)	Height of the stone weir HW (m)	Gross head available HG (m) $L_p*(\Delta y/\Delta x)+ Hw$
150	150	0.01	0.6	2.1

Table 6.4 Net head estimations

Intake volume flow rate (l/s)	Flow velocity in Intake pipe (m/s)	Reynolds number	friction factor	Dynamic head loss in Intake pipe H_{DL} (m)	Net available head H_N (m) ($H_G - H_{DL}$)
28	1.59	237317.30	0.00516	0.661	1.44
30	**1.70**	**254268.53**	**0.00510**	**0.750**	**1.35**
32	1.81	271219.77	0.00505	0.844	1.26

Figure 6.7 Proposed weir on the creek- Site1 (Taggerty, Victoria)

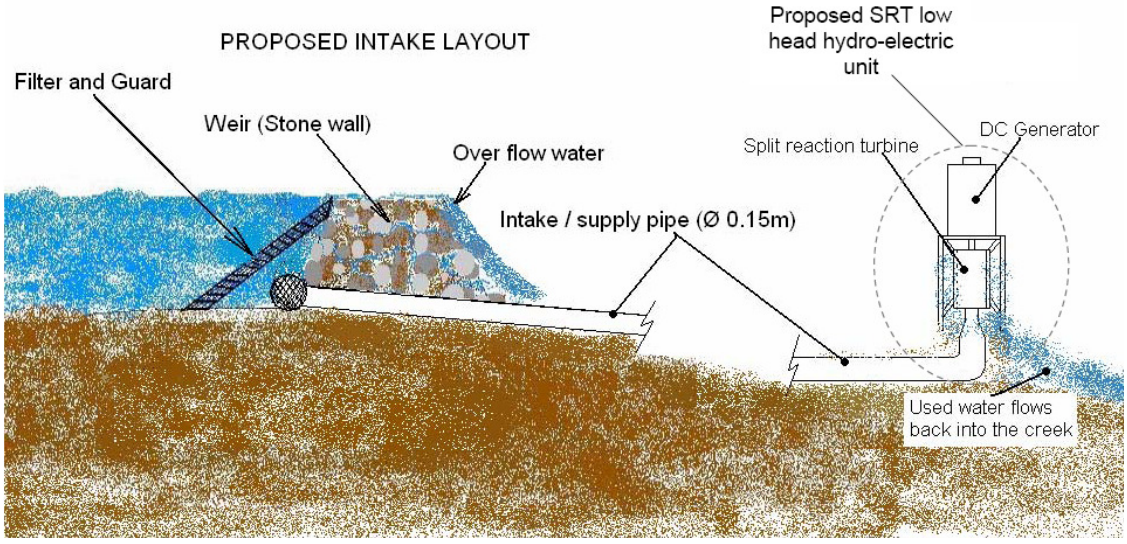

Figure 6.8 Sketch of proposed intake layout

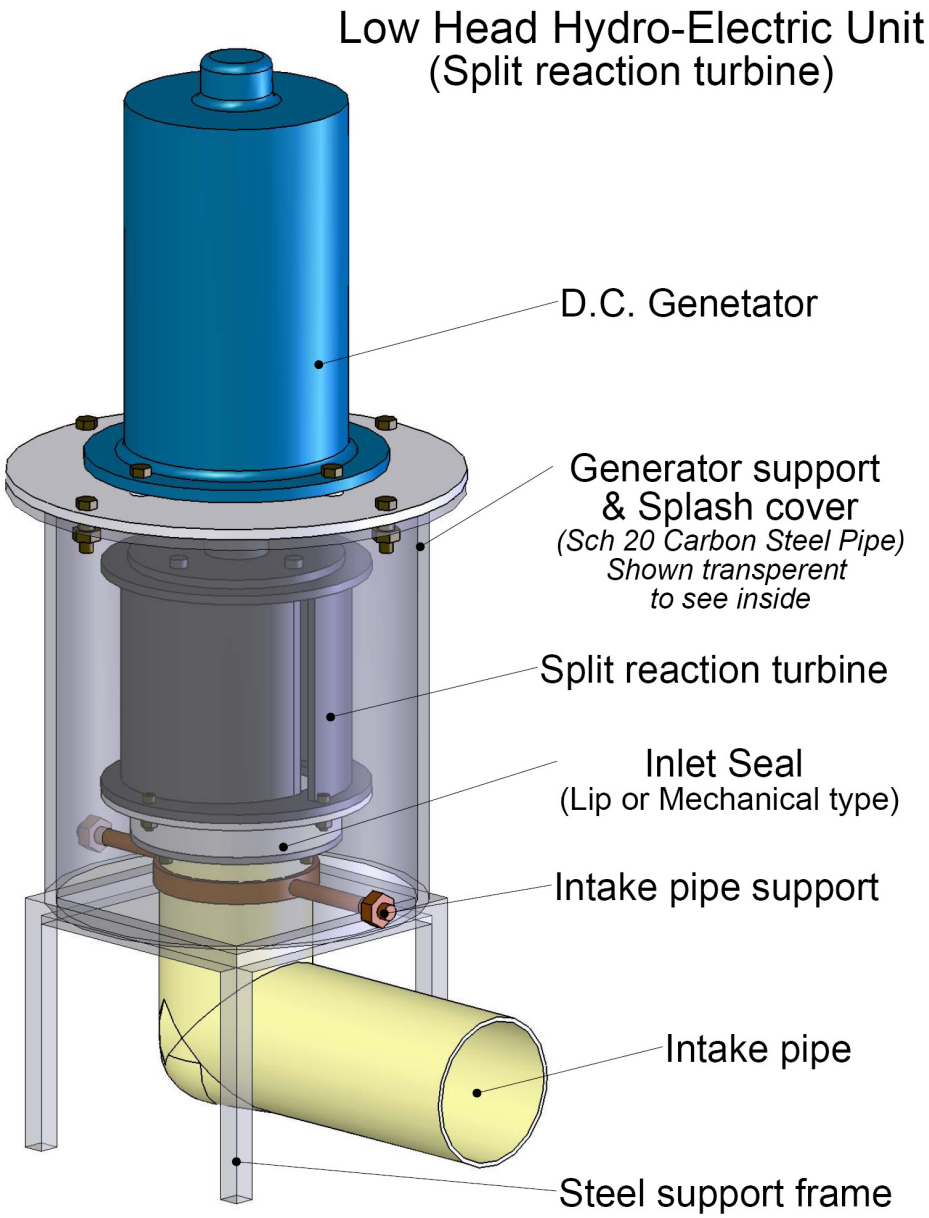

Figure 6.9 Proposed SRT low head hydro-electric unit

It can be seen from Table 6.4 that estimated net available head at the intake to the hydroelectric unit is 1.35m for a flow of 30 L/s. So the estimated potential hydro power is equal to 397 W. Assuming the energy conversation efficiency from hydro to electrical to be 50%, the estimated electrical power produced will be 198 W; i.e. 4.76kWh of daily energy production capacity.

As the nearest grid is 1.5km away a standalone system should be used with a 5kWh energy storage capacity in a 48V DC battery bank. Two methods can be used to charge the battery bank, first is with battery charger, i.e. indirect connection, and second is with direct coupling of the hydroelectric unit to the battery bank. The first option is more expensive and has its own limitations and disadvantages. While the second option is cheap but requires proper selection of DC generator and optimum turbine speed. A baldor DC motor with a rated DC voltage of 180V at 1750rpm can be used as a DC generator. Such an electric DC machine has a linear voltage to rotational speed characteristics, i.e. a 50V to 54V DC can be generated if the optimum rotational speed of the turbine is within at 500rpm to 525rpm. This voltage range of 50V to 54V is suitable for direct charging of 48V DC battery bank.

6.3.1.3 Split reaction turbine design

A net head of 1.35m and flow rate of 30L/s is selected from Table 6.4 for the design of the split reaction turbine. The assumptions made in the split reaction turbine design are; density of water equals to 1000kg/m³, gravitational acceleration equals to 9.81m/s², turbine optimum speed equals to 525rpm (55 rad/sec) and a conservative value of k-factor to be 0.1 (based on the experimental test results as discussed in chapter 5, see Figure 5.12 and Figure 5.24). The governing equations as discussed in chapter 2 are used in turbine dimension predictions. The optimum turbine diameter can be calculated using equation 2.41 and the total exit nozzle area can be calculated using the relation between the relative velocity, volume flow rate and exit nozzle area. Choice of two exit nozzles is made for this turbine, so the area of each nozzle would be half the total exit nozzle area. The choice of rectangular shape is made for exit nozzles with the exit nozzle height selected as 0.2m and so the exit nozzle width would be equal to the area for one nozzle divided by the exit nozzle height as shown in Table 6.5.

Table 6.5 Optimum diameter and exit nozzle dimension estimation

Net available head H_N (m)	Available flow rate (l/s)	Turbine k-factor	Turbine operational angular speed (rad/s)/(rpm)	Optimum turbine diameter (m)	Total exit nozzle area (m²)	Number of nozzles	Each exit nozzle height (m)	Each exit nozzle width (m)
1.44	28	0.1	55 / 525	0.208	0.0038	2	0.2	0.0094
1.35	**30**	**0.1**	**55 / 525**	**0.201**	**0.0042**	**2**	**0.2**	**0.0104**

1.26	32	0.1	55 / 525	0.195	0.0046	2	0.2	0.0115

The jet interference speed of the turbine with optimum diameter of 0.201m and exit nozzle width of 0.0104m can be calculated using equation 2.46; this should always be greater than the turbine operational speed as discussed in chapter 2. It can be seen from Table 6.6 that for a jet exit angle of $\theta = 0°$ and turbine wall thickness of 6mm (standard wall thickness of Ø150-250mm, Sch. 20 PVC pressure pipe), the jet interference speed is greater than the turbine operational speed, this is desired for optimum turbine operation.

Table 6.6 Non-interference speed check

Net available head (m) H_N	Optimum turbine diameter (m)	Turbine k-factor	Exit nozzle width (m) w	Turbine wall thickness (m) T	δ = w + t (m)	Turbine operational speed (rad/s)	Jet Interference speed (rad/s) ω_{int} $\theta = 0°$
1.44	0.208	0.1	0.0094	0.006	0.0154	55	62.81
1.35	**0.201**	**0.1**	**0.0104**	**0.006**	**0.0164**	**55**	**61.37**
1.26	0.195	0.1	0.0115	0.006	0.0175	55	59.89

Table 6.7 shows the turbine power estimation for the net available head and available flow rate; equations 2.1, 2.2, 2.9, 2.11 and 2.38 are used for this estimation. Final selection of a D.C. generator is based on this information.

Table 6.7 Turbine turbine power and efficiency estimation

Net available head H_N (m)	Available flow rate (l/s)	Turbine k-factor	Turbine operational angular speed (rad/s)	Optimum turbine diameter (m)	Turbine power (Watts)	Turbine efficiency (%)
1.44	28	0.1	55	0.208	276.28	69.85%
1.35	**30**	**0.1**	**55**	**0.201**	**277.51**	**69.85%**
1.26	32	0.1	55	0.195	276.28	69.85%

Baldor Permanent Magnet D.C. motor model number CDP3436 (0.56kW) is selected from the Baldor selection chart as shown in Table 6.8. Model CDP3436 (0.56kW) is selected over model CDP3326 (0.37kW) because the full load current of this model is high, it will protect the armature from overheat damage when operating at lower voltage than rated (i.e. at low rpm then rated rpm). From Table 6.8 and Table 6.9 it can be seen that when the DC generator is producing 208W of electrical power at 55rad/s, the generator output voltage would be around 54 V (Voltage constant $K_v = 0.9$) and the

generator output current would be about 3.85 amps which is very close to the full load armature current for model CDP3436.

Table 6.8 Baldor motor selection chart

Catalogue Model Number	Motor kW	Base rpm	Arm Volt (V)	Arm Full Load Amps	Voltage constant Kv (V/rad/sec)	Full load efficiency	List Price $A	NEMA Frame
CDP3306	0.18	1750	180	1.25	0.98	83%	440	56C
CDP3316	0.25	1750	180	1.6	0.98	84%	502	56C
CDP3326	0.37	1750	180	2.5	0.98	87%	567	56C
CDP3436	**0.56**	**1750**	**180**	**3.8**	**0.98**	**88%**	**684**	**56C**

Table 6.9 Electrical output from Baldor DC motor CDP343

Turbine power (Watts)	D.C. generator efficiency @ 50% of full load (%)	Electrical power output (Watts) $\dot{W}_E$ @55rad/s	DC Generator output voltage (Volts) $V_g = \omega * K_v$	DC Generator output current (Amps) $I_g = \dot{W}_E / V_g$	Daily electrical energy output (kWh)
276.28	75%	207.21	54	3.84	4.973
277.51	**75%**	**208.13**	**54**	**3.85**	**4.995**
276.28	75%	207.21	54	3.84	4.973

The generator output voltage of 54V is a good charging voltage for a 48V battery bank. With a blocking diode connected in between the DC generator and the batteries, discharge of energy from the battery into the generator can be prevented. This protection would be useful when voltage drops below 48V; voltage may decrease if available head drops due to some blockage at the entrance of intake pipe. A battery bank of four 12V, 115Ah batteries (Trojan Flooded Lead Acid Battery, Model 27TMX) connected in parallel would have energy storage capacity of 5.5kWh, which is sufficient for this particular site with a daily energy generation of 4.99kWh.

6.3.1.4 Selection of DC water pump

Daily water requirement of the farm on this site is 75m³. The shortest distance from the creek to the storage pond is about 500m with an average up slope of about 0.01; it means that a water pump with a minimum delivery head of 5m is required, so a DC water pump, which can deliver 75m³/day (i.e. 3.125m³/hr over 24hrs) with total energy consumption no more than 4.7kWh is required for this site.

Table 6.10 and Table 6.11 shows the estimated gross delivery head required to pump 3.125m³/hr through a presently installed 3 inch diameter delivery pipe. It can be seen that the gross delivery head of 5.12m is required to deliver water with a flow rate of 3.125m³/hr.

Table 6.10 Storage pond water supply system

Delivery pipe diameter (inch/mm)	Delivery pipe length (m)	Terrain up slope ($\Delta y/\Delta x$)	Daily water requirement (m^3)	Daily pump operation time (hrs)	Volume flow rate (m^3/hr)
3 / 75	500	0.01	75	24	3.125

Table 6.11 Delivery head requirement of water pump

Velocity (m/s)	Renolds number	friction factor	Dynamic head loss (m) H_D	Static head loss (m) H_S	Gross delivery head required (m) $H_D + H_S$
0.196	14714.62	0.0086	0.113	5	5.113

Figure 6.10 shows the pump selection curves for Conergy DC water pumps powered by battery. A 48V DC water pump by Conergy (Model 7442) can deliver 3.2 m³/hr to a delivery head of 5.5m, with power consumption of 182W, i.e. 4.37kWh of energy required to pump 75m³ in 24hrs.

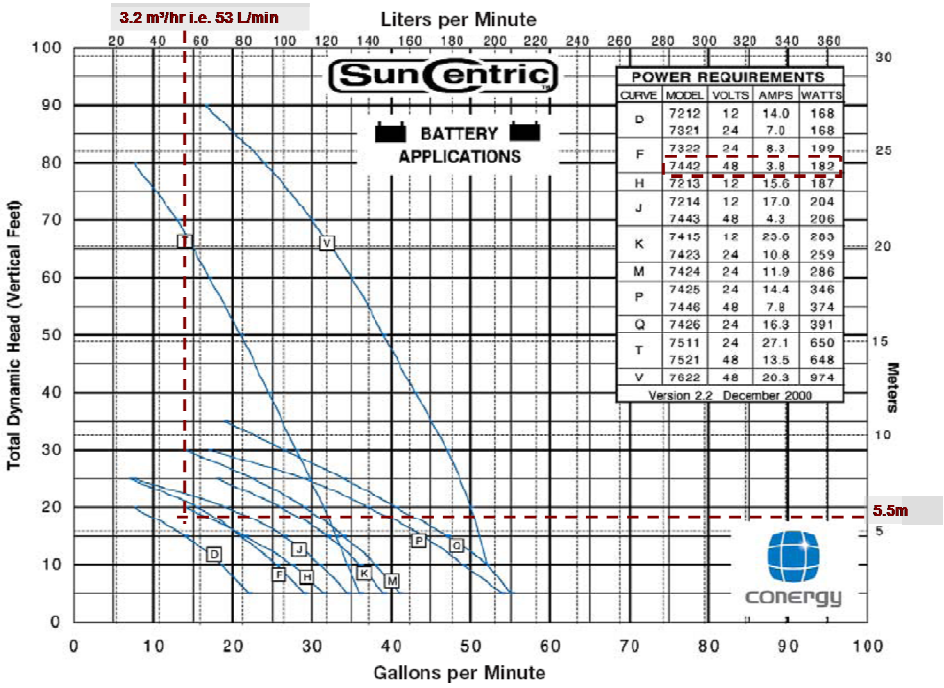

Figure 6.10 Conergy DC pump selection curves *(Ref. Conergy product resource)*

6.3.1.5 Costing of the hydro-electric installation

The PVC pipe that will carry the water from the creek to the hydroelectric unit will have diameter of 150mm and length of 150m. The cost of this PVC pipe is $23.35 (see Table - D-2, in Appendix D) per meter making the total material cost of the pipe to be $3502.

Table 6.12 Cost of intake pipe

Pipe cost $/m	Pipe Diameter (mm)	Pipe length (m)	Total pipe cost
23.35	150	150	$3502

The selected Baldor DC motor which may be used as a generator, costs $684 (www.baldor.com.au) and the cost to build the split reaction turbine and the support is about $250.

Table 6.13 Cost of DC generator and turbine with support

Generator type	Generator Model	Generator cost	Cost of turbine + support
D.C.	CDP3436	$684	$250

The total material cost for this hydroelectric set-up comes out to be $4236. The labour cost to install such a system is considered to be 100% of the material cost. So the total cost of to install this system will be $8472.

Table 6.14 Total cost of the hydro-electric installation

Total Material cost Pipe + Generator + Turbine	Labor cost 100% of material cost	Total Cost
$4236	$4236	$8472

Australian Federal Government supports installations of renewable energy systems in remote areas by giving a rebate 50% of the total cost, making the actual investment from the site owners to be only $4236.

6.3.1.6 Conclusion of case study

In conclusion of this case study it could be said that sufficient amount of power can be produced from the low head hydro resource available, which can in turn supply energy required for pumping 75m³/day. So the present petrol engine water pump can be replaced with the DC electric water pump powered by hydroelectric unit.

Chapter 7 Conclusion and Future work

7.1 Conclusion

In the conclusion of this thesis, it can be said that for global sustainable development it is very important to utilise renewable energy resources with low green house gas emissions. Additionally there is a huge technically exploitable hydropower potential available throughout the world, if utilized this can represent a significant fraction of the present global electricity consumption. Presently available low head micro hydro turbines are very expensive making them economically unattractive to be used for electricity production at an individual level. The high cost of presently available low head water turbines put an economical limitation to the utilization of the technically exploitable hydropower potential. Keeping this in mind research was conducted to achieve the main aim of this project of developing a low cost, high performance simple reaction water turbine for electricity production from low headwater resources. The task-oriented objectives are achieved and their conclusions are discussed in the following text.

From the theoretical analysis, it is seen that mass flow rate increases with the increase in the rotational speed due to the centrifugal pumping action. The variation of $\dot{m}$ with rotational speed is almost linear and the effect of supply head on the mass flow rate vanishes at high rotational speeds. It is also seen that for a practical situation with fluid frictional losses the simple reaction turbine will never experience the runaway condition of infinite speed.

It is seen from the theoretical investigation that the maximum power point would shift to a higher rotational speed for a given geometry of a turbine with increase in the supply head. It is also seen that the efficiency of the turbine is dependent on the k-factor and turbine efficiency would decrease with increase in the value of k-factor.

Further, it is seen from the theoretical investigation that the optimum diameter of the split reaction turbine is a function of supply head, rotational speed and k-factor and is independent of output power capacity of that turbine. Therefore, for a constant rotational speed and constant k-factor value, if head increases the corresponding optimum diameter

would increase. If the head and k-factor are kept constant, to achieve high rotational speed a smaller turbine diameter is required. At very high rotational speed the effect of static head on the optimum diameter starts to diminish. For a given power output at constant rotational speed and constant k-factor, a small diameter and tall turbine configuration would evolve at low static head, while under higher static heads the turbine would become large in diameter and would get shorter.

The phenomenon of jet-interference has been theoretically investigated in this research thesis. It shows how the jet-interference speed can be predicted for a turbine of known geometry. The disadvantage of the jet-interference is that it limits the power producing capacity of a turbine with a given diameter and operating speed, as this limits the allowable exit nozzle width. So it is important to consider jet-interference while designing a simple reaction turbine and especially the split reaction turbine developed in this research. A concept design of a self-governing simple reaction turbine has been presented with theoretical model.

The theoretical prediction of centrifugal pumping effect has been verified and validated from the experimental analysis and it is seen that the simple reaction turbine generates prominent centrifugal pumping effect with increase in rotational speed causing the mass flow rate to increase. When the turbine is stationary the mass flow rate is dependent on static head, but as the turbine starts to spin faster the effect of static head on the mass flow rate is experimentally seen to diminish as predicted in the theoretical investigation. Further, it is seen from the experimental investigation that the value of k-factor (fluid friction factor) increases with increase in relative velocity. However, the turbine shows efficiencies that do not vary greatly over a wide range of rotational speeds for different static head. With increase in static head, the maximum efficiency point and maximum power point move to higher rotational speed.

Stationary tests on CPT and all SRT prototypes showed a very close match between measured and estimated stationary torque values. In addition, the uncertainty analysis of the stationary test data showed a maximum instrumental uncertainty of ± 5%. This confirmed the reliability of the stationary test set-up and its instrumentation. It is also observed that the fluid frictional losses are mainly dependent on the exit velocity

(relative velocity) of the water leaving the turbine. This dependency of k-factor on relative velocity presents a possibility of testing any simple reaction turbine model only under stationary conditions at high pressures to simulate high relative velocity conditions and hence estimate the k-factor values at those high relative velocities. This estimated value of k-factor can then be used to predict the rotary performance (i.e. while power is extracted) of those simple reaction water turbines.

Power and power loss tests conducted on all simple reaction turbine prototypes show that cross pipe turbine design has a significant amount of power loss in turbine drag as compared to the SRT design. The reduced drag losses in the SRT are due to the disk shape rotor design. All the turbine prototypes show similar k-factor characteristics for stationary and rotary (i.e. while power is extracted) conditions. This helped to further confirm that the k-factor is a strong function of the relative velocity of the water leaving the turbine as is seen from the stationary tests. The maximum no-load speed of CPT is observed to be about 530rpm at 80kPa. Where as it is observed that SRT prototype1 (243mm diameter) runs at maximum no-load speed of 1365rpm at 50kPa supply pressure, further reducing the turbine diameter makes it spin at faster speeds as in case of SRT prototype2 (125mm diameter). This could reach a maximum no-load speed of about 2200rpm. The CPT design is not flexible to be manufactured with desired diameter and exit nozzle areas. It is not possible to make a small diameter CPT turbine with large nozzle exit area using standard pipefittings. The SRT design has the flexibility of changing the turbine diameter and exit nozzle area independent of each other.

It is seen from the comparison of power loss tests conducted on V-ring lip seal and NMS arrangement that, NMS has less frictional losses and these losses are almost a linear function of rotational speed; where as in case of V-ring lip seal the frictional losses depend on rotational speed and supply pressure. It was observed that a V-ring lip seal introduces high power loss at higher pressure; this is due to the large surface contact force between the stationary and rotary parts. While the V-ring seal are simple to use and install, they are also easily available and are inexpensive. Where as the NMS is not readily available for diameters above 100mm and they are very expensive.

Therefore, for the rotary seal at inlet of the turbine, a V-ring lip seal gives a very good seal with medium to low frictional power losses and are very inexpensive. These are simple to install and are easily available off the shelf products. While the nylon mechanical seal (NMS) have very good water sealing properties and have low frictional power loss, NMS are expensive and special products. So for remote area and micro hydro application a V-ring lip seal is an excellent rotary seal choice for any simple reaction turbine.

The turbine efficiency of CPT is about 55% (turbine efficiency), where as the turbine efficiency of SRT prototype1 is about 62% and SRT prototype2 is about 66%. This shows that the basic SRT design is a better option then CPT. In addition to this SRT design with some amount of split pipe overlap as exit nozzle guide for solid stream exit jets shows even higher energy conversion efficiency as demonstrated with SRT prototype2.

The power test results have demonstrated a good overall energy balance for all turbine prototypes. Further the uncertainty analysis of the power tests data shows a maximum instrumental uncertainty of ±6% (see Appendix C section C.3). This shows a good confidence in the experimental procedures, test set-up and the instrumentation used for the power tests.

SRT prototype 2 has been built to easily change the exit nozzle area as discussed in Chapter 3 section 3.2.2.3. SRT prototype 2 with 5.3mm (SRT-125D-120L-5.3W) exit nozzle width and 4.2mm (SRT-125D-120L-4.2W) exit width has been tested and their experimental results are supplied in Appendix B section B.1 and section B.2. These results show strong characteristic resemblance with SRT-125D-120L-8W. It is seen that as the nozzle exit area is reduced by reducing the exit nozzle width the power output drops and the overall efficiency of the hydroelectric system decreases due to inefficient operation of DC generator at part load. The turbine efficiency for all the SRT prototype 2 models is constant over range of supply head and rotational speed.

The SRT design is very flexible and can be modified to produce desired amount of power with no extra cost. The cost to build a 1kW “Split reaction turbine” including the cost of inlet port with V-ring rotary seal and the flange coupling for power

transmission would be about AU$250 to $300 (see Table 3.1 in Chapter 3). The cost of 1kW SRT is much lower as compared to other commercially available turbines as described by Harvey (Harvey, 2005) see Table 1.2 in Chapter 1.

The aim of this research to develop a low cost and high performance simple reaction water turbine for low head application has been achieved with fulfillment of all task oriented objectives. In the final conclusion of this thesis it can be confidently said that a "Split Reaction Turbine" (SRT) design is very flexible, it has good energy conversion efficiency and is an economic alternative to commercially available turbines for use in low head micro hydropower generation.

7.2 Future work

As the Split reaction turbine design has been optimised and tested in the laboratory a field trial will provide further necessary information for commercialisation of this turbine. The case study presented in this thesis at Taggerty site in Victoria, Australia, will provide a preliminary experience for real life installations of SRT. Future work will involve installation of split reaction turbines at a couple of different low head hydro sites and monitoring their performance over an extended period of time across all seasons. This will involve further low head site surveys in Australia or Overseas.

References

AINSWORTH, J. R. (1910) *"Science in modern life"*, The Gresham publishing company.

AKBARZADEH, A. (2001) Parametric Analysis of a Simple Reaction Water Turbine and its Application for Power Production from Low Head Reservoirs. *Fluids Engineering Division Summer Meeting.* New Orleans, Louisiana, USA, ASME.

AUSTRALIAN STANDARDS (2006) *AS/NZS 1477:2006 : PVC pipes and fittings for pressure applications*.

BARTLE, A. (2002) Hydropower potential and development activities. *Energy Policy,* 30**,** 1231-1239.

CENGEL Y., T. R. (2006) *Fundementals of Thermal-Fluid Sciences,* New York, Mc Graw Hill.

CONTI, J. J., HOLTBERG, P.D., & BEAMON, J.A. (2008) Annual Energy Outlook 2008. Energy Information Administration, US Department of Energy

DATE, A., AKBARZADEH, A. (2009) Design and cost analysis of low head simple reaction hydro turbine for remote area power supply, . *Renewable Energy,* 34**,** 409-415.

DATE, A., AKBARZADEH, A. (2005) Design Analysis and Investigation of a low head simple reaction water turbine. IN ANZSES (Ed.) *43rd ANZSES conference.* Dunedin, New Zealand.

DAUGHERTY, R. L., INGERSOLL, A.G. (1954) *"Fluid Mechanics with engineering applications"*, McGraw-Hill Book Company.

DROSG, M. (2007) *Dealing with Uncertainties : A Guide to Error Analysis,* Berlin, Heidelberg, Springer-Verlag Berlin Heidelberg.

DUNCAN, W. J., THOMAS, A.S., YOUNG D. (1970) *Mechanics of Fluids*, Edward Arnold.

ENFIELD, M. (2005) Banki-crossflow systems design guide. Planetary Power.

HARVEY, A. (2005) *MICRO-HYDRO TURBINE MANUAL - A guide to small-scale water power schemes*, ITDG Publishings.

HAU, E., RENOUARD, H. (2006) *Wind Turbines Fundamentals, Technologies, Application, Economics,* New York, Springer.

INCROPERA, F. P., DEWITT, D. P., (2002) *Fundamentals of Heat and Mass Transfer,* Brisbane, Juhn Wiley & Sons.

JEFFS, E. J. (1979) The application potential of hydro power. *Energy,* 4**,** 841-849.

KAYGUSUZ, K. (2004) Hydropower and the Worlds Energy Future. *Energy Sources,* 26**,** 215-224.

KHAN, M. J., IQBAL,M.T., QUAICOE,J.E. (2008) River current energy conversion systems: Progress, prospects and challenges. *Renewable and Sustainable Energy Reviews,* 12**,** 2177-2193.

KHENNAS, S., BARNETT, A. (2000) Micro-hydro power: An option for socio-economic development. IN SAYIGH, A. A. M. (Ed.) *World Renewable Energy Congress VI.* Oxford, Pergamon.

LEO, B. S., HSU, S. T. (1960) A simple reaction turbine as a solar engine. *Solar Energy,* 4**,** 16-20.

MENET, J. L. (2004) A double-step Savonius rotor for local production of electricity: a design study. *Renewable Energy,* 29**,** 1843-1862.

OAKEY, A. (1993) *Make your own Savonius rotor wind turbine : plans for water pumping and generating electricity,* Melbourne, Alternative Energy Association of Australia.

QUEK, S. (2001) Development of High head reaction turbine. *Department of Mechanical and Manufacturing Engineering.* Melbourne, RMIT University.

QUEK, W. (2003) Design, analysis and testing of a simple reaction turbine for power. *Department of Mechanical and Manufacturing Engineering.* Melbourne, RMIT University.

SAHA, U. K. & RAJKUMAR, M. J. (2006) On the performance analysis of Savonius rotor with twisted blades. *Renewable Energy,* 31**,** 1776-1788.

SCHLICHTING, H. (1955) *Boundary Layer Theory*, McGraw-Hill Book Co., Inc.

SEARS, F. W., ZEMANSKY, M. W. (1955) *University Physics*, Addison-Wesley Press.

SHEPHERD, D. G. (1956) *"Principles of turbomachinery"*, MacMillan company.

SOMMERS, G. L. (2004) Hydropower Resources. IN CLEVELAND, C. J. (Ed.) *Encyclopedia of Energy.* New York, Elsevier.

STERNBERG, R. (2008) Hydropower: Dimensions of social and environmental coexistence. *Renewable and Sustainable Energy Reviews,* 12**,** 1588-1621.

TAYLOR, R. (2004) Hydropower. IN J TRINNAMAN, A. C. (Ed.) *2004 Survey of Energy Resources (Twentieth Edition).* 20 ed. Oxford, Elsevier Science.

TURTON, R. K. (1995) *Principles of turbomachinery*, Chapman & Hall.

WADDELL, R., BRYCE, P. (1999) Micro-hydro systems for small communities. *Renewable Energy,* 16**,** 1257-1261.

WEBB, D. H. (1999) The design, development and testing of a Barker's Mill reaction water turbine. *Department of Mechanical and Manufacturing Engineering.* Melbourne, RMIT University.

WHITE, F. M. (1986) *Fluid Mechanics,* New York, McGraw-Hill Book Company.

WHITELAND, J. (1832) Suggested improvements in the construction of Barker's mill. *Journal of the Franklin Institute,* 14**,** 73-76.

WHYTE, W. S. (1985) *Basic metric surveying,* London; Boston, Butterworths.
WILSON, E. M. (1983) *Engineering Hydrology,* London, Macmillan.
WILSON, P. N. (1974) *Water turbines,* London, Her Majesty's Stationary Office.

Appendix A Building a Split reaction turbine model

A.1 Manufacturing of SRT prototype 2

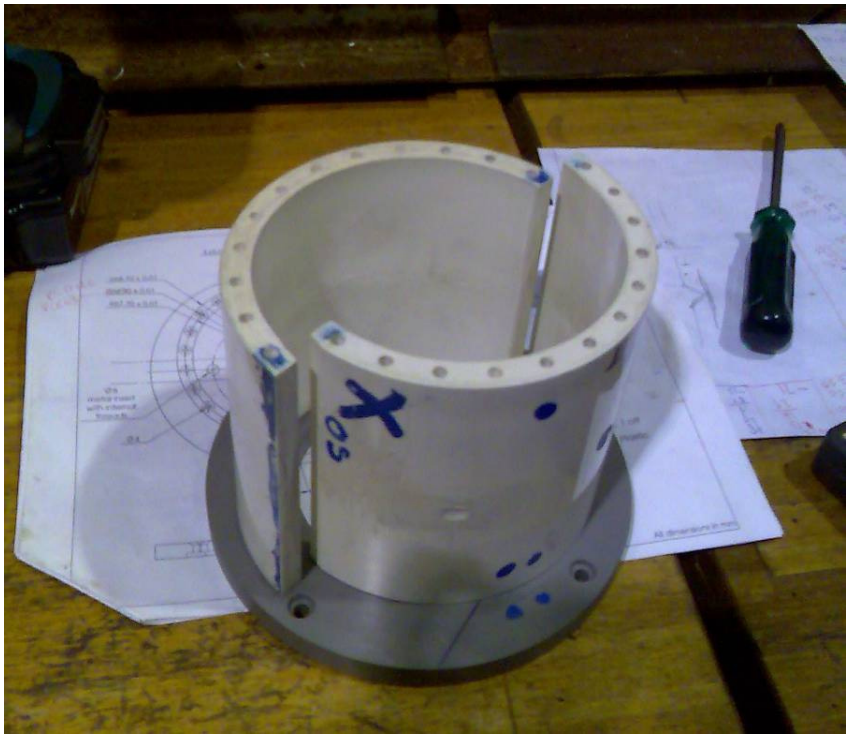

Figure - A.1 Split reaction turbine prototype 2

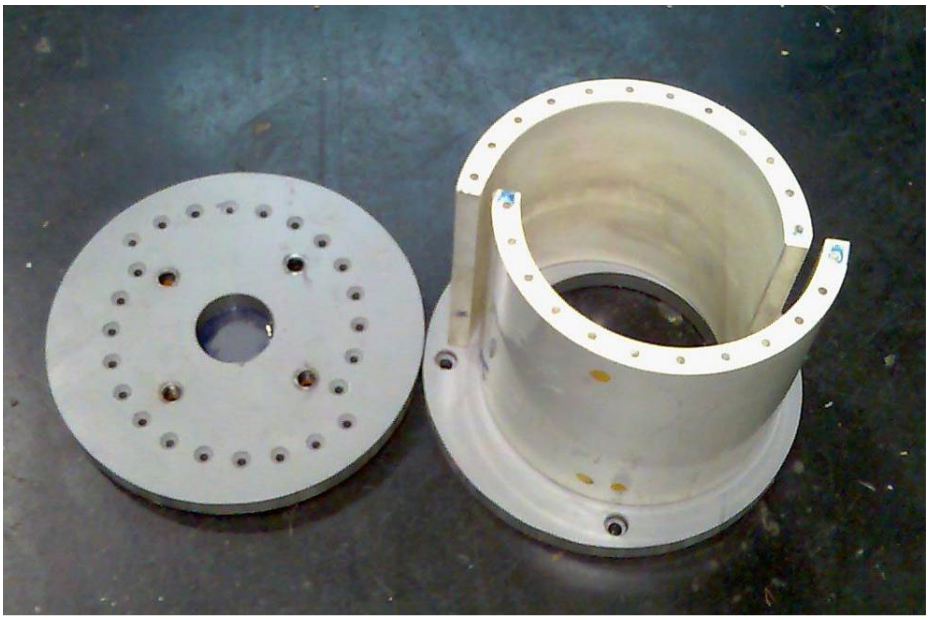

Figure - A.2 Split reaction turbine prototype 2

Figure - A.3 Split reaction turbine prototype 2

Figure - A.4 Split reaction turbine prototype 2

Figure - A.5 Split reaction turbine prototype 2

The top shaft flanged coupling can be bought off the shelf from the couple of manufacturers.

Figure - A.6 Shaft coupling by Watson Marine
(http://www.watsonmarine.com.au/watsonmarine/couplings.htm)

Figure - A.7 Shaft coupling by Teign Bridge
(http://www.teignbridge.co.uk/shaft_couplings.html)

Inlet port can be made from off the shelf stainless steel pipe flanges as shown in Figure - A.8; a welding neck type flange can be used, which will require very little machining.

CARBON & STAINLESS STEEL FLANGES • Dimensions & Weights

Class 150 Flanges to ASME B16.5

Nominal Size		Dimensions												Weight (kg)		
						Length Thru Hub		Bolt Drilling								
DN	NPS	Flange OD A mm	Flange Thickness D mm	Bore SOW SW B mm	Raised Face Diam. G mm	SOW, SW Threaded C mm	W Neck C mm	Circle Diam. K mm	Hole Diam. H mm	Bolts No.	Bolt Diam. In	RF Stud Bolt Length mm	RF Mach. Bolt Length mm	SOW SW	WN	Blind
15	1/2	88.9	11.2	22.4	35.1	15.8	47.8	60.4	15.7	4	1/2"	60.0	45.0	0.4	0.5	0.4
20	3/4	98.6	12.7	27.7	42.9	15.8	52.3	69.9	15.7	4	1/2"	65.0	50.0	0.6	0.7	0.6
25	1	108.0	14.2	34.5	50.8	17.5	55.6	79.2	15.7	4	1/2"	65.0	55.0	0.8	1.0	0.9
32	1 1/4	117.3	15.7	43.2	63.5	20.6	57.2	88.9	15.7	4	1/2"	70.0	55.0	1.0	1.3	1.2
40	1 1/2	127.0	17.5	49.5	73.2	22.4	62.0	98.6	15.7	4	1/2"	70.0	60.0	1.3	1.7	1.5
50	2	152.4	19.1	62.0	91.9	25.5	63.5	120.7	19.1	4	5/8"	80.0	65.0	2.1	2.6	2.4
65	2 1/2	177.8	22.4	74.7	104.6	28.5	69.9	139.7	19.1	4	5/8"	90.0	75.0	3.3	4.1	3.9
80	3	190.5	23.9	90.7	127.0	30.2	69.9	152.4	19.1	4	5/8"	90.0	75.0	3.9	4.9	4.9
90	3 1/2	215.9	23.9	103.4	139.7	31.8	71.4	177.8	19.1	8	5/8"	90.0	75.0	4.8	6.1	6.2
100	4	228.6	23.9	116.1	157.2	33.3	76.2	190.5	19.1	8	5/8"	90.0	75.0	5.3	6.8	7.0
125	5	254.0	23.9	143.8	185.7	36.6	88.9	215.9	22.4	8	3/4"	90.0	80.0	6.1	8.6	8.6
150	6	279.4	25.4	170.7	215.9	39.6	88.9	241.3	22.4	8	3/4"	100.0	85.0	7.5	10.6	11.3
200	8	342.9	28.4	221.5	269.7	44.5	101.6	298.5	22.4	8	3/4"	110.0	90.0	12.1	17.6	19.6
250	10	406.4	30.2	276.4	323.9	49.3	101.6	362.0	25.4	12	7/8"	115.0	95.0	16.5	24.0	28.8
300	12	482.6	31.8	327.2	381.0	55.6	114.3	431.8	25.4	12	7/8"	120.0	100.0	26.2	36.5	43.2
350	14	533.4	35.1	359.2	412.8	57.2	127.0	476.3	28.4	12	1"	130.0	110.0	34.6	48.4	58.1
400	16	596.9	36.6	410.5	469.9	63.5	127.0	539.8	28.4	16	1"	135.0	115.0	44.8	60.6	76.1
450	18	635.0	39.6	461.8	533.4	68.3	139.7	577.9	31.8	16	1 1/8"	150.0	125.0	48.9	68.3	93.7
500	20	698.5	42.9	513.1	584.2	73.2	144.5	635.0	31.8	20	1 1/8"	160.0	135.0	61.9	84.5	122.0
600	24	812.8	47.8	616.0	692.2	82.6	152.4	749.3	35.1	20	1 1/4"	175.0	145.0	86.9	115.0	185.0

Class 300 Flanges to ASME B16.5

Nominal Size		Dimensions												Weight (kg)		
						Length Thru Hub		Bolt Drilling								
DN	NPS	Flange OD A mm	Flange Thickness D mm	Bore SOW SW B mm	Raised Face Diam. G mm	SOW, SW Threaded C mm	W Neck C mm	Circle Diam. K mm	Hole Diam. H mm	Bolts No.	Bolt Diam. In	RF Stud Bolt Length mm	RF Mach. Bolt Length mm	SOW SW	WN	Blind
15	1/2	95.3	14.2	22.4	35.1	22.4	52.3	66.5	15.7	4	1/2"	65.0	55.0	0.6	0.8	0.6
20	3/4	117.3	15.7	27.7	42.9	25.4	57.2	82.6	19.1	4	5/8"	75.0	60.0	1.1	1.3	1.1
25	1	124.0	17.5	34.5	50.8	26.9	62.0	88.9	19.1	4	5/8"	80.0	65.0	1.4	1.5	1.4
32	1 1/4	133.4	19.1	43.2	63.5	26.9	65.0	98.6	19.1	4	5/8"	80.0	65.0	1.7	2.0	1.8
40	1 1/2	155.5	20.6	49.5	73.2	30.2	68.3	114.3	22.4	4	3/4"	90.0	75.0	2.5	2.9	2.7
50	2	165.1	22.4	62.0	91.9	33.3	69.9	127.0	19.1	8	5/8"	90.0	75.0	2.9	3.4	3.2
65	2 1/2	190.5	25.4	74.7	104.6	38.1	76.2	149.4	22.4	8	3/4"	100.0	85.0	4.3	5.2	4.9
80	3	215.9	28.4	90.7	127.0	42.9	79.2	168.1	22.4	8	3/4"	110.0	90.0	5.9	6.9	6.8
90	3 1/2	228.6	30.2	103.4	139.7	44.5	81.0	184.2	22.4	8	3/4"	110.0	95.0	7.3	8.7	8.7
100	4	254.0	31.8	116.1	157.2	47.8	85.9	200.2	22.4	8	3/4"	110.0	95.0	9.6	11.2	11.5
125	5	279.4	35.1	143.8	185.7	50.8	98.6	235.0	22.4	8	3/4"	120.0	100.0	12.3	15.1	15.6
150	6	317.5	36.6	170.7	215.9	52.3	98.6	269.7	22.4	12	3/4"	125.0	105.0	15.6	19.1	20.9
200	8	381.0	41.1	221.5	269.7	62.0	112.3	330.2	25.4	12	7/8"	140.0	110.0	24.2	29.9	34.3
250	10	444.5	47.6	276.4	323.9	66.5	117.3	387.4	28.4	16	1"	155.0	130.0	34.1	42.7	53.3
300	12	520.7	50.8	327.2	381.0	73.2	130.0	450.9	31.8	16	1 1/8"	170.0	145.0	49.8	61.8	78.8
350	14	584.2	53.8	359.2	412.8	76.2	142.7	514.4	31.8	20	1 1/8"	175.0	150.0	69.9	85.8	105.0
400	16	647.7	57.2	410.5	469.9	82.6	146.1	571.5	35.1	20	1 1/4"	190.0	160.0	88.1	106.0	137.0
450	18	711.2	60.5	461.8	533.4	88.9	158.8	626.7	35.1	24	1 1/4"	195.0	170.0	109.0	131.0	175.0
500	20	774.7	63.5	513.1	584.2	95.3	162.1	685.8	35.1	24	1 1/4"	205.0	180.0	134.0	158.0	221.0
600	24	914.4	70.0	616.0	692.2	106.4	168.1	812.8	41.1	24	1 1/2"	230.0	195.0	201.0	230.0	339.0

Class 600 Flanges to ASME B16.5

Nominal Size		Dimensions											Weight (kg)		
						Length Thru Hub		Bolt Drilling							
DN	NPS	Flange OD A mm	Flange Thickness D mm	Bore SOW SW B mm	Raised Face Diam. G mm	SOW, SW Threaded C mm	W Neck C mm	Circle Diam. K mm	Hole Diam. H mm	Bolts No.	Bolt Diam. In	RF Stud Bolt Length mm	SOW SW	WN	Blind
15	1/2	95.3	14.2	22.4	35.1	22.4	52.3	66.5	15.7	4	1/2"	80.0	0.7	0.9	0.8
20	3/4	117.3	15.7	27.7	42.9	25.4	57.2	82.6	19.1	4	5/8"	90.0	1.3	1.5	1.3
25	1	124.0	17.5	34.5	50.8	26.9	62.0	88.9	19.1	4	5/8"	90.0	1.5	1.8	1.6
32	1 1/4	133.4	20.6	43.2	63.5	28.4	66.5	98.6	19.1	4	5/8"	100.0	2.0	2.5	2.2
40	1 1/2	155.4	22.4	49.5	73.2	31.8	69.9	114.3	22.4	4	3/4"	105.0	3.0	3.5	3.3
50	2	165.1	25.4	62.0	91.9	36.6	73.2	127.0	19.1	8	5/8"	105.0	3.6	4.4	4.2
65	2 1/2	190.5	28.4	74.7	104.6	41.1	79.2	149.4	22.4	8	3/4"	120.0	5.3	6.4	6.1
80	3	209.6	31.8	90.7	127.0	46.0	82.6	168.1	22.4	8	3/4"	125.0	7.0	8.5	8.4
90	3 1/2	228.6	35.1	103.4	139.7	49.3	85.9	184.2	25.4	8	7/8"	140.0	8.8	10.7	11.0
100	4	273.1	38.1	116.1	157.2	53.8	101.6	215.9	25.4	8	7/8"	145.0	14.5	17.4	17.3
125	5	330.2	44.5	143.8	185.7	60.5	114.3	266.7	28.4	8	1"	165.0	24.4	29.2	29.4
150	6	355.6	47.8	170.7	215.9	66.5	117.3	292.1	28.4	12	1"	170.0	28.7	34.9	36.1
200	8	419.1	55.6	221.5	269.7	76.2	133.4	349.3	31.8	12	1 1/8"	195.0	43.4	53.9	58.9
250	10	508.0	63.5	276.4	323.9	85.9	152.4	431.8	35.1	16	1 1/4"	215.0	70.3	86.5	97.5
300	12	558.8	66.5	327.2	381.0	91.9	155.4	489.0	35.1	20	1 1/4"	220.0	84.2	103.0	124.0
350	14	603.3	69.9	359.2	412.8	93.7	165.1	527.1	38.1	20	1 3/8"	235.0	98.7	122.0	151.0
400	16	685.8	76.2	410.5	469.9	106.4	177.8	603.3	41.1	20	1 1/2"	255.0	142.0	170.0	214.0
450	18	743.0	82.6	461.8	533.4	117.3	184.2	654.1	44.5	20	1 5/8"	275.0	173.0	204.0	272.0
500	20	812.8	88.9	513.1	584.2	127.0	190.5	723.9	44.5	24	1 5/8"	290.0	220.0	254.0	349.0
600	24	939.8	101.6	616.0	692.2	139.7	203.2	838.2	50.8	24	1 7/8"	330.0	312.0	358.0	533.0

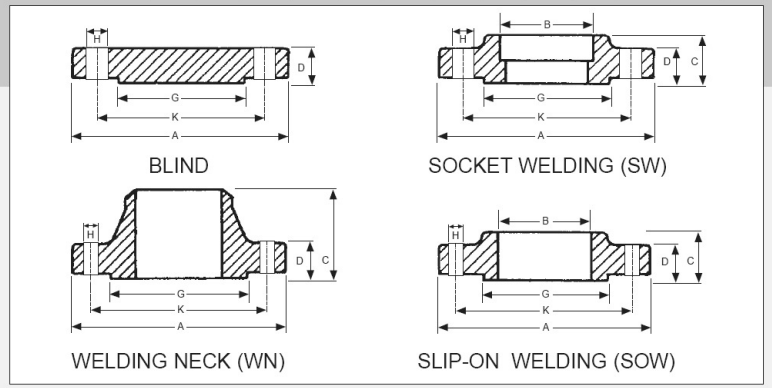

Note 1: All weights are approximate
Note 2: For Class 150, 300 the flange thickness "D" dimension includes approx. 1.5mm for the raised face height. For Class 600, 900, 1500, 2500 the flange thickness does not include the raised face height and approx. 6.4mm must be added to D dimension
Note 3: Bolt length dimensions incorporate the height of the raised face
Note 4: Welding Neck bore is derived from the pipe schedule

www.atlas-steels.com.au

Figure - A.8 Standard steel flange

Appendix B Measured and estimated performance data

B.1 Additional data on power loss experimental results

Table - B-1 Power loss estimation experimental results for DC motor alone

Motor supply voltage V_{in} (Volts)	Motor supply current I_{in} (Amps)	Turbine speed (rpm)	Estimated power Loss (V_{in} x I_{in}) (watts)
9.9	0.065	105	0.64
19.1	0.090	203	1.72
28.9	0.091	307	2.65
38.2	0.101	405	3.84
47.3	0.107	502	5.04
56.3	0.111	598	6.27
66.4	0.119	705	7.93
74.9	0.127	795	9.54
84.9	0.134	901	11.40
94.6	0.140	1004	13.25
103.8	0.147	1102	15.25
113.4	0.154	1204	17.49
122.9	0.162	1305	19.89
132.3	0.167	1405	22.13
141.5	0.172	1502	24.38
150.8	0.178	1601	26.78
160.5	0.183	1704	29.40
169.6	0.189	1800	32.07
179.2	0.194	1902	34.71
188.5	0.200	2001	37.63

Table - B-2 Power loss estimation experimental results for DC motor + SRT prototype 2 Turbine drag

Motor supply voltage V_{in} (Volts)	Motor supply current I_{in} (Amps)	Turbine speed (rpm)	Estimated power Loss (V_{in} x I_{in}) (watts)
11.1	0.207	118	2.3
19.1	0.293	203	5.6
28.4	0.339	301	9.6
37.9	0.386	402	14.6
47.6	0.391	505	18.6
56.6	0.397	601	22.5
65.9	0.412	700	27.2
75.3	0.432	799	32.5
85.2	0.436	904	37.1
94.4	0.446	1002	42.1
103.9	0.456	1103	47.4
113.2	0.465	1202	52.7
122.6	0.471	1301	57.7
132.0	0.477	1401	63.0
141.5	0.488	1502	69.0
151.2	0.497	1605	75.2
160.4	0.503	1703	80.7
169.7	0.507	1801	86.0
179.2	0.511	1902	91.5
189.2	0.519	2008	98.1

Table - B-3 Power loss estimation experimental results for DC motor + V-ring lip rotary seal + SRT prototype 2 Turbine drag @ 13.79kPa [2 PSI]

Motor supply voltage V_{in} (Volts)	Motor supply current I_{in} (Amps)	Turbine speed (rpm)	Estimated power Loss (V_{in} x I_{in}) (watts)
9.9	0.350	104	3.5
19.1	0.408	202	7.8
28.9	0.439	305	12.7
38.2	0.485	403	18.5
47.3	0.531	502	25.1
56.3	0.554	598	31.2
66.4	0.583	705	38.7
74.9	0.609	795	45.6
84.9	0.640	901	54.3
94.6	0.665	1003	62.9
103.8	0.691	1102	71.7
113.4	0.712	1204	80.7
122.9	0.734	1302	90.2
132.3	0.752	1405	99.6
141.5	0.769	1501	108.8
150.8	0.786	1601	118.6
160.5	0.806	1701	129.4
169.6	0.826	1800	140.0
179.2	0.840	1902	150.5
188.5	0.857	2003	161.6

Table - B-4 Power loss estimation experimental results for DC motor + V-ring lip rotary seal + SRT prototype 2 Turbine drag @ 41.37kPa [2 PSI]

Motor supply voltage V_{in} (Volts)	Motor supply current I_{in} (Amps)	Turbine speed (rpm)	Estimated power Loss (V_{in} x I_{in}) (watts)
9.5	1.923	101	18.3
18.7	1.383	198	25.8
28.1	1.236	298	34.7
38.0	1.164	403	44.2
47.3	1.148	502	54.3
56.5	1.125	600	63.6
66.4	1.126	705	74.8
75.5	1.138	802	86.0
85.0	1.159	902	98.5
94.0	1.192	998	112.1
103.1	1.220	1094	125.7
112.5	1.255	1194	141.1
122.8	1.284	1304	157.7
132.2	1.324	1403	175.0
141.6	1.363	1503	193.0
150.7	1.393	1600	210.0
160.5	1.433	1704	230.0
169.6	1.459	1800	247.4
179.0	1.485	1900	265.7
188.6	1.513	2002	285.4

Table - B-5 Power loss estimation experimental results for DC motor + NMS (Mechanical seal) + SRT prototype 2 Turbine drag

Motor supply voltage V_{in} (Volts)	Motor supply current I_{in} (Amps)	Turbine speed (rpm)	Estimated power Loss (V_{in} x I_{in}) (watts)
9.5	0.51	101	4.8
19.1	0.69	203	13.3
27.9	0.76	296	21.1
37.9	0.79	402	29.9
47.2	0.81	501	38.3
56.7	0.83	602	46.8
66.4	0.84	705	55.6
75.6	0.85	803	64.0
84.9	0.85	901	72.4
94.4	0.86	1002	81.1
103.8	0.87	1102	89.8
113.1	0.87	1201	98.4
121.4	0.87	1289	106.1
132.0	0.88	1401	116.0
140.8	0.88	1495	124.3
149.0	0.89	1582	132.0
160.7	0.89	1706	143.0
169.7	0.89	1802	151.6
179.1	0.90	1901	160.5
188.7	0.90	2003	169.7

B.2 Additional data on power test experimental results

Table - B-6 Power test experimental results for SRT-125D-120L-8W with V-ring seal @ 13.79kPa

Supply Pressure	Volume flow	Time	Estimated volume flow rate $\dot{V}$	Measured generator output voltage V_g	Measured generator output current I_g	Estimated electrical power output $\dot{W}_E$	Measured rotational speed of the turbine N	Angular speed of the turbine ω	Estimated input power $\dot{W}_{in}$ $\left(\dot{m}gh\right)$	Estimated overall efficiency η_o
kPa	m^3	sec	m^3/s	Volts	Amps	Watts	rpm	rad/s	Watts	%
13.79	0.2	12.99	0.0154	94.61	0.47	44.47	1004	105.13	212.0	20.98
13.79	0.2	13.78	0.0145	84.78	0.75	63.75	900	94.20	199.7	31.93
13.79	0.2	14.60	0.0137	75.45	0.97	73.44	801	83.84	188.5	38.96
13.79	0.2	15.57	0.0128	65.47	1.16	75.94	695	72.74	176.8	42.96
13.79	0.2	16.44	0.0121	56.61	1.36	77.00	601	62.90	167.4	46.00
13.79	0.2	17.35	0.0115	47.29	1.64	77.54	502	52.54	158.6	48.89
13.79	0.2	18.23	0.0109	38.15	1.89	72.10	405	42.39	151.0	47.75
13.79	0.2	19.08	0.0105	28.45	2.12	60.22	302	31.61	144.2	41.75
13.79	0.2	19.64	0.0102	20.82	2.22	46.20	221	23.13	140.2	32.97
13.79	0.2	20.10	0.0099	11.40	2.32	26.46	121	12.66	136.9	19.33

Table - B-7 Power test experimental results for SRT-125D-120L-8W with V-ring seal @ 13.79kPa

Estimated Power loss W_{loss}	Estimated generator turbine power $\dot{W}_T$ $\left(\dot{W}_E + \dot{W}_{loss}\right)$	Estimated turbine efficiency η	Relative velocity of the water jet V_r	Linear velocity of the turbine Nozzle U	Absolute velocity of the water jet V_a	k-factor	Estimated fluid frictional power loss $\dot{W}_{Ff}$ $\left(\frac{1}{2}\dot{m}kV_r^2\right)$	Estimated power loss in kinetic energy $\dot{W}_{Ke}$ $\left(\frac{1}{2}\dot{m}V_a^2\right)$	Estimated total output power $\dot{W}_{Out}$ $\left(\dot{W}_T + \dot{W}_{Ff} + \dot{W}_{Ke}\right)$
Watts	Watts	%	m/s	m/s	m/s		Watts	Watts	Watts
62.92	107.39	50.66	8.01	6.42	1.59	0.0734	19.33	36.15	162.86
54.43	118.19	59.19	7.54	5.75	1.79	0.0668	23.17	27.50	168.86
46.73	120.17	63.76	7.12	5.12	2.00	0.0616	27.29	21.33	168.79
38.85	114.80	64.93	6.68	4.44	2.23	0.0613	32.01	17.51	164.32
32.18	109.18	65.23	6.32	3.84	2.48	0.0594	37.33	14.40	160.91
25.49	103.03	64.96	5.99	3.21	2.78	0.0554	44.51	11.43	158.97
19.25	91.35	60.49	5.70	2.59	3.11	0.0540	53.10	9.61	154.06
12.97	73.19	50.75	5.45	1.93	3.52	0.0550	64.69	8.53	146.41
8.29	54.49	38.88	5.29	1.41	3.88	0.0555	76.53	7.90	138.93
2.82	29.28	21.39	5.17	0.77	4.40	0.0535	96.05	7.10	132.44

Table - B-8 Power test experimental results for SRT-125D-120L-8W with V-ring seal @ 41.37kPa

Supply Pressure	Volume flow	Time	Estimated volume flow rate $\dot{V}$	Measured generator output voltage V_g	Measured generator output current I_g	Estimated electrical power output $\dot{W}_E$	Measured rotational speed of the turbine N	Angular speed of the turbine ω	Estimated input power $\dot{W}_{in}$ $\left(\dot{m}gh\right)$	Estimated overall efficiency η_o
kPa	m^3	sec	m^3/s	Volts	Amps	Watts	rpm	rad/s	Watts	%
41.37	0.2	7.76	0.0257	160.71	0.83	133.25	1706	178.56	1064.1	12.52
41.37	0.2	8.04	0.0248	150.34	2.02	304.02	1596	167.05	1027.0	29.60
41.37	0.2	8.27	0.0241	141.68	2.87	406.07	1504	157.42	998.9	40.65
41.37	0.2	8.55	0.0233	132.07	3.41	449.76	1402	146.74	965.3	46.59
41.37	0.2	8.86	0.0225	122.18	3.75	458.17	1297	135.75	931.8	49.17
41.37	0.2	9.16	0.0218	113.23	4.01	454.05	1202	125.81	901.5	50.37
41.37	0.2	9.46	0.0211	103.90	4.30	446.78	1103	115.45	872.9	51.18
41.37	0.2	9.77	0.0204	94.29	4.54	428.26	1001	104.77	845.5	50.65
41.37	0.2	10.08	0.0198	84.97	4.67	396.54	902	94.41	819.2	48.41
41.37	0.2	10.38	0.0192	75.55	4.79	362.03	802	83.94	795.5	45.51
41.37	0.2	10.67	0.0187	65.75	4.92	323.31	698	73.06	773.9	41.78
41.37	0.2	10.95	0.0182	56.05	5.04	282.62	595	62.28	754.1	37.48
41.37	0.2	11.19	0.0178	46.91	5.17	242.42	498	52.12	737.8	32.86

Table - B-9 Power test experimental results for SRT-125D-120L-8W with V-ring seal @ 41.37kPa

Estimated Power loss W_{loss}	Estimated generator turbine power $\dot{W}_T$ $\left(\dot{W}_E + \dot{W}_{loss}\right)$	Estimated turbine efficiency η	Relative velocity of the water jet V_r	Linear velocity of the turbine Nozzle U	Absolute velocity of the water jet V_a	k-factor	Estimated fluid frictional power loss $\dot{W}_{Ff}$ $\left(\frac{1}{2}\dot{m}kV_r^2\right)$	Estimated power loss in kinetic energy $\dot{W}_{Ke}$ $\left(\frac{1}{2}\dot{m}V_a^2\right)$	Estimated total output power $\dot{W}_{Out}$ $\left(\dot{W}_T + \dot{W}_{Ff} + \dot{W}_{Ke}\right)$
Watts	Watts	%	m/s	m/s	m/s		Watts	Watts	Watts
242.00	375.26	35.26	13.40	10.90	2.49	0.1236	79.86	285.28	740.40
219.94	523.95	51.02	12.93	10.20	2.73	0.1174	92.41	243.60	859.96
202.25	608.32	60.90	12.58	9.61	2.96	0.1075	105.97	205.24	919.53
183.44	633.20	65.60	12.15	8.96	3.19	0.1040	118.82	179.17	931.19
164.98	623.14	66.88	11.73	8.29	3.44	0.1007	133.31	156.03	912.48
149.05	603.10	66.90	11.35	7.68	3.67	0.1007	146.43	141.29	890.81
133.24	580.02	66.45	10.99	7.05	3.94	0.0968	163.68	123.26	866.96
117.79	546.05	64.58	10.64	6.40	4.25	0.0916	184.23	106.03	836.31
103.61	500.15	61.05	10.31	5.77	4.55	0.0904	204.77	95.22	800.14
90.10	452.14	56.84	10.02	5.13	4.89	0.0869	229.80	83.79	765.72
76.93	400.24	51.72	9.74	4.46	5.28	0.0813	260.90	72.20	733.34
64.75	347.37	46.06	9.49	3.80	5.69	0.0784	295.15	64.44	706.96
54.08	296.50	40.19	9.29	3.18	6.11	0.0764	332.43	58.76	687.69

Table - B-10 Power test experimental results for SRT-125D-120L-8W with NMS @ 13.79kPa

Supply Pressure	Volume flow	Time	Estimated volume flow rate $\dot{V}$	Measured generator output voltage V_g	Measured generator output current I_g	Estimated electrical power output $\dot{W}_E$	Measured rotational speed of the turbine N	Angular speed of the turbine ω	Estimated input power $\dot{W}_{in}$ $\left(\dot{m}gh\right)$	Estimated overall efficiency η_o
kPa	m^3	sec	m^3/s	Volts	Amps	Watts	rpm	rad/s	Watts	%
13.79	0.2	12.61	0.0158	99.10	0.41	40.63	1052	110.11	218.3	18.61
13.79	0.2	12.98	0.0154	94.39	0.48	45.31	1002	104.88	212.0	21.37
13.79	0.2	14.18	0.0141	80.07	0.71	56.85	850	88.97	194.1	29.29
13.79	0.2	14.95	0.0134	71.78	0.86	61.40	762	79.76	184.1	33.35
13.79	0.2	16.06	0.0124	60.48	1.07	64.64	642	67.20	171.4	37.71
13.79	0.2	16.43	0.0121	56.52	1.15	64.76	600	62.80	167.5	38.65
13.79	0.2	17.37	0.0115	47.19	1.33	62.73	501	52.44	158.5	39.59
13.79	0.2	18.10	0.0110	39.56	1.47	58.03	420	43.96	152.1	38.16
13.79	0.2	18.69	0.0107	33.23	1.62	53.83	353	36.93	147.3	36.55
13.79	0.2	19.44	0.0103	23.64	1.82	43.10	251	26.27	141.6	30.44
13.79	0.2	19.74	0.0101	18.84	1.97	37.12	200	20.93	139.5	26.62
13.79	0.2	19.98	0.0100	14.13	2.18	30.85	150	15.70	137.8	22.39

Table - B-11 Power test experimental results for SRT-125D-120L-8W with NMS @ 13.79kPa

Estimated Power loss W_{loss}	Estimated generator turbine power $\dot{W}_T$ $\left(\dot{W}_E + \dot{W}_{loss}\right)$	Estimated turbine efficiency η	Relative velocity of the water jet V_r	Linear velocity of the turbine Nozzle U	Absolute velocity of the water jet V_a	k-factor	Estimated fluid frictional power loss $\dot{W}_{Ff}$ $\left(\frac{1}{2}\dot{m}kV_r^2\right)$	Estimated power loss in kinetic energy $\dot{W}_{Ke}$ $\left(\frac{1}{2}\dot{m}V_a^2\right)$	Estimated total output power $\dot{W}_{Out}$ $\left(\dot{W}_T + \dot{W}_{Ff} + \dot{W}_{Ke}\right)$
Watts	Watts	%	m/s	m/s	m/s		Watts	Watts	Watts
85.46	126.09	57.77	8.24	6.72	1.52	0.0712	18.27	38.28	182.64
81.13	126.44	59.63	8.01	6.40	1.60	0.0695	19.78	34.29	180.51
68.03	124.88	64.35	7.33	5.43	1.90	0.0628	25.31	23.74	173.93
60.49	121.89	66.21	6.95	4.87	2.08	0.0611	28.95	19.72	170.56
50.25	114.89	67.02	6.47	4.10	2.37	0.0597	34.93	15.55	165.37
46.68	111.44	66.52	6.33	3.84	2.49	0.0563	37.73	13.69	162.85
38.29	101.03	63.76	5.98	3.20	2.78	0.0563	44.49	11.58	157.10
31.46	89.50	58.85	5.74	2.68	3.06	0.0545	51.59	9.92	151.01
25.82	79.64	54.08	5.56	2.26	3.31	0.0558	58.40	9.22	147.27
17.29	60.39	42.65	5.35	1.60	3.74	0.0544	71.93	7.99	140.32
13.04	50.16	35.97	5.27	1.28	3.99	0.0531	80.44	7.45	138.05
8.88	39.73	28.83	5.20	0.96	4.25	0.0522	90.06	7.06	136.84

Table - B-12 Power test experimental results for SRT-125D-120L-8W with NMS @ 41.37kPa

Supply Pressure	Volume flow	Time	Estimated volume flow rate $\dot{V}$	Measured generator output voltage V_g	Measured generator output current I_g	Estimated electrical power output $\dot{W}_E$	Measured rotational speed of the turbine N	Angular speed of the turbine ω	Estimated input power $\dot{W}_{in}$ $\left(\dot{m}gh\right)$	Estimated overall efficiency η_o
kPa	m^3	sec	m^3/s	Volts	Amps	Watts	rpm	rad/s	Watts	%
41.37	0.1	6.65	0.0300	207.05	1.58	328.00	2198	230.06	1242.6	26.40
41.37	0.1	6.92	0.0289	194.99	2.02	393.02	2070	216.66	1193.8	32.92
41.37	0.1	7.07	0.0282	188.02	2.34	440.17	1996	208.91	1168.5	37.67
41.37	0.1	7.39	0.0270	174.55	2.82	492.45	1853	193.95	1116.9	44.09
41.37	0.1	7.72	0.0259	161.55	3.21	518.94	1715	179.50	1070.1	48.49
41.37	0.1	8.07	0.0247	148.37	3.55	526.98	1575	164.85	1023.9	51.47
41.37	0.1	8.45	0.0236	135.65	3.88	525.85	1440	150.72	977.5	53.79
41.37	0.1	8.87	0.0225	122.27	4.24	518.88	1298	135.86	931.1	55.73
41.37	0.1	9.01	0.0222	117.75	4.34	511.58	1250	130.83	916.7	55.80
41.37	0.1	9.39	0.0213	105.98	4.65	493.04	1125	117.75	879.3	56.07
41.37	0.1	9.69	0.0206	96.74	4.90	473.93	1027	107.49	852.3	55.61
41.37	0.1	9.89	0.0202	90.24	5.09	459.51	958	100.27	834.8	55.05
41.37	0.1	10.15	0.0197	82.43	5.35	441.36	875	91.58	813.7	54.24
41.37	0.1	10.45	0.0191	72.72	5.69	413.77	772	80.80	790.2	52.36
41.37	0.1	10.73	0.0186	63.59	5.98	380.55	675	70.65	769.5	49.45
41.37	0.1	11.08	0.0180	51.81	6.42	332.61	550	57.57	745.5	44.62

Power test experimental results for SRT-125D-120L-8W with NMS @ 41.37kPa

Estimated Power loss W_{loss}	Estimated generator turbine power $\dot{W}_T$ $\left(\dot{W}_E + \dot{W}_{loss}\right)$	Estimated turbine efficiency η	Relative velocity of the water jet V_r	Linear velocity of the turbine Nozzle U	Absolute velocity of the water jet V_a	k-factor	Estimated fluid frictional power loss $\dot{W}_{Ff}$ $\left(\frac{1}{2}\dot{m}kV_r^2\right)$	Estimated power loss in kinetic energy $\dot{W}_{Ke}$ $\left(\frac{1}{2}\dot{m}V_a^2\right)$	Estimated total output power $\dot{W}_{Out}$ $\left(\dot{W}_T + \dot{W}_{Ff} + \dot{W}_{Ke}\right)$
Watts	Watts	%	m/s	m/s	m/s		Watts	Watts	Watts
176.47	504.47	40.60	15.64	14.05	1.59	0.1447	38.16	531.78	1074.40
165.45	558.47	46.78	15.03	13.23	1.80	0.1414	46.63	460.78	1065.87
159.12	599.29	51.29	14.71	12.76	1.95	0.1345	53.84	411.04	1064.17
146.93	639.39	57.25	14.06	11.84	2.22	0.1280	66.35	341.60	1047.34
135.25	654.19	61.13	13.47	10.96	2.51	0.1180	81.47	276.93	1012.59
123.48	650.46	63.53	12.89	10.07	2.82	0.1080	98.58	222.02	971.06
112.21	638.05	65.27	12.31	9.20	3.10	0.1057	113.71	189.09	940.85
100.42	619.31	66.51	11.72	8.30	3.43	0.1030	132.09	159.28	910.68
96.46	608.04	66.33	11.54	7.99	3.55	0.1004	139.76	148.17	895.97
86.18	579.22	65.87	11.07	7.19	3.88	0.0972	159.89	126.56	865.67
78.16	552.09	64.78	10.73	6.56	4.17	0.0930	178.70	110.28	841.07
72.54	532.05	63.74	10.51	6.12	4.39	0.0887	194.05	98.81	824.92
65.80	507.17	62.33	10.24	5.59	4.65	0.0866	212.72	89.34	809.23
57.48	471.26	59.64	9.95	4.93	5.01	0.0820	240.11	77.50	788.87
49.68	430.23	55.91	9.69	4.31	5.37	0.0800	268.48	69.82	768.53
39.69	372.30	49.94	9.39	3.52	5.87	0.0796	310.47	63.16	745.92

Table - B-13 Power test experimental results for SRT-125D-120L-5.3W with V-ring seal @ 13.79kPa

Supply Pressure	Volume flow	Time	Estimated volume flow rate $\dot{V}$	Measured generator output voltage V_g	Measured generator output current I_g	Estimated electrical power output $\dot{W}_E$	Measured rotational speed of the turbine N	Angular speed of the turbine ω	Estimated input power $\dot{W}_{in}$ $\left(\dot{m}gh\right)$	Estimated overall efficiency η_o
kPa	m^3	sec	m^3/s	Volts	Amps	Watts	rpm	rad/s	Watts	%
13.79	0.1	9.86	0.0101	93.01	0.15	14.29	987	103.35	139.5	10.24
13.79	0.1	10.63	0.0094	81.29	0.35	28.47	863	90.33	129.5	21.99
13.79	0.1	11.37	0.0088	70.65	0.53	37.48	750	78.50	121.0	30.98
13.79	0.1	12.27	0.0081	58.69	0.72	42.46	623	65.21	112.2	37.85
13.79	0.1	13.08	0.0076	47.95	0.91	43.75	509	53.28	105.2	41.58
13.79	0.1	13.58	0.0073	41.17	1.02	41.93	437	45.74	101.4	41.37
13.79	0.1	14.10	0.0071	33.63	1.15	38.76	357	37.37	97.6	39.71
13.79	0.1	14.59	0.0068	25.72	1.32	33.90	273	28.57	94.4	35.93
13.79	0.1	14.87	0.0067	20.16	1.41	28.50	214	22.40	92.5	30.80
13.79	0.1	15.03	0.0066	16.49	1.50	24.66	175	18.32	91.6	26.93

Table - B-14 Power test experimental results for SRT-125D-120L-5.3W with V-ring seal @ 13.79kPa

Estimated Power loss W_{loss}	Estimated generator turbine power $\dot{W}_T$ $\left(\dot{W}_E + \dot{W}_{loss}\right)$	Estimated turbine efficiency η	Relative velocity of the water jet V_r	Linear velocity of the turbine Nozzle U	Absolute velocity of the water jet V_a	k-factor	Estimated fluid frictional power loss $\dot{W}_{Ff}$ $\left(\frac{1}{2}\dot{m}kV_r^2\right)$	Estimated power loss in kinetic energy $\dot{W}_{Ke}$ $\left(\frac{1}{2}\dot{m}V_a^2\right)$	Estimated total output power $\dot{W}_{Out}$ $\left(\dot{W}_T + \dot{W}_{Ff} + \dot{W}_{Ke}\right)$
Watts	Watts	%	m/s	m/s	m/s		Watts	Watts	Watts
61.51	75.80	54.33	7.95	6.31	1.64	0.0656	21.01	13.64	110.45
51.52	79.99	61.77	7.38	5.52	1.87	0.0644	16.47	16.35	112.81
42.89	80.37	66.43	6.90	4.79	2.10	0.0628	13.10	19.41	112.88
33.72	76.18	67.90	6.40	3.98	2.41	0.0617	10.28	23.71	110.16
25.95	69.70	66.24	6.00	3.25	2.75	0.0605	8.31	28.76	106.77
21.27	63.20	62.36	5.78	2.79	2.98	0.0598	7.34	32.74	103.28
16.28	55.04	56.38	5.57	2.28	3.28	0.0585	6.41	38.16	99.62
11.27	45.17	47.87	5.38	1.75	3.63	0.0585	5.79	45.18	96.13
7.90	36.40	39.34	5.28	1.37	3.91	0.0581	5.43	51.24	93.07
5.73	30.39	33.19	5.22	1.12	4.10	0.0579	5.24	55.86	91.50

Table - B-15 Power test experimental results for SRT-125D-120L-5.3W with V-ring seal @ 41.37kPa

Supply Pressure	Volume flow	Time	Estimated volume flow rate $\dot{V}$	Measured generator output voltage V_g	Measured generator output current I_g	Estimated electrical power output $\dot{W}_E$	Measured rotational speed of the turbine N	Angular speed of the turbine ω	Estimated input power $\dot{W}_{in}$ $\left(\dot{m}gh\right)$	Estimated overall efficiency η_o
kPa	m^3	sec	m^3/s	Volts	Amps	Watts	rpm	rad/s	Watts	%
41.37	0.1	5.91	0.0169	158.35	0.45	71.26	1681	175.94	699.0	10.19
41.37	0.1	6.13	0.0163	147.99	0.85	125.79	1571	164.43	673.8	18.67
41.37	0.1	6.33	0.0158	138.10	1.19	164.84	1466	153.44	652.3	25.27
41.37	0.1	6.57	0.0152	127.45	1.68	214.75	1353	141.61	628.2	34.19
41.37	0.1	6.76	0.0148	119.82	1.97	235.96	1272	133.14	610.9	38.62
41.37	0.1	7.00	0.0143	109.74	2.27	249.63	1165	121.94	589.5	42.34
41.37	0.1	7.22	0.0138	100.70	2.53	254.64	1069	111.89	571.9	44.53
41.37	0.1	7.42	0.0134	92.22	2.75	253.97	979	102.47	556.1	45.67
41.37	0.1	7.73	0.0129	79.79	3.00	239.36	847	88.65	534.1	44.82
41.37	0.1	7.91	0.0126	71.87	3.18	228.56	763	79.86	521.7	43.81
41.37	0.1	8.10	0.0123	63.11	3.30	208.28	670	70.13	509.4	40.88
41.37	0.1	8.33	0.0120	52.38	3.52	184.52	556	58.19	495.5	37.24
41.37	0.1	8.51	0.0117	42.77	3.65	156.27	454	47.52	484.9	32.22

Table - B-16Power test experimental results for SRT-125D-120L-5.3W with V-ring seal @ 41.37kPa

Estimated Power loss W_{loss}	Estimated generator turbine power $\dot{W}_T$ $\left(\dot{W}_E + \dot{W}_{loss}\right)$	Estimated turbine efficiency η	Relative velocity of the water jet V_r	Linear velocity of the turbine Nozzle U	Absolute velocity of the water jet V_a	k-factor	Estimated fluid frictional power loss $\dot{W}_{Ff}$ $\left(\frac{1}{2}\dot{m}kV_r^2\right)$	Estimated power loss in kinetic energy $\dot{W}_{Ke}$ $\left(\frac{1}{2}\dot{m}V_a^2\right)$	Estimated total output power $\dot{W}_{Out}$ $\left(\dot{W}_T + \dot{W}_{Ff} + \dot{W}_{Ke}\right)$
Watts	Watts	%	m/s	m/s	m/s		Watts	Watts	Watts
236.90	308.16	44.08	13.28	10.74	2.54	0.1232	183.64	54.45	546.25
215.06	340.85	50.59	12.80	10.04	2.76	0.1198	159.98	62.11	562.94
195.14	359.98	55.18	12.40	9.37	3.03	0.1098	133.07	72.18	565.23
174.71	389.47	62.00	11.94	8.65	3.29	0.1054	114.05	82.16	585.68
160.71	396.68	64.93	11.61	8.13	3.48	0.1043	103.82	89.38	589.87
143.05	392.68	66.61	11.20	7.45	3.76	0.1010	90.35	100.55	583.57
127.99	382.63	66.91	10.87	6.83	4.03	0.0959	78.28	112.51	573.42
114.57	368.54	66.27	10.57	6.26	4.31	0.0915	68.69	124.86	562.08
96.08	335.44	62.81	10.15	5.41	4.74	0.0878	58.38	144.74	538.56
85.06	313.62	60.12	9.91	4.88	5.04	0.0839	51.96	159.96	525.54
73.53	281.81	55.32	9.68	4.28	5.40	0.0786	45.34	179.41	506.56
60.37	244.89	49.42	9.42	3.55	5.86	0.0756	40.14	205.82	490.85
49.49	205.76	42.43	9.22	2.90	6.31	0.0735	36.57	233.61	475.94

Table - B-17 Power test experimental results for SRT-125D-120L-5.3W with NMS @ 13.79kPa

Supply Pressure	Volume flow	Time	Estimated volume flow rate $\dot{V}$	Measured generator output voltage V_g	Measured generator output current I_g	Estimated electrical power output $\dot{W}_E$	Measured rotational speed of the turbine N	Angular speed of the turbine ω	Estimated input power $\dot{W}_{in}$ $\left(\dot{m}gh\right)$	Estimated overall efficiency η_o
kPa	m^3	sec	m^3/s	Volts	Amps	Watts	rpm	rad/s	Watts	%
13.79	0.1	9.60	0.0104	97.50	0.00	0.00	1035	108.33	143.3	0.00
13.79	0.1	11.06	0.0090	75.02	0.24	17.96	796	83.36	124.5	14.43
13.79	0.1	12.39	0.0081	56.94	0.51	29.06	604	63.27	111.1	26.17
13.79	0.1	13.12	0.0076	47.29	0.68	32.16	502	52.54	104.9	30.66
13.79	0.1	13.76	0.0073	38.62	0.87	33.43	410	42.91	100.1	33.41
13.79	0.1	14.34	0.0070	29.67	1.04	30.88	315	32.97	96.0	32.18
13.79	0.1	14.69	0.0068	23.55	1.17	27.58	250	26.17	93.7	29.44
13.79	0.1	14.91	0.0067	18.93	1.33	25.12	201	21.04	92.3	27.22
13.79	0.1	15.02	0.0066	16.49	1.41	23.32	175	18.32	91.6	25.44
13.79	0.1	15.16	0.0066	12.25	1.50	18.34	130	13.61	90.8	20.21

Table - B-18 Power test experimental results for SRT-125D-120L-5.3W with NMS @ 13.79kPa

Estimated Power loss W_{loss}	Estimated generator turbine power $\dot{W}_T$ $\left(\dot{W}_E + \dot{W}_{loss}\right)$	Estimated turbine efficiency η	Relative velocity of the water jet V_r	Linear velocity of the turbine Nozzle U	Absolute velocity of the water jet V_a	k-factor	Estimated fluid frictional power loss $\dot{W}_{Ff}$ $\left(\frac{1}{2}\dot{m}kV_r^2\right)$	Estimated power loss in kinetic energy $\dot{W}_{Ke}$ $\left(\frac{1}{2}\dot{m}V_a^2\right)$	Estimated total output power $\dot{W}_{Out}$ $\left(\dot{W}_T + \dot{W}_{Ff} + \dot{W}_{Ke}\right)$
Watts	Watts	%	m/s	m/s	m/s		Watts	Watts	Watts
83.99	83.99	58.62	8.17	6.62	1.55	0.0692	23.99	12.53	120.51
63.43	81.40	65.39	7.10	5.09	2.01	0.0624	14.18	18.15	113.72
47.06	76.12	68.54	6.33	3.86	2.47	0.0605	9.76	24.52	110.40
38.38	70.53	67.26	5.98	3.21	2.77	0.0597	8.11	29.17	107.82
30.62	64.05	64.02	5.70	2.62	3.08	0.0588	6.94	34.49	105.48
22.65	53.52	55.77	5.47	2.01	3.46	0.0570	5.93	41.59	101.04
17.21	44.79	47.81	5.34	1.60	3.74	0.0563	5.45	47.60	97.84
13.12	38.24	41.44	5.26	1.28	3.98	0.0559	5.18	52.92	96.34
10.96	34.28	37.40	5.22	1.12	4.11	0.0563	5.10	56.02	95.40
7.22	25.56	28.16	5.18	0.83	4.34	0.0556	4.90	62.11	92.58

Table - B-19 Power test experimental results for SRT-125D-120L-5.3W with NMS @ 41.37kPa

Supply Pressure	Volume flow	Time	Estimated volume flow rate $\dot{V}$	Measured generator output voltage V_g	Measured generator output current I_g	Estimated electrical power output $\dot{W}_E$	Measured rotational speed of the turbine N	Angular speed of the turbine ω	Estimated input power $\dot{W}_{in}$ $\left(\dot{m}gh\right)$	Estimated overall efficiency η_o
kPa	m^3	sec	m^3/s	Volts	Amps	Watts	rpm	rad/s	Watts	%
41.37	0.1	5.20	0.0192	196.41	0.40	77.88	2085	218.23	794.3	9.81
41.37	0.1	5.51	0.0181	178.18	0.98	174.56	1892	197.98	748.8	23.31
41.37	0.1	5.86	0.0170	160.09	1.63	261.67	1699	177.87	704.8	37.13
41.37	0.1	6.13	0.0163	146.68	2.04	298.94	1557	162.98	673.1	44.41
41.37	0.1	6.41	0.0156	133.85	2.35	315.20	1421	148.72	644.1	48.94
41.37	0.1	6.78	0.0147	118.53	2.66	315.52	1258	131.70	608.9	51.82
41.37	0.1	7.05	0.0142	107.33	2.90	311.75	1139	119.26	585.6	53.24
41.37	0.1	7.27	0.0137	98.52	3.10	305.59	1046	109.47	567.6	53.84
41.37	0.1	7.50	0.0133	89.33	3.26	290.87	948	99.26	550.5	52.84
41.37	0.1	7.65	0.0130	83.20	3.35	278.52	883	92.45	539.6	51.61
41.37	0.1	7.79	0.0128	77.55	3.40	264.06	823	86.17	530.2	49.81
41.37	0.1	7.92	0.0126	71.52	3.43	245.02	759	79.47	521.1	47.02

Table - B-20Power test experimental results for SRT-125D-120L-5.3W with NMS @ 41.37kPa

Estimated Power loss W_{loss}	Estimated generator turbine power $\dot{W}_T$ $\left(\dot{W}_E + \dot{W}_{loss}\right)$	Estimated turbine efficiency η	Relative velocity of the water jet V_r	Linear velocity of the turbine Nozzle U	Absolute velocity of the water jet V_a	k-factor	Estimated fluid frictional power loss $\dot{W}_{Ff}$ $\left(\frac{1}{2}\dot{m}kV_r^2\right)$	Estimated power loss in kinetic energy $\dot{W}_{Ke}$ $\left(\frac{1}{2}\dot{m}V_a^2\right)$	Estimated total output power $\dot{W}_{Out}$ $\left(\dot{W}_T + \dot{W}_{Ff} + \dot{W}_{Ke}\right)$
Watts	Watts	%	m/s	m/s	m/s		Watts	Watts	Watts
166.74	244.62	30.80	15.09	13.33	1.77	0.1429	312.45	29.94	587.01
150.21	324.77	43.37	14.23	12.09	2.14	0.1306	239.38	41.39	605.53
133.94	395.61	56.13	13.39	10.86	2.53	0.1189	181.75	54.59	631.95
121.99	420.92	62.53	12.79	9.95	2.84	0.1112	147.98	65.53	634.43
110.62	425.82	66.11	12.24	9.08	3.16	0.1030	120.12	77.57	623.51
97.14	412.67	67.78	11.57	8.04	3.53	0.1012	99.72	91.57	603.96
87.36	399.11	68.16	11.13	7.28	3.85	0.0965	84.57	104.63	588.31
79.70	385.29	67.88	10.79	6.69	4.10	0.0953	76.06	115.38	576.73
71.75	362.62	65.87	10.46	6.06	4.40	0.0917	66.77	128.83	558.22
66.47	344.99	63.93	10.25	5.65	4.61	0.0899	61.65	138.55	545.20
61.62	325.68	61.43	10.07	5.26	4.81	0.0880	57.22	148.40	531.30
56.45	301.47	57.86	9.90	4.85	5.05	0.0841	51.92	160.53	513.92

Table - B-21 Power test experimental results for SRT-125D-120L-4.2W with V-ring seal @ 13.79kPa

Supply Pressure	Volume flow	Time	Estimated volume flow rate $\dot{V}$	Measured generator output voltage V_g	Measured generator output current I_g	Estimated electrical power output $\dot{W}_E$	Measured rotational speed of the turbine N	Angular speed of the turbine ω	Estimated input power $\dot{W}_{in}$ $\left(\dot{m}gh\right)$	Estimated overall efficiency η_o
kPa	m^3	sec	m^3/s	Volts	Amps	Watts	rpm	rad/s	Watts	%
13.79	0.1	12.33	0.0081	98.68	0.00	0.00	1003	104.98	111.6	0.00
13.79	0.1	13.95	0.0072	78.33	0.24	18.80	796	83.33	98.7	19.06
13.79	0.1	15.49	0.0064	61.04	0.42	25.64	620	64.94	88.8	28.86
13.79	0.1	16.56	0.0060	49.19	0.58	28.53	500	52.33	83.1	34.34
13.79	0.1	17.44	0.0057	39.21	0.76	29.80	399	41.71	78.9	37.76
13.79	0.1	18.07	0.0055	31.29	0.89	27.82	318	33.28	76.2	36.53
13.79	0.1	18.59	0.0054	23.59	1.05	24.81	240	25.10	74.0	33.50
13.79	0.1	18.99	0.0053	16.08	1.19	19.11	163	17.11	72.5	26.36
13.79	0.1	19.09	0.0052	13.54	1.26	17.01	138	14.40	72.1	23.60

Table - B-22 Power test experimental results for SRT-125D-120L-4.2W with V-ring seal @ 13.79kPa

Estimated Power loss W_{loss}	Estimated generator turbine power $\dot{W}_T$ $\left(\dot{W}_E + \dot{W}_{loss}\right)$	Estimated turbine efficiency η	Relative velocity of the water jet V_r	Linear velocity of the turbine Nozzle U	Absolute velocity of the water jet V_a	k-factor	Estimated fluid frictional power loss $\dot{W}_{Ff}$ $\left(\frac{1}{2}\dot{m}kV_r^2\right)$	Estimated power loss in kinetic energy $\dot{W}_{Ke}$ $\left(\frac{1}{2}\dot{m}V_a^2\right)$	Estimated total output power $\dot{W}_{Out}$ $\left(\dot{W}_T + \dot{W}_{Ff} + \dot{W}_{Ke}\right)$
Watts	Watts	%	m/s	m/s	m/s		Watts	Watts	Watts
62.80	62.80	56.27	8.03	6.41	1.62	0.066	17.09	10.59	90.48
46.36	65.16	66.05	7.10	5.09	2.01	0.062	11.10	14.43	90.69
33.54	59.18	66.62	6.39	3.97	2.42	0.060	7.95	18.93	86.07
25.35	53.89	64.85	5.98	3.20	2.78	0.058	6.20	23.32	83.41
18.84	48.64	61.64	5.68	2.55	3.13	0.057	5.27	28.02	81.93
13.92	41.75	54.80	5.48	2.03	3.45	0.056	4.65	32.82	79.21
9.36	34.16	46.14	5.33	1.53	3.79	0.055	4.17	38.65	76.98
5.10	24.21	33.40	5.21	1.04	4.17	0.054	3.89	45.70	73.79
3.70	20.72	28.74	5.19	0.88	4.31	0.054	3.81	48.48	73.01

Table - B-23 Power test experimental results for SRT-125D-120L-4.2W with V-ring seal @ 41.37kPa

Supply Pressure	Volume flow	Time	Estimated volume flow rate $\dot{V}$	Measured generator output voltage V_g	Measured generator output current I_g	Estimated electrical power output $\dot{W}_E$	Measured rotational speed of the turbine N	Angular speed of the turbine ω	Estimated input power $\dot{W}_{in}$ $\left(\dot{m}gh\right)$	Estimated overall efficiency η_o
kPa	m^3	sec	m^3/s	Volts	Amps	Watts	rpm	rad/s	Watts	%
41.37	0.1	7.65	0.0130	157.62	0.00	0.00	1602	167.68	539.7	0.00
41.37	0.1	7.90	0.0126	147.88	0.20	29.27	1503	157.31	522.3	5.60
41.37	0.1	8.15	0.0123	138.23	0.44	61.31	1405	147.06	506.8	12.10
41.37	0.1	8.39	0.0119	129.87	0.71	92.86	1320	138.16	492.1	18.87
41.37	0.1	8.62	0.0116	121.80	0.99	120.41	1238	129.58	478.8	25.15
41.37	0.1	8.93	0.0112	111.28	1.35	150.22	1131	118.38	462.2	32.50
41.37	0.1	9.24	0.0108	101.04	1.64	165.85	1027	107.49	447.0	37.10
41.37	0.1	9.56	0.0104	90.52	1.96	177.27	920	96.29	431.7	41.06
41.37	0.1	9.84	0.0101	81.17	2.23	180.68	825	86.35	419.6	43.07
41.37	0.1	10.14	0.0098	70.64	2.43	171.77	718	75.15	407.2	42.18
41.37	0.1	10.38	0.0096	61.29	2.61	159.96	623	65.21	397.7	40.22
41.37	0.1	10.62	0.0094	50.77	2.83	143.43	516	54.01	388.6	36.91

Table - B-24 Power test experimental results for SRT-125D-120L-4.2W with V-ring seal @ 41.37kPa

Estimated Power loss W_{loss}	Estimated generator turbine power $\dot{W}_T$ $\left(\dot{W}_E + \dot{W}_{loss}\right)$	Estimated turbine efficiency η	Relative velocity of the water jet V_r	Linear velocity of the turbine Nozzle U	Absolute velocity of the water jet V_a	k-factor	Estimated fluid frictional power loss $\dot{W}_{Ff}$ $\left(\frac{1}{2}\dot{m}kV_r^2\right)$	Estimated power loss in kinetic energy $\dot{W}_{Ke}$ $\left(\frac{1}{2}\dot{m}V_a^2\right)$	Estimated total output power $\dot{W}_{Out}$ $\left(\dot{W}_T + \dot{W}_{Ff} + \dot{W}_{Ke}\right)$
Watts	Watts	%	m/s	m/s	m/s		Watts	Watts	Watts
221.12	221.12	40.97	12.94	10.24	2.70	0.120	131.05	47.64	399.81
202.06	231.33	44.29	12.53	9.61	2.92	0.116	114.62	53.75	399.70
183.98	245.30	48.40	12.15	8.98	3.17	0.106	96.03	61.68	403.01
168.94	261.80	53.20	11.80	8.44	3.36	0.105	87.14	67.32	416.26
155.00	275.41	57.53	11.48	7.91	3.57	0.103	78.42	73.64	427.47
137.63	287.85	62.28	11.08	7.23	3.85	0.099	67.94	82.97	438.76
121.65	287.50	64.31	10.72	6.56	4.16	0.095	59.01	93.28	439.78
106.13	283.40	65.64	10.35	5.88	4.47	0.095	52.92	104.36	440.67
93.14	273.82	65.26	10.06	5.27	4.79	0.092	47.28	116.23	437.33
79.39	251.16	61.67	9.77	4.59	5.18	0.088	41.51	131.88	424.55
67.98	227.94	57.31	9.54	3.98	5.56	0.084	36.68	148.36	412.98
56.00	199.43	51.32	9.32	3.30	6.02	0.078	31.81	170.27	401.51

Table - B-25 Power test experimental results for SRT-125D-120L-4.2W with NMS @ 13.79kPa

Supply Pressure	Volume flow	Time	Estimated volume flow rate $\dot{V}$	Measured generator output voltage V_g	Measured generator output current I_g	Estimated electrical power output $\dot{W}_E$	Measured rotational speed of the turbine N	Angular speed of the turbine ω	Estimated input power $\dot{W}_{in}$ $\left(\dot{m}gh\right)$	Estimated overall efficiency η_o
kPa	m^3	sec	m^3/s	Volts	Amps	Watts	rpm	rad/s	Watts	%
13.79	0.1	12.27	0.0081	99.86	0.00	0.00	1015	106.24	112.2	0.00
13.79	0.1	13.32	0.0075	85.79	0.20	17.16	872	91.27	103.3	16.61
13.79	0.1	14.68	0.0068	69.36	0.43	29.83	705	73.79	93.7	31.82
13.79	0.1	15.63	0.0064	59.23	0.60	35.54	602	63.01	88.1	40.35
13.79	0.1	16.44	0.0061	49.78	0.75	37.34	506	52.96	83.7	44.60
13.79	0.1	17.34	0.0058	39.75	0.91	36.17	404	42.29	79.4	45.56
13.79	0.1	18.10	0.0055	30.50	1.07	32.77	310	32.45	76.0	43.10
13.79	0.1	18.56	0.0054	22.83	1.22	27.95	232	24.28	74.1	37.70
13.79	0.1	19.15	0.0052	9.94	1.79	17.75	101	10.57	71.9	24.70

Table - B-26 Power test experimental results for SRT-125D-120L-4.2W with NMS @ 13.79kPa

Estimated Power loss W_{loss}	Estimated generator turbine power $\dot{W}_T$ $\left(\dot{W}_E + \dot{W}_{loss}\right)$	Estimated turbine efficiency η	Relative velocity of the water jet V_r	Linear velocity of the turbine Nozzle U	Absolute velocity of the water jet V_a	k-factor	Estimated fluid frictional power loss $\dot{W}_{Ff}$ $\left(\frac{1}{2}\dot{m}kV_r^2\right)$	Estimated power loss in kinetic energy $\dot{W}_{Ke}$ $\left(\frac{1}{2}\dot{m}V_a^2\right)$	Estimated total output power $\dot{W}_{Out}$ $\left(\dot{W}_T + \dot{W}_{Ff} + \dot{W}_{Ke}\right)$
Watts	Watts	%	m/s	m/s	m/s		Watts	Watts	Watts
46.74	46.74	41.67	8.07	6.49	1.58	0.070	18.56	10.17	75.47
38.21	55.37	53.60	7.43	5.57	1.86	0.062	12.81	12.93	81.11
31.86	61.68	65.80	6.74	4.51	2.24	0.053	8.18	17.02	86.88
24.42	59.95	68.08	6.34	3.85	2.49	0.056	7.17	19.76	86.89
18.79	56.13	67.05	6.02	3.23	2.79	0.049	5.39	23.59	85.11
14.72	50.89	64.10	5.71	2.58	3.13	0.050	4.69	28.18	83.76
12.24	45.01	59.20	5.47	1.98	3.49	0.053	4.37	33.55	82.93
12.60	40.55	54.70	5.33	1.48	3.85	0.047	3.58	39.86	83.99
15.09	32.85	45.70	5.17	0.65	4.52	0.047	3.29	53.36	89.49

Table - B-27Power test experimental results for SRT-125D-120L-4.2W with NMS @ 41.37kPa

Supply Pressure	Volume flow	Time	Estimated volume flow rate $\dot{V}$	Measured generator output voltage V_g	Measured generator output current I_g	Estimated electrical power output $\dot{W}_E$	Measured rotational speed of the turbine N	Angular speed of the turbine ω	Estimated input power $\dot{W}_{in}$ $\left(\dot{m}gh\right)$	Estimated overall efficiency η_o
kPa	m^3	sec	m^3/s	Volts	Amps	Watts	rpm	rad/s	Watts	%
41.37	0.1	6.62	0.0151	216.90	0.00	0.00	2056	215.19	623.5	0.00
41.37	0.1	7.04	0.0142	191.90	0.63	120.90	1852	193.84	586.3	20.62
41.37	0.1	7.33	0.0136	172.00	0.98	168.56	1720	180.03	563.6	29.91
41.37	0.1	7.63	0.0131	153.00	1.28	195.84	1598	167.21	541.3	36.18
41.37	0.1	8.06	0.0124	136.50	1.64	223.70	1425	149.18	512.3	43.67
41.37	0.1	8.53	0.0117	121.50	1.85	224.78	1265	132.40	484.0	46.44
41.37	0.1	8.98	0.0111	109.00	2.05	223.45	1105	115.66	459.8	48.60
41.37	0.1	9.41	0.0106	92.10	2.35	216.44	962	100.66	438.5	49.35
41.37	0.1	9.76	0.0102	80.70	2.57	207.40	843	88.20	423.2	49.01
41.37	0.1	9.96	0.0100	73.90	2.71	200.27	772	80.77	414.4	48.32
41.37	0.1	10.18	0.0098	66.50	2.83	188.20	694	72.68	405.5	46.41
41.37	0.1	10.36	0.0096	60.40	2.98	179.99	631	66.01	398.6	45.15

Table - B-28 Power test experimental results for SRT-125D-120L-4.2W with NMS @ 41.37kPa

Estimated Power loss W_{loss}	Estimated generator turbine power $\dot{W}_T$ $\left(\dot{W}_E + \dot{W}_{loss}\right)$	Estimated turbine efficiency η	Relative velocity of the water jet V_r	Linear velocity of the turbine Nozzle U	Absolute velocity of the water jet V_a	k-factor	Estimated fluid frictional power loss $\dot{W}_{Ff}$ $\left(\frac{1}{2}\dot{m}kV_r^2\right)$	Estimated power loss in kinetic energy $\dot{W}_{Ke}$ $\left(\frac{1}{2}\dot{m}V_a^2\right)$	Estimated total output power $\dot{W}_{Out}$ $\left(\dot{W}_T + \dot{W}_{Ff} + \dot{W}_{Ke}\right)$
Watts	Watts	%	m/s	m/s	m/s		Watts	Watts	Watts
164.25	164.25	26.34	14.95	13.14	1.81	0.143	240.37	24.68	429.31
146.85	267.75	45.67	14.06	11.84	2.22	0.128	178.72	34.95	481.42
135.68	304.24	53.99	13.51	10.99	2.52	0.115	142.90	43.25	490.39
125.38	321.22	59.34	12.98	10.21	2.77	0.110	121.31	50.13	492.65
110.98	334.68	65.33	12.29	9.11	3.17	0.098	91.75	62.40	488.83
97.70	322.47	66.62	11.61	8.09	3.52	0.100	78.42	72.52	473.41
84.54	307.99	66.98	11.03	7.06	3.96	0.091	61.40	87.28	456.68
72.84	289.27	65.96	10.52	6.15	4.37	0.090	52.63	101.19	443.10
63.18	270.58	63.94	10.15	5.39	4.76	0.085	44.77	116.02	431.38
57.45	257.72	62.18	9.94	4.93	5.01	0.084	41.55	125.53	424.80
51.24	239.43	59.04	9.72	4.44	5.29	0.083	38.60	136.95	414.98
46.13	226.12	56.73	9.56	4.03	5.53	0.083	36.67	147.23	410.02

Appendix C Uncertainty analysis

All scientifically relevant quantities must be assigned an uncertainty, as discussed by Manfred Drosg (Drosg, 2007). The uncertainty is a statistical measure of data quality. It shows how well the data, i.e., the best estimate, fits the (unknown) true value. However, it does not specify the actual deviation between these two values. No data value is of any use whatsoever in a scientific context without a statement on its uncertainty.

If a data value y has an (absolute) uncertainty Δy, we can get the degree of exactness by dividing Δy by y, thus obtaining a dimensionless quantity, the relative (or fractional or percentage) uncertainty σ_r, (Drosg, 2007)

$$\sigma_r = \Delta y / y \qquad 7.1$$

The absolute uncertainty Δy is not suited for comparisons. In the following example we can see how the absolute uncertainty cannot be used for comparison,

In first case the length of a machine part is measured to be 44.89mm ±0.1mm, and in second case the distance from a point on the earth's surface to a certain point on the moon's surface is known to be 384400 km ±0.001 km; both the absolute uncertainties cannot compared with each other. Thus, it is obvious that the quality of a measurement is not necessarily determined by the absolute uncertainties.

The total uncertainty ΔF of a result $F = F(x_1, x_2, x_3, ...)$ is calculated by adding all n individual (independent) uncertainty components ΔF_{xi} in quadrature according to the *law of error propagation*:(Drosg, 2007)

$$\Delta F = \sqrt{(\Delta F_{x1})^2 + (\Delta F_{x2})^2 + (\Delta F_{x3})^2 + ...} = \sqrt{\sum_{i=1}^{n} (\partial F / \partial x_i)^2 * (\Delta x_i)^2} \qquad 7.2$$

The above uncertainty analysis procedure is applied to all the experimental data obtained in this research to estimate the performance and the accompanying uncertainties in the results.

C.1 Uncertainty analysis of stationary test results

Table - C-1 shows the measured results from a stationary test conducted on split reaction turbine prototype 1 with mean turbine diameter Ø243mm and total exit nozzle area of 0.00144m². The volume flow rate of the water flowing through the turbine is equal to the measured water volume (0.2m³) divided by the measured time. The relative velocity V_r of water jets at both the exit nozzles is equal to the measured volume flow rate divided by the total exit nozzle area. Using this velocity and equation 2.38 the value of k-factor was calculated. Ideally, the torque produced at the shaft T_{shaft} should be equal to the estimated torque, i.e. product of absolute velocity V_a, total mass flow rate $\dot{m}$ and mean turbine radius R as shown is equation 2.10. In this case as the turbine is stationary (i.e. $\omega = 0 \,\&\, \therefore U = 0$) the absolute velocity V_a is equal to the relative velocity V_r. Further the force F_{LC} measured by the load cell is equal to the strain indicator reading divided by the load cell calibration factor. Therefore, the torque at the shaft is equal to the product of the measured force and the torque arm length L_{arm} which is 0.19m.

Relative uncertainty in measurement of supply pressure with Floyd's pressure gauge is ± 1.0%. Relative uncertainty in measurement of the flow through turbine using Omega flow meter is ± 2.0%. Relative uncertainty in measurement of time using a standard stop watch is +/-3.0% up to 10sec, there after ±1.5%. Relative uncertainty in measurement of static force using Dana Load Cell 20kgf is ±1%. Based on this information the relative uncertainty of estimated torque and measured is calculated and is shown in Table - C-6 and Table - C-7.

The uncertainty analysis of the experimental data from stationary test shows that the estimated torque has an relative uncertainty of ±4.41% (see Table - C-6) and the measured torque has an relative uncertainty of ±1.13% (see Table - C-7). This shows that the experimental producer used has a good level of confidence.

Table - C-1 Stationary test results for split reaction turbine prototype 1

Supply Pressure	Volume flow	Time	Volume flow rate (V_{dot})	Measured force (F_{LC})	Exit Velocity (v)	Mass flow rate (m_{dot})	Estimated Shaft Torque (T_{est})	Measured Shaft torque (T)	Percentage uncertainty in the estimated and measured torque $(T - T_{est}) / T_{est}$	Estimated stationary k-factor
kPa	m^3	sec	m^3/s	(N)	m/s	kg/s	N-m	N-m	%	
10	0.2	31.61	0.00633	314	16.74	4.394	3.378	3.181	-6.21%	0.0358
15	0.2	25.87	0.00773	467	24.90	5.368	5.042	4.731	-6.57%	0.0411
20	0.2	22.47	0.00890	619	33.00	6.181	6.684	6.270	-6.60%	0.0470
25	0.2	20.15	0.00993	774	41.27	6.893	8.312	7.841	-6.02%	0.0524
30	0.2	18.45	0.01084	908	48.41	7.528	9.916	9.198	-7.80%	0.0587
35	0.2	17.13	0.01168	1070	57.05	8.108	11.502	10.839	-6.12%	0.0648
40	0.2	16.07	0.01245	1205	64.24	8.642	13.068	12.207	-7.06%	0.0711
45	0.2	15.20	0.01316	1363	72.67	9.140	14.617	13.807	-5.86%	0.0773
50	0.2	14.46	0.01383	1529	81.52	9.607	16.146	15.489	-4.25%	0.0836
55	0.2	13.83	0.01446	1673	89.20	10.044	17.650	16.947	-4.15%	0.0904

$$\dot{V} = \frac{V}{t}$$

$$\frac{\partial \dot{V}}{\partial V} = \frac{1}{t}\partial V$$

$$\frac{\partial \dot{V}}{\partial t} = -\frac{V}{t^2}\partial t$$

$$\frac{\Delta \dot{V}}{\dot{V}} = \frac{\sqrt{\left(\frac{1}{t}\Delta V\right)^2 + \left(-\frac{V}{t^2}\Delta t\right)^2}}{\dot{V}}$$

Table - C-2 Uncertainty in the volume flow rate estimation for SRT prototype 1

Absolute uncertainty	Absolute uncertainty	Absolute uncertainty	Relative uncertainty
± 2%	± 1.5%	± ΔV_{dot}	± ΔV_{dot} / V_{dot}
ΔV (m^3)	Δt (sec)	(m^3/s)	
0.004	0.474	0.000158	2.50%
0.004	0.388	0.000193	2.50%
0.004	0.337	0.000223	2.50%
0.004	0.302	0.000248	2.50%
0.004	0.277	0.000271	2.50%
0.004	0.257	0.000292	2.50%
0.004	0.241	0.000311	2.50%
0.004	0.228	0.000329	2.50%
0.004	0.217	0.000346	2.50%
0.004	0.207	0.000362	2.50%

$$\dot{m} = \frac{\rho V}{t}$$

$$\frac{\partial \dot{m}}{\partial Q} = \frac{\rho}{t}\partial Q$$

$$\frac{\partial \dot{m}}{\partial t} = -\frac{\rho * Q}{t^2}\partial t$$

$$\frac{\Delta \dot{m}}{\dot{m}} = \frac{\sqrt{\left(\frac{\rho}{t}\Delta Q\right)^2 + \left(-\frac{\rho * Q}{t^2}\Delta t\right)^2}}{\dot{m}}$$

Table - C-3 Uncertainty in the mass flow rate estimation for SRT prototype 1

Absolute uncertainty	Relative uncertainty
± Δm_{dot}	± Δm_{dot} / m_{dot}
(kg/s)	
0.158	2.50%
0.193	2.50%
0.223	2.50%
0.248	2.50%
0.271	2.50%
0.292	2.50%
0.311	2.50%
0.329	2.50%
0.346	2.50%
0.362	2.50%

$$A = l \times w$$

$$\frac{\partial A}{\partial l} = w \times \partial l$$

$$\frac{\partial A}{\partial w} = l \times \partial w$$

$$\frac{\Delta A}{A} = \frac{\sqrt{(w \times \Delta l)^2 + (l \times \Delta w)^2}}{A}$$

Exit nozzle length = 120±0.3mm
Width of each exit nozzle = 6±0.15mm
Total width of exit nozzle = 12±0.3mm

Table - C-4 Uncertainty in the exit nozzle area estimation of SRT prototype 1

Absolute uncertainty	Relative uncertainty
Area (m²)	± ΔA/A
± ΔA	
3.618E-05	2.51%
3.618E-05	2.51%
3.618E-05	2.51%
3.618E-05	2.51%
3.618E-05	2.51%
3.618E-05	2.51%
3.618E-05	2.51%
3.618E-05	2.51%
3.618E-05	2.51%
3.618E-05	2.51%

$$v = \frac{\dot{V}}{A}$$

$$\frac{\partial v}{\partial \dot{V}} = \frac{1}{A} \partial \dot{V}$$

$$\frac{\partial v}{\partial A} = -\frac{\dot{V}}{A^2} \partial A$$

$$\frac{\Delta v}{v} = \frac{\sqrt{\left(\frac{1}{A}\Delta \dot{V}\right)^2 + \left(-\frac{\dot{V}}{A^2}\Delta A\right)^2}}{v}$$

Table - C-5 Uncertainty in the exit velocity estimation for SRT prototype 1

Absolute uncertainty	Relative uncertainty
Velocity ± Δv	± Δv/v
(m/s)	
0.156	3.54%
0.190	3.54%
0.219	3.54%
0.244	3.54%
0.267	3.54%
0.287	3.54%
0.306	3.54%
0.324	3.54%
0.340	3.54%
0.356	3.54%

$$T_{estimated} = \dot{m} * v_a * R$$

$$\omega = 0; U = 0; \Rightarrow \therefore v_a = v_r = v$$

$$T_{estimated} = \dot{m} * v * R$$

$$\frac{\delta T_{estimated}}{\delta \dot{m}} = v * R * \partial \dot{m}$$

$$\frac{\delta T_{estimated}}{\delta v} = \dot{m} * R * \partial v$$

$$\frac{\delta T_{estimated}}{\delta R} = \dot{m} * v * \partial R$$

$$\frac{\Delta T_{estimated}}{T_{estimated}} = \frac{\sqrt{\left(v * R * \Delta \dot{m}\right)^2 + \left(\dot{m} * R * \Delta v\right)^2 + \left(v * \dot{m} * \Delta R\right)^2}}{T_{estimated}}$$

Table - C-6 Uncertainty in the estimated torque for SRT prototype 1

Absolute uncertainty	Absolute uncertainty	Relative uncertainty
Radius 121.5±1mm	Estimated torque	Estimated torque
ΔR (m)	ΔT_{est} (Nm)	± $\Delta T_{est} / T_{est}$
0.001	0.149	4.41%
0.001	0.223	4.41%
0.001	0.295	4.41%
0.001	0.367	4.41%
0.001	0.438	4.41%
0.001	0.508	4.41%
0.001	0.577	4.41%
0.001	0.645	4.41%
0.001	0.713	4.41%
0.001	0.779	4.41%

$$T_{shaft} = F_{LC} * L_{arm}$$

$$\frac{\partial T_{shaft}}{\partial F_{LC}} = L_{arm} * \partial F_{LC}$$

$$\frac{\partial T_{shaft}}{\partial L_{arm}} = F_{LC} * \partial L_{arm}$$

$$\frac{\Delta T_{shaft}}{T_{shaft}} = \frac{\sqrt{(L_{arm} * \Delta F_{LC})^2 + \sqrt{(F_{LC} * \Delta L_{arm})^2}}}{T_{shaft}}$$

Table - C-7 Uncertainty in the shaft torque estimation for SRT prototype 1

Absolute uncertainty	Absolute uncertainty	Relative uncertainty
Measured Force	Torque arm length (190±1mm)	Measured shaft torque
$\pm \Delta F_{LC}$ (N)	$\pm \Delta L_{arm}$ (m)	$\pm \Delta T_{sh} / T_{sh}$
0.17	0.0010	1.13%
0.25	0.0010	1.13%
0.33	0.0010	1.13%
0.41	0.0010	1.13%
0.48	0.0010	1.13%
0.57	0.0010	1.13%
0.64	0.0010	1.13%
0.73	0.0010	1.13%
0.82	0.0010	1.13%
0.89	0.0010	1.13%

Table - C-8 Measured and estimated data from a stationary test on the cross pipe turbine

Pressure kPa	Flow ltr	Vol flow m^3	Time sec	Flow rate l/s	Flow rate m^3/s	Strain Indicator reading	Measured force N	Exit Velocity m/s	Estimated Torque N-m	Shaft torque N-m	%error	k-factor
10	100	0.1	58.43	1.711	0.0017	125	6.66	4.312	1.476	1.406	-4.96%	0.076
20	100	0.1	41.44	2.413	0.0024	242	12.90	6.079	2.934	2.722	-7.76%	0.082
30	100	0.1	33.95	2.945	0.0029	387	20.63	7.420	4.371	4.354	-0.39%	0.090
40	100	0.1	29.48	3.392	0.0034	503	26.82	8.545	5.797	5.659	-2.44%	0.096
50	100	0.1	26.43	3.783	0.0038	621	33.11	9.531	7.211	6.986	-3.22%	0.101
60	100	0.1	24.19	4.135	0.0041	764	40.73	10.417	8.614	8.595	-0.22%	0.106
70	100	0.1	22.44	4.456	0.0045	876	46.70	11.228	10.007	9.855	-1.55%	0.111
80	100	0.1	21.03	4.755	0.0048	991	52.84	11.980	11.392	11.148	-2.19%	0.115

Table - C-9 Uncertainty analysis of CPT stationary test results

Absolute uncertainty	Absolute uncertainty	Absolute uncertainty	Absolute uncertainty		Absolute uncertainty	Absolute uncertainty		Absolute uncertainty	Absolute uncertainty	Relative uncertainty	Absolute uncertainty	Relative uncertainty	Absolute uncertainty	Relative uncertainty
± 2%	±1.5%	±	±	±	±	±	±	±	±	Estimated	±	±	±	Shaft
ΔV	Δt	ΔVdot	Δmdot	A	ΔA	Δ*v*	R	ΔR	$\Delta T_{estimated}$	± ΔT/T	ΔFLC	ΔLarm/L	Larm	±ΔT/T
0.002	0.876	0.0000428	0.0428	0.000397	0.0000032	0.113	0.2	0.001	0.054	3.66%	0.067	0.10%	0.211	1.11%
0.002	0.622	0.0000603	0.0603	0.000397	0.0000032	0.160	0.2	0.001	0.107	3.66%	0.129	0.10%	0.211	1.11%
0.002	0.509	0.0000736	0.0736	0.000397	0.0000032	0.195	0.2	0.001	0.160	3.66%	0.206	0.10%	0.211	1.11%
0.002	0.442	0.0000848	0.0848	0.000397	0.0000032	0.224	0.2	0.001	0.212	3.66%	0.268	0.10%	0.211	1.11%
0.002	0.397	0.0000946	0.0946	0.000397	0.0000032	0.250	0.2	0.001	0.264	3.66%	0.331	0.10%	0.211	1.11%
0.002	0.363	0.0001034	0.1034	0.000397	0.0000032	0.273	0.2	0.001	0.315	3.66%	0.407	0.10%	0.211	1.11%
0.002	0.337	0.0001114	0.1114	0.000397	0.0000032	0.295	0.2	0.001	0.366	3.66%	0.467	0.10%	0.211	1.11%
0.002	0.315	0.0001189	0.1189	0.000397	0.0000032	0.314	0.2	0.001	0.417	3.66%	0.528	0.10%	0.211	1.11%

Table - C-10 Measured and estimated data from a stationary test on the SRT prototype 2 with 8mm exit nozzle width

Pressure kPa	Flow ltr	Vol flow m^3	Time sec	Flow rate l/s	Flow rate m^3/s	Strain Indicator reading	Measured force N	Exit Velocity m/s	Estimated Torque N-m	Shaft torque N-m	%error	k-factor
5	100	0.1	16.85	5.936	0.00594	95	5.06	3.092	1.120	1.069	4.55%	0.046
10	100	0.1	11.93	8.380	0.00838	192	10.24	4.365	2.231	2.160	3.19%	0.050
15	100	0.1	9.77	10.239	0.01024	288	15.36	5.333	3.331	3.240	2.73%	0.055
20	100	0.1	8.47	11.802	0.01180	384	20.47	6.147	4.426	4.320	2.38%	0.059
25	100	0.1	7.59	13.171	0.01317	482	25.69	6.860	5.511	5.420	1.65%	0.063
30	100	0.1	6.94	14.400	0.01440	575	30.66	7.500	6.588	6.470	1.80%	0.067
35	100	0.1	6.44	15.526	0.01553	669	35.69	8.087	7.659	7.530	1.68%	0.070
40	100	0.1	6.04	16.569	0.01657	766	40.85	8.629	8.722	8.620	1.17%	0.074
45	100	0.1	5.70	17.543	0.01754	860	45.88	9.137	9.777	9.680	0.99%	0.078

Table - C-11 Uncertainty analysis of stationary test results for SRT prototype 2 with 8mm exit nozzle width

Absolute uncertainty	Absolute uncertainty	Absolute uncertainty	Absolute uncertainty		Absolute uncertainty	Absolute uncertainty		Absolute uncertainty	Absolute uncertainty	Relative uncertainty	Absolute uncertainty	Absolute uncertainty	Absolute uncertainty	Relative uncertainty
± 2%	±1.5%	±	±	±	±	±	±	±	±	Estimated	±	±	±	Shaft
ΔV	Δt	ΔVdot	Δmdot	A	ΔA	Δν	R	ΔR	$\Delta T_{estimated}$	± ΔT/T	ΔFLC	ΔLarm	Larm	±ΔT/T
0.002	0.253	0.000148	0.148	0.00192	0.000036	0.0969	0.061	0.001	0.048	4.33%	0.0506	0.0010	0.211	1.11%
0.002	0.179	0.000210	0.210	0.00192	0.000036	0.1368	0.061	0.001	0.097	4.33%	0.1024	0.0010	0.211	1.11%
0.002	0.293	0.000369	0.369	0.00192	0.000036	0.2171	0.061	0.001	0.189	5.68%	0.1536	0.0010	0.211	1.11%
0.002	0.254	0.000426	0.426	0.00192	0.000036	0.2503	0.061	0.001	0.251	5.68%	0.2047	0.0010	0.211	1.11%
0.002	0.228	0.000475	0.475	0.00192	0.000036	0.2793	0.061	0.001	0.313	5.68%	0.2569	0.0010	0.211	1.11%
0.002	0.208	0.000519	0.519	0.00192	0.000036	0.3054	0.061	0.001	0.374	5.68%	0.3066	0.0010	0.211	1.11%
0.002	0.193	0.000560	0.560	0.00192	0.000036	0.3293	0.061	0.001	0.435	5.68%	0.3569	0.0010	0.211	1.11%
0.002	0.181	0.000597	0.597	0.00192	0.000036	0.3514	0.061	0.001	0.495	5.68%	0.4085	0.0010	0.211	1.11%
0.002	0.171	0.000633	0.633	0.00192	0.000036	0.3720	0.061	0.001	0.555	5.68%	0.4588	0.0010	0.211	1.11%

C.2 Uncertainty analysis of power loss test results

Table - C-12 shows measured and estimated quantities from a power test conducted on SRT prototype 1 with V-ring lip. The total power loss is estimated as product of supply voltage and supply current. Where as the torque loss is estimated by dividing the power loss by the angular speed of the turbine; the uncertainty in the estimation of torque loss is based on this definition and is predicted using the instrumental uncertainties in the basic measured data.

Table - C-12 Measured and estimated quantities from power loss test of SRT prototype1 with V-ring seal

DC motor + Turbine drag + V-ring lip @ 50kPa					
(Measured)			(Estimated)		
Supply Voltage V (Volt)	Supply Current I (Amp)	Turbine Speed (rpm)	Angular speed ω (rad/sec)	Power Loss V*I (Watt)	Torque Loss $T_{loss} = V * I / \omega$ (Nm)
9.5	4.01	101	10.57	38.2	3.784
18.7	2.62	198	20.72	48.9	2.360
28.1	2.18	298	31.19	61.2	1.962
38.0	1.92	403	42.18	72.9	1.780
47.3	1.81	502	52.54	85.6	1.629
56.5	1.76	600	62.80	99.7	1.588
66.4	1.74	705	73.79	115.9	1.552
75.5	1.76	802	83.94	132.7	1.551
85.0	1.77	902	94.41	150.2	1.573
94.0	1.79	998	104.46	168.6	1.614
103.1	1.82	1094	114.51	187.8	1.652
112.5	1.86	1194	124.97	209.2	1.674
122.8	1.90	1304	136.49	232.8	1.706
132.2	1.91	1403	146.85	252.8	1.722
141.6	1.94	1503	157.31	274.6	1.746
150.7	1.96	1600	167.47	294.7	1.760
160.5	1.99	1704	178.35	319.1	1.789
169.6	2.01	1800	188.40	340.9	1.809
179.0	2.03	1900	198.87	363.1	1.832
188.6	2.05	2002	209.54	386.7	1.845

Therefore by partially differentiating the torque loss equation to solve for the relative uncertainty in $\frac{\Delta T_{loss}}{T_{loss}}$ following equation is derived,

$$\frac{\Delta T_{loss}}{T_{loss}} = \frac{\sqrt{\left(\frac{V}{\omega}\Delta I\right)^2 + \left(\frac{I}{\omega}\Delta V\right)^2 + \left(-\frac{V \times I}{\omega^2}\Delta\omega\right)^2}}{T_{loss}}$$

Relative uncertainty in measurement of rotational speed using Yokogawa tachometer Model 3632 is ±1rpm up to 2000rpm. Relative uncertainty in measurement of voltage output using a standard multi-meter is ±1.50%. Relative uncertainty in measurement of current output using a standard multi-meter is ±2.50 %. Based on this information and the above equation the relative uncertainty of loss torque is calculated and is shown in Table - C-13.

Table - C-13 Uncertainty analysis of the torque loss

ΔV Absolute uncertainty of supply voltage	ΔI Absolute uncertainty of supply current	$\Delta\omega$ Absolute uncertainty of angular speed	ΔT_{loss} Absolute uncertainty of loss torque	$\frac{\Delta T_{loss}}{T_{loss}}$ Relative uncertainty of loss torque
0.143	0.100	0.009904	0.105329	2.92%
0.280	0.066	0.005052	0.068795	2.92%
0.421	0.055	0.003357	0.057206	2.92%
0.569	0.048	0.002482	0.050416	2.92%
0.709	0.045	0.001993	0.047498	2.92%
0.848	0.044	0.001667	0.046286	2.92%
0.996	0.044	0.001419	0.045784	2.92%
1.133	0.044	0.001247	0.046092	2.92%
1.275	0.044	0.001109	0.046375	2.92%
1.410	0.045	0.001002	0.047057	2.92%
1.546	0.046	0.000914	0.047825	2.92%
1.687	0.046	0.000838	0.048804	2.92%
1.843	0.047	0.000767	0.049729	2.92%
1.982	0.048	0.000713	0.05019	2.92%
2.124	0.048	0.000666	0.050891	2.92%
2.261	0.049	0.000625	0.051305	2.92%
2.408	0.050	0.000587	0.052162	2.92%
2.543	0.050	0.000556	0.052754	2.92%
2.685	0.051	0.000526	0.053232	2.92%
2.829	0.051	0.000500	0.053804	2.92%

C.3 Uncertainty analysis of power test results

Table - C-14 and Table - C-15 shows the measured results from a power test conducted on SRT prototype1 with mean turbine diameter Ø243mm and total exit nozzle area of 0.00144m². The volume flow rate (m³/s) of the water flowing through the turbine is equal to the measured water volume (0.4m³) divided by the measured time. The electrical power output is calculated as a product of generator output voltage and current. The hydro power input is calculated as a product of mass flow rate times gravitational acceleration times the supply head, i.e. $\dot{m}\,gh$. The electrical efficiency is calculated as the percentage ratio of electrical output power divided by the hydro input power.

The generator torque (i.e. shaft torque) is the actual torque produced by the turbine. It is the sum of electrical torque plus the torque loss (i.e. DC motor/generator + turbine air drag + rotary seal friction). It is calculated as discussed in section 4.5 of Chapter 4. $T_g = K_t * I_g + T_{loss}$, Here K_t is the DC generator torque constant and $T_{loss} = \dfrac{\dot{W}_{loss}}{\omega}$ is the torque loss estimated from the power loss experiments as discussed in section 4.5 and 4.6 of Chapter 4 and section C.2 of Appendix C. From the generator torque the turbine power $\dot{W}_T$ is calculated as $T_g * \omega$.

The relative velocity V_r of water jets at both the exit nozzles is equal to the measured volume flow rate (m³/s) divided by the total exit nozzle area (0.00144m²). Linear velocity of the nozzle U is calculated as a product of rotor radius and angular speed. Absolute velocity of the water jet is calculated as difference between the relative velocity of water jet and the linear velocity of the turbine i.e. $V_r - U$. Using the relative velocity value and equation 2.38 (see Chapter 2) the value of k-factor is calculated. The fluid frictional power loss $\dot{W}_{Ff}$ is calculated as $\left(\frac{1}{2}\dot{m}\,kV_r^{\,2}\right)$, and the power loss in the kinetic energy leaving the turbine with exiting water jet $\dot{W}_{Ke}$ is calculated as $\left(\frac{1}{2}\dot{m}V_a^{\,2}\right)$.

The total output power is calculated as $\dot{W}_{Out} = \dot{W}_T + \dot{W}_{Ff} + \dot{W}_{Ke}$.

For the uncertainty analysis of the quantities estimated from the data collected in the power test, the instrumental relative uncertainties are used. Relative uncertainty in measurement of supply pressure with Floyd's pressure gauge is ±1.0%. Relative uncertainty in measurement of the water flow through turbine using Omega flow meter is ± 2.0%. Relative uncertainty in measurement of time using a standard stop watch is +/- 3.0% up to 10sec and there after ±1.5%. Relative uncertainty in measurement of rotational speed using Yokogawa tachometer Model 3632 is ±1rpm up to 2000rpm. Relative uncertainty in measurement of voltage output using a standard multi-meter is ±1.50%. Relative uncertainty in measurement of current output using a standard multi-meter is ±2.50 %.

Further the relative uncertainty in the torque loss estimation is calculated in section C.2 of Appendix C which is used as a basis to do further uncertainty analysis in this section. The relative uncertainty of torque loss is calculated as ±2.92% (see Table - C-13, Appendix C).

The relative manufacturing uncertainty in the total exit nozzle area is considered as ±1% (i.e. for a total exit nozzle area of 1440mm², the manufacturing uncertainty of 14.4 mm²). The relative manufacturing uncertainty in the turbine mean radius is considered to be ±0.08% (i.e. for a turbine mean radius of 121.5mm the manufacturing uncertainty of ±0.1mm).

$\dot{W}_{Out} = \dot{W}_{T} + \dot{W}_{Ff} + \dot{W}_{Ke}$ The relative uncertainty in the estimation of the total output power $\dot{W}_{Out}$ is calculated as maximum ±5.02% (see Table - C-17). The relative uncertainty in the estimation of the hydro input power $\dot{W}_{In}$ is calculated as ±2.70% (see Table - C-17). From these calculated quantities of the relative uncertainties it is confirmed that the experimental procedures used for conducting the performance power test on the simple reaction turbines in this research have very high level of confidence.

Table - C-14 Measured and estimated quantities from a power test on SRT prototype-1 with V-ring lip seal @ 50kPa supply pressure

Supply Pressure	Volume flow	Time	Estimated volume flow rate $\dot{V}$	Measured generator output voltage V_g	Measured generator output current I_g	Estimated electrical power output $\dot{W}_E$	Measured rotational speed of the turbine N	Angular speed of the turbine ω	Estimated input power $\dot{W}_{in}$ $\left(\dot{m}gh\right)$	Estimated overall efficiency η_E
kPa	m^3	sec	m^3/s	Volts	Amps	Watts	rpm	rad/s	Watts	%
50	0.4	15.46	0.0258	126.3	0.00	0.0	1341	140.36	1291.4	0.00
50	0.4	16.38	0.0244	115.6	1.14	132.1	1228	128.48	1218.5	10.84
50	0.4	17.14	0.0233	107.3	2.19	235.0	1139	119.18	1164.5	20.18
50	0.4	18.00	0.0222	98.8	3.27	322.6	1049	109.76	1109.1	29.09
50	0.4	18.98	0.0210	90.2	4.27	385.0	958	100.28	1051.9	36.60
50	0.4	20.08	0.0199	81.3	5.27	428.3	863	90.34	994.1	43.08
50	0.4	21.13	0.0189	72.7	6.11	444.0	771	80.74	944.4	47.01
50	0.4	22.20	0.0180	64.8	6.91	447.8	688	71.99	899.2	49.80
50	0.4	23.41	0.0171	56.4	7.78	439.0	599	62.67	852.6	51.49
50	0.4	24.46	0.0163	49.0	8.35	409.0	520	54.43	816.0	50.12
50	0.4	25.71	0.0155	39.8	8.92	355.1	423	44.22	776.5	45.73
50	0.4	26.58	0.0150	33.0	8.93	294.2	350	36.62	750.8	39.19
50	0.4	27.62	0.0145	24.1	9.21	222.2	256	26.79	722.6	30.75

Table - C-15 Estimated quantities from a power test on SRT prototype-1 with V-ring lip seal @ 50kPa supply pressure

Estimated torque loss T_{loss}	Estimated generator input torque T_g $\left(K_t * I_g + T_{loss}\right)$	Estimated generator turbine power $\dot{W}_T$ $\left(T_g * \omega\right)$	Relative velocity of the water jet V_r	Linear velocity of the turbine Nozzle U	Absolute velocity of the water jet V_a	k-factor	Estimated fluid frictional power loss $\dot{W}_{Ff}$ $\left(\frac{1}{2}\dot{m}kV_r^2\right)$	Estimated power loss in kinetic energy $\dot{W}_{Ke}$ $\left(\frac{1}{2}\dot{m}V_a^2\right)$	Estimated total output power $\dot{W}_{Out}$ $\left(\dot{W}_T + \dot{W}_{Ff} + \dot{W}_{Ke}\right)$
Nm	Nm	Watts	m/s	m/s	m/s		Watts	Watts	Watts
1.72	1.72	242.00	17.94	17.05	0.88	0.2149	892.65	10.06	1144.70
1.70	2.73	350.11	16.92	15.61	1.31	0.2000	697.97	21.01	1069.09
1.68	3.65	434.86	16.17	14.48	1.69	0.1838	559.93	33.41	1028.19
1.66	4.60	504.79	15.40	13.34	2.07	0.1708	449.56	47.49	1001.84
1.65	5.49	550.03	14.61	12.18	2.43	0.1640	368.15	61.91	980.09
1.64	6.38	576.04	13.81	10.98	2.83	0.1565	296.57	79.69	952.30
1.63	7.13	575.78	13.12	9.81	3.31	0.1405	228.29	103.31	907.38
1.64	7.86	565.64	12.49	8.75	3.74	0.1317	184.69	125.90	876.23
1.65	8.66	542.51	11.84	7.61	4.23	0.1267	151.45	152.32	846.27
1.68	9.19	500.39	11.33	6.61	4.72	0.1191	124.79	181.79	806.98
1.74	9.77	432.18	10.78	5.37	5.41	0.1081	97.60	227.36	757.13
1.83	9.86	361.16	10.43	4.45	5.98	0.1016	82.94	268.41	712.52
2.03	10.32	276.61	10.04	3.26	6.78	0.0980	71.31	332.26	680.19

Following equations are used to calculate the absolute uncertainties in Table - C-16,

$$\Delta k = \sqrt{\left(\frac{2g \times \Delta H}{V_r^{\,2}}\right)^2 + \left(\frac{2R\omega^2 \Delta R}{V_r^{\,2}}\right)^2 + \left(\frac{2\omega R^2 \Delta \omega}{V_r^{\,2}}\right)^2 + \left(\frac{-1}{\left(V_r^{\,2}\right)^2}\left(2gH + R^2\omega^2\right) \times \Delta V_r\right)};$$

$$\Delta \dot{V} = \sqrt{\left(\frac{1}{t}\Delta V\right)^2 + \left(-\frac{V}{t^2}\Delta t\right)^2};$$

$$\Delta \dot{m} = \sqrt{\left(\frac{\rho}{t}\Delta V\right)^2 + \left(-\frac{\rho * V}{t^2}\Delta t\right)^2};$$

$$\Delta U = \sqrt{(\omega \times \Delta R)^2 + (R \times \Delta \omega)^2};$$

$$\Delta V_r = \sqrt{\left(\frac{1}{A}\Delta \dot{V}\right)^2 + \left(-\frac{\dot{V}}{A^2}\Delta A\right)^2};$$

$$\Delta V_a = \sqrt{\Delta U^2 + \Delta V_r^{\,2}};$$

Table - C-16 Calculated absolute uncertainties for the power test conducted on the SRT prototype1 with V-ring seal @ 50kPa supply pressure

Absolute uncertainty in measured supply head ΔH	Absolute uncertainty in measured volume flow ΔV	Absolute uncertainty in measured time Δt	Absolute uncertainty in the estimated flow rate $\Delta \dot{V}$	Absolute uncertainty in the estimated mass flow rate $\Delta \dot{m}$	Absolute uncertainty in the total exit nozzle area ΔA	Absolute uncertainty in the turbine mean radius ΔR	Absolute uncertainty in the estimated angular speed $\Delta \omega$	Absolute uncertainty in the estimated relative velocity ΔV_r	Absolute uncertainty in the estimated linear velocity of turbine ΔU	Absolute uncertainty in the estimated absolute velocity ΔV_a	Absolute uncertainty in the estimated k-factor Δk
± m	± m³	± sec	± m³/s	± kg/s	± m²	± m	± rad/s	± m/s	± m/s	± m/s	±
0.051	0.0080	0.2318	0.00065	0.6470	0.0000144	0.0001	0.0007	0.4838	0.0140	0.4840	0.0039
0.051	0.0080	0.2457	0.00061	0.6105	0.0000144	0.0001	0.0008	0.4565	0.0128	0.4566	0.0042
0.051	0.0080	0.2571	0.00058	0.5834	0.0000144	0.0001	0.0009	0.4363	0.0119	0.4364	0.0045
0.051	0.0080	0.2699	0.00056	0.5557	0.0000144	0.0001	0.0010	0.4155	0.0110	0.4156	0.0048
0.051	0.0080	0.2846	0.00053	0.5270	0.0000144	0.0001	0.0010	0.3941	0.0100	0.3942	0.0053
0.051	0.0080	0.3012	0.00050	0.4981	0.0000144	0.0001	0.0012	0.3724	0.0090	0.3725	0.0058
0.051	0.0080	0.3170	0.00047	0.4732	0.0000144	0.0001	0.0013	0.3538	0.0081	0.3539	0.0063
0.051	0.0080	0.3330	0.00045	0.4505	0.0000144	0.0001	0.0015	0.3369	0.0072	0.3369	0.0069
0.051	0.0080	0.3512	0.00043	0.4272	0.0000144	0.0001	0.0017	0.3194	0.0063	0.3195	0.0076
0.051	0.0080	0.3669	0.00041	0.4088	0.0000144	0.0001	0.0019	0.3057	0.0054	0.3057	0.0082
0.051	0.0080	0.3856	0.00039	0.3890	0.0000144	0.0001	0.0024	0.2909	0.0044	0.2909	0.0090
0.051	0.0080	0.3988	0.00038	0.3762	0.0000144	0.0001	0.0029	0.2813	0.0037	0.2813	0.0096
0.051	0.0080	0.4143	0.00036	0.3620	0.0000144	0.0001	0.0039	0.2707	0.0027	0.2707	0.0104

Following equations are used to calculate the absolute and relative uncertainties in Table - C-17,

$$\Delta \dot{W}_E = \sqrt{\left(V_g * \Delta I_g\right)^2 + \left(I_g * \Delta V_g\right)^2} ;$$

$\Delta T_{loss} = \pm 2.92\%(T_{loss})$, here ±2.92% is taken from the previous analysis discussed in section C.2 of Appendix C;

$$\Delta T_g = \sqrt{\left(K_t \Delta I_g\right)^2 + \left(\Delta T_{loss}\right)^2} ;$$

$$\Delta \dot{W}_T = \sqrt{\left(\omega \times \Delta T_g\right)^2 + \left(T_g \times \Delta \omega\right)^2} ;$$

$$\Delta \dot{W}_{Out} = \sqrt{\left(\Delta \dot{W}_T\right)^2 + \left(\Delta \dot{W}_{Ke}\right)^2 + \left(\Delta \dot{W}_{Ff}\right)^2} ;$$

$$\frac{\Delta \dot{W}_{out}}{\dot{W}_{out}} = \frac{\sqrt{\left(\Delta \dot{W}_T\right)^2 + \left(\Delta \dot{W}_{Ke}\right)^2 + \left(\Delta \dot{W}_{Ff}\right)^2}}{\dot{W}_{out}};$$

$$\Delta \dot{W}_{in} = \sqrt{\left(g * H * \Delta \dot{m}\right)^2 + \left(g * \dot{m} * \Delta H\right)^2} ;$$

$$\frac{\Delta \dot{W}_{in}}{\dot{W}_{in}} = \frac{\sqrt{\left(g * H * \Delta \dot{m}\right)^2 + \left(g * \dot{m} * \Delta H\right)^2}}{\dot{W}_{in}};$$

Table - C-17 Calculated absolute and relative uncertainties for the power test conducted on the SRT prototype1 with V-ring seal @ 50kPa supply pressure

Absolute uncertainty in the measured generator output voltage ΔV_g	Absolute uncertainty in the measured generator output current ΔI_g	Absolute uncertainty in the estimated electrical power output $\dot{\Delta W}_E$	Absolute uncertainty in the estimated torque loss ΔT_{loss}	Absolute uncertainty in the estimated generator input torque ΔT_g	Absolute uncertainty in the estimated generator turbine power $\dot{\Delta W}_T$	Absolute uncertainty in the estimated fluid frictional power loss $\dot{\Delta W}_{Ff}$	Absolute uncertainty in the estimated power loss in kinetic energy $\dot{\Delta W}_{Ke}$	Absolute uncertainty in the estimated total output power $\dot{\Delta W}_{Out}$	Relative uncertainty in the estimated total output power $\frac{\dot{\Delta W}_{Out}}{\dot{W}_{Out}}$	Absolute uncertainty in the estimated hydro input power $\dot{\Delta W}_{in}$	Relative uncertainty in the estimated hydro input power $\frac{\dot{\Delta W}_{in}}{\dot{W}_{in}}$
± Volts	± Amps	± W	± Nm	± Nm	± W	± W	± W	± W	± %	± W	± %
1.89	0.000	0.00	0.0503	0.0503	7.07	55.51	11.03	57.04	4.98%	34.83	2.70%
1.73	0.029	3.85	0.0495	0.0563	7.24	44.05	14.62	46.97	4.39%	32.87	2.70%
1.61	0.055	6.85	0.0490	0.0711	8.47	36.02	17.24	40.82	3.97%	31.41	2.70%
1.48	0.082	9.41	0.0485	0.0908	9.96	29.63	19.11	36.64	3.66%	29.92	2.70%
1.35	0.107	11.22	0.0481	0.1112	11.15	24.90	20.18	33.93	3.46%	28.37	2.70%
1.22	0.132	12.49	0.0478	0.1327	11.99	20.79	21.07	31.93	3.35%	26.81	2.70%
1.09	0.153	12.94	0.0477	0.1513	12.22	17.04	22.26	30.58	3.37%	25.47	2.70%
0.97	0.173	13.06	0.0478	0.1693	12.19	14.65	22.89	29.79	3.40%	24.25	2.70%
0.85	0.195	12.80	0.0482	0.1891	11.85	12.80	23.34	29.14	3.44%	23.00	2.70%
0.73	0.209	11.92	0.0490	0.2023	11.01	11.39	23.99	28.75	3.56%	22.01	2.70%
0.60	0.223	10.35	0.0509	0.2157	9.54	10.02	25.10	28.66	3.79%	20.94	2.70%
0.49	0.223	8.58	0.0534	0.2165	7.93	9.29	26.14	28.85	4.05%	20.25	2.70%
0.36	0.230	6.48	0.0593	0.2245	6.02	8.65	27.81	29.74	4.37%	19.49	2.70%

Table - C-18 Calculated absolute and relative uncertainties for the power test conducted on the SRT prototype2 with V-ring seal and exit nozzle width of 8mm @ 41.37kPa supply pressure

Absolute uncertainty in the measured generator output voltage ΔV_g	Absolute uncertainty in the measured generator output current ΔI_g	Absolute uncertainty in the estimated electrical power output $\dot{\Delta W}_E$	Absolute uncertainty in the estimated torque loss ΔT_{loss}	Absolute uncertainty in the estimated generator input torque ΔT_g	Absolute uncertainty in the estimated generator turbine power $\dot{\Delta W}_T$	Absolute uncertainty in the estimated fluid frictional power loss $\dot{\Delta W}_{Ff}$	Absolute uncertainty in the estimated power loss in kinetic energy $\dot{\Delta W}_{Ke}$	Absolute uncertainty in the estimated total output power $\dot{\Delta W}_{Out}$	Relative uncertainty in the estimated total output power $\frac{\dot{\Delta W}_{Out}}{\dot{W}_{Out}}$	Absolute uncertainty in the estimated hydro input power $\dot{\Delta W}_{in}$	Relative uncertainty in the estimated hydro input power $\frac{\dot{\Delta W}_{in}}{\dot{W}_{in}}$
± Volts	± Amps	± W	± Nm	± Nm	± W	± W	± W	± W	± %	± W	± %
2.41	0.021	3.89	1.36	0.0396	0.0441	7.88	26.80	43.13	5.89%	39.98	3.75%
2.26	0.051	8.86	1.32	0.0384	0.0611	10.21	23.57	42.17	4.94%	38.57	3.75%
2.13	0.072	11.84	1.28	0.0375	0.0771	12.14	21.26	41.74	4.53%	37.42	3.75%
1.98	0.085	13.11	1.25	0.0365	0.0880	12.91	19.03	41.17	4.42%	36.17	3.75%
1.83	0.094	13.36	1.22	0.0355	0.0950	12.90	17.08	40.54	4.44%	34.93	3.75%
1.70	0.100	13.24	1.18	0.0346	0.1004	12.63	15.56	40.06	4.51%	33.85	3.75%
1.56	0.108	13.03	1.15	0.0337	0.1065	12.30	14.19	39.73	4.59%	32.77	3.75%
1.41	0.114	12.49	1.12	0.0328	0.1117	11.70	13.03	39.44	4.72%	31.71	3.75%
1.27	0.117	11.56	1.10	0.0320	0.1143	10.79	10.38	29.77	3.73%	22.12	2.70%
1.13	0.120	10.55	1.07	0.0313	0.1169	9.81	9.79	29.61	3.87%	21.48	2.70%
0.99	0.123	9.43	1.05	0.0307	0.1196	8.74	9.29	29.61	4.04%	20.86	2.70%
0.84	0.126	8.24	1.04	0.0304	0.1223	7.62	8.87	29.86	4.22%	20.32	2.70%
0.70	0.129	7.07	1.04	0.0303	0.1252	6.52	8.55	30.39	4.42%	19.88	2.70%

Table - C-19 Calculated absolute and relative uncertainties for the power test conducted on the CPT prototype with V-ring seal @ 80kPa supply pressure

Absolute uncertainty in the measured generator output voltage ΔV_g	Absolute uncertainty in the measured generator output current ΔI_g	Absolute uncertainty in the estimated electrical power output $\Delta \dot{W}_E$	Absolute uncertainty in the estimated torque loss ΔT_{loss}	Absolute uncertainty in the estimated generator input torque ΔT_g	Absolute uncertainty in the estimated generator turbine power $\Delta \dot{W}_T$	Absolute uncertainty in the estimated fluid frictional power loss $\Delta \dot{W}_{Ff}$	Absolute uncertainty in the estimated power loss in kinetic energy $\Delta \dot{W}_{Ke}$	Absolute uncertainty in the estimated total output power $\Delta \dot{W}_{Out}$	Relative uncertainty in the estimated total output power $\frac{\Delta \dot{W}_{Out}}{\dot{W}_{Out}}$	Absolute uncertainty in the estimated hydro input power $\Delta \dot{W}_{in}$	Relative uncertainty in the estimated hydro input power $\frac{\Delta \dot{W}_{in}}{\dot{W}_{in}}$
± Volts	± Amps	± W	± Nm	± Nm	± W	± W	± W	± W	± %	± W	± %
0.74	0.000	0.00	4.79	0.1399	7.69	8.78	12.30	16.58	3.78%	13.44	2.69%
0.69	0.016	0.88	4.55	0.1328	6.84	8.23	12.43	16.04	3.69%	13.07	2.69%
0.66	0.026	1.33	4.42	0.1291	6.46	7.97	12.50	15.81	3.64%	12.88	2.69%
0.63	0.036	1.76	4.27	0.1247	6.04	7.67	12.60	15.59	3.62%	12.65	2.69%
0.60	0.047	2.19	4.11	0.1201	5.67	7.38	12.70	15.40	3.59%	12.42	2.69%
0.57	0.056	2.48	3.99	0.1164	5.39	7.16	12.80	15.29	3.59%	12.24	2.69%
0.53	0.066	2.75	3.83	0.1119	5.07	6.92	12.92	15.18	3.60%	12.02	2.69%
0.49	0.078	3.00	3.67	0.1071	4.75	6.66	13.08	15.12	3.63%	11.78	2.69%
0.45	0.092	3.20	3.48	0.1015	4.42	6.38	13.33	15.12	3.69%	11.51	2.69%
0.40	0.102	3.21	3.32	0.0970	4.09	6.17	13.58	15.18	3.77%	11.30	2.69%
0.37	0.110	3.18	3.22	0.0941	3.85	6.02	13.81	15.27	3.85%	11.15	2.69%
0.32	0.123	3.05	3.08	0.0900	3.47	5.82	14.24	15.50	3.97%	10.92	2.69%
0.28	0.137	2.97	3.01	0.0878	3.22	5.67	14.66	15.79	4.06%	10.76	2.69%
0.23	0.151	2.72	2.99	0.0874	2.86	5.54	15.23	16.21	4.19%	10.61	2.69%

Appendix D Potential site survey

D.1 Potential sites

Table - D-1 List of other potential sites in Victoria, Australia (Survey results)

Result of survey: Potential hydro sites in Victoria, Australia			
Location	**Head**	**Flow**	**Description**
Narbethong	10m	12 liters/sec	Small Creek
Beechforest	5m min	11 litres/sec	1km creek frontage
Narbethong near Healesville	9m	10 liters/sec	Small Creek
Aberfeldy	over 10m	12-15 litres/min	spring fed dam
Scenes Creek (Great Ocean Road)		12 liters/sec	Small Creek
Beachworth	9m	10 liters/sec	Small creek
Berwick	5-10m	10 liters/sec	Small Creek
Bruarong near Yackandandah	12m	12 liters/sec	Have existing Platypus turbine
Launching Place	5m min	16 litres/sec	Small Creek
Belgrave	10m	10 liters/sec	Creek with intermittant flow
Tatong - NthE Vict	10m +	15 liters/sec	Fast flowing creek
Yackandandah	4-5m	10 liters/sec	spring

D.2 Additional information on case study

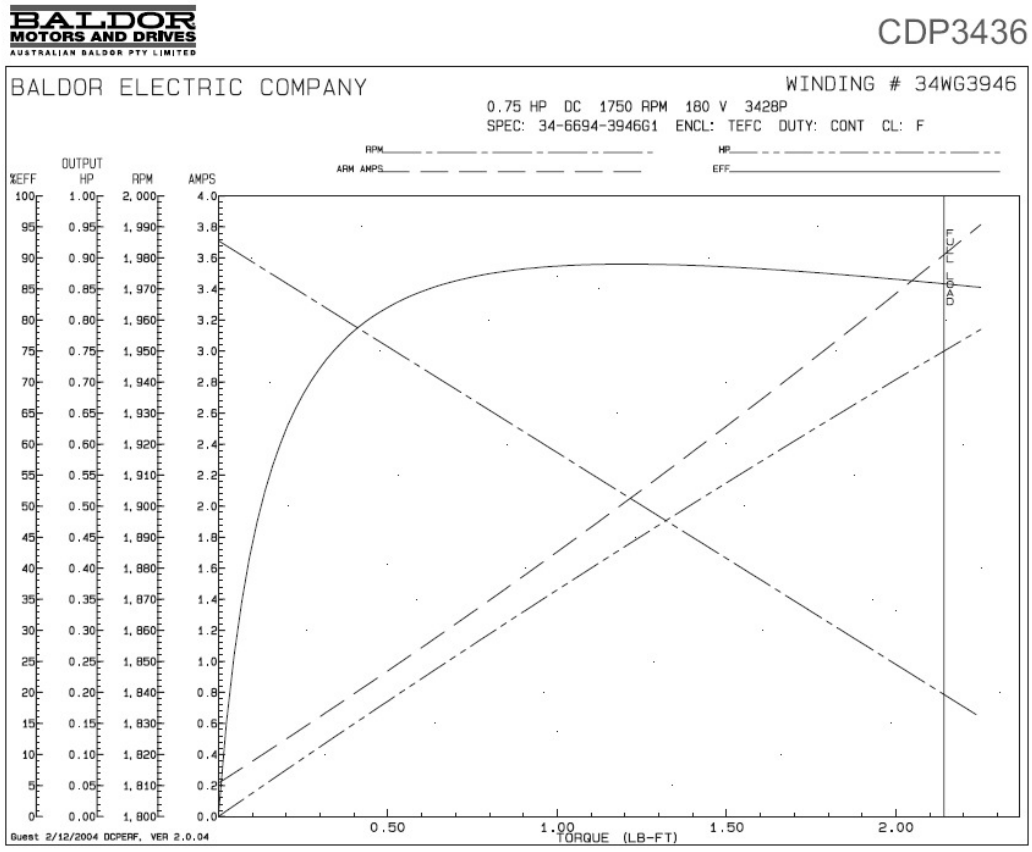

Figure - D.1 Performance curves of selected D.C. generator (Site1: Taggerty)

Table - D-2 Price list of PVC pipes

Ref Code	Item Description	Unit	Rate	Mark Up %	Supp Code
Trade Heading:	***Drainage***				*(Continued)*
PL14375	E.O 100 mm Access Coupling	No	9.64		
PL14376	E.O 100 mm Slip Coupling	No	20.25		
PL14377	E.O 100 mm Inspection Tee	No	18.66		
	- 150mm Dia Sewer Pipework				
PL14385	6000 mm long PVC Pipe	m	23.35		
	- 150mm Dia Sewer Fittings				
PL14387	E.O 150 mm Bend [15 Deg]	No	21.68		
PL14388	E.O 150 mm Bend [45 Deg]	No	23.93		
PL14389	E.O 150 mm Bend [88 Deg]	No	37.74		
PL14390	E.O 150 mm Junction [100 x 150 PI]	No	32.98		
PL14391	E.O 150 mm Junction [150 x 150 PI]	No	53.49		
PL14392	E.O 150 mm Access Coupling	No	16.91		
PL14393	E.O 150 mm Inspection Tee	No	46.90		
	CAST IRON DUCT COVERS AND FRAMES				
	- Supply & Fix Covers and Frames				
PL14430	Light Duty	No	216.00		
PL14431	Medium Duty	No	296.46		

Appendix E Test Rig Instrumentation

E.1 Additional information on instrumentation

BALDOR MOTORS AND DRIVES
AUSTRALIAN BALDOR PTY LIMITED

CDP3603

DC Motor Performance Data

Winding: 36WGZ507	Type: 3649P	Enclosure: TEFC

Nameplate Data		General Characteristics	
Rated Output (HP)	3 HP	Armature Resistance	0.3209 ohms
RPM	1750	Commutating Winding Resistance	
Armature Volts	180	Series Winding Resistance	
Armature Amps	14	Shunt Winding Resistance	
Field Volts		Armature Inductance	
Field Amps		Armature Inertia	
Rating - Duty	40C AMB-CONT	Maximun rated RPM with field weakening	
Power Supply Code	K	Maximum allowable inrush amps	
		Full Load Temperature Rise	

Load Characteristics at 180 Armature Volts

Load Point	1	2	3	4	5	6	7
Armature Amps	0.4	3.37	6.34	9.01	12.28	13.51	20.45
RPM	1860	1844	1827	1813	1795	1788	1750
Torque (LB-FT)	0	2	4	5.8	8	8.83	13.5

Figure - E.1 Data Sheet for the DC motor/generator used in the turbine test rig

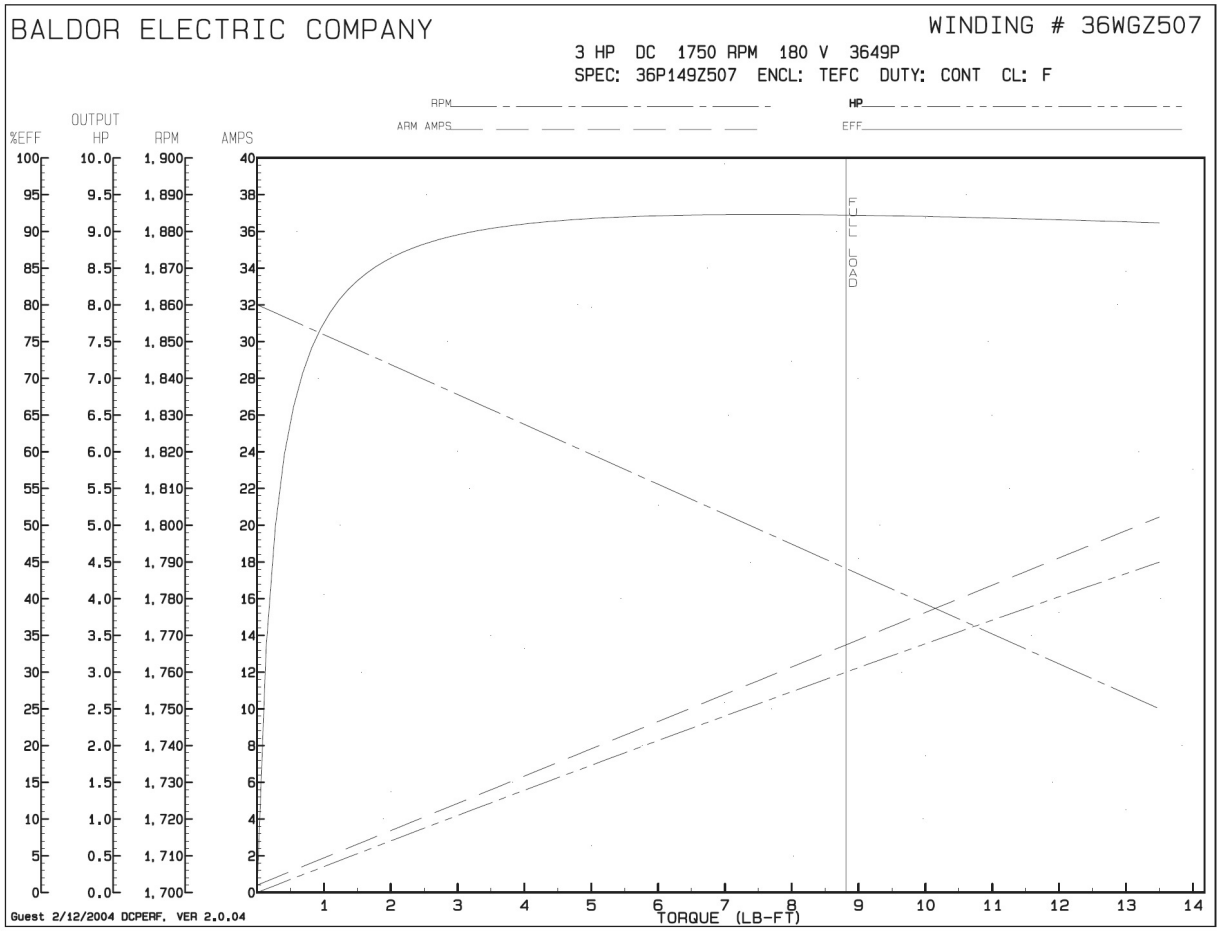

Figure - E.2 Performance curves for the DC motor/generator used in the turbine test rig

ANOTHER QUALITY PRODUCT FROM

Australian Valve & Filter Industries Pty Ltd
248 Wolseley Place, Thomastown, Vic 3074
Tel (03) 9460 5444 Fax (03) 9460 5510
Email avfi@avfi.com.au Web www.avfi.com.au

REMOVABLE ELEMENT WOLTMAN WATER METER

Working Condition

Water temperature:
- ⩽ 50°C for cold potable water meter
- ⩽ 90°C for hot water meter

Water pressure: ⩽ 16 Bar

Maximum Permissible Error

a) In the lower zone from Qmin inclusive up to but excluding Qt is ± 5%
b) In the upper zone from Qt inclusive up to and including Qs is:
Cold potable water meter ± 2%
Hot water meter ± 3%

Description

The OMEGA is a heavy duty water meter used to measure the volume of water passing through pipelines in, water supply, industrial and irrigation markets.
Due to its hermetically sealed register and magnetic drive transmission, this meter is well known for its long life as only its impeller and transmission shaft are in contact with the water.

Features

- High quality fusion bonded epoxy coated
- Available with reed switch pulse output
- Removable and interchangeable measuring element
- Meets or exceeds international standard ISO4064 class B
- Flow rate and resettable display available
- Low pressure loss even at high flow rates
- Magnetic transmission allows register to keep completely dry
- Flanges to Australian standard 2129

Note:

Standard pulse 50mm to 125mm 1 pulse per 100 litres. 150mm to 200mm 1 pulse per 1000 litres, 250mm to 500mm 1 pulse per 10,000 litres. Others available on request.
Hot water version to 90 deg C available on request.

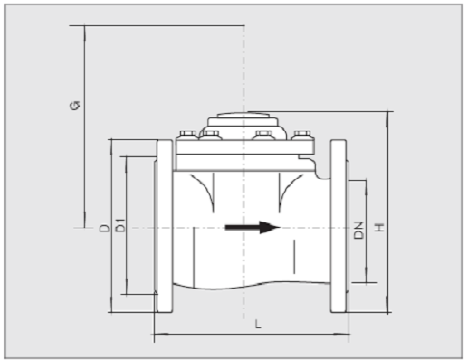

Main Technical Data

Size mm	Class	q_s Max. Flow	q_p Nominal Flow	q_t Transitional Flow	q_{min} Min. Flow	Min. Reading	Max. Reading
		m^3/h				m^3	
50	B	30	15	3.0	0.75	0.01	999999
65	B	50	25	5	0.75	0.01	999999
80	B	80	40	8.0	1.2	0.01	999999
100	B	120	60	12	1.8	0.01	999999
125	B	200	100	20	3.0	0.01	999999

Pressure Loss Curve

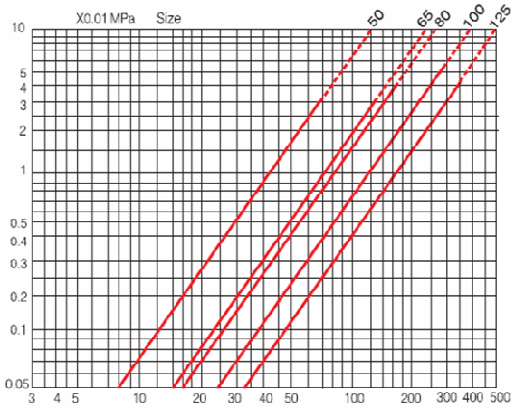

Dimensions and Weight

Size	Length L	Height H	G	Connecting Flange			Weight kg
	mm			D Outer Dia mm	D1 Bolt Circle Dia mm	Connecting Bolt (Pcs)	
50	310	256	400	150	114	4xM18	14
65	200	242	360	165	127	4xM18	13
80	225	275.8	400	185	146	4xM18	16
100	250	285.8	400	215	178	8xM18	18
125	250	275	360	255	210	8xM18	20

Figure - E.3 Data sheet and performance curves for water flow meter used in the turbine test rig

LOWARA

FHE - FHS - FHF SERIES
HYDRAULIC PERFORMANCE TABLE 50 Hz, 2 POLES

PUMP TYPE	POWER		Q = DELIVERY																												
			l/min	0	100	150	200	250	300	400	500	600	700	800	1000	1200	1400	1600	1800	2000	2300	2500	3000	3600	4500	5300	6200
			m³/h	0	6	9	12	15	18	24	30	36	42	48	60	72	84	96	108	120	138	150	180	216	270	318	372
	kW	HP	H = TOTAL HEAD METERS COLUMN OF WATER																												
32-125/07*	0,75	1	16,9	15,8	14,6	13	11	8,7																							
32-125/11*	1,1	1,5	21,9	20,7	19,6	18,1	16,3	14,2	9																						
32-160/15*	1,5	2	27,3	25,9	24,5	22,7	20,5	17,8	11																						
32-160/22*	2,2	3	34,7	33,3	32	30,2	28	25,3	18,8																						
32-200/30	3	4	44,2	41,5	39,8	37,7	35,2	32,2	24,6																						
32-200/40	4	5,5	54,4	52	50	47,7	45	41,9	34,6	26																					
32-250/55	5,5	7,5	79	74,7	71	67	62	55,6	37																						
32-250/75	7,5	10	99	95,3	92	88	83	76	58,3																						
40-125/11*	1,1	1,5	14,5				13,7	13	11,3	8,8	5,8																				
40-125/15*	1,5	2	18,1				17,2	16,7	15	12,7	9,6	6																			
40-125/22*	2,2	3	24,5				23,5	23	21	18,8	15,8	12,3	8,2																		
40-160/30	3	4	31,5				30	29,5	27,5	24,5	21,5	17,4																			
40-160/40	4	5,5	38				37	36	34	31,5	28,5	24,5	20																		
40-200/55	5,5	7,5	46,5				45	44	41,5	38,5	34,5	29,5																			
40-200/75	7,5	10	57				55	54	52	49	45,5	41	36																		
40-250/**	11	15	64				60	59	56	53	49	45	39																		
40-250/110	11	15	72				68	67	65	61	57	52	47																		
40-250/150	15	20	85				81	80	77	74	70	65	60																		
50-125/22*	2,2	3	17							16	15,1	14	12,8	9,8	6,2																
50-125/30	3	4	20							19,5	18,8	18	16,9	14,1	10,5																
50-125/40	4	5,5	24							23,5	23	22,5	21,5	19	15,8	11,8															
50-160/55	5,5	7,5	32							31,5	30,5	29,5	28	24,5	20,5	14,8															
50-160/75	7,5	10	40							39	38	37	36	33	29	24															
50-200/**	11	15	50,5							48	47	45	43	38,5	32,5	25,5															
50-200/110	11	15	58							55	54	53	50	46	40	33															
50-250/150	15	20	68							65	64	63	61	56	50	41															
50-250/185	18,5	25	77							74	73	72	70	66	60	52															
50-250/220	22	30	86							84	83	81	80	75	70	61	51														
65-125/40	4	5,5	19										17,5	16	14,5	13	11														
65-125/55	5,5	7,5	23										21,5	20,5	19	17,5	16	14													
65-125/75	7,5	10	27										26	25	24,5	23	22	20	18												
65-160/**	11	15	33										32	31	30	28	26	24	21,5												
65-160/110	11	15	36										35	34	33	31,5	30	28	25,5												
65-160/150	15	20	42										41,5	41	40	38,5	37	35	33	29,5											
65-200/150	15	20	45										46	45	43	41	39	36,5	34												
65-200/185	18,5	25	52										53	52	51	49	47	44,5	42												
65-200/220	22	30	59										60	59	58	56	54	52	49,5	44,5											
65-250/200	22	30	62										62	60	58	55,5	52	48,5	44	36,5											
65-250/300	30	40	76										75	74	73	70,5	67,5	64	61	54											
65-250/370	37	50	90										88,5	87	86	84	81	78	74,5	68,5											
80-160/110	11	15	27													27,5	27	26	24,5	22,5	21	16									
80-160/150	15	20	33													33	32	31	30	28	26	22									
80-160/185	18,5	25	39													38,5	37,5	36,5	35,5	34	32,5	28,5	22								
80-200/220	22	30	48													47,5	46,5	45	43,5	41	38,5	32,5									
80-200/300	30	40	60													60	59	58	57	54,5	52	47	39								
80-250/370	37	50	71													71	69	67	65	61	58	49									
80-250/450	45	61	80													81	80	78	76	72,5	70	62									
80-250/550	55	75	92													94	93	91	89,5	86,5	84	77	66								
100-160/220	22	30	33,3																31,8	31	30,3	28,2	25,5	20,3	15,3						
100-160/300	30	40	43																40,8	40	39,2	37,2	34,7	29,3	23,7	16					
100-200/300	30	40	49,5																47	45,8	44,7	41,5	37,3	29,3	20						
100-200/370	37	50	56																54,3	53,3	52,4	49,8	45,8	38	29,5						

* * / 92 - 9,2 kW - 12,5 HP - FHE / 110A - 11 kW - 15 HP - FHS-FHF

Figure - E.4 Performance data sheet for water pump used in the turbine test rig

LOWARA

FH 65 SERIES
OPERATING CHARACTERISTICS at 2900 rpm 50 Hz, 2 POLES

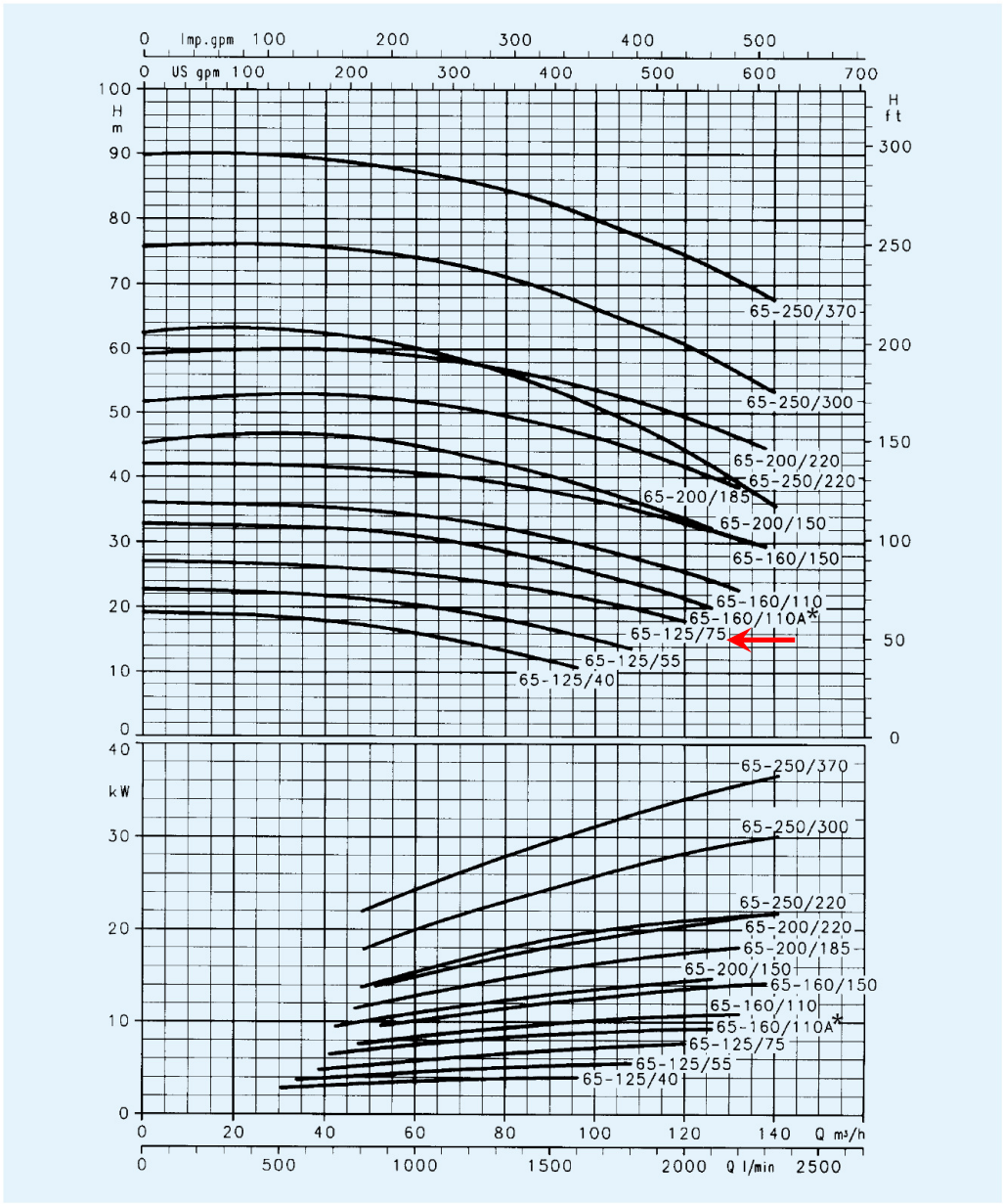

* /92 - 9,2 kW - 12,5 HP for version FHE - /110A - 11 kW - 15 HP for version FHS-FHF

Please verify with the price list the availability of model type FHE-FHS-FHF
These performances are valid for liquids with density ρ = 1.0 kg/dm³ and kinematic viscosity γ = 1 mm²/sec.

Figure - E.5 Performance curves for water pump used in the turbine test rig

LOWARA

DIMENSIONS AND WEIGHTS, FHE 2 POLES SERIES

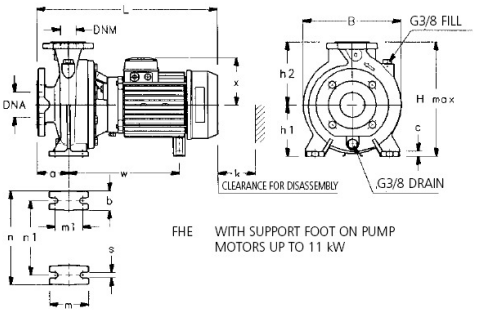

FHE WITH SUPPORT FOOT ON PUMP
MOTORS UP TO 11 kW

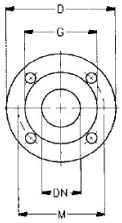

FLANGES

DN	D	M	G	HOLES N°	HOLES Ø	MAX. THICKNESS
32	140	100	78	4	18	18
40	150	110	88	4	18	18
50	165	125	102	4	18	20
65	185	145	122	4	18	20

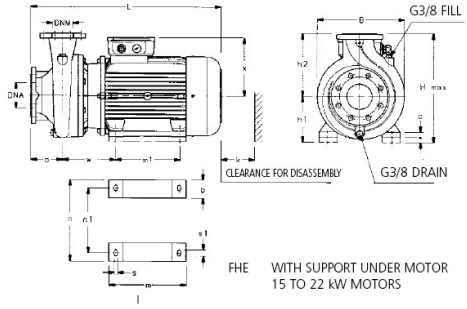

FHE WITH SUPPORT UNDER MOTOR
15 TO 22 kW MOTORS

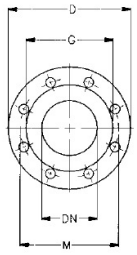

FLANGES

DN	D	M	G	HOLES N°	HOLES Ø	MAX. THICKNESS
80	200	160	138	8	18	22
100	220	180	158	8	18	22

PUMP TYPE	PUMP						SUPPORT										B	H max.	L	k	WEIGHT kg
	DNM	DNA	a	h2	w	x	b	c	c1	h1	m	m1	n	n1	s	s1					
FHE 32-125/07	32	50	80	140	235	129	50	12	–	112	100	70	190	140	14	–	233	252	443	86	27
FHE 32-125/11	32	50	80	140	235	129	50	12	–	112	100	70	190	140	14	–	233	252	443	86	28
FHE 32-160/15	32	50	80	160	235	129	50	12	–	132	100	70	240	190	14	–	235	292	443	86	31
FHE 32-160/22	32	50	80	160	235	129	50	12	–	132	100	70	240	190	14	–	235	292	443	86	34
FHE 32-200/30	32	50	80	180	283	121	50	12	–	160	100	70	240	190	14	–	285	340	461	86	43
FHE 32-200/40	32	50	80	180	290	133	50	12	–	160	100	70	240	190	14	–	285	340	487	86	49
FHE 40-125/11	40	65	80	140	235	129	50	12	–	112	100	70	210	160	14	–	233	252	443	88	30
FHE 40-125/15	40	65	80	140	235	129	50	12	–	112	100	70	210	160	14	–	233	252	443	88	31
FHE 40-125/22	40	65	80	140	235	129	50	12	–	112	100	70	210	160	14	–	233	252	443	88	33
FHE 40-160/30	40	65	80	160	283	121	50	12	–	132	100	70	240	190	14	–	250	292	461	88	36
FHE 40-160/40	40	65	80	160	290	133	50	12	–	132	100	70	240	190	14	–	250	292	487	88	42
FHE 40-200/55	40	65	100	180	311	150	50	12	–	160	100	70	265	212	14	–	285	340	553	88	59
FHE 40-200/75	40	65	100	180	311	150	50	12	–	160	100	70	265	212	14	–	285	340	553	88	64
FHE 40-250/92	40	65	100	225	278	191	65	14	–	180	125	95	320	250	14	–	335	405	604	107	91
FHE 40-250/110	40	65	100	225	278	191	65	14	–	180	125	95	320	250	14	–	335	405	604	107	99
FHE 40-250/150	40	65	100	225	208	232	50	22	20	180	260	210	318	254	13	23	335	412	688	107	123
FHE 50-125/22	50	65	100	160	235	129	50	12	–	132	100	70	240	190	14	–	255	292	463	92	37
FHE 50-125/30	50	65	100	160	285	121	50	12	–	132	100	70	240	190	14	–	255	292	481	92	39
FHE 50-125/40	50	65	100	160	292	133	50	12	–	132	100	70	240	190	14	–	255	292	507	92	45
FHE 50-160/55	50	65	100	180	313	150	50	12	–	160	100	70	265	212	14	–	285	340	553	92	68
FHE 50-160/75	50	65	100	180	313	150	50	12	–	160	100	70	265	212	14	–	285	340	553	92	72
FHE 50-200/92	50	65	100	200	280	191	50	12	–	160	100	70	265	212	14	–	305	360	604	92	81
FHE 50-200/110	50	65	100	200	280	191	50	12	–	160	100	70	265	212	14	–	305	360	604	92	86
FHE 50-250/150	50	65	100	225	208	232	50	22	20	180	260	210	318	254	13	23	340	412	688	107	123
FHE 50-250/185	50	65	100	225	208	232	50	22	20	180	304	254	318	254	13	23	340	412	732	107	135
FHE 50-250/220	50	65	100	225	208	232	50	22	20	180	304	254	318	254	13	23	340	412	732	107	149
FHE 65-125/40	65	80	100	180	292	133	65	14	–	160	125	95	280	212	14	–	285	340	507	105	64
FHE 65-125/55	65	80	100	180	313	150	65	14	–	160	125	95	280	212	14	–	285	340	553	105	72
FHE 65-125/75	65	80	100	180	313	150	65	14	–	160	125	95	280	212	14	–	285	340	553	105	76
FHE 65-160/92	65	80	100	200	278	191	65	14	–	160	125	95	280	212	14	–	331	360	604	112	95
FHE 65-160/110	65	80	100	200	278	191	65	14	–	160	125	95	280	212	14	–	331	360	604	112	103
FHE 65-160/150	65	80	100	200	208	232	50	22	–	160	260	210	318	254	13	23	331	392	688	112	127
FHE 65-200/150	65	80	100	225	208	232	50	22	20	180	260	210	318	254	13	23	335	412	688	112	127
FHE 65-200/185	65	80	100	225	208	232	50	22	20	180	304	254	318	254	13	23	335	412	732	112	139
FHE 65-200/220	65	80	100	225	208	232	50	22	20	180	304	254	318	254	13	23	335	412	732	112	153
FHE 65-250/220	65	80	100	250	208	232	50	22	40	200	304	254	318	254	13	23	332	450	732	112	159
FHE 80-160/110	80	100	125	225	278	191	65	14	–	180	125	95	320	250	14	–	332	405	629	129	109
FHE 80-160/150	80	100	125	225	208	232	50	22	20	180	260	210	318	254	13	23	332	412	713	129	133
FHE 80-160/185	80	100	125	225	208	232	50	22	20	180	304	254	318	254	13	23	332	412	757	129	145
FHE 80-200/220	80	100	125	250	208	232	50	22	20	180	304	254	318	254	13	23	332	430	757	129	159

Figure - E.6 Dimensions and weight of the water pump used in the turbine test rig

3631 00, 3632 00 & 3633 00
Pocket Tachometers

3631 00
50 (W) × 220 (H) × 30 (D) mm
210g

3632 00
50 (W) × 180 (H) × 30 (D) mm 210g excludes probe

3633 00
50 (W) × 240 (H) × 30 (D) mm
270g

New, pocket digital tachometers provide easy one-hand operation. The 3631 and 3632 operate from photo probe, and the 3633 uses a contact rubber tip or surface speed wheel. These pocket-sized tachometers are ideal tools for safe and simple measurement of rotational speed.

3631 & 3632
- **SAFE TO OPERATE WITH NO CONTACT WITH MACHINE**
- **CRISP TONE SOUNDS AND ◄ MARK DISPLAYED WHEN THE BEAM OF LIGHT IS ON TARGET**
- **ANALOG OUTPUT, AND PROBE LEAD FOR HARD TO GET AT LOCATIONS ... 3632**

3633
- **SURFACE SPEED WHEELS (OPTIONAL)**

COMMON TO ALL MODELS
- **UP TO 19,999 rpm IN TWO RANGES**
- **0.1 rpm RESOLUTION UP TO 1,999.9 rpm**
- **SAMPLE (MEAS)/HOLD MODE SELECTOR**
- **PALM-SIZE PACKAGE**

SPECIFICATIONS

Common to 3631 to 3633
Sample Rate: 0.5 to 1s (1s on 3633 20,000 rpm range)
Type of Display: 5-digit LCD
Maximum Reading: 19999
Overrange Indication: - - - - display
Low Battery Indication: B mark display
Mode Selector: MEAS, HOLD, or LOCK (continuous measurement)
Operating Temperature Range: 0 to 50°C (32 to 122°F)
Power Source: Single 9 V battery (IEC 6F22, Energieblock 9 V or equivalent), approx. 7 hours of continuous operation
Spares: B9691AL reflective tapes (10 sheets/unit)... for 3631 or 3632 (order q'ty; 1 unit), B9691 LA rubber tips (3 pcs./unit)... for 3633 (order q'ty; 1 unit)

Analog Output (3632 only)
Output Voltage: 0.1 V/1,000 rpm to 2.0 V/20,000 rpm
Accuracy: ±5% of range
Ripple Noise: Less than 0.1 Vp-p
Response Time: Within 1s (to reading within 90% of final value)
Output Impedance: Approx. 1 kΩ

Optional Accessories for 3633: Surface speed wheel... B9691 LD (m/min), B9691LP (mm/s)

Model	3631	3632	3633
Measurement System	Touchless, using a photo probe and reflective tape		Touch, using a contact rubber tip (standard) , or surface speed wheel (optional)
Measuring Ranges:	2,000rpm range .... 60.0 to 1,999.9rpm 20,000rpm range .... 60 to 19,999rpm		2,000rpm range .... 6.0 to 1,999.9rpm 20,000rpm range .... 1 to 19,999rpm
Resolution	0.1rpm on 2,000rpm range, 1rpm on 20,000rpm range		
Accuracy	2,000rpm range: ±0.1rpm for 60 to 400rpm ±0.2rpm for 400 to 1,200rpm ±0.3rpm for 1,200 to 1,999rpm 20,000rpm range: ±1rpm for 60 to 4,000rpm ±2rpm for 4,000 to 12,000rpm ±3rpm for 12,000 to 19,999rpm		2,000rpm range: ±0.1rpm for 6 to 160rpm ±0.2rpm for 160 to 1,000rpm ±0.3rpm for 1,000 to 1,800rpm 20,000rpm range: ±2rpm for 1 to 19,999rpm
Effective Measurement Distance between Photo Probe and Reflective Tape	*30 to 300mm	*5 to 50mm	—
	*At light projection angle of within ±30°, and reflective tape size of 10mm by 10mm		
Reflective Light Input	Buzzer sounds, and ◄ mark displayed		—
Standard Accessories	Soft case ... 1 pc, 9V battery ... (1 pc, built-in) , reflective tapes (10×90mm) ... 10 sheets, tripod adapter ... 1 pc		Soft case ... 1 pc, 9V battery ... (1 pc, built-in) , rubber tips (B9691LA) ... 3 pcs
	—	Probe fixture ... 1 set, analog output lead ...1 set	

Figure - E.7 Data sheet for the tachometer used in the turbine testing

V-RING

General

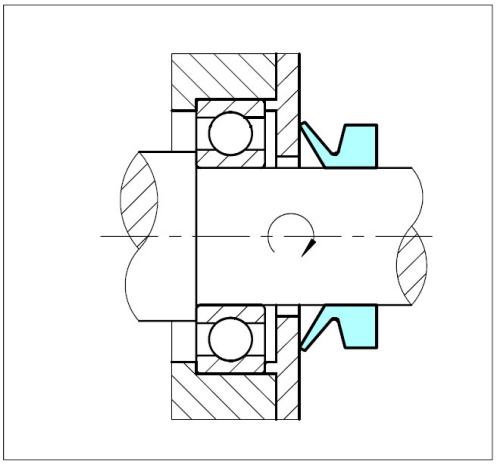

Figure 53 Method of operation of the V-Ring

The V-RING is a unique all-rubber seal for rotary shafts. Developed in the 1960's by FORSHEDA AB, it has been used successfully by OEMs and on the replacement market world wide in a broad range of applications.

The V-Ring is the perfect seal to prevent the ingress of dirt, dust, water or combinations of these media while positively retaining grease. With its unique design and performance the V-Ring can be used with a wide range of bearing types. It can also be used as a secondary seal to protect primary seals that do not perform well in hostile environments.

Description and advantages

The V-Ring is normally stretched and mounted directly on the shaft, where it is held in position by the inherent tension of the rubber body. It rotates with the shaft and seals axially against a stationary counterface, perpendicular to the shaft. The counterface can be the side wall of a bearing or a washer, stamping, bearing housing, or even the metal case of an oil seal. The sealing lip is flexible and applies only a relatively light contact pressure against the counter-face and yet is still sufficient to maintain the sealing function. The low contact pressure (that varies with the fitted width) allows the seal to run dry in many applications.

Due to influence of the centrifugal force, the contact pressure of the lip decreases with increased speed. This means that frictional losses and heat are kept to a minimum, resulting in excellent wear characteristics and extended seal life. Once breakaway friction is overcome, the friction reduce steadily until around the 10 -15 m/s range, when it reduces quite quickly. In the 15 - 20 m/s range the friction reduces to zero. The V-Ring then serves as a clearance seal and deflector. The power loss due to seal friction develops as shown in Fig. 54.

The flexible lip and hinge allow the V-Ring to function even in the presence of a certain amount of run-out, eccentricity and shaft misalignment. Contact our local B+S company for advice on these and other application issues.

V-Rings are made entirely of rubber without fabric or sheet metal reinforcement. They are, therefore, particularly easy to install. V-Rings can be stretched and, depending on size, installed over flanges, pulleys and bearing housings without costly dismantling. For larger sizes they can even be supplied as cut rings and joined by vulcanisation on site.

Design

V-Rings are available in seven standard cross-sections to meet various space and application requirements.

The cross-sections of profiles A and S increase with the shaft diameter, whilst the other types have the same cross-section for the whole diameter range.

Profile A is the most common and available for shaft diameters from 2.7 to 2020 mm, inclusive.

Profile S is wide and tapered, which provides a very firm hold on the shaft. The rings are available for shaft diameters from 4.5 to 210 mm.

Profiles L and LX have narrow axial cross sections making them suitable for compact arrangements and are often used in combination with labyrinth seals. Available for shaft diameters from 105 (135 for LX) to 2025 mm.

Profiles RME, RM and AX are heavy duty V-Rings that are designed primarily for large high speed bearing arrangements, I. E. rolling mill and papermaking machine applications. Additionally they can be used as secondary seals for heavy duty applications where the primary seal has to be protected against water and or particulate contamination. The RME, RM and AX types can be axially and radially located on the shaft with the especially designed clamping bands (see page 138). Available for shaft diameters from 300mm and up.

Larger V-Ring sizes are available as spliced seals. For more details please contact your local B+S company.

Figure - E.8 General information of Busak+Shamban V-ring lip seal

Temperature resistance

Exposure to higher temperatures accelerate the ageing of rubber, the elongation decreases, the compression set increases, and finally the material becomes hard and brittle. Cracks at the sealing edge are a typical indication that the seal has been exposed to excessively high temperature. The ageing of the rubber has an appreciable negative influence on the useful life of the seal.

The temperature limits for the principal materials are illustrated in Figure 55. They should only be regarded as approximate, since the media and time of exposure also affect the materials.

The temperature ranges within the shaded areas indicate temperatures that can be allowed for only certain periods of time. The higher the temperature, the shorter the service life. If the maximum temperature is exceeded, the elastomer may suffer permanent set or damage. Special elastomers are available for use in cold temperatures. If the elastomer is subjected to temperatures lower than the recommended values it will become hard and brittle, however it will regain its properties as soon as the temperature rises again.

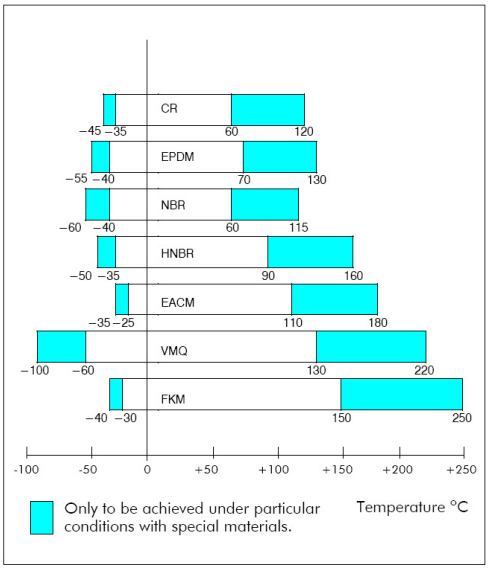

Figure 55 Temperature recommendations for V-Rings

Oil and solvent resistance

Since the V-Ring is used primarily for sealing grease lubricated bearings exposed to water splash, dirt, dust, scale etc. the normal choice of compound is Nitrile Rubber (N6T50) 510. However innumerable types of oil are available on the market and each of these has different effect on rubber. In addition, a given type of oil from different manufacturers may have different influence.

It is the additives in the oil that may affect the rubber. Especially so for hypoid oils, that contain sulphur. Since sulphur is used as the vulcanising agent for nitrile rubber it will initiate a secondary curing at temperatures above +80°C. As a result of that, nitrile rubber will become hard and brittle. Hydrogenated Nitrile and Fluorinated rubbers, which are not vulcanised with sulphur, may therefore be considered for use with this type of oil. Oxidised oils represent another example illustrating the difficulty of tabulating the oil resistance of rubber materials. These oils are oxidised during operation and their properties will therefore change substantially. Such oils break down silicone rubber.Solvents could generally cause deterioration or swelling of the rubber however mixtures of different solvents may cause considerably more damage than a single solvent. An example of this is mixing methanol and hydrocarbons.

For further information on oil and solvent resistance we recommend you to be in contact with your local B+S company.

Application instructions

The V-RING is normally fully exposed to the medium to be sealed. The requirements on the shaft and the counterface are mainly dependent on the medium and the peripheral speed.

Shaft design

The V-Ring is in most cases fitted on a rotating shaft. The requirements regarding diameter tolerances and surface roughness of the shaft are fairly moderate. As the V-Ring is an all-rubber seal it can be stretched to a varying degree and be used for a wide range of shaft diameters.

In applications where low power loss and long lifetime are important it is recommended that the V-Ring size is selected, so that the shaft diameter falls between the minimum and nominal values within the recommended range. This is because the contact pressure of the sealing lip increases with the shaft diameter, due to the stretch of the V-Ring. At a higher stretch, a harder contact pressure is generated, causing an accelerated wear of the sealing lip. In order to prevent the V-Ring from sliding along the shaft, and to ensure the correct installation width, it is

Figure - E.9 Operating temperature and sealing fluid information for Busak+Shamban V-ring lip seal

always recommended to arrange an axial support, especially for small cross-section profiles and larger shaft sizes, for example V-Ring type A, L and LX.

The surface roughness of the shaft should in general not exceed Ra 6.3 µm. For sealing fluids and fine particles, a maximum of Ra 3.2 µm is recommended. Sharp edges and burrs, which can damage the V-Ring must be avoided.

Counter-face design

The condition of the counter-face has a great influence on the sealing function. The medium to be sealed and the peripheral speed of the shaft determine the requirements regarding surface roughness and material of the counter-face. It is important that it is smooth and flat without any sharp edges. To achieve the full effect of the flinger action, the V-Ring should always be designed in a relatively open space. Equally important is to keep the gap between the shaft and the counter-face as small as possible, in order to prevent entry of the V-Ring lip during the installation. Recommended application dimensions are given in the dimension tables.

Material and material hardness

Cold rolled steel sheet, stainless steel or zinc plated sheet are excellent materials for the counter-face. However, the choice of material is highly dependent on the medium to be sealed.

For normal running conditions, conventional mild steel with a hardness of min. 125 HB is sufficient. For sealing against grease, oil and dry particles no further surface treatment is required. With an increase in speed and the presence of abrasive particles the hardness of the counter-face must also be increased.

The following materials are normally used :

Material	Hardness HB	Medium
Mild Steel	125-150	Water splash, sand, dust
Grey Cast Iron	190-270	Water splash, sand, dust
Sinter Bronze	100-160	Water, dust
Stainless Steel (Cr/Ni 18-8, C 0.1%)	150-200	Water
Stainless Steel (Cr/Ni 18-8, C 0.15%) Work-hardened	350	Water and abrasive particles
Acid Proof Steel	180-200	Chemicals
Tungsten Carbide	350-500	Water and scale
Forged Steel	200-255	Water and scale
Die-cast Aluminium	90-160	Water splash

Surface treatment

When the counter-face is exposed to water or other corrosive media, it must be protected accordingly.

Mild steel surfaces should either be zinc-plated and chromated, chromium plated, treated with an anticorrosion spray, or painted. The choice of treatment will depend on the overall running conditions.

Where the seal is immersed in water, stainless steel is recommended. However, due to the poor thermal conductivity stainless steel should not be used in dry running conditions unless the speed is slow (<1 m/s).

Surface finish

The rate of abrasion of the V-Ring is influenced by a number of factors, one of which is the surface finish of the counter-face. The choice of surface finish will depend on the medium to be sealed and the shaft speed as well. It is not only the surface finish value as such that is important, but also the surface character. For turned surfaces, it is recommended to buff the surface with fine emery cloth to remove any sharp peaks arising from the turning operation.

Surfaces with too fine finish, e.g. certain cold rolled steel surfaces, may cause a suction effect between the V-Ring lip and the counter-face resulting in noise problems and uneven running (so-called stick-slip effect).

The counterface surface must be free from scratch marks and other surface damages within the sealing area. This is important when sealing fluids and fine particles are present.

Guide to recommended surface finish

Surface finish µm Ra	Speed m/s	Medium
0.4-0.8	> 10	Oil, water, scale, fibre
0.8-1.6	5-10	Oil splash, grease, water splash
1.6-2.0	1-5	Grease, dust, water splash, scale
2.0-2.5	<1	Grease, dust

The surface finish should not be lower than Ra 0.05 µm.

Flatness

The flatness of the counter-face is of importance, especially at higher shaft speeds.

The maximum permissible flatness deviation is normally defined as 0.4 mm per 100 mm.

Figure - E.10 Information of counter surface material and finish for V-ring lip seal

Installation

Axial support

When used to retain oil and grease, an axial support for the V-Ring is always required. For applications with a lower degree of stretch than recommended in the dimension tables (e.g. for ease of assembly) or with a shaft speed exceeding 6-8 m/s (depending on the rubber compound selected) an axial support is also necessary.

An axial support can ensure that the correct installation width relative to the counter-face is maintained for blind assemblies.

The V-Ring must always be supported over its entire base. The axial support should be designed in accordance with Figure 56. The dimensions A, c, d_1, d_3 and B_1 are shown in the dimension tables.

Calculation of the axial support diameter d_5 is as follows;

V-Ring type	Diameter d5
A, S	d_1 + 0.5 x c
L, LX	d_1 + 3 mm
RM, RME	d_1 + 10 mm
AX	d_1 + 9 mm

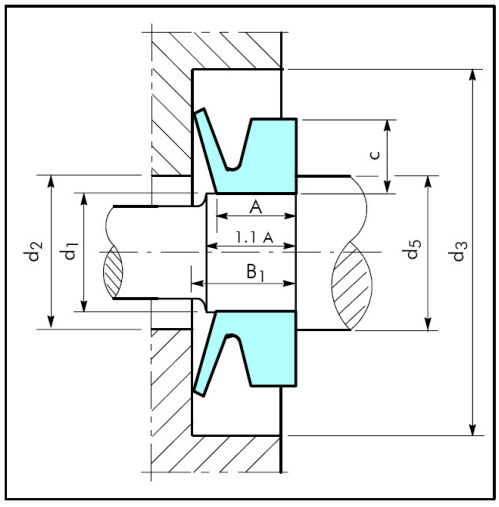

Figure 56 Axial support

Radial retention

When the V-Ring is fitted on the shaft, the body of the V-Ring is subject to a centrifugal force and tends to move or even lift off from the shaft at a certain speed.

At shaft speeds over 10-12 m/s, depending on the V-Ring material, the V-Ring in general requires radial retention.

The speed when radial retention is required is also dependent on the degree of stretch of the V-Ring. V-Rings larger than 2000 mm should always be fitted with radial retention, irrespective of the operating speed.

The radial retention can be designed as a recess, in which the V-Ring body fits, or consist of a number of separate clamping segments. Please contact your local B+S company for further guidance.

The clamping band type A or RM are other useful alternatives. See page 138.

Stationary assembly

In cases where the peripheral speed of the shaft exceeds 10-12 m/s an alternative method to radial clamping is to mount the V-Ring on a stationary component in the unit. The contact pressure of the lip will remain constant, as there will be no centrifugal force acting upon the lip.

In comparison to a rotating V-Ring, friction and power loss will be higher resulting in somewhat shorter service life. In order to compensate for this the following steps should be taken:

Counter-face surface finish:
machine to max. 0.8 µm Ra

V-Ring stretch:
maximum 4-6%

Axial interference:
keep to the minimum requirements for compensation of the axial movement within the assembly.

At higher peripheral speed adequate lubrication and heat transfer from the counter-face are required.

Torque

The torque, and consequently the power loss due to the friction of the seal, is often of such a magnitude that it should be taken into consideration when deciding seal type. This applies particularly in the case of small electrical motors, conveyor rollers or any unit where low friction is an important requirement.

Figure - E.11 Installation guide for V-ring lip seal

The power losses are influenced by many factors such as the seal design and compound, surface finish of the counter-face, fitted width and stretch, speed, medium, lubricant, temperature etc.

For this reason it is difficult to give exact torque values for all running conditions.

Generally speaking, the power losses resulting from a V-Ring are always lower than a corresponding radial oil seal.

Grease lubrication gives higher power losses than oil lubrication or dry running.

By applying a suitable low friction dry film lubricant on the counter-face surface the friction and the heat generated can be reduced.

An increase of the fitted width of the V-Ring, giving a reduced lip pressure, will also lower the friction. However, the total axial movement in the assembly must be considered in order not to exceed the tolerances shown in the dimension tables.

Whenever detailed information about power losses is required, consult your local B+S company.

Installation guidelines

When the V-Ring is used as a grease seal/contaminant excluder, the V-Ring is normally mounted on the outside of a bearing housing, with or without, axial support.

General rules:

1. The V-Ring, the counter-face and the shaft should be clean.
2. The shaft should preferably be dry and free from grease or oil, particularly when the V-Ring is mounted without axial support.
3. The lip of the V-Ring should be lubricated with a thin film of grease or silicone oil.
4. In cases when friction must be reduced to a minimum, coat the counter-face with a low friction agent, and do not apply grease to the lip.
5. Ensure that the V-Ring is mounted with a uniform stretch around the shaft.

When the V-Ring is mounted on the shaft the outer diameter of the lip is reduced. Unless the stretch is uniform this reduction will vary around the periphery. This may lead to partial entry of the lip in the bore of the counter-face when the seal is pushed into position.

In the case of large diameter seals a uniform stretch can be achieved by inserting a blunt screwdriver or a piece of string under the V-Ring body and running it around the shaft twice. Take care not to damage seal or shaft.

The most convenient method of assembling large diameter V-Ring's, to ensure uniform stretch, is to mark off the body of the V-Ring and the shaft or seating with six equidistant marks. The marks should then be matched together when the V-Ring is fitted in position.

For more detailed installation instructions, contact your local B+S company.

Clamping band

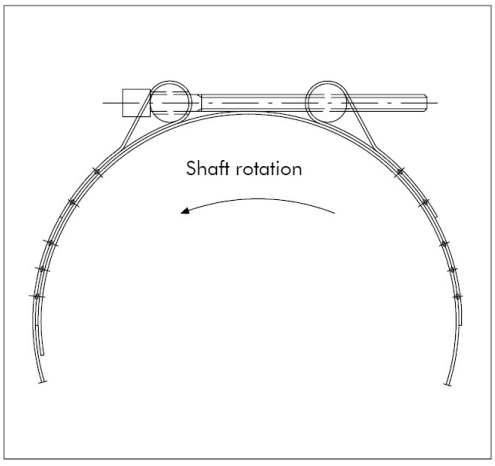

Figure 57 Clamping band RM

FORSHEDA Clamping Band RM

For clamping large diameter V-Rings of the RM and RME types, the FORSHEDA Clamping Band RM is recommended.

Together with Clamping Band RM a special series of "low stretch" V-Rings can be used for shaft diameters larger than 1500 mm. This will reduce torque and facilitate the fitting of the V-Ring.

When ordering the Clamping Band RM, simply state the shaft diameter for which the clamping band is intended. Each clamping band comprises a set of standard lengths measuring 1000 mm and 1500 mm depending on the size, standard attachments and, if necessary, an adjustable length and two set of rivets. When the parts are assembled, the clamping band will fit the specific V-Ring.

Figure - E.12 Installation guide and power loss factors for V-ring lip seal

Dimension table - V-Ring type A

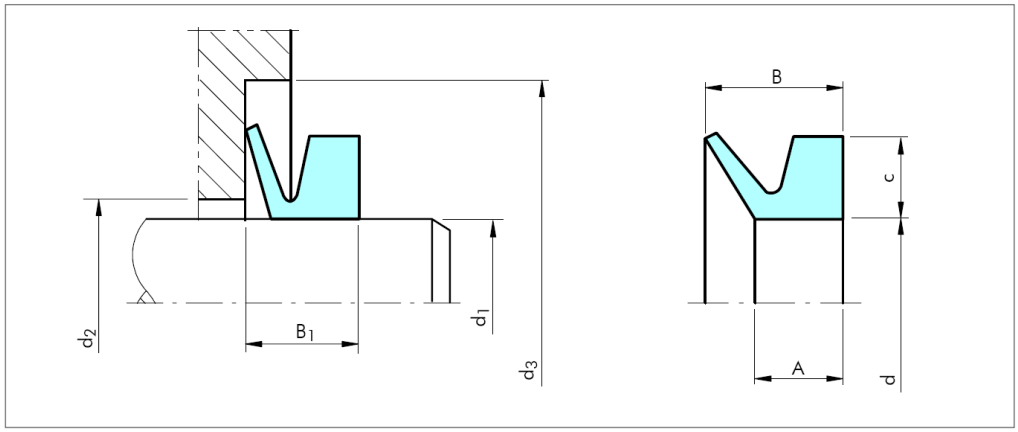

Figure 59 Installation drawing

When the shaft diameter d_1 is on the boundary between two sizes of V-Ring, select the larger V-Ring.
All dimensions in mm.

Table XL Profile dimensions - assembly dimensions

For shaft diameter d_1	Inside diameter d	Height of cross-section c	Dimension A	Free width B	Maximum d_2	Minimum d_3	Fitted width B_1	V-Ring FORSHEDA Ref.	Part number
2.7 - 3.5	2.5	1.5	2.1	3.0	d_1 + 1	d_1 + 4	2.5 ±0.3	V-3A	TWVA00030
3.5 - 4.5	3.2	2	2.4	3.7	d_1 + 1	d_1 + 6	3.0 ±0.4	V-4A	TWVA00040
4.5 - 5.5	4	2	2.4	3.7	d_1 + 1	d_1 + 6	3.0 ±0.4	V-5A	TWVA00050
5.5 - 6.5	5	2	2.4	3.7	d_1 + 1	d_1 + 6	3.0 ±0.4	V-6A	TWVA00060
6.5 - 8.0	6	2	2.4	3.7	d_1 + 1	d_1 + 6	3.0 ±0.4	V-7A	TWVA00070
8.0 - 9.5	7	2	2.4	3.7	d_1 + 1	d_1 + 6	3.0 ±0.4	V-8A	TWVA00080
9.5 - 11.5	9	3	3.4	5.5	d_1 + 1	d_1 + 9	4.5 ±0.6	V-10A	TWVA00100
11.5 - 12.5	10.5	3	3.4	5.5	d_1 + 1	d_1 + 9	4.5 ±0.6	V-12A	TWVA00120
12.5 - 13.5	11.7	3	3.4	5.5	d_1 + 1	d_1 + 9	4.5 ±0.6	V-13A	TWVA00130
13.5 - 15.5	12.5	3	3.4	5.5	d_1 + 1	d_1 + 9	4.5 ±0.6	V-14A	TWVA00140
15.5 - 17	14	3	3.4	5.5	d_1 + 1	d_1 + 9	4.5 ±0.6	V-16A	TWVA00160
17.5 - 19	16	3	3.4	5.5	d_1 + 1	d_1 + 9	4.5 ±0.6	V-18A	TWVA00180
19 - 21	18	4	4.7	7.5	d_1 + 2	d_1 + 12	6.0 ±0.8	V-20A	TWVA00200
21 - 24	20	4	4.7	7.5	d_1 + 2	d_1 + 12	6.0 ±0.8	V-22A	TWVA00220
24 - 27	22	4	4.7	7.5	d_1 + 2	d_1 + 12	6.0 ±0.8	V-25A	TWVA00250
27 - 29	25	4	4.7	7.5	d_1 + 2	d_1 + 12	6.0 ±0.8	V-28A	TWVA00280
29 - 31	27	4	4.7	7.5	d_1 + 2	d_1 + 12	6.0 ±0.8	V-30A	TWVA00300
31 - 33	29	4	4.7	7.5	d_1 + 2	d_1 + 12	6.0 ±0.8	V-32A	TWVA00320
33 - 36	31	4	4.7	7.5	d_1 + 2	d_1 + 12	6.0 ±0.8	V-35A	TWVA00350
36 - 38	34	4	4.7	7.5	d_1 + 2	d_1 + 12	6.0 ±0.8	V-38A	TWVA00380
38 - 43	36	5	5.5	9.0	d_1 + 2	d_1 + 15	7.0 ±1.0	V-40A	TWVA00400
43 - 48	40	5	5.5	9.0	d_1 + 2	d_1 + 15	7.0 ±1.0	V-45A	TWVA00450
48 - 53	45	5	5.5	9.0	d_1 + 2	d_1 + 15	7.0 ±1.0	V-50A	TWVA00500
53 - 58	49	5	5.5	9.0	d_1 + 2	d_1 + 15	7.0 ±1.0	V-55A	TWVA00550
58 - 63	54	5	5.5	9.0	d_1 + 2	d_1 + 15	7.0 ±1.0	V-60A	TWVA00600
63 - 68	58	5	5.5	9.0	d_1 + 2	d_1 + 15	7.0 ±1.0	V-65A	TWVA00650

Figure - E.13 V-ring seal dimensions and part numbers

For shaft diameter d_1	Inside diam-eter d	Height of cross-section c	Dimension A	Free width B	Maximum d_2	Minimum d_3	Fitted width B_1	V-Ring FORSHEDA Ref.	Part number
68 - 73	63	6	6.8	11.0	d_1 + 3	d_1 + 18	9.0 ±1.2	V-70A	TWVA00700
73 - 78	67	6	6.8	11.0	d_1 + 3	d_1 + 18	9.0 ±1.2	V-75A	TWVA00750
78 - 83	72	6	6.8	11.0	d_1 + 3	d_1 + 18	9.0 ±1.2	V-80A	TWVA00800
83 - 88	76	6	6.8	11.0	d_1 + 3	d_1 + 18	9.0 ±1.2	V-85A	TWVA00850
88 - 93	81	6	6.8	11.0	d_1 + 3	d_1 + 18	9.0 ±1.2	V-90A	TWVA00900
93 - 98	85	6	6.8	11.0	d_1 + 3	d_1 + 18	9.0 ±1.2	V-95A	TWVA00950
98 - 105	90	6	6.8	11.0	d_1 + 3	d_1 + 18	9.0 ±1.2	V-100A	TWVA01000
105 - 115	99	7	7.9	12.8	d_1 + 4	d_1 + 21	10.5 ±1.5	V-110A	TWVA01100
115 - 125	108	7	7.9	12.8	d_1 + 4	d_1 + 21	10.5 ±1.5	V-120A	TWVA01200
125 - 135	117	7	7.9	12.8	d_1 + 4	d_1 + 21	10.5 ±1.5	V-130A	TWVA01300
135 - 145	126	7	7.9	12.8	d_1 + 4	d_1 + 21	10.5 ±1.5	V-140A	TWVA01400
145 - 155	135	7	7.9	12.8	d_1 + 4	d_1 + 21	10.5 ±1.5	V-150A	TWVA01500
155 - 165	144	8	9.0	14.5	d_1 + 4	d_1 + 24	12.0 ±1.8	V-160A	TWVA01600
165 - 175	153	8	9.0	14.5	d_1 + 4	d_1 + 24	12.0 ±1.8	V-170A	TWVA01700
175 - 185	162	8	9.0	14.5	d_1 + 4	d_1 + 24	12.0 ±1.8	V-180A	TWVA01800
185 - 195	171	8	9.0	14.5	d_1 + 4	d_1 + 24	12.0 ±1.8	V-190A	TWVA01900
195 - 210	180	8	9.0	14.5	d_1 + 4	d_1 + 24	12.0 ±1.8	V-199A	TWVA01990
190 - 210	180	15	14.3	25.0	d_1 + 10	d_1 + 45	20.0 ±4.0	V-200A	TWVA02000
210 - 235	198	15	14.3	25.0	d_1 + 10	d_1 + 45	20.0 ±4.0	V-220A	TWVA02200
235 - 265	225	15	14.3	25.0	d_1 + 10	d_1 + 45	20.0 ±4.0	V-250A	TWVA02500
265 - 290	247	15	14.3	25.0	d_1 + 10	d_1 + 45	20.0 ±4.0	V-275A	TWVA02750
290 - 310	270	15	14.3	25.0	d_1 + 10	d_1 + 45	20.0 ±4.0	V-300A	TWVA03000
310 - 335	292	15	14.3	25.0	d_1 + 10	d_1 + 45	20.0 ±4.0	V-325A	TWVA03250
335 - 365	315	15	14.3	25.0	d_1 + 10	d_1 + 45	20.0 ±4.0	V-350A	TWVA03500
365 - 390	337	15	14.3	25.0	d_1 + 10	d_1 + 45	20.0 ±4.0	V-375A	TWVA03750
390 - 430	360	15	14.3	25.0	d_1 + 10	d_1 + 45	20.0 ±4.0	V-400A	TWVA04000
430 - 480	405	15	14.3	25.0	d_1 + 10	d_1 + 45	20.0 ±4.0	V-450A	TWVA04500
480 - 530	450	15	14.3	25.0	d_1 + 10	d_1 + 45	20.0 ±4.0	V-500A	TWVA05000
530 - 580	495	15	14.3	25.0	d_1 + 10	d_1 + 45	20.0 ±4.0	V-550A	TWVA05500
580 - 630	540	15	14.3	25.0	d_1 + 10	d_1 + 45	20.0 ±4.0	V-600A	TWVA06000
630 - 665	600	15	14.3	25.0	d_1 + 10	d_1 + 45	20.0 ±4.0	V-650A	TWVA06500
665 - 705	630	15	14.3	25.0	d_1 + 10	d_1 + 45	20.0 ±4.0	V-700A	TWVA07000
705 - 745	670	15	14.3	25.0	d_1 + 10	d_1 + 45	20.0 ±4.0	V-725A	TWVA07250
745 - 785	705	15	14.3	25.0	d_1 + 10	d_1 + 45	20.0 ±4.0	V-750A	TWVA07500
785 - 830	745	15	14.3	25.0	d_1 + 10	d_1 + 45	20.0 ±4.0	V-800A	TWVA08000
830 - 875	785	15	14.3	25.0	d_1 + 10	d_1 + 45	20.0 ±4.0	V-850A	TWVA08500
875 - 920	825	15	14.3	25.0	d_1 + 10	d_1 + 45	20.0 ±4.0	V-900A	TWVA09000
920 - 965	865	15	14.3	25.0	d_1 + 10	d_1 + 45	20.0 ±4.0	V-950A	TWVA09500
965 - 1015	910	15	14.3	25.0	d_1 + 10	d_1 + 45	20.0 ±4.0	V-1000A	TWVAX1000
1015 - 1065	955	15	14.3	25.0	d_1 + 10	d_1 + 45	20.0 ±4.0	V-1050A	TWVAX1050
1065 - 1115	1000	15	14.3	25.0	d_1 + 10	d_1 + 45	20.0 ±4.0	V-1100A	TWVAW1100
1115 - 1165	1045	15	14.3	25.0	d_1 + 10	d_1 + 45	20.0 ±4.0	V-1150A	TWVAW1150
1165 - 1215	1090	15	14.3	25.0	d_1 + 10	d_1 + 45	20.0 ±4.0	V-1200A	TWVAW1200
1215 - 1270	1135	15	14.3	25.0	d_1 + 10	d_1 + 45	20.0 ±4.0	V-1250A	TWVAW1250
1270 - 1320	1180	15	14.3	25.0	d_1 + 10	d_1 + 45	20.0 ±4.0	V-1300A	TWVAW1300
1320 - 1370	1225	15	14.3	25.0	d_1 + 10	d_1 + 45	20.0 ±4.0	V-1350A	TWVAW1350
1370 - 1420	1270	15	14.3	25.0	d_1 + 10	d_1 + 45	20.0 ±4.0	V-1400A	TWVAW1400
1420 - 1470	1315	15	14.3	25.0	d_1 + 10	d_1 + 45	20.0 ±4.0	V-1450A	TWVAW1450
1470 - 1520	1360	15	14.3	25.0	d_1 + 10	d_1 + 45	20.0 ±4.0	V-1500A	TWVAW1500
1520 - 1570	1405	15	14.3	25.0	d_1 + 10	d_1 + 45	20.0 ±4.0	V-1550A	TWVAW1550
1570 - 1620	1450	15	14.3	25.0	d_1 + 10	d_1 + 45	20.0 ±4.0	V-1600A	TWVAW1600
1620 - 1670	1495	15	14.3	25.0	d_1 + 10	d_1 + 45	20.0 ±4.0	V-1650A	TWVAW1650
1670 - 1720	1540	15	14.3	25.0	d_1 + 10	d_1 + 45	20.0 ±4.0	V-1700A	TWVAW1700
1720 - 1770	1585	15	14.3	25.0	d_1 + 10	d_1 + 45	20.0 ±4.0	V-1750A	TWVAW1750
1770 - 1820	1630	15	14.3	25.0	d_1 + 10	d_1 + 45	20.0 ±4.0	V-1800A	TWVAW1800
1820 - 1870	1675	15	14.3	25.0	d_1 + 10	d_1 + 45	20.0 ±4.0	V-1850A	TWVAW1850
1870 - 1920	1720	15	14.3	25.0	d_1 + 10	d_1 + 45	20.0 ±4.0	V-1900A	TWVAW1900
1920 - 1970	1765	15	14.3	25.0	d_1 + 10	d_1 + 45	20.0 ±4.0	V-1950A	TWVAW1950
1970 - 2020	1810	15	14.3	25.0	d_1 + 10	d_1 + 45	20.0 ±4.0	V-2000A	TWVAW2000

Figure - E.14 V-ring seal dimensions and part numbers

Appendix F

F.1 Theoratical analysis of turbine jet-interference

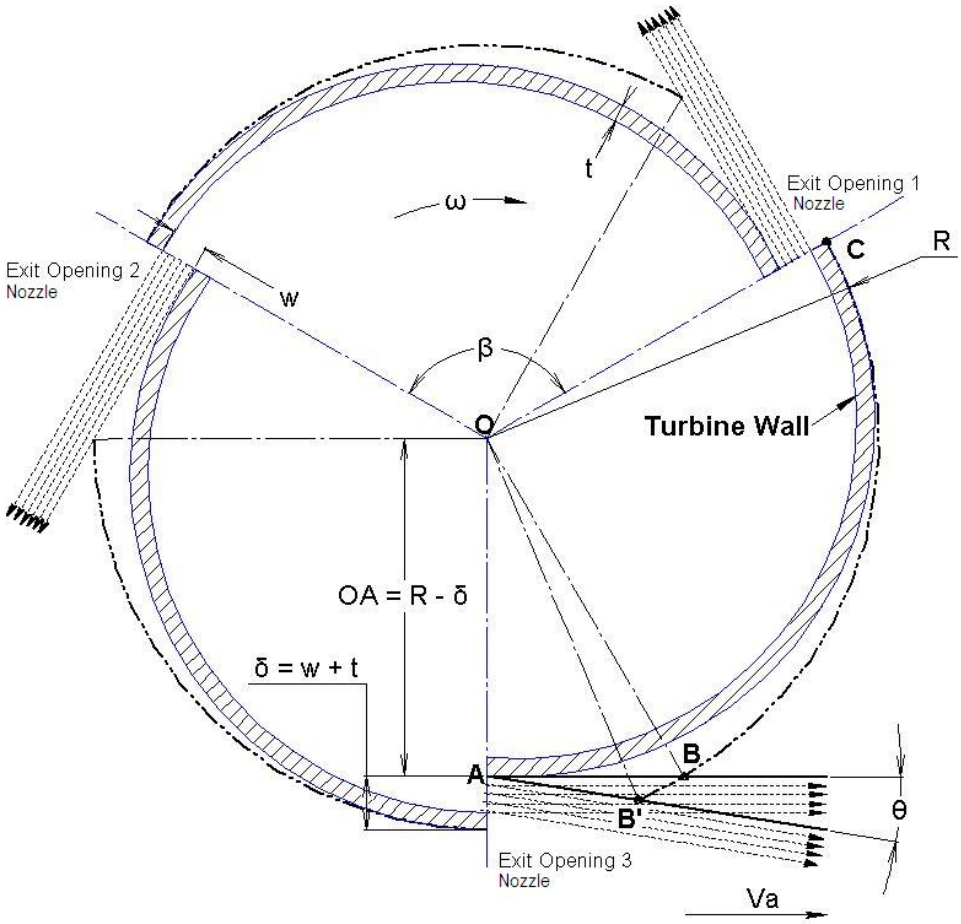

Figure - F.1 Interference of rotor and jet

$\delta = w + t$

When $t_{CB'} = t_{AB'}$

$$\frac{\hat{COB'}}{\omega} = \frac{AB'}{V_a}$$

$$\frac{AB'}{\sin \angle AOB'} = \frac{OB'}{\sin \angle OAB'}$$

$$AB' = \frac{OB'}{\sin \angle OAB'} \times \sin \angle AOB'$$

Where, $OB' = OB = OC = R$

$$\angle OAB' = \frac{\pi}{2} + \theta$$

$$\frac{OA}{\sin \angle AB'O} = \frac{OB'}{\sin \angle OAB'}$$

$$\sin \angle AB'O = OA \times \frac{\sin \angle OAB'}{OB'}$$

$$\angle AB'O = ArcSin\left(OA \times \frac{\sin \angle OAB'}{OB'} \right)$$

$$\angle AB'O = ArcSin\left[(R - \delta) \times \frac{\sin\left(\frac{\pi}{2} + \theta \right)}{R} \right]$$

$$\angle AOB' = \pi - \angle OAB' - \angle AB'O$$

$$\angle AOB' = \pi - \left(\frac{\pi}{2} + \theta \right) - ArcSin\left[(R - \delta) \times \frac{\sin\left(\frac{\pi}{2} + \theta \right)}{R} \right]$$

$$\angle AOB' = \frac{\pi}{2} - \theta - ArcSin\left[(R - \delta) \times \frac{\sin\left(\frac{\pi}{2} + \theta \right)}{R} \right]$$

$$\angle COB' = \beta - \angle AOB'$$

$$\angle COB' = \beta - \frac{\pi}{2} + \theta + ArcSin\left[(R - \delta) \times \frac{\sin\left(\frac{\pi}{2} + \theta \right)}{R} \right]$$

$$AB' = \frac{OB'}{\sin \angle OAB'} \times \sin \angle AOB'$$

$$AB' = \frac{R}{\sin\left(\frac{\pi}{2}+\theta\right)} \times \sin\left(\frac{\pi}{2} - \theta - ArcSin\left[(R-\delta)\times\frac{\sin\left(\frac{\pi}{2}+\theta\right)}{R}\right]\right)$$

$$\frac{\beta - \frac{\pi}{2} + \theta + ArcSin\left[(R-\delta)\times\frac{\sin\left(\frac{\pi}{2}+\theta\right)}{R}\right]}{\omega} = \frac{\frac{R}{\sin\left(\frac{\pi}{2}+\theta\right)} \times \sin\left(\frac{\pi}{2} - \theta - ArcSin\left[(R-\delta)\times\frac{\sin\left(\frac{\pi}{2}+\theta\right)}{R}\right]\right)}{V_a}$$

$$V_a = V_r - U$$

$$V_a = V_r - R\omega$$

$$\therefore \frac{\beta - \frac{\pi}{2} + \theta + ArcSin\left[(R-\delta)\times\frac{\sin\left(\frac{\pi}{2}+\theta\right)}{R}\right]}{\omega} = \frac{\frac{R}{\sin\left(\frac{\pi}{2}+\theta\right)} \times \sin\left(\frac{\pi}{2} - \theta - ArcSin\left[(R-\delta)\times\frac{\sin\left(\frac{\pi}{2}+\theta\right)}{R}\right]\right)}{V_r - R\omega}$$

$$\therefore \omega = \frac{\beta - \frac{\pi}{2} + \theta + ArcSin\left[(R-\delta)\times\frac{\sin\left(\frac{\pi}{2}+\theta\right)}{R}\right]}{\frac{R}{\sin\left(\frac{\pi}{2}+\theta\right)} \times \sin\left(\frac{\pi}{2} - \theta - ArcSin\left[(R-\delta)\times\frac{\sin\left(\frac{\pi}{2}+\theta\right)}{R}\right]\right)} \times \left(V_r - R\omega\right)$$

$$\therefore \omega = C \times \left(V_r - R\omega\right)$$

$$Where \Rightarrow C = \frac{\beta - \frac{\pi}{2} + \theta + ArcSin\left[(R-\delta)\times\frac{\sin\left(\frac{\pi}{2}+\theta\right)}{R}\right]}{\frac{R}{\sin\left(\frac{\pi}{2}+\theta\right)} \times \sin\left(\frac{\pi}{2} - \theta - ArcSin\left[(R-\delta)\times\frac{\sin\left(\frac{\pi}{2}+\theta\right)}{R}\right]\right)}$$

$$\therefore \omega_{\max} = \frac{C \times V_r}{(1+CR)}$$

$$\therefore V_r = \sqrt{\frac{1}{(1+k)}} \times \sqrt{2gH + R^2\omega^2}$$

$$\therefore \omega = \frac{C \times \left[\sqrt{\frac{1}{(1+k)}} \times \sqrt{2gH + R^2\omega^2} \right]}{(1+CR)}$$

$$\therefore \omega^2 = \left(\frac{C}{(1+CR)} \right)^2 \cdot \frac{1}{(1+k)} \times \left(2gH + R^2\omega^2 \right)$$

$$\therefore \omega^2 = C_1 2gH + C_1 R^2 \omega^2$$

$$Where \Rightarrow C_1 = \left(\frac{C}{(1+CR)} \right)^2 \cdot \frac{1}{(1+k)}$$

$$\therefore \omega^2 (1 - C_1 R^2) = C_1 2gH$$

$$\therefore \omega_{\max} = \sqrt{\frac{C_1 2gH}{(1 - C_1 R^2)}}$$